Arnan Araza

Assessment, Uncertainties and Applications of Global Above-ground Biomass Maps from Earth Observation

2023

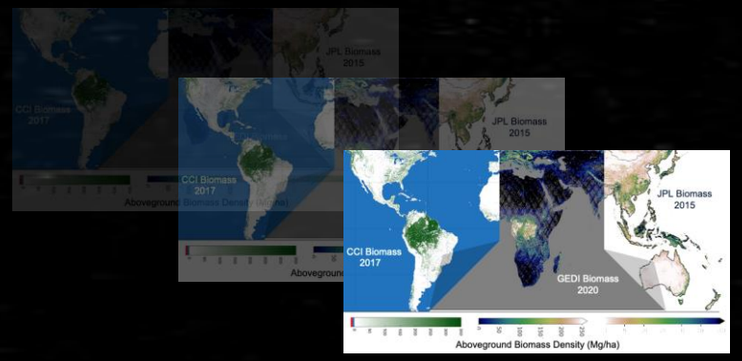

Assessment,
Uncertainties and
Applications of

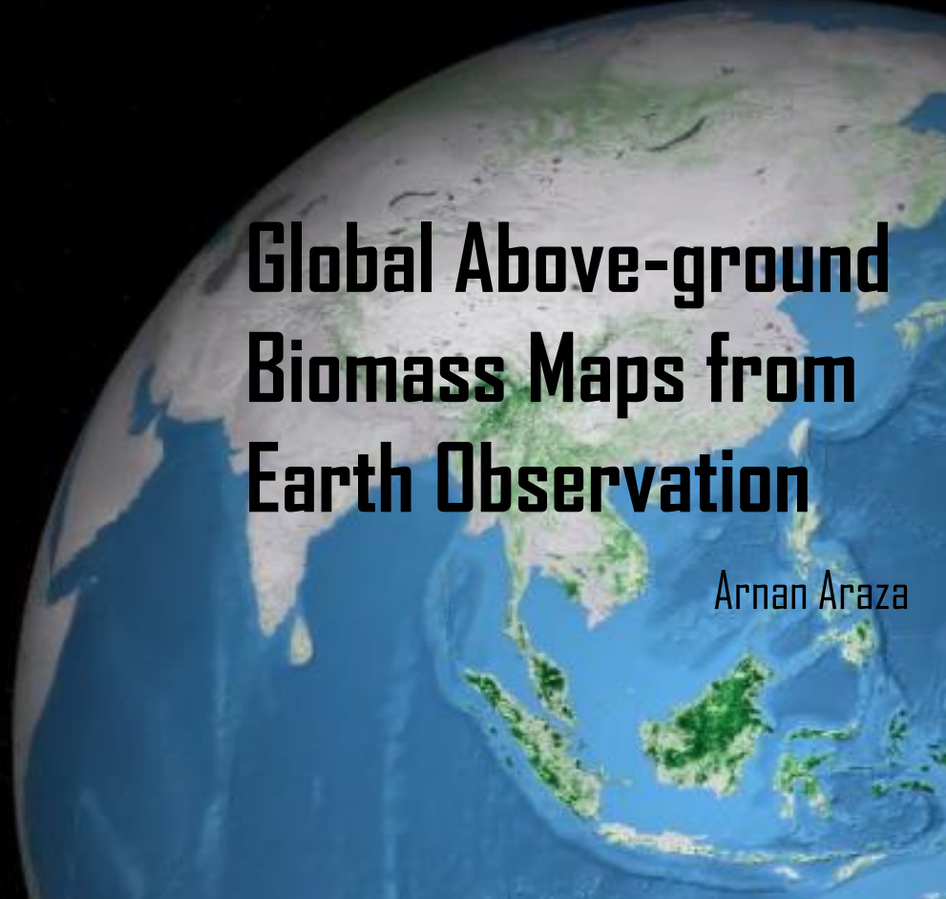

Global Above-ground Biomass Maps from Earth Observation

Arnan Araza

Propositions

1. Regional bias in global above-ground biomass (AGB) maps makes map-based AGB estimates unreliable.
   (this thesis)

2. The assessments of global AGB and AGB change maps suffer from limited reference data.
   (this thesis)

3. Claiming that machine learning models are 'physics-aware' or 'physics-based' is fundamentally flawed and misleading.

4. Obesity will remain unresolved regardless of the amount of research devoted to it.

5. Smartphones do more harm than good to human welfare.

6. Government projects are often co-terminus with implementing politicians and hence unsustainable.

Propositions belonging to the thesis entitled
Assessment, Uncertainties and Applications of Global Above-ground Biomass Maps from Earth Observation

Arnan Araza
Wageningen, 6 June 2023

Assessment, Uncertainties and Applications of Global Above-ground Biomass Maps from Earth Observation

Thesis

Arnan Araza

Thesis committee

Promotors:
Prof. Dr Martin Herold
Professor of Remote Sensing
Wageningen University & Research

Prof. Dr Lars Hein
Personal chair, Environmental Systems Analysis
Wageningen University & Research

Co-promotor:
Dr Sytze de Bruin
Associate Professor, Laboratory of Geo-information Science and Remote Sensing
Wageningen University & Research

Other members:
Prof. Dr Gerard Heuvelink, Wageningen University & Research
Dr Michael Schlund, University of Twente, Enschede
Dr Maxime Réjou-Méchain, Institut de recherche pour le développement, Marseille France
Dr Nuno Carvalhais, Max-Planck-Institut für Biogeochemie, Jena Germany

This research was conducted under the auspices of the C.T. de Wit Graduate School
of Production Ecology & Resource Conservation (PE&RC)

Assessment, Uncertainties and Applications of Global Above-ground Biomass Maps from Earth Observation

Arnan Araza

Thesis
submitted in fulfilment of the requirements for the degree of doctor at Wageningen University
by the authority of the Rector Magnificus
Prof. Dr A.P.J. Mol,
in the presence of the
Thesis Committee appointed by the Academic Board
to be defended in public
on Tuesday 6 June, 2023
at 4 p.m. in the Omnia Auditorium.

Arnan Araza
Assessment, Uncertainties and Applications of global Above-ground biomass maps from Earth Observation
186 pages.

PhD thesis, Wageningen University, Wageningen, The Netherlands (2023)
With references, with summary in English

DOI: https://doi.org/10.18174/630094
ISBN: 978-94-6447-695-8

Contents

Chapter 1

Introduction

1.1 Context

1.1.1 Above-ground biomass and climate change

The global terrestrial forest and woody vegetation are vital assets of our planet because of the enormous ecosystem services they provide to mankind. Forests store and sequester atmospheric carbon, which is the most valuable ecosystem service in the context of climate change. To mitigate climate change, the ideal scenario is to avoid carbon emissions from forest deforestation and degradation, while enriching forest lands through afforestation, reforestation and sustainable forest management. Important to this global target are essential climate variables (ECV), a set of globally explicit variables that jointly characterize the Earth's climate for climate science and policy (Bojinski et al., 2014). The concept of ECV is spearheaded by the Global Climate Observing System under the United Nations and the International Council for Science. Among the ECVs is forest aboveground biomass (AGB), a direct measure of carbon stocks defined as the aboveground standing dry mass from trees and other woody vegetation, expressed as mass per unit area typically Mg ha $^{-1}$ (GCOS, 2010).

1.1.2 How is AGB measured?

Directly measuring AGB involves destructive harvesting and weighing of trees but this unsustainable practice has long been replaced by non-destructive estimation methods. The indirect way of AGB estimation requires tree measurements of diameter and preferably height measurements, which are then supplied to allometric models to estimate tree-level biomass. Allometric models are created using data from destructively measured AGB and may vary from one tree species to another. Historically, biomass estimates of trees are usually aggregated to spatial units such as forest inventory plots and forest stands to estimate the productivity of forest plantations. However, obtaining this information at large scales (e.g., regional to national) is hindered mainly by inaccessible forest areas, insufficient funding and long survey time (McRoberts & Tomppo, 2007). These are the same reasons that hinder re-measurements after a certain period. As such, the AGB estimation has become dependent on remote sensing data. Aircraft and satellites have onboard instruments that can detect and measure various forms of energy, such as visible light, infrared, and scattered radio waves, and use this information to create images. Using remote sensing data as auxiliary variables, biomass can be estimated over large unit areas such as forest stands, administrative units and the whole country area. This process produces more precise estimates than using forest inventory alone (McRoberts et al., 2005).

1.1.3 AGB remote sensing through the decades

Biomass estimates are also possible at the pixel level of the remote sensing data to produce an AGB map. Remote sensing of AGB has a long history. In the 1980-2000s, biomass remote sensing was mainly motivated by the need to estimate the primary productivity of lands. Examples are the use of Synthetic Aperture Radar (radar) to estimate the biomass of Australian woodlands (Lucas et al., 2000) and Normalized Difference Vegetation Index (NDVI) from Landsat (optical) to determine the African dry land productivity potential (Tucker et al., 1985). The "AGB sensing" properties of radar sensors is the signal sensitivity to forest structure while optical signals indicate the greenness of canopy and leaves. Since the early 2000s, forest AGB maps intended for global carbon cycle research have emerged. A notable example is the first Amazon AGB map derived using MODIS-based NDVI that allowed carbon stock estimates of countries and climate zones (Saatchi et al., 2007). There were also demonstrations about the potential of airborne Light Detection and Ranging (LiDAR) to detect the forest vertical structure and hence AGB at local to regional scales (Dubayah & Drake, 2000). In the later decades, the development of mapping AGB is evident from the rapid increase of products and associated scientific papers. Using Landsat alone, there have been at least 20 AGB maps produced in a variety of study areas (Nguyen et al., 2019). Using SAR, at least 50 studies that applied unique data and estimation methods were recorded (Sinha et al., 2015).

The number of AGB maps at pantropical to global scales is increasing, thanks to the increasing satellite missions and the availability of Earth Observation (EO) data. For example, Landsat archive has been publicly available since 2008 onwards. Literature reviews revealed at least 15 global AGB maps exist as of the year 2019 using different mapping methods (Rodríguez-Veiga et al., 2017; Zhang et al., 2019). For instance, the pantropical AGB maps of Saatchi et al. (2011b) and Baccini et al. (2012) were based on a two-step mapping method. First, local estimates of AGB are obtained from models that correlate plot AGB and height from spaceborne LiDAR. Second, a global sample of these local AGB estimates is used as calibration data to fit models that either use individual or combined optical and radar data. Several maps are solely based on radar data or spaceborne LiDAR data such as maps from Climate Change Initiative (CCI) (Santoro & Cartus, 2019) and Global Ecosystem Dynamics Investigation (Dubayah et al., 2020), respectively. The CCI maps in particular did not use calibration data since AGB is estimated directly from radar signals using deterministic models. The current list of global AGB maps is expected to further increase because of at least four radar satellite missions dedicated to forest monitoring. A prominent example is the BIOMASS mission, the first satellite operating with a P-band wavelength, capable of penetrating the forest canopy for better forest structure retrievals (Quegan et al., 2019). Listed below are the main pantropical to global AGB maps produced using state-of-the-art remote sensing.

Table 1.1: Table showing a list of pantropical to global AGB maps.

AGB map	Spatial scale	Pixel size	Epoch	Reference
Avitabile	pantropical	1km	2007	Avitabile et al. (2016)
GEDI	pantropical	1km	2020	Duncanson et al. (2022)
Saatchi	pantropical	1km	2000	Saatchi et al. (2011b)
Baccini Pan-tropical	pantropical	1km	2007	Baccini et al. (2012)
Baccini Global	global	30m	2000	GlobalForestWatch (2002)
Chen	global	1km	2007	Chen et al. (2018)
Hu	global	1km	2004	Hu et al. (2016)
Kindermann	global	55km	2005	Kindermann et al. (2008)
GEOCARBON	global	1km	2008	Avitabile et al. (2014); Santoro et al. (2015)
GlobBiomass	global	100m	2010	Santoro et al. (2020)
Ruesch-Gibbs	global	1km	2000	Ruesch & Gibbs (2008)
Yang	global	1km	2005	Yang et al. (2020)
Zhang	global	1km	2000	Zhang & Liang (2020)
Alnaiz	global	1km	2000-2019	Alaniz et al. (2022)
Baccini time series	pantropical	250 m	2003-2014	Baccini et al. (2017)
CCI Biomass	global	100 m	2010,2017,2018	Santoro & Cartus (2019)
JPL time seires	global	10 km	2010-2019	Xu et al. (2021)
Liu	global	27.5km	1993-2012	Liu et al. (2015)
LVOD SMOS	global	25 km	2010-2019	Yang et al. (2022)
Scatterometer AGB	global	25 km	1990-2020	Santoro et al. (2022a)
LVOD time series	global	25 km	1988-2008	Liu et al. (2012)
WRI Flux model	global	30 m	2000-2020	Harris et al. (2021)

1.2 AGB map assessment and uncertainties

1.2.1 AGB map uncertainty

Just like any EO product, global AGB maps are affected by uncertainty mainly because satellite data are indirect measures of biomass. Uncertainty in this context is the range where the unknown map error resides. Remote sensing data suffer from the well-known signal saturation in high biomass areas wherein a constant AGB value is recorded (Lucas et al., 2000). Remote sensing signals in low biomass areas are prone to mixed soil and vegetation components (Réjou-Méchain et al., 2019) and environmental effects such as rain and snow (Santoro et al., 2015). For maps produced using regression models that relate plot AGB to satellite data (calibrated models), the uncertainty of the predicted map AGB is inherited from plot errors due to tree measurements and the allometric model of choice (Chave et al., 2004). These errors are elaborated below in section 1.2.3. Moreover, calibrated models are prone to bias the predictions to the mean of the observations (Rodríguez-Veiga et al., 2019). For maps produced from deterministic models (not using calibration data), the map uncertainty sources originate from the model itself and its parameters. These enumerated uncertainty sources mostly contribute to the consistently observed pattern in current AGB maps which is an overestimation of low biomass and underestimation of high biomass (Rodríguez-Veiga et al., 2019).

1.2.2 Map validation and reference data

Global AGB maps should undergo independent map validation to evaluate map accuracy and reliability. This standard operating procedure is the main stipulation of the recently published CEOS AGB Validation Protocol (Duncanson et al., 2021). Independent validation mainly involves the comparison of the maps with an independent reference dataset that is not used in map production and is preferably implemented by entities other than map producers. The common sources of reference data are National Forest Inventories (NFI) plots and permanent research plots. The validation involves comparing the AGB between plots and maps either at the plot level (plot-pixel) or aggregated levels (plot-grid cells). The comparison is evaluated by classical accuracy metrics like mean error (bias) and root mean square error (RMSE) typically for a number of AGB bins.

1.2.3 Reference data uncertainty

Plot uncertainties originate from tree measurement errors particularly errors from the measurement equipment and even human errors. When biomass is estimated from these measurements, another uncertainty contributor stems from the use of allometric models (Chave et al., 2004). In the absence of allometric models specific to tree species, generalized models are used such as regional to pantropical models and these alternative models introduce uncertainties. It is also possible that the species-level model used needs to incorporate other tree parameters like wood density. Furthermore, the reference data constitute a global sample that is opportunistic (ad-hoc sample). Such a sample may require prerequisites before being designated as reference data such as an analysis of environmental representativity (Labrière et al., 2022) or sampling assumptions (de Bruin et al., 2020). There are also a number of uncertainty sources when comparing plots and maps. Plots and map pixels have spatial mismatches that result in highly uncertain AGB estimates especially when plots are small i.e., <0.1 ha (Réjou-Méchain et al., 2019). Such mismatch may worsen due to plot geo-location errors from imprecise global positioning systems. Moreover, plots are often surveyed in forest areas while pixels can cover both forest and non-forest areas. Lastly, plots and maps do not always represent the same epoch.

1.2.4 Map assessment

Given that the plots are not error-free, the premise of map assessment in this thesis is to consider the uncertainties of both the map and the plots before their AGB comparison (plot-map comparison). This notion also concerns the accuracy metrics used e.g., root mean square difference (RMSD). The next consideration in map assessments is the choice of aggregation level where the reference data and map AGB are compared. The main reason for aggregating is that certain map users prefer coarse resolution maps as explained in the next section. Another motivation is that the averaging reduces random errors of the

estimated AGB at the pixel and plot levels. The grid cells need to be have representative plots and one way to attain this is to select grid cells only if the plots inside are above a minimum threshold (Fazakas et al., 1999; de Bruin et al., 2019; Xu et al., 2021). Herein we refer to map assessment as the comparison of the AGB between plots and maps that are both uncertain.

1.3 AGB map applications and users

The users of global AGB maps employ the maps as input data to meet their needs and targets. They can be categorized as global and national users. Global users are mostly modellers of the global carbon cycle and climate who are using coarse inputs >1 km to their models. These users relied on biomass and carbon inputs at the level of major climatic zones until the availability of spatially explicit AGB. The climate modellers also use AGB maps to evaluate the results of Dynamic Global Vegetation Models (DGVM) which results are used for reporting global carbon budgets (Friedlingstein et al., 2022). The national users are countries that use the maps to generate the statistics required for Greenhouse Gas reporting (GHG) in compliance with the United Nations Framework Convention on Climate Change (UNFCCC). Countries also use maps under the context of Reducing Emissions from Deforestation and Degradation (REDD+) where countries perform monitoring, reporting and verification (MRV) of emissions as basis for incentive provisions. Countries rely on AGB maps and associated forest changes to capture emissions related to every land-use changes while monitoring emissions in a timely manner. Map users are explicit about map accuracy and uncertainty requirements. Global modellers prefer maps that are unbiased as possible with a pixel-level relative uncertainty of <20% (Quegan & Ciais, 2018). The GHG reporting guidelines also stipulate that the estimates need to be unbiased and the uncertainties need to be reduced as far as practicable (Eggleston et al., 2006). The GHG reporting follows the International Panel on Climate Change (IPCC) tiers about carbon reporting quality and applicability: Tier 1 = regional to global estimates; Tier 2 = national estimates; Tier 3 = high-quality national estimates. Statistics derived from global AGB maps were evaluated to be equivalent to Tier 1 estimates but with the potential to go beyond Tier 1 once map error corrections are implemented (Langner et al., 2014).

There are promising national applications for global AGB maps. One is national carbon accounting under the UN System of Environmental-Economic Accounting (UNSEEA) (UN, 2021). The UNSEEA framework is a spatially explicit system that analyze ecosystems, where national or sub-national maps of ecosystem type, condition and ecosystem services are compiled. Countries started to adopt the framework after UNSEEA became an international statistical standard in 2021. Another innovative application of a global AGB map together with forest disturbance data is a carbon monitoring system capable of reporting monthly carbon emissions for REDD+ (Csillik et al., 2022).

The global AGB maps play a role in the Global Stocktake events, a venue where countries reiterate their pledges in the last Paris Agreement. The first stocktake has started in 2021-2023 and will be repeated every five years. The kickoff of the event was at the UN Climate Change Conference (COP) 26 in 2021 where five global AGB maps were also presented and showcased: `https://www.earthdata.nasa.gov/maap-biomass/`. This initiative was part of the Biomass Harmonization where leading space agencies cooperate to guide national users about space-based AGB data.

1.4 Towards AGB change assessment

Recently, multi-date AGB maps at global scales were produced as a reflection of the growing EO data, see Table 1.1. Besides AGB maps of single epochs, maps of AGB dynamics can have great user interest and a wider range of applications (Herold et al., 2019). A survey among climate modellers in 2019 revealed that most modellers prefer time series AGB maps whenever possible preferably at >1 km pixel size (Peylin et al., 2019). Moreover, national carbon accounting frameworks like UNFCCC and UNSEEA need annual updates.

Two methods are commonly used to obtain an estimate of biomass change (ΔAGB). The stock change approach involves deriving ΔAGB by differencing AGB maps from different epochs. In contrast, with the "gain-loss" approach, land use specific carbon emission and removal factors are used to derive an estimate of ΔAGB starting from an initial estimate of AGB for a given epoch (McRoberts et al., 2020). Both methods provide maps of ΔAGB. The current data sources include at least eight ΔAGB data sources (Table 1.1). The data sources cover epochs 1990-2020, two of them have annual AGB maps i.e., Xu et al. (2021); Santoro et al. (2022a). Regardless of the method, ΔAGB maps are subject to map assessments. Similar to assessing single epochs, the ΔAGB assessment needs to consider map and plot uncertainties. This time, uncertainties from > 1 period need to be accounted since re-measured reference data are used.

1.5 This thesis

1.5.1 Research gaps

Past studies that assessed global AGB maps are limited to regional, pan-tropical and pan-European scales. All studies disregarded the uncertainties of the reference data in the plot-map comparisons. The main hurdle of a global-scale assessment is the lack of an ideal global sample of forest biomass obtained using a probability-based sampling design. Sampling the world's forests is extremely expensive and it is unclear which institutions are responsible for the funding and implementation of the ground sample. This situation is even more problematic for assessing ΔAGB where reference data are more limited.

This is one of the main reasons why there are no ΔAGB map assessments so far. Moreover, the current validation protocols for AGB map assessments are intended for maps of single epochs. While there are already several of ΔAGB totals from country to major climatic zones, what is missing is the spatial map-map comparisons that can identify the consistency of ΔAGB among maps and identify areas where maps disagree on ΔAGB. Identifying hotspot regions of ΔAGB at high spatial resolutions is also important for local policy implications (UN, 2021). The user preference for spatial resolution also pushes for ΔAGB map assessments over different aggregation levels. Such an exercise informs whether indeed systematic differences persist after averaging and how the estimates between the reference data and maps compare from fine to coarse aggregation levels. These issues need more attention now given the increasing number of global AGB maps that will also increase the burden of users with respect to map selection. Without map assessments to guide them, users may select a product subjectively. Worse, they might select a biased map without considering other map products leading to the propagation of map errors to the user's final outputs like climate projections and national carbon accounts.

The usability of global AGB map products for national applications such as GHG reporting, REDD+ MRV and UNSEEA accounting lacks actual demonstrations. Not all REDD+ countries have produced their AGB maps and previous UNSEEA country cases mostly relied on alternative data sources (not actual AGB data) for carbon accounting. The start of the 2020 decade is a reasonable time to pilot country use cases of global AGB products under frameworks that concern map assessment and uncertainty. Priority countries need to be those under the threat of deforestation and degradation and representing at least tropical, temperate and boreal eco-zones. The country cases would matter more if priority countries have existing reference data. Map assessment tools that maintain the data privacy of countries need to be devised. Aside from the assessment outputs, countries need accuracy assessments, which account for sampling effects and other sources of uncertainty. Lastly, carbon accounting of stocks and flows needs an associated uncertainty. Sources of uncertainties include spatially correlated map errors or any associated activity data used e.g., disturbance data. To summarize the research problems are: (1) global AGB maps are biased and reference data are affected by uncertainty; (2) there is a lack of a global AGB map assessment and uncertainty framework and its demonstration; (3) an exploratory assessment of ΔAGB is needed; (4) and country carbon statistics derived from global AGB maps need uncertainty estimates.

1.5.2 Role of this thesis

Map assessment framework

This thesis develops and implements a framework for global AGB map assessment and uncertainty of global AGB products. Actual applications of the framework are both demonstrated for global and national users. Map assessments make use of a compilation

of global reference data and this can be sourced both from publicly available data and private data under data-use agreements. The collated reference data needs to undergo quality filtering and their plot AGB needs uncertainty estimates and harmonization with map AGB estimates to correct for forest area mismatches. The framework applies these preliminary steps to produce a globally distributed >116,000 observations from a collection of NFIs, research plots and local AGB maps from airborne LiDAR (herein called LiDAR) as reference data. One of the main steps in the assessment framework is the estimation of AGB averages over grid cells using plot uncertainties as weights allowing uncertain plots to have less impact on the averaging. This step paves the way to implement a model-based method to minimize map systematic differences (bias adjustment) as a means to integrate the AGB of plots and maps. This step is subsequently followed by a geostatistical approach (precision modelling) to account for spatially correlated map errors when aggregating pixels over larger areas of interest such as a land cover class, country and continent. An associated online map assessment tool is developed to implement the framework.

Exploratory assessment of ΔAGB

This thesis explores the assessment of the ΔAGB from four recent global ΔAGB products using re-measured NFIs and LiDAR as reference data. Maps need to be assessed at different aggregation levels given the varying user preferences in map resolution. The map assessments are complemented by map-map comparisons to identify regions that show consistent ΔAGB estimates spatially. This analysis strengthens the identification of hotspot regions of AGB loss and gains. The results of the AGB and ΔAGB comparisons are helpful not only to map users but also to map producers for improving AGB retrieval methods in certain regions where map AGB estimates disagree with reference data and with most of the other map products. Lastly, the strengths and limitations of each reference data are identified and discussed.

National applications of global AGB maps

This thesis demonstrates the use of global AGB maps for two national applications that both require high-resolution map inputs First, using the global ΔAGB products, spatial carbon fluxes are mapped and used as the main input for developing carbon accounts following the UNSEEA framework. This thesis accounts for the carbon flux prediction error at the pixel level and the UNSEEA class aggregation, resulting in the first UNSEEA carbon accounts with reported uncertainties. This method is piloted in five case countries with reference data. Unique from this demonstration is the representativity analysis of the country data in relation to carbon flux. Another national application of this thesis involves an integration of a bias-adjusted global AGB map into a carbon monitoring framework in the context of REDD+ that identifies carbon emissions at high spatial (10 m) and temporal resolutions (monthly). African countries are currently subject to

this monthly carbon MRV. Aside from map uncertainty, the uncertainty related to the disturbance data is accounted in deriving the uncertainty of the monthly country stocks and emissions.

1.5.3 Research questions

This thesis aims to answer the following research questions:

1. How can the accuracy and uncertainty of global AGB maps be assessed using different reference data sources?
2. Which sources of uncertainty affect the assessment and applications of global AGB maps?
3. What is the effect of spatial aggregation on ΔAGB assessments?
4. How global AGB maps and their assessment support both global and national map users?

1.5.4 Thesis overview

The succeeding chapters of this thesis are based on four separate journal papers. Chapter 2 involves a framework for assessing the accuracy and uncertainty of four global aboveground biomass maps (Araza et al., 2022a). The maps represent different epochs and have associated uncertainty layers needed for the map assessment and uncertainty modelling (bias and precision). Chapter 2 shows assessments of these maps at 0.1° spatial resolution which are particularly useful for global climate and carbon modellers. The total pantropical AGB over time and their uncertainties are one of the main results of Chapter 2. Chapter 3 is about the past decade ΔAGB comparisons from four multitemporal global maps including maps produced from stock differencing and gain-loss methods (Araza et al., 2023). This exploratory assessment of ΔAGB involves comparisons of plots and maps at different aggregation levels to cater different map resolution requirement of users; and map-map comparisons to assess ΔAGB consistency. What makes the study exploratory is the objective to collate ΔAGB reference data for the first time in literature while assessing their geographic and eco-zone coverages. Chapters 2 and 3 are global scale assessments that both follow the same reference data quality filtering and uncertainty assessment of prominent plot error sources. Chapters 4 and 5 are national applications for two different carbon accounting systems. Chapter 4 is about the spatial predictions and uncertainties of forest carbon fluxes used for UNSEEA carbon accounting of five case countries (Chapter 4, Araza et al. under review). Carbon fluxes are predicted using the Chapter 3 high-resolution maps among other environmental data; NFI and LiDAR reference data and an ensemble machine learning framework. Carbon stocks (CCI 2010 map) and flows (predicted carbon fluxes) are aggregated at UNSEEA class and country levels while accounting for residual uncertainties. Chapter 5 demonstrates a

carbon emission reporting system for all African countries at high spatial and temporal resolution suitable for REDD+ MRV (Csillik et al., 2022). Carbon emissions and their uncertainties are estimated using a bias-adjusted AGB map as baseline biomass and the associated forest disturbances afterward (gain-loss) (Reiche et al., 2021). Lastly, Chapter 6 summarizes the learning from the previous chapters and details the outlooks and further application of the map assessment framework and the global AGB maps. These discussions are in line with the upcoming forest-oriented satellites and increasing international initiatives supporting permanent AGB reference datasets. Also mentioned in Chapter 6 are associated parallel studies that relate to this thesis i.e., (Araza et al., 2021c, 2022b). The diagram showing the overview of the thesis is shown in Figure 1.1.

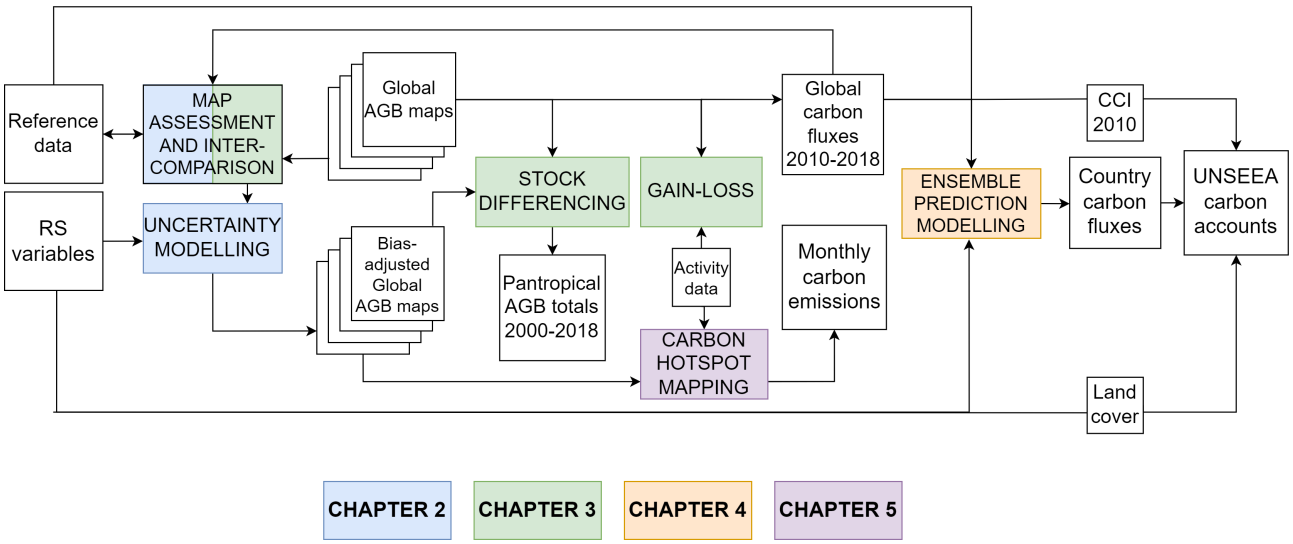

Figure 1.1: Flowchart of the main components of the thesis highlighting the main methodology for each chapter.

Chapter 2

A comprehensive framework for assessing the accuracy and uncertainty of global above-ground biomass maps

This chapter is based on:

Araza, A., De Bruin, S., Herold, M., Quegan, S., Labriere, N., Rodriguez-Veiga, P., ... & Lucas, R. (2022). A comprehensive framework for assessing the accuracy and uncertainty of global above-ground biomass maps. *Remote Sensing of Environment, 272,* 112917.

Abstract

Over the past decade, several global maps of above-ground biomass (AGB) have been produced, but they exhibit significant differences that reduce their value for climate and carbon cycle modelling, and also for national estimates of forest carbon stocks and their changes. The number of such maps is anticipated to increase because of new satellite missions dedicated to measuring AGB. Objective and consistent methods to estimate the accuracy and uncertainty of AGB maps are therefore urgently needed. This paper develops and demonstrates a framework aimed at achieving this. The framework provides a means to compare AGB maps with AGB estimates from a global collection of National Forest Inventories and research plots that accounts for the uncertainty of plot AGB errors. This uncertainty depends strongly on plot size, and is dominated by the combined errors from tree measurements and allometric models (inter-quartile range of their standard deviation (SD) = 30-151 Mg ha^{-1}). Estimates of sampling errors are also important, especially in the most common case where plots are smaller than map pixels (SD = 16-44 Mg ha^{-1}). Plot uncertainty estimates are used to calculate the minimum-variance linear unbiased estimates of the mean forest AGB when averaged to 0.1°. These are used to assess four AGB maps: Baccini (2000), GEOCARBON (2008), GlobBiomass (2010) and CCI Biomass (2017). Map bias, estimated using the differences between the plot and 0.1° map averages, is modelled using Random Forest regression driven by variables shown to affect the map estimates. The bias model is particularly sensitive to the map estimate of AGB and tree cover, and exhibits strong regional biases. Variograms indicate that AGB map errors have map-specific spatial correlation up to a range of 50-104 km, which increases the variance of spatially aggregated AGB map estimates compared to when pixel errors are independent. After bias adjustment, total pantropical AGB and its associated SD are derived for the four map epochs. This total becomes closer to the value estimated by the Forest Resources Assessment after every epoch and shows a similar decrease. The framework is applicable to both local and global-scale analysis, and is available at `https://github.com/arnanaraza/PlotToMap`. Our study therefore constitutes a major step towards improved AGB map validation and improvement.

2.1 Introduction

Above-ground biomass (AGB) is the total mass of material stored in the living stems, branches and leaves of vegetation, and is often described as a biomass density, with units of mass per unit area. AGB is recognised by Global Climate Observing System (GCOS) as an Essential Climate Variable (ECV), primarily because it is intimately related to both emissions of CO_2 to the atmosphere arising from Land Use Change and fire, and uptake of CO_2 from the atmosphere due to vegetation growth (GCOS, 2016). However, it has much wider significance because of its value to human societies for energy, materials and other ecosystem services, and is also important in forest management and for policy initiatives such as Reducing Emissions from Deforestation and forest Degradation (REDD+). As a result, there have been major efforts to map forest AGB using Earth Observation (EO) data (Herold et al., 2019); at least 15 AGB maps for five epochs have been derived at pan-tropical to global scales according to meta-analyses by Rodríguez-Veiga et al. (2017) and Zhang et al. (2019).

Further maps are anticipated because of new missions dedicated to measuring forest structure and AGB, including the Global Ecosystem Dynamics Investigation (GEDI) LiDAR mission (Dubayah et al., 2020), the NASA-ISRO Synthetic Aperture Radar (NISAR) (Kellogg et al., 2020) and BIOMASS satellite (Quegan et al., 2019).

Current AGB maps were derived using different methods and data sources (Langner et al., 2014; Rodríguez-Veiga et al., 2017; Mitchard et al., 2013; Réjou-Méchain et al., 2019). This leads to significant disagreements between them that reduce their value for estimating carbon stocks in global and national applications. In addition, the maps have specific, individual error properties, rendering them unreliable for biomass change analysis, despite representing different epochs (Herold et al., 2019).

The accuracy of AGB estimates is normally quantified by characterising their error, i.e., the difference between the estimated and true AGB; this is normally unknown unless trees are destructively harvested to obtain their true weight. Ideally, the full error distribution would be known, but accuracy is commonly described statistically using various moments of the error distribution. Often, only two moments of the error are considered: the bias, which is the mean value of the error, and the precision, which quantifies the spread in the distribution of random errors around this mean (Dieck, 2007). These random errors are often less troublesome since their dispersion can be reduced by averaging, but this does not reduce bias.

There are many potential sources of bias in AGB estimation, including methodological, human and equipment biases when measuring tree dimensions; the use of incorrect allometric models when estimating tree AGB from these measurements; factors affecting EO signals such as saturation at high biomass, and mixed soil and vegetation components influencing signals from low biomass areas (Réjou-Méchain et al., 2019); and variations in

the EO signal due to environmental effects such as rain and snow (Santoro et al., 2015). As a result, a consistently observed pattern in current AGB maps derived from space data is overestimation of low biomass and underestimation of high biomass (Réjou-Méchain et al., 2019; Rodríguez-Veiga et al., 2019).

Assessment of the accuracy of an AGB map has to take into account both errors in the map itself and in the reference data used to validate it (Duncanson et al., 2021). Reference data are commonly in situ plot measurements (plot data), whose uncertainty can be quantified using methods described in the Committee for Earth Observing Satellites (CEOS) AGB validation protocol (Duncanson et al., 2021). Plot uncertainties originating from tree measurements have rigorously been assessed at local scales (McRoberts et al., 2016; Chave et al., 2004; Harmon et al., 2015; Rejou-Mechain et al., 2017), and their propagation into AGB maps has been assessed at local (Chen et al., 2015) and regional scales (Rodríguez-Veiga et al., 2016). At larger scales, Avitabile & Camia (2018) accounted for both plot and map uncertainties in four pan-European maps using independent plot data to evaluate map bias and precision.

Consistent accuracy and uncertainty assessment of continental and global scale AGB maps are hampered by the lack of a global reference dataset (Schimel et al., 2015; Rodríguez-Veiga et al., 2017). Sampling the world's forests is highly labour-intensive and expensive, and forest inventory data are often not open access. National Forest Inventories (NFIs) have been established only in a limited set of countries, of which a minority are in tropical areas (McRoberts & Tomppo, 2007). In addition, NFIs in the tropics are often incomplete or unrepresentative because forest regions may be remote, inaccessible, or located in conflict areas. Efforts have recently started to centralize and standardize AGB plot data. The Forest Observation System (FOS) provides access to thousands of plot data (Schepaschenko et al., 2019), and the standardization of plot data from large plots and LiDAR-derived transects has been advocated (Chave et al., 2019b). Other data sources, such as the Global Forest Biodiversity Initiative (GFBI) (Liang et al., 2016), provide data to researchers by request and GFBI also encourages the contribution of data. Fine-resolution AGB maps from LiDAR can also be used as an alternative to plot data for AGB map validation (McRoberts et al., 2019a) and provide high-quality AGB estimates over more extended areas than forest inventories (Labriere et al., 2018). Nevertheless, there are only a few fine-resolution AGB maps, open access data sources and proprietary plot data that can be used under data-use agreements. The consequent lack of a consistently sampled reference AGB dataset has consequences for statistical inference, which is only possible under certain assumptions and requires the data to be accompanied by uncertainty estimates (de Bruin et al., 2019; McRoberts et al., 2020; Duncanson et al., 2021).

Using a collection of plot datasets with uncertainty estimates across the globe offers several opportunities. Firstly, differences between plot measurements and global AGB

maps can reveal regional patterns that may be explainable by environmental and/or ecological variables (de Bruin et al., 2019). This would allow these differences to be predicted using model-based approaches. For example, Tsutsumida et al. (2019) identified geographical areas with high AGB errors, attributing error hotspots to local land-use practices. Secondly, global data can be used to investigate bias and develop bias reduction methods. As examples, Xu et al. (2016) and Zhang & Liang (2020) applied random forest regression to model and remove AGB map bias, whilst Avitabile et al. (2016) combined weighted linear averaging with bias removal methods when fusing the Saatchi et al. (2011b) and Baccini et al. (2012) pantropical maps. Thirdly, the availability of plot-level uncertainties allows evaluation of the extent to which plot-map differences can be attributed to map error.

A key GCOS principle for climate monitoring is that random errors and time-dependent biases in satellite observations and derived products should be identified (GCOS, 2016), and more generally map users prefer AGB maps to be unbiased and to have spatially explicit uncertainty information (Quegan & Ciais, 2018). The latter should include information on the spatial correlation of map errors since this is needed to model the precision of AGB estimates derived by averaging and summing map pixel values at coarser grids or countries (de Bruin et al., 2019). In this paper, we propose a model-based framework designed to meet these needs using a global opportunistic sample of plot data to assess four AGB maps. This allows four questions to be addressed: (1) What is the error contribution from different plot error sources? (2) How can map bias be assessed? (3) How can map users and producers benefit from this framework? (4) How can the framework be applied to derive the total AGB and its uncertainty in the pantropics in different periods?

2.2 Materials and Methods

2.2.1 A framework for comparing plot and map estimates of AGB

The framework first pre-processes plot data to minimise forest area (where "forest" is set to be 30-m pixels with >10% tree cover (Hansen et al., 2013a)) and temporal mismatches with the AGB maps (section 2.2.2), and then has three main analysis steps highlighted in Figure 3.1. Although plot estimates of AGB may be biased if an incorrect allometric model is used, this bias will tend to be small if local allometric models are used, as is often the case for NFIs and research plots (Chave et al., 2014). Hence we here assume they are unbiased and, after quantifying their uncertainties (section 2.2.3), use them to calculate the minimum-variance linear unbiased (MVLU) estimates of the mean AGB within 0.1° grid cells, together with their uncertainties (section 2.2.4). This allows the biases in the maps to be quantified. Map bias and the spatial correlation of random map errors are then modelled, respectively using spatial covariates and variograms of AGB residuals as inputs (section 2.2.5), and applied to four global AGB maps (Baccini,

GEOCARBON, GlobBiomass and CCI Biomass; see section 2.2.2). Finally, we estimate the total pantropical AGB for each map epoch, together with their confidence intervals, and compare them with the values from the 2020 Forest Resource Assessment (UN-FAO, 2020) (section 2.2.6).

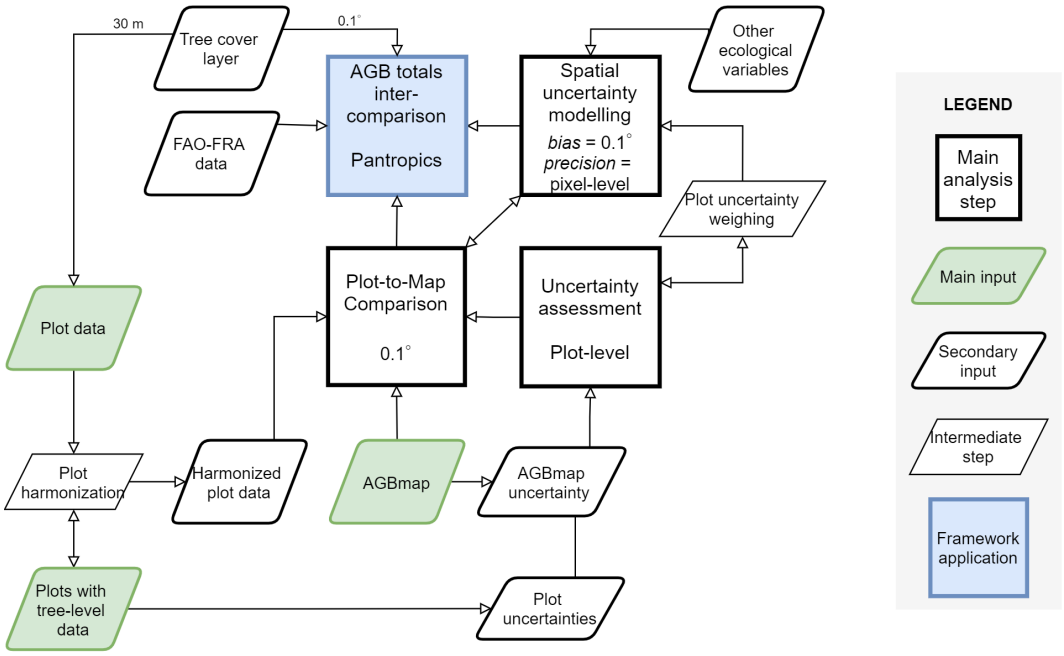

Figure 2.1: Schematic of the framework indicating the three main inputs and three analysis steps leading to the comparison between plot and map estimates of AGB and the totals of the latter. Note the two-way link between the plot-to-map comparison and uncertainty modelling, indicating the assessment of map accuracy.

2.2.2 Data inputs

Three types of input data are needed to implement the framework: (1) plot estimates of AGB, which we refer to as plot data; (2) plot data with tree-level measurements (at least tree diameter), referred to as plots with tree data; and (3) global AGB maps.

Plot data

We used a global collection of plot data from NFIs (often derived using systematic sampling) and research network plots; the latter were mainly in the tropics, where they make up a quarter of the tropical plots. Most plot data were obtained under data-use agreements (see Table S1 for the plot metadata). From them, we selected a subset meeting the following criteria. Plots should:

1. not have been used for AGB map calibration;
2. have precise coordinates to at least four decimal places in decimal degrees;

3. have been measured within ten years of the map epoch (McRoberts et al., 2015);
4. have plot-level AGB estimated using all trees with a diameter at breast height (DBH) of 10 cm or greater;
5. not have been deforested in the period between the inventory and the map epoch, according to forest loss data (Hansen et al., 2013a);
6. have comprehensive metadata that contains information about field measurement, allometric model and sampling scheme used;
7. have an associated report or other publication.

This yielded a total of at most 116,181 (out of a possible 225,698) globally distributed plots to be used as reference data. Their coverage was assessed against: (a) world regions and tree cover; (b) biomes defined by specific precipitation and temperature regimes (Iremonger & Gerrand, 2011); (c) strata derived from tree cover and population density, in order to assess plot coverage in forests with and without human disturbance (Figure 3.2). The plot data cover all biomes (though some, such as portions of boreal and tropical rainforest, are under-represented) and they extend over all the population density and tree cover strata.

The size of individual plots ranges from 0.02 ha to 25 ha, with a median size of 0.20 ha, and they cover a total area of 18,192 ha. The plot measurements took place between 1996 and 2018, and their AGB values were estimated using allometric models deemed appropriate for their forest area by the data providers. The mean plot AGB is 100.70 Mg ha^{-1} with a standard deviation (SD) of 158.31 Mg ha^{-1}. More comprehensive plot summary statistics are shown in Table S2.

Harmonizing plot and map data

Comparisons between plot and map data are only meaningful if they share common spatial and temporal characteristics. This requires applying two pre-processing steps to the plot data. For plots surveyed either before or after the map epoch, the first uses forest growth data and the number of years between the plot and map estimates to adjust the plot AGB to the date of the map data (Avitabile & Camia, 2018). We used the growth data from model-based estimates derived from chronosequences and permanent plots for the tropics and subtropics (Suarez et al., 2019), and for temperate and boreal regions (Buendia et al., 2019); these are improvements of the estimates in the IPCC 2006 report. Specific growth data are used depending on the forest type, ecological region, forest age and continent. The second step deals with the different areas of the forest plots and the AGB map support unit (i.e., the original pixel size or a coarser grid cell). Note that the map provides an estimate of AGB within each support unit, but this may include non-woody and non-forest areas, especially in heterogeneous and fragmented landscapes (Chave et al., 2004; Nascimento & Laurance, 2002). AGB maps including non-forest woody vegetation are also preferred by some users, including climate modellers (Quegan

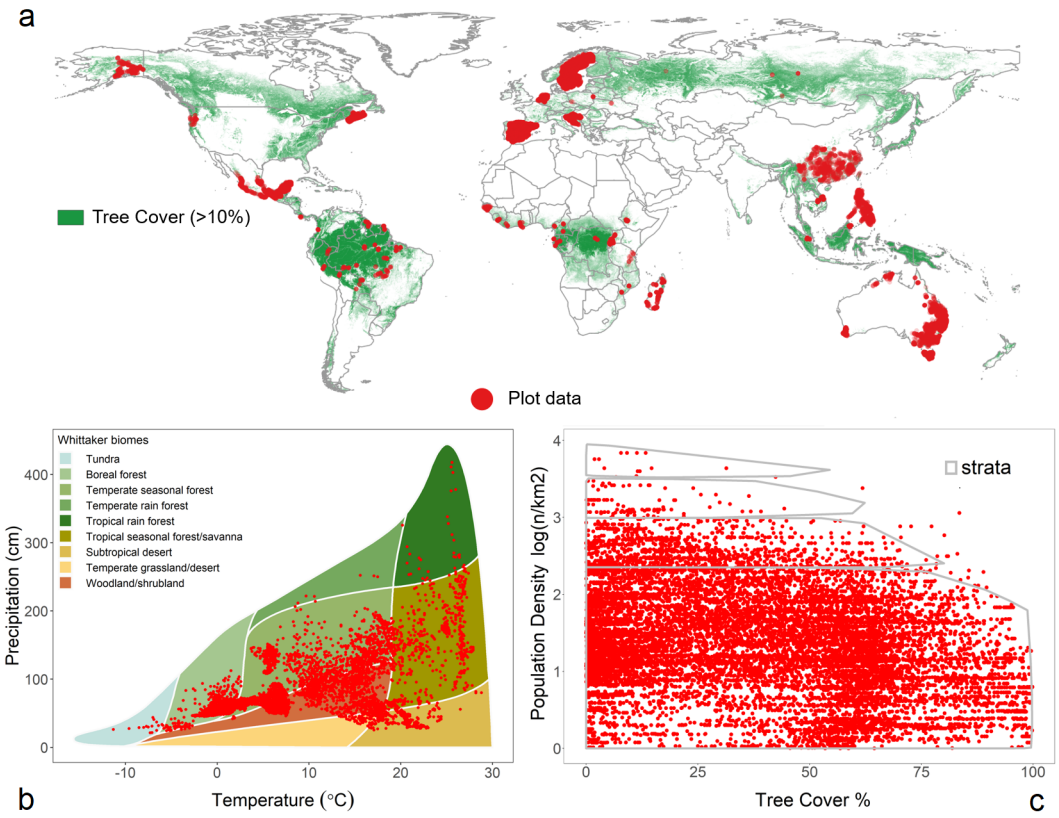

Figure 2.2: Distribution of the plot data: (a) within countries and areas with $> 10\%$ tree cover (Hansen et al., 2013a); (b) within ecological regions or biomes (Whittaker, 1975) as a function of rainfall and temperature; (c) within strata with and without possible man-made forest disturbances as indicated by a scatterplot of log2-scaled human population density (Balk & Yetman, 2004) against tree cover percentage.

& Ciais, 2018). To provide an estimate of the same quantity from plot data, we assume that the plot data properly represent the forested part of the support unit and other types of land cover have negligible AGB. Then for plots smaller than the support unit, the plot-based estimate of the AGB in the support unit (or average AGB for coarser grid cells) is given by multiplying the plot AGB by the forest fraction (0-1), where this is derived by defining forests as areas with at least 10% tree cover (following Food and Agriculture Organization guidelines (UN-FAO, 2010)) and using the 30-m tree cover layer by Hansen et al. (2013a).

AGB maps

From the AGB maps listed in Table S3, four were selected on the basis of three criteria: (1) global extent; (2) open access; (3) accompanying maps of uncertainty (referred to as an SD layer). The Baccini map (epoch 2000), is based on the two-step method of Baccini et al. (2012) that first establishes a statistical model relating space-

borne LiDAR metrics to AGB reference plots, allowing AGB estimation at the LiDAR footprints. These AGB estimates are then used to calibrate a statistical model which estimates AGB from Landsat reflectance, thus generating a global AGB map accessible at `https://www.globalforestwatch.org/`. The available SD layer of the Baccini map includes estimates of errors from allometric models, the LiDAR-based model and the Landsat-based model, and is currently limited to the pantropics, but the provision of the global layer on the Global Forest Watch platform is planned (Table S3). The GEO-CARBON 2007-2010 map (Avitabile et al., 2014) was produced by combining a refined pantropical map (Avitabile et al., 2016) (a fusion of the Saatchi et al. (2011b) and Baccini et al. (2012) maps) with the boreal map of Santoro et al. (2015), to obtain global coverage. The SD layer of the refined pantropical map is estimated using a procedure based on error stratification, whereas that of the boreal map accounts for random variation in the radar backscatter intensity used to predict growing stock volume (GSV) and AGB. The GlobBiomass 2010 and the CCI Biomass 2017 version 1 maps were produced from spaceborne synthetic aperture radar (SAR) images of backscattered intensity (Santoro & Cartus, 2019; Santoro et al., 2020), from which GSV was estimated using physically-based models and then converted to AGB by scaling for wood density and biomass expansion factors estimated from empirical models (Santoro et al., 2020). The SD layers of the two maps account for random errors in radar data and from the biomass retrieval process and its parameters using a first-order Taylor series approach. The Baccini and GEO-CARBON maps are limited to forest areas, while GlobBiomass and CCI Biomass maps include non-forest areas.

2.2.3 Uncertainty in estimating AGB from plot data

The plot harmonization described in section 2.2.2 involves adjusting plot values to minimize temporal and areal mismatches between the plot and map estimates, both of which involve uncertainty. Another cause of difference between the true AGB in a map pixel and its estimate from plot data comes from sampling errors since plots are typically smaller than map pixels (Baccini et al., 2007). This section describes the methods used to estimate the SDs of these error sources.

Plot measurement and allometric model errors

Non-destructive forest inventory is the traditional method used to estimate tree AGB, but has an uncertainty of 5-44% at the stand scale (Burt et al., 2020). Tree measurement errors originate from uncalibrated surveying tools and human errors, which propagate into the allometric model used to estimate AGB from tree diameter (and height) per tree, and then into aggregation at plot-level (Rejou-Mechain et al., 2017). The cumulative error from tree measurement and allometric models is termed “measurement error” in this study.

To estimate the uncertainty in measurement errors (SD_{me}), plots with tree data were used to estimate how errors in individual tree measurements propagate into biomass estimates at plot-level. We used data from 8,457 plots, ranging from 0 to 25 ha in size and with a total of 267,907 trees. These plots are within all the major climatic zones (tropics, sub-tropics, temperate and boreal) and across eight countries, of which the majority are in the tropics. However, plots with tree data constitute only 7.4% of all plot data used in our analysis. A two-step approach was therefore implemented to predict SD_{me} for all plots using a model calibrated on the plots with tree data.

The first step estimated tree-level errors due to uncertainty in tree parameters (wood density, diameter and tree height). Tree wood density data and their uncertainty were obtained from global and regional databases (Chave et al., 2009). For trees without height data, stem diameter was used to estimate height, H, using the Weibull height-diameter model (equation 2.1). This three-parameter estimator of H has been tested within tropical forests (Feldpausch et al., 2012), temperate coniferous forests in Norway (Mahanta & Borah, 2014) and China (Zhang et al., 2014), boreal forests (Zhang et al., 2018), and coniferous forests in the Philippine Highlands (Anacioco et al., 2018):

$$H = a(1 - \exp(-(DBH/b)^{c})) \tag{2.1}$$

where DBH is diameter at breast height and a, b and c are fitted coefficients.

Errors arising from the parameters in the biomass allometric model, such as model coefficients and residual standard errors, were also considered. These data are derived from the dataset of destructive tree measurements provided in Chave et al. (2014). The overall error propagation included the probability distributions of the tree and allometric model parameters and was implemented by running 1000 Monte Carlo simulations using the *AGBmonteCarlo* function of the *BIOMASS R* package (Rejou-Mechain et al., 2017). The outputs are estimates of AGB and its SD_{me} for each tree, which were aggregated to plot-level.

In the second step, a random forest (RF) model trained on the SD_{me} of the 8,457 plots using climatic zones, AGB and plot size as covariates was used to predict SD_{me} for all plots. The RF model predictions were tested using an independent random subset containing a third (n=2,819) of the plots with tree data. The evaluation of the model resulted in an R^2 of 0.86 and Root Mean Square Error (RMSE) of 22.1 Mg ha^{-1}.

Temporal differences

The correction for plot and map temporal mismatch introduces errors caused by uncertainties in the growth rate, for which data are available per forest type, biome and continent. To derive the temporal uncertainty for the plots, SD_{td}, we multiplied the SD of the growth data in Table 4.9 of IPCC 2019 (Buendia et al., 2019), SD_{gr}, in Mg ha^{-1} yr^{-1},

by the difference between the plot survey year (PY) and the map epoch (MY):

$$SD_{\text{td}} = SD_{\text{gr}} * |MY - PY| \tag{2.2}$$

Sampling error

The sampling error can be significant, especially when the AGB exhibits large local variability since plots are often smaller than map pixels (Baccini et al., 2007). To estimate this within-pixel sampling error, spatial configurations using measured data from 8-60 ha plots and 5-250 m EO footprints were simulated by Rejou-Mechain et al. (2014). For each simulation, configurations of both plot and pixel were randomly located. For simulations where plots are smaller than pixels, the RMSE was computed and normalized by the mean AGB of the footprint to derive a Coefficient of Variation (CV).

We adopted the results of Figure 6 and Table S2 of Rejou-Mechain et al. (2014) to train an RF model to predict CV as a function of plot size and AGB map pixel size. We evaluated the model using one-third of the total set of plots (n=38,289) which yielded an R^2 of 0.81 and an RMSE of 0.07. The CV was then converted into the SD of sampling error (SD_{se}) by multiplying by the mean AGB of all the plot data ($\bar{\mu}AGB$) (equation 2.3).

$$SD_{\text{se}} = \bar{\mu}AGB * CV \tag{2.3}$$

Plot-level uncertainty

Assuming the three error sources are independent, the uncertainty in the estimate of the mean AGB within a map pixel using plot data, SD_{p}, is then given by:

$$SD_{\text{p}} = \sqrt{{SD_{\text{me}}}^2 + {SD_{\text{td}}}^2 + {SD_{\text{se}}}^2} \tag{2.4}$$

The SDs of the three main plot error sources and the maps were analyzed for each map over three groups of plot sizes: large plots (1-25 ha), plots of moderate size (0.3-1 ha) and smaller plots, usually from NFIs (<0.3 ha); and over biomass ranges (<150, 150-300, and >300 Mg ha^{-1}). The same grouping was also used to summarize the SD layers of the maps.

2.2.4 Comparison of plot and map estimates of AGB

Aggregation to 0.1° grid cells

The plot data were compared with the AGB maps in 0.1° grid cells (referred to below as default AGB maps), which is a spatial scale comparable to those typically used in global carbon cycle and climate models. Non-forest pixels (taken to have AGB = 0) were

included for Baccini and GEOCARBON prior to aggregation to avoid biasing the 0.1° AGB averages if only forest pixels are used. For each grid-cell i, its average AGB was estimated from the map data by averaging the AGB estimates at each pixel in the cell; and from the plot data by the MVLU estimate under the assumption that the plot data are unbiased. The MVLU estimate is the weighted average of each plot estimate of AGB, x, inside the grid cell i, where the weight is inversely proportional to the variance of x. Hence the plot-based estimate of the AGB of the grid cell has uncertainty $SD_{\mathrm{pG}}(i)$ given by equation (3.1), where the summation is over all plots in the grid cell.

$$SD_{\mathrm{pG}}(i) = \sqrt{1/\sum(1/{SD_{\mathrm{p}}}^2(x))} \tag{2.5}$$

Only grid cells containing at least 5 plots were selected; on average these cells contained 15 plots, with an average total area of 2.3 ha. Around 46% of the total number of available grid cells were excluded from this selection process. Similar studies have also set minimum plot numbers to select grid cells for map assessment, e.g., Fazakas et al. (1999); Baccini et al. (2012, 2017); Xu et al. (2021). Although in some cases these plots may not properly represent the grid cell, notably when they are research plots lying in particular types of forest, only 4% globally and 24% of the tropical plots used for analysis are research plots. This issue is discussed further in section 2.4.3, and Figs. S1 and S2.

Evaluation of differences between plot and map estimates of AGB

Plot and map estimates of AGB were tabulated and compared in AGB bins of width 50 Mg ha^{-1}. For each bin, the following accuracy metrics were computed: Root Mean Squared Difference ($RMSD$) between map and plot AGB at 0.1° (AGB_{mG} and AGB_{pG}) for all grid cells within the bin (n) (equation 2.6); and the Mean Difference MD (equation 2.7), which is interpreted as map bias or simply "bias". Scatterplots were also used to locate transitions from map overestimation to underestimation and AGB ranges exhibiting little bias. The scatterplots have a higher number of AGB bins than the tabulated results.

$$RMSD = \sqrt{\sum_{i=1}^{n} \frac{\left(AGB_{\mathrm{mG}}(i) - AGB_{\mathrm{pG}}(i)\right)^2}{n}} \tag{2.6}$$

$$MD = (\bar{\mu}AGB_{\mathrm{mG}} - \bar{\mu}AGB_{\mathrm{pG}}) \tag{2.7}$$

Map error conformity

We assessed whether the reported map SD is consistent with the plot SD and the other uncertainty components at 0.1° using a metric denoted as map error conformity (EC). Map uncertainty is classified as optimistic (OP) or pessimistic (PE) according to equation 2.8.

$$EC = \begin{cases} OP & \text{if } (\bar{\mu}SD_{\mathrm{mG}}{}^2) \leq RMSD^2 - MD^2 - (\bar{\mu}\mathrm{SD}_{\mathrm{pG}}{}^2)PE \\ & \text{otherwise} \end{cases} \quad (2.8)$$

2.2.5 Spatial uncertainty

This section details the model-based approach to predicting bias and the geostatistical approach to modeling precision when aggregating map SD over the tropics. The restriction to the tropics is because the extra-tropical SD layer is not currently available for the Baccini map (section 2.2.2), and since most plots with tree-level data used for measurement error estimation are in the tropics.

The Random Forest algorithm

We used RF (Breiman, 2001) to model and predict bias. RF is a non-parametric ensemble model of decision trees from bootstrapped samples of the training data and produces averaged predictions (RF regression). We implemented RF using the *ranger R* package (Wright & Ziegler, 2017). This provides a standard error (SE) of the RF model, calculated using the infinitesimal jackknife approach (Wager et al., 2014) along with a function *case.weights* that prioritizes data with higher weights when forming the bootstrap samples, and hence the trees of the RF model.

Bias modelling

We modelled bias using RF regression and data at 0.1° to form weighted bootstrap samples. The model used open access sources of spatially exhaustive covariates that were considered to have a possible influence on bias (Chave et al., 2004; Rejou-Mechain et al., 2014; Santoro et al., 2015), all averaged to 0.1°. We first tested 10 covariates, including the AGB map itself, its reported uncertainty, slope, aspect, tree cover, elevation, rainfall, temperature, biomes, longitude and latitude. Using all and partial combinations of the covariates, we created multiple RF models using the default RF hyperparameters. The models were evaluated using a randomly held-out 30% of the 0.1° data to assess the proportion of the variance of residuals explained by the model. We then visually inspected the bias for indications of geographic correlation among covariates, as suggested in Meyer et al. (2019). After this initial investigation, we limited the covariates to the five listed in Table 4.1, which also gives brief metadata on the final covariates.

The predictive power of the covariates in the RF model was assessed by the Variable Importance Measure (VIM) and Partial Dependence Plots (PDP). VIM is the mean decrease in accuracy of an RF model after data permutation of a covariate, while a PDP shows the marginal effect of covariates on bias prediction. We normalized and ranked the VIM for every AGB map. The PDPs are displayed as matrices, color-coded with bias and with the axes labelled by the values of a covariate pair, e.g., bias plotted against AGB map and tree cover.

Under the assumption that the error in the estimated bias is normally distributed, we derived the 95% confidence intervals (CI) of the predicted bias ($\widehat{MD}$) using the SE from the RF model (equation 2.9). The estimated bias was then subtracted from the default 0.1° AGB map at all grid cells where the 95% CI of bias does not include zero. The corrected AGB maps (referred to as bias-adjusted) were then compared with the plot estimates at 0.1° using a third of the total grid cells independent from the data used for bias modelling.

$$95\%CI = \widehat{MD} \pm 1.96 * SE \tag{2.9}$$

Table 2.1: Covariates used in bias modelling, with a brief description, unit and spatial resolution.

Covariates	Label	Data description	Data unit	Original spatial pixel size (m)
AGB map	AGB	The AGB maps according to Baccini, GEOCARBON, GlobBiomass, and CCI Biomass	Mg ha^{-1}	30,1000,100,100
Map uncertainty layer	SD	SD of propagated errors from RS inputs and biomass model parameters when predicting AGB_{map}	Mg ha^{-1}	30,1000,100,100
slope	SL	Terrain steepness computed from SRTM v4.1 (Jarvis et al., 2008)[1] using the Horn 1981 algorithm suited for rough terrain	% rise	30
aspect	ASP	Orientation of slope with respect to compass direction	degrees	30
tree cover	TC	Tree cover percentage. Source data varies between maps: Baccini = TC2000-GFC; GEOCARBON and GlobBiomass and CCI Biomass = TC2010-GFC	1-100	30,30,30

[1] *Used GTOPO30 (GTOPO30-global, 2002) for latitudes over 60 degrees north*

Uncertainty of the aggregated AGB map over the tropics

Model-based inference (as used in this study) has to account for spatial correlation in map errors when summing or averaging over an area. Furthermore, the variance of map errors may vary over space (heteroscedasticity). To account for the latter, the AGB residual, $AGB_{\mathrm{R}}(x)$, defined as map-plot difference at plot location x, was scaled by the map SD; this assumes the SD of the residuals is proportional to the map SD at that point (equation 6.1):

$$SR(x) = \frac{AGB_R(x)}{SD_m(x)} \tag{2.10}$$

where $SR(x)$ is the scaled residual and $SD_{\mathrm{m}}(x)$ is the map SD. This scaling was assumed to transform the residuals to homoscedasticity.

We then generated variogram models, $\gamma(h)$ in equation 6.2, to estimate the spatial correlation of SR at spatial lag h, where x is a plot location, and the errors are assumed to be statistically stationary:

$$\gamma(h) = \frac{1}{2}\,\mathrm{Var}[SR(x) - SR(x+h)] \tag{2.11}$$

As proposed in Christensen (2011), the variograms were adjusted for the variance of plot errors by subtracting the mean $SD_{\mathrm{p}}/SD_{\mathrm{m}}$ from the nugget of the variograms. Using the adjusted variograms, $SD_{\mathrm{m}}(i)$ was computed using the covariances estimated at the original map scale within each grid cell. An identical procedure was adopted when estimating the SD in the total pantropical AGB for each map (section 2.3.4). This step is based on the covariances $\sigma_{i,j}$ of grid cell pairs i and j $(1 \ldots \mathrm{n})$, derived after convoluting the adjusted variograms from the original map pixel size to 0.1° following the procedure of Kyriakidis (2004). These covariances of the map error component yielded the variance and hence SD of the total estimated AGB within the tropical belt (SD_{trop}) (equation 2.12):

$$\mathrm{SD}_{\,\mathrm{trop}} = \sqrt{\sum_{i=1}^{n}\sum_{j=1}^{n}\sigma_{i,j}} \tag{2.12}$$

For each AGB map, this was transformed to a 95% CI of the subsequent pantropical AGB corresponding to each map epoch.

2.2.6 Total pantropical AGB

The total pantropical AGB (-25° to 25° latitude) estimated from bias-adjusted maps were compared to that given by the default 0.1° maps i.e., not adjusted for bias. The 2020 Forest Resource Assessment (FRA) (UN-FAO, 2020) data for 2000, 2010 and 2017 (2017 as the average of 2015 and 2020) were also used to assess how AGB data compares with map estimates over time. Since the FRA provides AGB only in forest areas, we used 0.1° tree cover maps to remove 0.1° grid cells whose forest cover was less than a given threshold, chosen to produce a pantropical forest area close to that reported in the FRA. We used the Hansen et al. (2013a) tree cover from 2000 for the 2000 map and from 2010 for the 2010 and 2017 maps.

2.3 Results

2.3.1 Uncertainty as a function of plot size and AGB

For plots < 0.3 ha, the inter-quartile range of SD was 30-151 Mg ha^{-1} for measurement error and 16-44 Mg ha^{-1} for sampling error (Figure 2.3). The SD of measurement error

decreased sharply for larger plots and increased slightly as AGB increased. The sampling errors were also affected by map pixel size. For instance, GEOCARBON (1 km pixels) had consistently higher SD than Baccini (30 m pixels). Plots that were temporally adjusted for epoch 2000 (Baccini) and 2017 (CCI Biomass) exhibited slightly higher temporal SDs than for the other two maps because of the longer periods that had to be bridged between the map epoch and plot inventory date (Table S1), but the temporal error had the lowest SD of the three error sources. On average among the maps, the estimated SD of each error was 93.9 Mg ha^{-1} (measurement), 51.6 Mg ha^{-1} (sampling) and 24.6 Mg ha^{-1} (temporal), equivalent to 73, 22 and 5% of the total variance, respectively. Map SDs exhibited very different magnitudes, but high map AGB values were always associated with higher map SD.

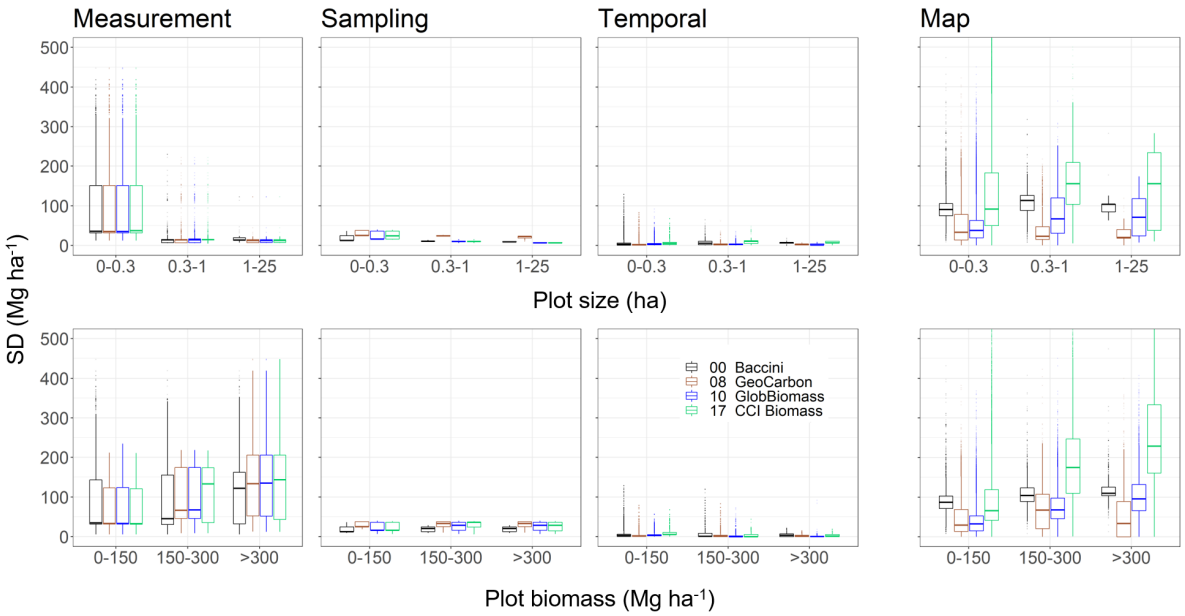

Figure 2.3: Boxplots of plot-level SD for measurement error, sampling error and temporal adjustment as a function of plot size and AGB, color-coded and labelled according to the AGB map they are compared with; the horizontal bar indicates the median and the boxes show the inter-quartile range. Also depicted are boxplots of map SD as a function of plot size and AGB.

2.3.2 Plot-to-map comparison

Comparisons between map and plot estimates of AGB at 0.1° in Figure 2.4 and Table 2.2 show that, while all the maps overestimate lower biomass and underestimate higher biomass, the transition point from over- to under-estimation differs. For example, the Baccini map starts to underestimate AGB at around 150 Mg ha^{-1}, whereas for the other maps this occurs around 200 Mg ha^{-1}. For all maps, the largest underestimation of AGB was in the highest biomass bin. GEOCARBON has the smallest underestimation for values of AGB $>$ 300 Mg ha^{-1}, while the GlobBiomass and CCI Biomass maps have the

lowest absolute MD over the range 50-200 Mg ha^{-1}. The inter-quartile ranges of the binned AGB map values do not overlap with the 1:1 line below 50 Mg ha^{-1} and above 300 Mg ha^{-1}, indicating bias dominates random errors for those bins.

The map error conformity (EC) in Table 2.2 shows that overall, GEOCARBON is optimistic about map precision whilst CCI Biomass is pessimistic. The precision estimates for the Baccini and GlobBiomass maps tend to be optimistic for low AGB and pessimistic for high AGB.

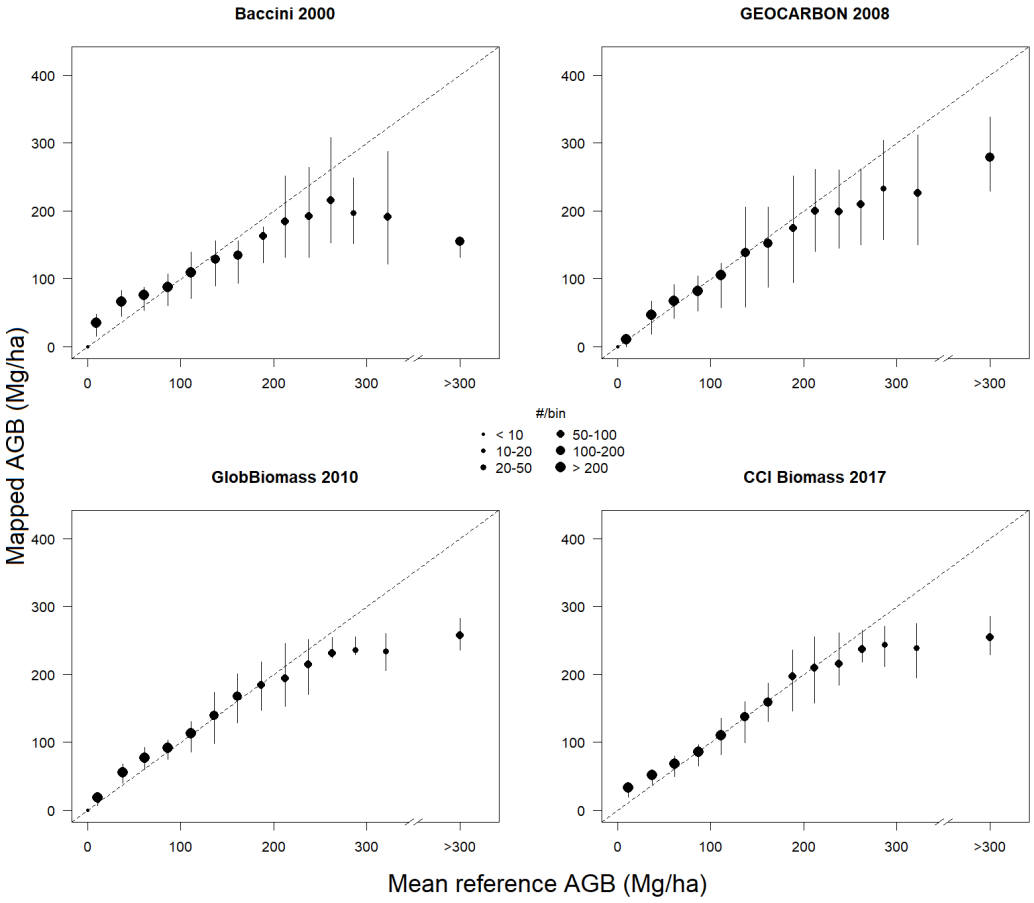

Figure 2.4: Map estimates of AGB aggregated to 0.1° against mean plot AGB within 0.1° grid cells for all four AGB maps. The number of grid cells are: Baccini=6,561; GEOCARBON=6,521; GlobBiomass=6,201; and CCI Biomass=2,612 originating from plot datasets ±10 years apart than the map epoch (see section 2.2.2 and Table S2). Each circle represents an AGB bin and its size denotes the number of grid cells in the bin, while the whiskers correspond to the 25th and 75th quartile range of the map AGB.

Table 2.2: Summary statistics of the plot-to-map comparison: mean plot and map AGB, MD (bias), RMSD, and mean variances of plot and map AGB errors per biomass bin at 0.1°. The EC column lists whether the SD layer provided with the map is optimistic (OP) or pessimistic (PE) about map precision.

AGB bin	AGB_{pG}	AGB_{mG}	MD	RMSD	$SD_{pG}{}^2$	$SD_{mG}{}^2$	EC
Baccini	- - - - - - -	- - - - - - -	- Mg ha^{-1} -	- - - - -			
0-50	19	46	27	38	13325	6348	OP
50-100	69	80	11	45	27435	11208	OP
100-150	121	117	-4	50	17645	12188	OP
150-200	173	146	-27	70	12846	12976	OP
200-250	225	188	-37	103	11849	14709	PE
250-300	270	209	-61	109	11283	15750	PE
300-400	337	192	-146	174	10009	14982	PE
>400	793	147	-647	761	33181	15161	PE
GEOCARBON							
0-50	23	17	-5	26	11771	2221	OP
50-100	70	65	-5	42	24989	8727	OP
100-150	121	122	1	80	20325	9356	OP
150-200	173	183	10	93	14528	6764	OP
200-250	225	190	-34	84	15285	7334	OP
250-300	272	232	-41	90	12224	3158	OP
300-400	338	287	-51	105	20454	2436	OP
>400	680	269	-411	511	72987	131	OP
GlobBiomass							
0-50	23	35	12	22	11373	1112	OP
50-100	70	83	12	29	24674	3236	OP
100-150	120	123	3	47	19805	6188	OP
150-200	171	174	3	55	14042	9731	OP
200-250	225	205	-20	59	14644	12843	PE
250-300	273	233	-41	61	10135	15076	PE
300-400	337	238	-99	110	23175	16465	OP
>400	700	263	-437	520	72682	21374	PE
CCI Biomass							
0-50	22	40	19	29	6845	13304	PE
50-100	72	75	3	31	21218	59323	PE
100-150	122	122	-1	50	19363	74641	PE
150-200	172	174	2	57	14824	167434	PE
200-250	224	212	-12	61	16401	211949	PE
250-300	274	240	-34	58	9347	135659	PE
300-400	339	245	-93	107	19736	84973	PE
>400	680	253	-426	503	71469	227242	PE

2.3.3 Spatial bias

The fraction of the variance of the bias explained by the RF models ranged from 24 to 36% over the AGB maps. Map AGB and tree cover were the most important predictors in the models (Figure S3 and Table S4). The proportion of 0.1° grid cells for which the 95% CI of the bias prediction included 0 Mg ha^{-1} ranged from 4 to 15% across the AGB maps, so most grid cells were corrected for bias.

Systematic underestimation is particularly obvious over the tropical rainforests of the Amazon, the Congo basin and insular Southeast Asia (Figure 2.5), but also occurs in parts of other climatic zones, particularly the sub-tropical zone of China and southeast Australia, the temperate zone of Spain and USA, and the boreal zone of Russia and Canada. There is no obvious common spatial pattern of overestimation among the maps. The GEOCARBON map has the smallest underestimation in the tropics, followed by the CCI Biomass map. The GlobBiomass map exhibits the largest overestimation in the temperate regions, while the Baccini map has the largest overestimation in the boreal zone.

2.3.4 Estimates of total pan-tropical AGB

The default and bias-adjusted maps, and the FRA all show a decrease in the total pan-tropical AGB from 2000 to 2017 (Table 2.3), but with important differences. The bias-adjusted maps give higher total AGB than the default maps for all years since they correct for map underestimation in high AGB regions. The 95% CIs for the estimated total AGBs take account of the map-specific spatial correlation in AGB map errors (see convoluted variograms in Figure S5, which exhibit sills from 0.11-0.38 and nugget = 0, and the modified SDs in 0.1° grid cells in Figure S6). The differences between the three estimates decrease from 2000 to 2017, though the bias-adjusted estimate is still 6.9 Petagrams (Pg) greater than the FRA estimate in 2017.

Table 2.3: Pantropical forest AGB with 95% CI estimated from the default and bias-adjusted maps. Also shown are estimates derived from FRA data for these three years. The forest areas of map-based AGB estimates are set as the closest possible area to the FRA forest area based on a 0.1° tree cover threshold. The analysis includes all pantropical countries but without the pantropical portions of China and Australia.

Year	AGB (Pg)			Forest area (mil. ha)		95% CI (Pg)	
	Default	This study	FRA	Map-based	FRA	Default	This study
2000	354.47	406.38	302.69	1939.28	1998.20	5.83	0.88
2010	279.35	314.20	290.97	1928.98	1907.77	7.93	5.09
2017	277.60	296.20	283.78	1928.98	1849.50	14.10	1.57

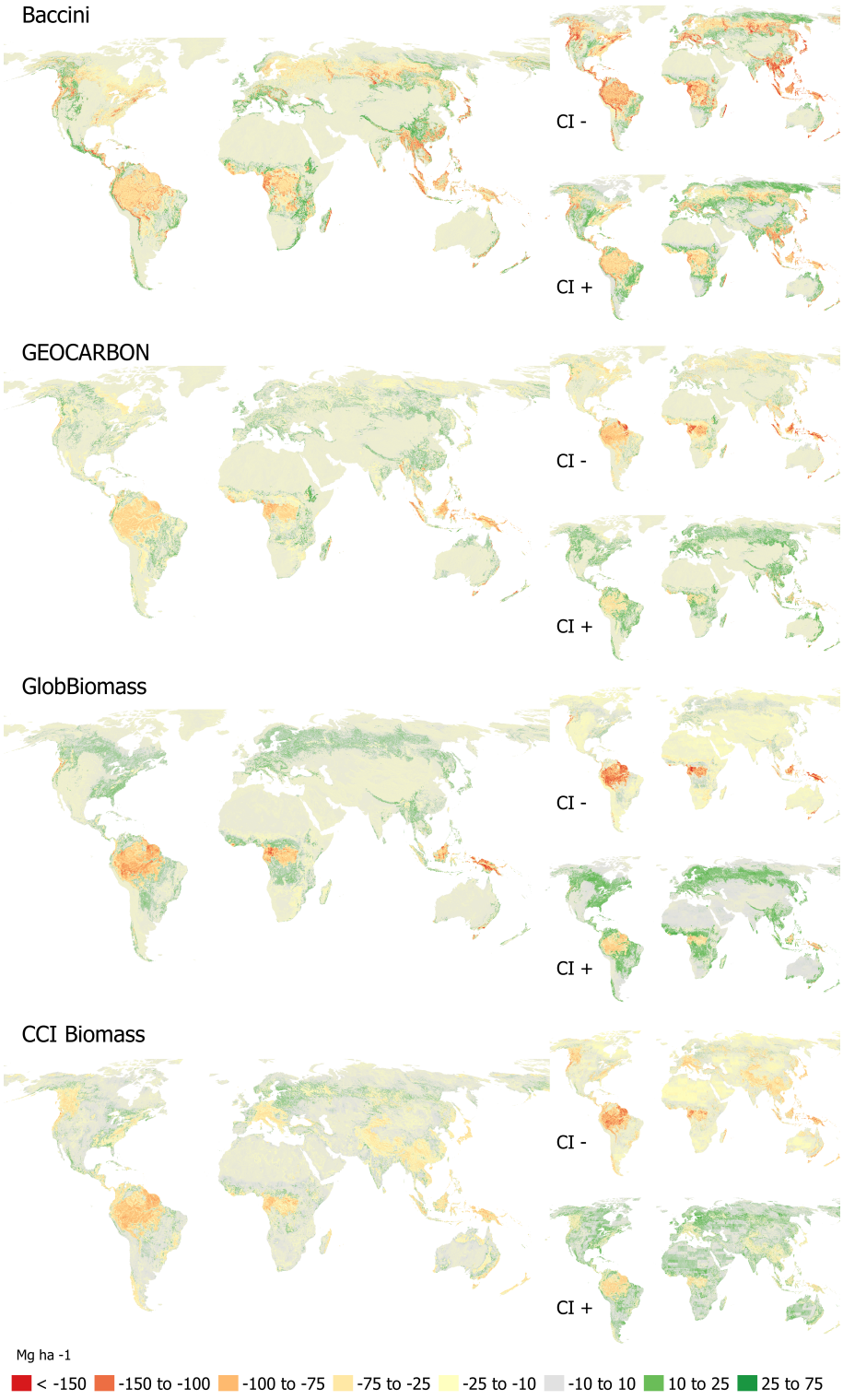

Figure 2.5: The predicted bias of global biomass maps in 0.1° grid cells and their 95% CI: lower (CI-) and upper (CI+). There is a 95% chance that the bias lies within the (CI-, CI+) interval.

2.4 Discussion

2.4.1 Uncertainty drivers in plot-to-map comparison

The largest contributor to plot SD (73%) was measurement error (which includes allometric model errors), which is much larger for smaller plots and increases slightly with higher biomass. Most of the plot data come from small plots (mostly NFIs) in which there are fewer trees. Combined with geolocation errors causing trees near the plot boundary to be included or excluded, this produces large uncertainties (Réjou-Méchain et al., 2019). Moreover, around 34% of the plots smaller than 0.3 ha are extra-tropical, and may be subject to erroneous uncertainty estimates due to the use of the wrong allometric model (Chen et al., 2015). Generic allometric models similar to Chave et al. (2014) for non-tropical forests are not yet developed. The uncertainty of measurement error is probably best estimated by the data producers themselves and its provision would be a useful addition to the data quality requirements for current and upcoming plot data (see section 2.2.2).

Sampling errors in the range 16-44 Mg ha^{-1} were estimated for small plots when map pixel size and forest cover were taken into account (see section 2.2.2). They tend to be amplified when small plots are compared with large map pixels (Rejou-Mechain et al., 2014), as observed in the GEOCARBON results (1 km pixel size, Figure 2.3), which has the highest SD for this error. This occurs partly because forest structure tends to be non-uniform over short distances (Chave et al., 2004; Saatchi et al., 2011a), especially on slopes (Rejou-Mechain et al., 2014) and when there are very big trees (de Castilho et al., 2006). However, the influence of forest structure variability tends to decrease as plot size increases, e.g., Saatchi et al. (2011a) found that the CV of sampling error was 80% smaller for 1 ha plots than for 0.01 ha plots in the tropics. As well as plot size, the number and spatial spread of plots inside a map pixel affects sampling errors (Næsset et al., 2015; Bradford et al., 2010). Several randomly placed samples may be better at capturing the mean AGB of a forest region than a single large sample covering the same total area (Nascimento & Laurance, 2002). LiDAR data may also be useful as reference data since LiDAR-based AGB maps typically cover substantial areas and hence provide samples covering the whole range of AGB in a landscape. This will prevent biases arising from preferential sampling, which is often implicit in the selection of research plots (Duncanson et al., 2021). Whenever available, these maps would be preferred over the research plots themselves as reference data.

Uncertainty from plot temporal adjustment was largest for the AGB maps of 2000 and 2017 because of the longer periods between the map epoch and plot inventory date (Table S1), but was a small contributor to total plot uncertainty. Improvements might be possible by stratifying the growth data to capture the growth of disturbed forests under different management intensities and natural disturbances (Suarez et al., 2019). Such estimates

could be complemented by forest age maps (Besnard et al., 2021).

Map SDs exhibited very different magnitudes as a result of the use of different data, different AGB estimation methods and different ways of propagating uncertainty (section 2.2.2). However, high map AGB values are always associated with higher map SD (though not necessarily a higher CV) (Rodríguez-Veiga et al., 2017). If plots are used for calibration, such as in the Baccini map, large measurement errors may contribute a significant part of the total error propagated to the map (Rejou-Mechain et al., 2017). AGB maps produced without in situ calibration avoid such errors, but are vulnerable to model uncertainties (Santoro et al., 2011). For example, the SDs for GlobBiomass and CCI Biomass arise mainly from limitations in the model converting backscatter to GSV and uncertainty in its parameters (Santoro et al., 2020).

All AGB maps tended to overestimate low AGB and underestimate high AGB. Numerous studies, summarized in Réjou-Méchain et al. (2019) and Duncanson et al. (2021), show similar effects, as a result of several intertwined factors. Both optical and radar sensors are known to saturate for higher values of AGB (Zhao et al., 2016; Rodríguez-Veiga et al., 2019), which inevitably leads to underestimation of AGB. However, the factors causing map overestimation for lower AGB are more complex. For radar-based maps, it is largely driven by imperfect allometric models (Santoro, 2020) and the influence of soil moisture and roughness (Santoro et al., 2011). For maps derived using optical data, it is possibly a result of fitting saturated EO data to plot data in the regression models, particularly if plots are limited to certain forest conditions but used to calibrate models predicting AGB globally (Rodríguez-Veiga et al., 2019). The smaller map bias in mid-range AGB values is expected for regression methods, which often force the mean of the training data and predictions to be equal. Similar behaviour for the model-based approaches used by GlobBiomass and CCI Biomass may reflect higher sensitivity of radar backscatter to AGB and reduced soil effects in this AGB range. GEOCARBON has the closest match to plot data for AGB $>$ 200 Mg ha^{-1}, possibly because its bias removal method used a plot dataset in the tropics which may overlap with our plot data. However, this effect is not easy to quantify as here the comparison is with plot data after the harmonization process (section 2.2.2).

2.4.2 Bias and precision modelling

The model-based approach to predicting bias at 0.1° yields broad-scale spatial patterns of map over- and underestimation that exhibit significant similarities between the four maps (Figure 2.5), and are also similar to patterns observed in Avitabile et al. (2016) for two global maps and Tsutsumida et al. (2019) for regional maps. Error hotspots, mainly of map underestimation, stand out in the regions of agreement and disagreement between the maps (Figure 2.6). Such hotspots occur regardless of the methods used to produce the maps (Xu et al., 2016) whenever there are sufficient reference data to compare with

the maps (Avitabile et al., 2016; Rodríguez-Veiga et al., 2019). However, insufficient and unrepresentative reference data may cause incorrect estimation of map bias and hence erroneous map correction (Avitabile et al., 2016). We attempted to counteract this effect by reducing the plot-based estimates of AGB at 0.1° when non-forest areas exist in grid cells (section 2.2.2). The plots used here cover all major ecological zones, though some zones are under-sampled, and are subject to large measurement errors. These plot errors are accounted for when creating the training data, as explained in section 2.2.5. For example, training data within areas with high map underestimation, such as the Tasmanian forests, were mostly small plots, so received lower weights and hence had a lower chance to become training data. A similar situation is observed in Sweden.

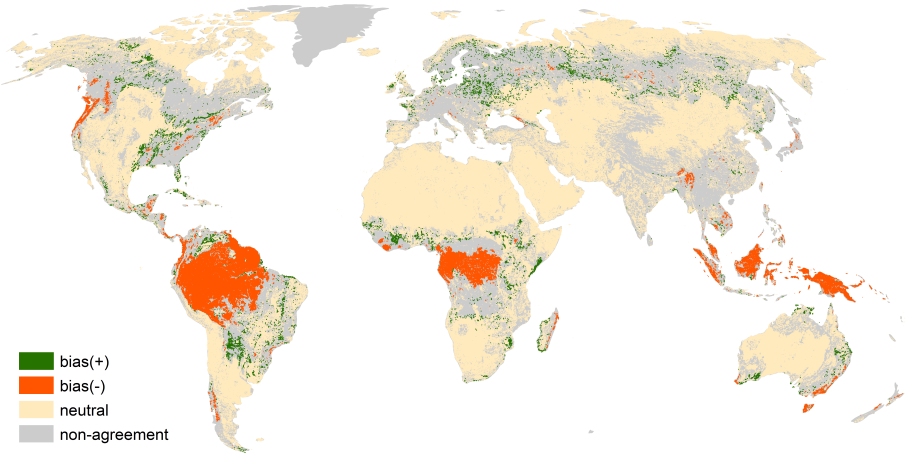

Figure 2.6: Map of grid cells where the biases in the four AGB maps shown in Figure 2.5 at 0.1° for 2000, 2008, 2010 and 2017 agree and disagree; overestimation or bias(+) in all maps, i.e., 10 < bias < 50; underestimation or bias(-) in all maps, i.e., -150 < bias < -10; neutral in all maps, i.e., -10 < bias < 10. All numerical values are in Mg ha^{-1}. All other areas are in the non-agreement class.

The Variable Importance Measure (Table S4) and Partial Dependency Plots (PDP; Figure S3) indicate that the predicted bias is most sensitive to map AGB and tree cover, but this is also clear from Figure 2.5. In particular, the PDPs show that map underestimation of at least 60 Mg ha^{-1} mostly occurs when AGB >300 Mg ha^{-1} and canopy cover is in the range 60-90%. Furthermore, bias in the radar-based maps, e.g., CCI Biomass, is sensitive to steep northeasterly slopes because of the look geometry of the sensor and incorrect pre-processing of the SAR data for moderate and steep terrain (Santoro & Cartus, 2019). These observations may help in developing improved AGB estimators that combat such deficiencies.

Spatial autocorrelation analysis revealed spatial dependency in errors up to lags of 50-104 km, depending on the map (Figure S5). Short-range autocorrelation of residuals (<5 km) comes from localized forest structure (Guitet et al., 2015; Mascaro et al., 2014). However, longer-range autocorrelation is found from our plot data, which are mostly from NFIs that

are configured to sample the forest over short distances (e.g., using nested plots) while also representing regional to country scales. Similar effects were found in other large-scale studies (Baccini et al., 2012; Avitabile et al., 2011; Ploton et al., 2020b). Large scale AGB mapping often uses environmental variables, e.g., topography (Baccini et al., 2012) and climate (Hernández-Stefanoni et al., 2020), as predictors, and these exhibit long-range spatial dependency that may transfer into the AGB error structure (Ploton et al., 2020b). This may also affect the two radar-based maps as the GSV and biomass expansion factor used for AGB estimation are mapped with climatic variables as inputs (Santoro et al., 2020; Santoro, 2020). The variograms also indicate that the map SD layers need to be improved. In the variogram models shown in Figure S5, the residuals are scaled by the map SD, so the SDs are incorrect when the sills deviate from 1 (see "default variogram" in Figure S5). Further evidence for the need to adjust the SDs is given by the map error conformity measures (Table 2.2). Overly pessimistic estimated SD for the CCI Biomass 2017 map has already been corrected in its updated version (Santoro, 2020).

2.4.3 Strengths and limitations of the framework

A core GCOS principle is that estimates of AGB should as far as possible be unbiased. This study provides a comprehensive framework for meeting this principle by estimating the bias and uncertainty in AGB maps (Figure 3.1). It can be adapted to the requirements of different map users or producers (Herold et al., 2019) but requires estimates of uncertainty in both plots and maps, and careful vetting of the quality and suitability of plot data. Open source tools estimating plot uncertainty (e.g., *BIOMASS* and *Plot2Map*) are of great value for this. *BIOMASS* has not been widely tested other than in tropical regions, though is currently being tested in extra-tropical forests. We also provide an interactive online tool for users of the framework and open source software (which can be readily updated) that offers more flexibility in pre-processing plot data and comparing plot and map AGB estimates (`https://github.com/arnanaraza/PlotToMap`). Countries with constraints on sharing plot data could use such tools while maintaining national data privacy.

Bias-adjusted maps of AGB and its uncertainty in 0.1° or larger grid cells can be used in climate and carbon modelling (see Figure S4). They can also provide estimates of national AGB over time, and its uncertainty, to assist carbon accounting based on NFI sampling (McRoberts & Tomppo, 2007) and to enhance local AGB estimates (Næsset et al., 2020; Toan et al., 2011). In addition, they can provide baseline AGB values when more frequent estimation of carbon emissions is desirable (Csillik & Asner, 2020).

Information on local to regional map biases and their dependence on terrain and forest variables (Table S4, Figure S3) may help to trace the factors causing such bias. Moreover, map producers should find the analyses of spatial error structure from variograms and map error conformity informative. For more precise maps, our variograms that account for

measurement errors (i.e., with zero nugget) and our optimized method of SD aggregation can be adapted.

The application of the uncertainty framework to estimating pantropical AGB showed a persistent temporal decline in stocks and increasing agreement between the map-based estimates and the estimate from FRA over time. This may reflect both increasing quality of forest AGB data from countries (Nesha et al., 2021) and improving map accuracy, and suggests that we can have more confidence in more recent estimates of pantropical forest AGB. However, the large disagreements between the map-based and FRA estimates of AGB in 2000 indicate that long-term AGB change estimation based on differences in AGB maps is likely to be unreliable. Further analysis of AGB change from these estimates will be addressed in a follow-up study.

The limitations in the uncertainty framework reported here pertain to the plot dataset, plot selection bias, methodological limitations and data requirement issues. Most plot data with tree-level measurements lack tree height, so we estimated height with the Weibull model, but this model may not apply in all biomes, such as woodlands and mangrove forests. We also lacked tree-level data in non-tropical regions, so estimates of measurement errors for plots in these regions are subject to revision. The fact that the plot dataset in the boreal regions is concentrated in two countries may also limit global application of the framework.

Plot selection bias will arise if the plots inside a 0.1° grid cell do not provide a random sample of the AGB within the cell. For example, if they are selected to lie within high AGB areas within a diverse forest landscape, their weighted average would overestimate the AGB at 0.1°. Research plots, which make up 4% of the total dataset but 24% in the tropics, are particularly prone to this effect. To analyze how this might affect our analysis we examined the variability of tree cover at grid scale and plot locations, and treated this as a proxy for AGB variation (Avitabile & Camia, 2018). This analysis yielded a set of grid cells without preferential samples (referred to as strict filtering of the plot dataset; see Figure S1 for the specific steps). Assessment of the GlobBiomass map at pantropical and global scales against the filtered plot dataset (based on the tree cover for the same epoch (Hansen et al., 2013a)) gave results differing only slightly from use of the current dataset (see Figure S1). This suggests that preferential sampling had little effect on our analysis. Possible reasons for this are that almost the same number of grid cells were excluded under the current approach and the strict filter (56% and 57% in the pantropics, respectively), and that many of the grid cells selected were the same under both approaches, particularly in tropical high AGB areas e.g., 77% of the tropical grid cells where GlobBiomass >250 Mg ha^{-1} used in the current approach were also used after strict filtering (Figure S2). Though we used several grid cells containing research plots, these are mainly plots with area >0.60 ha located in forests that visually exhibit homogeneous canopy cover. Nonetheless, the bias seen in the corrected maps when AGB

>300 Mg ha^{-1} may be exacerbated by the lack of representative plot data, even if the minimum number of plots inside grid cells is increased. This AGB range was only covered by research plots in Tasmanian and Amazonian forests, and most of them were excluded from the bias modelling since the weighted bootstrapping limits the use of small plots with high AGB.

A number of possibilities exist for improving the bias modelling. Using additional covariates, such as AGB texture and canopy height, may help (Xu et al., 2021). Additional plot data, preferably large plots, are desirable both to compensate for those with high variance and, more importantly, to increase spatial coverage since a large training dataset is needed to capture local AGB error patterns (Xu et al., 2016). Selected values from local AGB maps, if they exist, can be added to the training data in under-sampled areas (McRoberts et al., 2019b). We also plan to assess different cross-validations of the bias model. In addition, the use of harmonized plots at coarser scales, e.g., 1 km from forestry concessions (Ploton et al., 2020a) and 25 km from NFIs (Menlove & Healey, 2020) are also options, given their extensive forest coverage.

2.5 Conclusions

1. The comprehensive uncertainty framework developed in this paper can correct existing AGB maps for bias, within the limitations of the bias model. Such maps, with their associated SDs at coarser scales, are particularly useful in the context of climate and carbon cycle modelling. The analysis of spatial bias and models of spatial error correlation provide valuable information to both map users and producers on local to regional map errors.

2. The estimates of bias in the AGB maps exhibit spatial patterns that largely reflect AGB itself. The bias models would benefit from additional plot data and local AGB maps within poorly represented regions i.e., LiDAR-based maps will be preferred over plot data whenever available.

3. The spatial uncertainty modelling was hindered by plot AGB uncertainty arising principally from measurement and sampling errors, which tends to be especially large in regions where only small plots are available. It would be helpful if NFIs included some larger plots to serve multiple purposes, including the assessment of global AGB maps.

4. Both map-based and FRA estimates of pantropical AGB show a decline from 2000 to 2017, and become increasingly close with time, despite the datasets and methods used being quite different for different map epochs. However, there is still a difference of 6.9 Pg between the map-based and FRA estimate in 2017.

Chapter 3

Past decade above-ground biomass change comparisons from four multi-temporal global maps

This chapter is based on:

Araza, A., Herold, M., De Bruin, S., Ciais, P., Gibbs, D. A., Harris, N., ... & Hein, L. (2023). Past decade above-ground biomass change comparisons from four multi-temporal global maps. International Journal of Applied Earth Observation and Geoinformation, 118, 103274.

Abstract

Above-ground biomass (AGB) is considered an essential climate variable that underpins our knowledge and information about the role and climate actions of changing forests in mitigating climate change. The availability of satellite-based AGB and change (ΔAGB) products has increased in recent years. We assessed the past-decade net ΔAGB derived from four recent global multi-date AGB maps: ESA-CCI maps, WRI-Flux model, JPL time series, and SMOS-LVOD time series. Our assessments explore and use different reference data sources with biomass re-measurements within the past decade. The reference data comprise National Forest Inventory (NFI) plot data, local ΔAGB maps from airborne LiDAR, and selected Food and Agriculture Organization - Forest Resource Assessment country data from countries with well-developed monitoring capacities. Map to reference data comparisons were performed at levels ranging from 100 m to 25 km spatial scale. The comparisons revealed that LiDAR data compared most reasonably with the maps, while the comparisons using NFI only showed some agreements at aggregation levels <10 km. Regardless of the aggregation level, AGB losses and gains according to the map comparisons were consistently smaller than the reference data. Map-map comparisons at 25 km highlighted that the maps consistently captured some AGB losses in known deforestation hotspots. The comparison also identified several carbon sink regions consistently detected by all maps. However, disagreement between maps is still large in key forest regions such as the Amazon basin. The overall ΔAGB map cross-correlation between maps varied in the range 0.11-0.29 (r). Reported ΔAGB magnitudes were largest in the high-resolution datasets including the CCI map differencing (stock change) and Flux model (gain-loss) methods, while they were smallest according to the coarser-resolution LVOD and JPL time series products, especially for AGB gains. Our results suggest that ΔAGB assessed from current maps can be biased and any use of the estimates should take that into account. Currently, ΔAGB reference data are sparse especially in the tropics but that deficit needs to be alleviated by upcoming LiDAR data networks in the context of Supersites and GEO-Trees.

3.1 Introduction

The above-ground biomass (AGB) content in forests represents the amount of carbon they store and hence changes in AGB correspond to the amount of CO_2 emitted to or removed from the atmosphere. This function of AGB and their changes (ΔAGB) defines them as an essential climate variable being an important input for global climate models and a necessity for countries in their mandated carbon accounting (Herold et al., 2019). Monitoring the spatial and temporal dynamics of AGB benefits from Earth Observation (EO) and a wider range of observations from space that shall enable a more accurate estimation of AGB is anticipated (Rodríguez-Veiga et al., 2017).

Two approaches are commonly used to obtain an estimate of ΔAGB. The stock change approach consists of estimating ΔAGB by differencing AGB maps from different epochs. Sources of such an approach include the Climate Change Initiative (CCI) Biomass AGB maps for the epochs 2010, 2017 and 2018 with a 100 m pixel size produced using radar remote sensing (Santoro & Cartus, 2019). Another example is the recent L-band Vegetation Optical Depth (LVOD) global AGB dataset with a pixel size of 25 km (Wigneron et al., 2021; Yang et al., 2022). In contrast, with the "gain-loss" approach land use specific carbon emission and removal factors are used to derive an estimate of ΔAGB starting from an initial estimate of AGB for a given epoch (McRoberts et al., 2020). One example is Harris et al. (2021), wherein a baseline AGB map, annual forest loss and gain maps, and activity data specific to deforestation, fire, agriculture and forestry were used to assess net carbon fluxes in the past two decades at 30 m spatial resolution. Xu et al. (2021) used a similar approach that paired annual AGB maps with activity data for carbon fluxes analysis from 2000 to 2019 at the spatial scale of 10 km.

Independent map assessments should be a standard operating procedure for EO-based products (Nightingale et al., 2010; Duncanson et al., 2021). Map assessment in this context involves the comparison of ΔAGB from maps and a reference dataset, i.e., using in-situ data from repeated AGB measurements. A common source of reference data used is represented by measurements collected at sample plots by a National Forest Inventory (NFI) data. Data from NFIs in extra-tropical countries are commonly being used for ΔAGB assessments and subsequent analysis mainly because these NFIs are well-established. Most NFIs, however, are not open-access data, which constrains their use for assessments beyond country scales. Yet, countries have used NFI data to report AGB statistics (means and totals) every five years as part of United Nation's Forest Resource Assessment (FRA). The FRA data was used in global-scale studies related to ΔAGB analysis, e.g., as a basis for comparison with map-based estimates aggregated to countries in multiple periods (Xu et al., 2021; Araza et al., 2022a). At local scales, airborne LiDAR-based ΔAGB maps provide precise estimates. While forest height derived from LiDAR is highly correlated with AGB, the local estimates they provide are considered more reliable than the ΔAGB from plot data as –unlike plots– LiDAR covers whole landscapes

(Næsset et al., 2015). These features have allowed LiDAR as a reliable AGB reference data (Duncanson et al., 2021). Given that most LiDAR campaigns are being repeated for monitoring forest ecosystems, a long list of local LiDAR-based ΔAGB assessments is available. A good example is the study of Nguyen et al. (2020) that used periodic LiDAR-based AGB to validate an AGB time series.

The ΔAGB map assessments concern the spatial resolution i.e., aggregation level over which ΔAGB is assessed. The choice of spatial resolution often depends on the map use (Quegan & Ciais, 2018; Herold et al., 2019). Global map users such as carbon and climate modellers commonly use coarse resolution maps (>1 km) as inputs to global models (Quegan & Ciais, 2018). In contrast, most country-level applications prefer fine-resolution maps that are more informative about highly localized forest area changes such as small-scale mining and slash-and-burn farming. For instance, high-resolution ΔAGB maps serve as input for carbon monitoring, reporting and verification (MRV) (Csillik et al., 2022), and ecosystem accounting (Hein et al., 2020b). Because of this, it makes sense to iterate map assessments over a range of aggregation levels to determine at what resolution the plot and pixel averages best match (Moreno et al., 2016; Santoro et al., 2022a). Such an exercise would also inform the map users how the maps compare with certain reference data.

Global ΔAGB assessment is challenged by several factors. First, there is a lack of readily available and globally suitable reference data because global mapping of multi-temporal AGB has only recently started. Second, the uncertainty about ΔAGB assessed from a global product is large. For instance, changes driven by slow regrowth and degradation are challenging to be detected from satellites (Ryan et al., 2011; Santoro & Cartus, 2019). Third, the current good practices for AGB map validation (Duncanson et al., 2021) and map-reference data comparisons (Araza et al., 2022a) concern AGB maps of single epochs. Multi-date AGB mapping studies have either assessed their products for single epochs or skipped map assessments all together. Lastly, not all ΔAGB data sources directly provide ΔAGB. Converting CO_2 and carbon maps into AGB is straightforward, but sometimes the map products combine the carbon of above-ground and below-ground components (Xu et al., 2021) and occasionally even soil components are included (Harris et al., 2021).

Here we present an exploratory assessment of four ΔAGB maps that represent the past decade. The maps were specifically derived from the CCI maps; carbon flux produced using the Harris et al. (2021) method; the Xu et al. (2021) maps and the LVOD maps herein called as CCI, Flux, JPL, LVOD, respectively. Given the lack of a consistent global ΔAGB reference dataset, map-map comparisons are used to assess consistency among the maps in reporting AGB gains and losses. We (1) compile several ΔAGB reference data sources and assess their suitability for map assessment; (2) compare the ΔAGB between reference data and maps at different spatial aggregation levels; and (3) spatially assess the mutual consistency of ΔAGB maps.

3.2 Materials and methods

3.2.1 Overview of the methods

The assessment of four global ΔAGB Mg ha^{-1} is outlined in Figure 3.1. Preliminary steps that include forest masking, modification of the original carbon flux model and other pre-processing steps all made sure that the maps have comparable ΔAGB. To assess the ΔAGB maps, we used three types of AGB dataset with repeated measurements as reference data: airborne LiDAR-based AGB maps (LiDAR), NFI plots and FRA. To make the map-reference data comparisons meaningful, we further selected subsets of the reference data based on data quality criteria and we applied the same forest mask (used for the maps) based on a forest definition set as > 30% tree cover at 30 m pixel size (Hansen et al., 2013b). Then, the ΔAGB of the reference data and maps were aggregated and compared at five aggregation levels between 100 m and 25 km. The reference data uncertainty were estimated and used as weights for the aggregation step. At 25 km, we assessed the level of agreement among them through spatial analysis and cross-correlation. Note that the units of the aggregation level and map pixel size are both referred similarly e.g., 25 km.

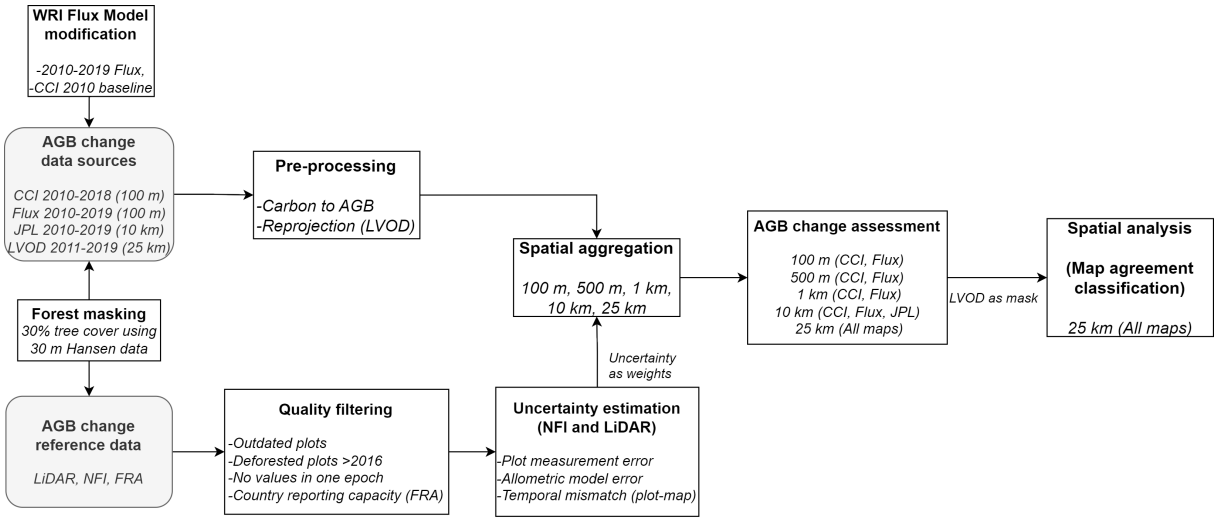

Figure 3.1: Overview of the steps undertaken until the assessment and spatial analysis of ΔAGB maps.

3.2.2 ΔAGB maps

CCI Biomass maps

The European Space Agency Climate Change Initiative (ESA-CCI) Biomass dataset consist of annual global AGB maps with a pixel size of 100 m. The most recent version includes maps for the epochs 2010, 2017 and 2018, and we selected the 2010 and 2018

epochs for our analysis. Each map was derived from synthetic aperture radar (SAR) data where the signal is in the form of backscatter intensity. The SAR input data are then integrated into a physically-based model, accounting for the individual contributions to the backscattered signal from the forest canopy and the ground below the canopy (Santoro & Cartus, 2019; Santoro et al., 2021). The CCI modelling approach is reinforced by allometric equations that relate the canopy density to forest height and then height to AGB (Santoro et al., 2022b). These allometries were derived from the AGB of GlobBiomass dataset (Santoro et al., 2021), and the canopy density and canopy height metrics based spaceborne LiDAR observations. The CCI map comes with associated standard deviation (SD) layers where propagation of uncertainties from the model inputs and AGB retrieval process are estimated by first-order Taylor series approximation.

Carbon flux model

The carbon flux model of Harris et al. (2021) was modified to obtain the net above-ground carbon fluxes attributed to AGB change between 2010 and 2019. Net fluxes in this context are defined as the difference between the carbon emitted and removed by woody vegetation. The default starting year of the model (2000) was changed and the model was initiated with the AGB map, the primary forest and the tree cover for the year 2010. The CCI 2010 map provided the baseline AGB resulting into carbon fluxes at 100 m spatial resolution and we also adjusted the model duration to a 9 years period. We further modified the model to exclude fluxes of other gases aside from CO_2 (CH_4 and N_2O) and excluded below-ground carbon and soil carbon components from the computations. The derived CO_2 was then converted to carbon flux based on the 12/44 carbon-CO_2 proportion and the carbon flux was converted to ΔAGB through division by 0.49 being the conversion factor used by most large-scale carbon mapping. The flux model accounts for the uncertainties (SD) from all major inputs such as the activity data and emission-removal factors, which are estimated at major climatic zone level.

JPL time series AGB

The JPL product (Xu et al., 2021) retrieves AGB from remote sensing data following a two-step approach. First, in every 10 km grid cell covering field plots, AGB mapping is performed based on the relationship between field plot AGB and vegetation height derived from spaceborne data and airborne LiDAR, and backscatter intensity from spaceborne radar data. The resulting grid cells are then used to train and test machine learning models using covariates from MODIS optical data, topographic and climatic variables. At the pixel level, Xu et al. (2021) estimated and summed the uncertainties related to model residual, model parameter estimation error and plot measurement error. The 10 km time series of above-ground carbon maps were first divided by 0.49 to obtain AGB. We used the average of 2009-2011 and 2017-2019 to derive ΔAGB. This step allows comparison with the other ΔAGB maps and reduces the inter-annual variability in the original time

series.

SMOS-LVOD time series AGB

Lastly, we used the 25 km LVOD time series AGB products (Wigneron et al., 2021; Yang et al., 2022) derived from observations by the Soil Moisture and Ocean Salinity (SMOS) satellite. Spatially explicit estimates of LVOD were derived every year between 2010 and 2019. Filtering individual images was done to mitigate the signal noises but resulted in partial coverage of east Asia. Temporal aggregates of the LVOD product are results of a temporal decorrelation method to reduce the seasonal effects related to water content. The uncertainty of the LVOD dataset primarily comes from the AGB reference biomass map used. The LVOD dataset was originally projected to an Equal-Area Scalable Earth (EASE) system. We re-projected the map to WGS 84 using bilinear interpolation. Note that owing to data availability, 2011 was used as the starting point for ΔAGB assessment by LVOD.

More information about the ΔAGB maps are shown in Table S2 including the different remote sensing data applied, spatial resolution, temporal resolution, validation method and forest masking.

3.2.3 ΔAGB reference data

NFIs

The first set of reference data consists of re-measured National Forest Inventories (NFI) plot data from Belgium, the Netherlands, Philippines and Sweden where the first and second measurements were surveyed at least five years apart. The re-measurements allowed estimation of ΔAGB. The NFIs have plot-level AGB estimated by the data sources, but without uncertainty estimates. We then estimated plot uncertainty from measurement and allometric model error as a function of AGB, eco-zone and plot size. We used the prediction model described in Araza et al. (2022a) developed from an extensive plot database spread over all major eco-zones. The model followed an error propagation method of parameters from tree measurements such as diameter, height and wood density and the parameters of the AGB allometric model such as the model coefficients and residual standard errors. The AGB of the reference data was also adjusted to reduce the effects of temporal mismatches between the reference and maps. The AGB of datasets surveyed $\pm >2$ years apart from the map epoch were subjected to this step using growth data from the 2019 Intergovernmental Panel on Climate Change (IPCC) (Buendia et al., 2019). Biomass is either added or reduced depending on the number of years between the inventory date and map epoch. The associated annual uncertainty owing to these adjustments was also estimated based on the reported IPCC growth data uncertainties.

LiDAR

The second reference data comprises local AGB maps derived in forests with re-measured plot inventories and two airborne LiDAR campaigns between 2010 and 2019. Maps of ΔAGB were derived by differencing AGB maps from the two survey periods. Data sources include maps from Brazil (Longo et al., 2016) and the USA (Johnson et al., 2010) where AGB mapping involved calibration of LiDAR height and plot AGB using power-law models. We also used LiDAR-based maps from research projects in Bulgaria, Czech Republic, Costa Rica, Poland and Spain derived using regression models that relate height and AGB. The LiDAR maps resampled to 100 m were used. Some of these maps have associated SD layers all estimated using Monte Carlo error propagation involving errors from the calibration dataset and the associated height-AGB model parameters.

FRA

The third set of reference data are country-level estimates of ΔAGB from FRA reports, derived by differencing the reported AGB 2018 and 2010, where 2018 was computed as the average of 2015 and 2020 AGB. We selected the FRA data based on the capability of countries to conduct NFIs and derive FRA variables using remote sensing. We followed the FRA capacity categories based on a scale of 1 to 5 (1=very poor; 5=very good). Selected countries belonging to east Asia were excluded because of incomplete map coverage as explained in Section 3.2.2. The AGB from the FRA data does not have associated uncertainty estimates.

Reference data quality assessment

We further selected subsets of the reference data:

1. NFI plots were filtered using tree cover loss datasets Hansen et al. (2013b) to retain only plots without forest area changes after the latest measurement and prior to 2018 map epoch. We also discarded plots more than 10 years apart from the map epoch;
2. LiDAR pixels were discarded if there are AGB values in one epoch but without values in the other epoch;
3. FRA data were limited to countries with re-measured NFI or with "very good" NFI reporting capacity since 2010.

We reported the number of reference data retained after quality filtering compared to the original data, and mapped the coverage of the selected reference data over eco-zones based on Whittaker's biome (Whittaker, 1975). The coverage per eco-zone and country determined the suitability of reference data for global map assessments. For each reference dataset, histograms of the AGB distribution in two epochs are shown in Figure S1. We also derived the ΔAGB density for NFI and LiDAR to assess the ΔAGB distribution at

every aggregation level (section 3.2.4). We aim to assess how the ΔAGB (losses, gains and no changes) are depicted from fine to coarse levels depending on the reference data. More information about the reference data is shown in Table S1 and their maps are shown in Figure S2.

3.2.4 Map-reference data ΔAGB comparisons

The past-decade net ΔAGB from the map products and the reference data were compared at different spatial resolutions i.e., grid cells. The details of the comparisons are shown in Table 3.1 showing the grid cell selection.

Table 3.1: Details of the ΔAGB map-reference data comparisons and the selection of grid cells.

Assessment spatial scale	NFI grid cell selection criteria	LiDAR grid cell selection criteria	Map product
100x100 m^2 (100 m)	all	all	CCI, Flux
500x500 m^2 (500 m)	all	all	CCI, Flux
1x1 km^2 (1 km)	>1 plots	all	CCI, Flux
10x10 km^2 (10 km)	>4 plots	>14 pixels	CCI, Flux, JPL
25 km	>9 plots	>19 pixels	all

Grid cells were used if they met the minimum number of reference data inside grid cells (Xu et al., 2021; Araza et al., 2022a), see 2nd column of Table 3.1. This way, grid cells >1 km with very few reference data were excluded from the analysis. The AGB averages per epoch from NFI plots and LiDAR pixels at grid cells were estimated as weighted means where reference data with high uncertainty received smaller weights in the averaging. The weights $W(x)$ were inversely proportional to the variance ${SD_{\mathrm{p}}}^2$ of an NFI plot or a LIDAR pixel x as shown in Eq. 3.1 (Araza et al., 2022a).

$$W(x) = 1/{SD_{\mathrm{p}}}^2(x) \tag{3.1}$$

The AGB averages of both reference data and maps were assured to correspond to a forest mask defined as 30 m pixels > 30 % tree cover (Hansen et al., 2013b). This step was separately done per epoch and for each aggregation level. Subjected to this harmonization are the ΔAGB maps from CCI and LVOD (see Table S2) and the LiDAR reference data. Particularly, the maps were resampled to 30 m to match the forest mask pixel size. All non-forest pixels were masked out then the remaining pixels were averaged for each aggregation level. The assessment at 25 km level included FRA as reference data. We simply used the FRA country average AGB for the needed epochs, which are subject to the country forest definition. The ΔAGB comparisons of grid cell averages between the reference data and maps were assessed using statistical measures including mean difference (MD), Root Mean Square Difference (RMSD), coefficient of determination (R^2) and Nash-Sutcliffe Efficiency

(NSE). These evaluations were implemented for each aggregation level and summarized as color-coded matrices per ΔAGB bin. Herein, ΔAGB comparisons pertain to map-reference data ΔAGB comparisons, which were also displayed as scatterplots and per ΔAGB bin. We also refer to map AGB loss and gain underestimation whenever ΔAGB estimates from reference data are higher than the map estimates.

3.2.5 Map-map ΔAGB comparisons

The 25 km ΔAGB maps were masked using the LVOD product for geographical comparability. The latitudinal profiles of the masked ΔAGB maps were graphed to depict regional patterns of ΔAGB. Then, the level of agreement among the ΔAGB maps was spatially assessed depending on the sign of the ΔAGB. We first classified ΔAGB into "loss" (net loss), "gain" (net gain) and "no change". Here we assume ΔAGB 7 to -7 Mg ha^{-1} as "no change" based on a conservative SD of 9-year growth rate defined in Table 14 of IPCC 2019 for global analysis (Buendia et al., 2019). The threshold avoids erroneous labelling of small ΔAGB values, which can be very uncertain (Ryan et al., 2011; Santoro et al., 2022a). The ΔAGB pixels were finally classified as follows: (1) all products agree on "loss"; (2) all products agree on "gain"; (3) all products agree on "no change"; (4) 2 products agree on "loss", other 2 not "loss" and disagree with each other; (5) 2 products agree on "gain", other 2 not "gain" and disagree with each other; (6) 2 products agree on "no change", other 2 not "no change" and disagree with each other; (7) 3 products disagree. We also assessed cross-correlation among the 25 km ΔAGB maps indicated by Pearson's correlation coefficient (r).

3.3 Results

3.3.1 Reference data for ΔAGB global comparisons

The spatial distribution of the reference datasets are shown in Figure 3.2. The number of discarded data was largest for FRA (90%) since most countries do not have repeated NFIs (see Table S3). More than half of the NFI plots (56%) were excluded either because they were outdated (see Section 3.2.3) or the sites were deforested after the 2nd measurement and before 2018. Almost no LiDAR pixels (<1%) were filtered out as reference since the repeated LiDAR surveys all took place in the past decade and almost all pixels had valid data in both epochs. The reference data are mostly found in the temperate and tropics but under-represents them as well as the other eco-zones. The selected FRA data, though small in size, come from all eco-zone. Despite its smaller size, the NFI dataset has broader eco-zone coverage than the LiDAR dataset. That is because NFIs are surveyed over entire countries while LiDAR campaigns are typically confined to forests. We had no access to NFIs and LiDAR data from Africa and Australia.

The ΔAGB distributions from LiDAR and NFI data at different aggregation levels are

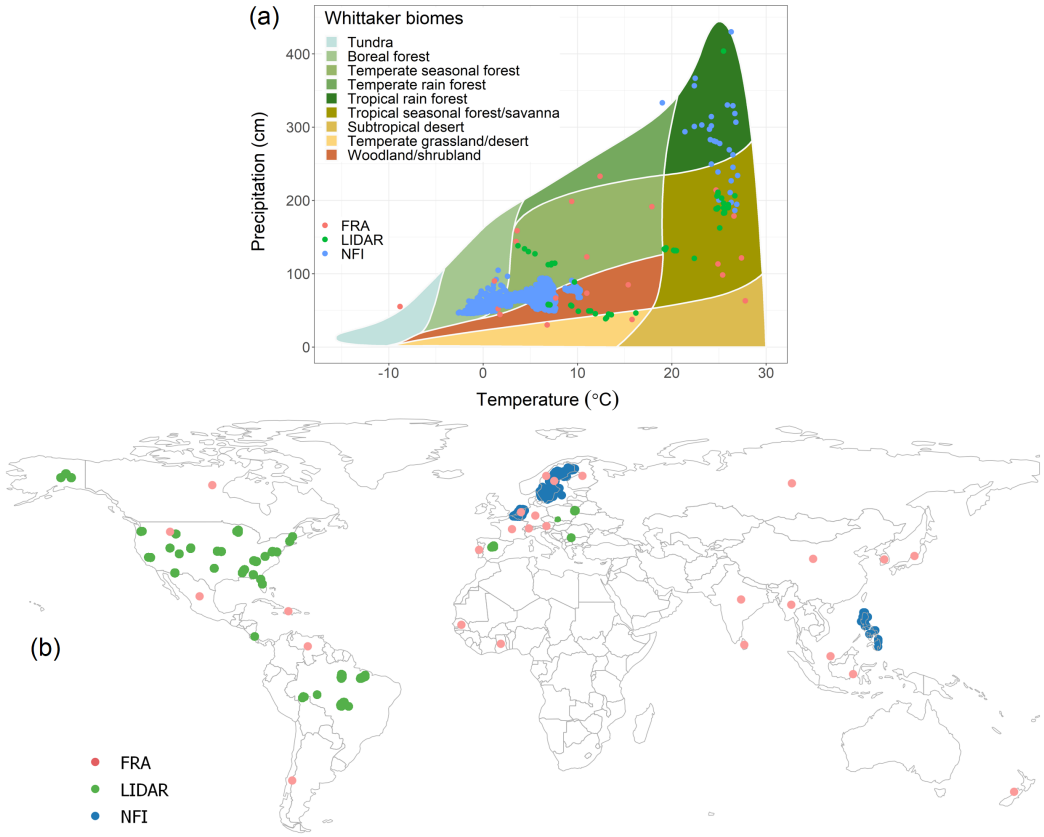

Figure 3.2: Coverage of the reference data per major ecological zone (a) and the map of the selected reference data (b). The reference data are already quality-filtered, see Section 3.2.3.

shown in Figure 3.3. The highest density of data is observed for small ΔAGB but there are also several reference data implying large AGB gains and losses. Owing to spatial averaging, the density of data increases towards small ΔAGB from fine to coarse aggregation levels, especially for NFI data. The NFI captured larger AGB gains (until 1 km), while LiDAR captured more AGB losses throughout all aggregation levels. These results suggest LIDAR data showed consistent ΔAGB distributions across the aggregation levels. These observations are influenced by the forest types where the reference data are located, i.e., forest plantations for NFIs and disturbed forests for LiDAR (Table S1).

3.3.2 ΔAGB comparisons at different aggregation levels.

Figure 3.4 compares the ΔAGB derived from the CCI and Flux maps with respect to the corresponding NFI and LiDAR values for all aggregation levels (left to right). While the averaging resulted in a decrease in scattering especially in small ΔAGB (i.e., RMSD), the mean difference (MD) is still prominent particularly for AGB loss regardless of the spatial scale. The LiDAR comparisons sustain a level of agreement with the two maps throughout all spatial scales, while some level of agreement is evident only until the 1 km comparison for NFIs. Often, the number of NFI plots inside coarse grid cells is limited e.g., 5-6 plots

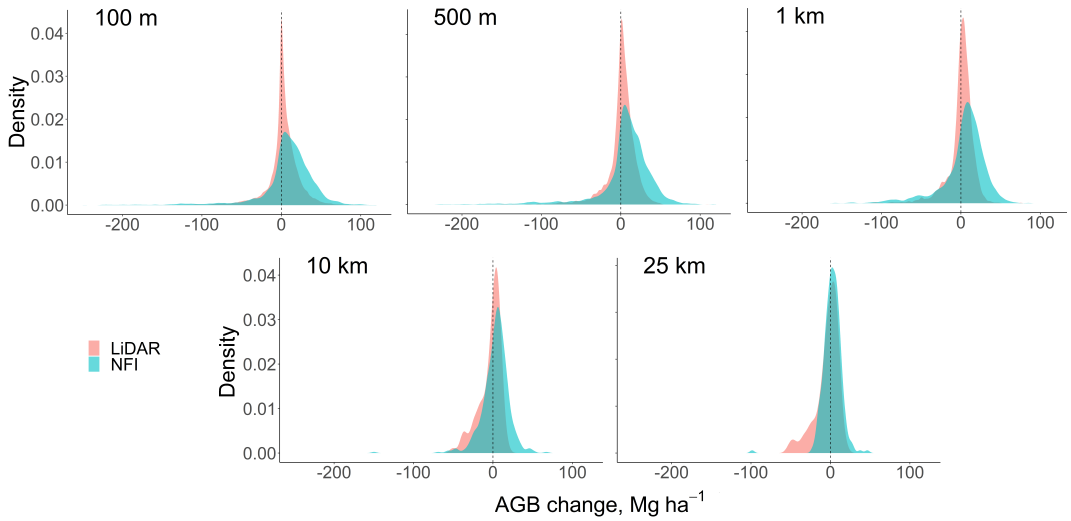

Figure 3.3: ΔAGB distributions from NFI and LiDAR data for the five aggregation levels.

per 10 km cell (Figure S2). The effect of spatial averaging is further observed in the coloured matrices of MD and RMSD per ΔAGB bin in Figure 3.5. Another observation in Figure 3.4 particularly for the 100-500 m comparisons is the different distribution of ΔAGB between CCI and Flux ΔAGB bins with no to minimal changes based on reference data.

Figure 3.6 shows the ΔAGB comparisons for all map products against reference data aggregated to a common spatial resolution of 25 km. At such a coarse level, map estimates show some level of agreement with LiDAR data. For all maps, agreement is substantially reduced when using NFI data as the reference. The comparisons with the FRA show that countries with re-measured NFI (mostly reporting gains) agree differently with the maps. These variations among maps will be the focus in the spatial analysis results.

3.3.3 ΔAGB spatial analysis and map-map comparisons

Figure 3.7(a) shows the inter-comparison of ΔAGB maps. The magnitude and ranges of ΔAGB vary among the maps. The CCI and Flux maps display the largest AGB changes in time as indicated by higher colour contrast in the map and higher fluctuations in their latitudinal profile graphs (Figure S3). Examples are depicted in the CCI results for regions such as east US, south Amazon basin and Madagascar (-18°), and South American countries along -42°; and for high gains in the temperate region for the Flux results. These are regions where the CCI and Flux disagree. Except for LVOD AGB loss, the changes are not very evident in the two time series products (JPL and LVOD). The maps in Figure 3.7(a) mostly agree in regions where net AGB loss is prominent such as southwest Amazon, Siberian boreal forests, west and central Africa and Indonesia. Consensus about net forest gains is evident in China, western Canada, African savannahs and in a few patches within Europe and Amazon basin; but disagreement is evident in central Amazonia. Separate

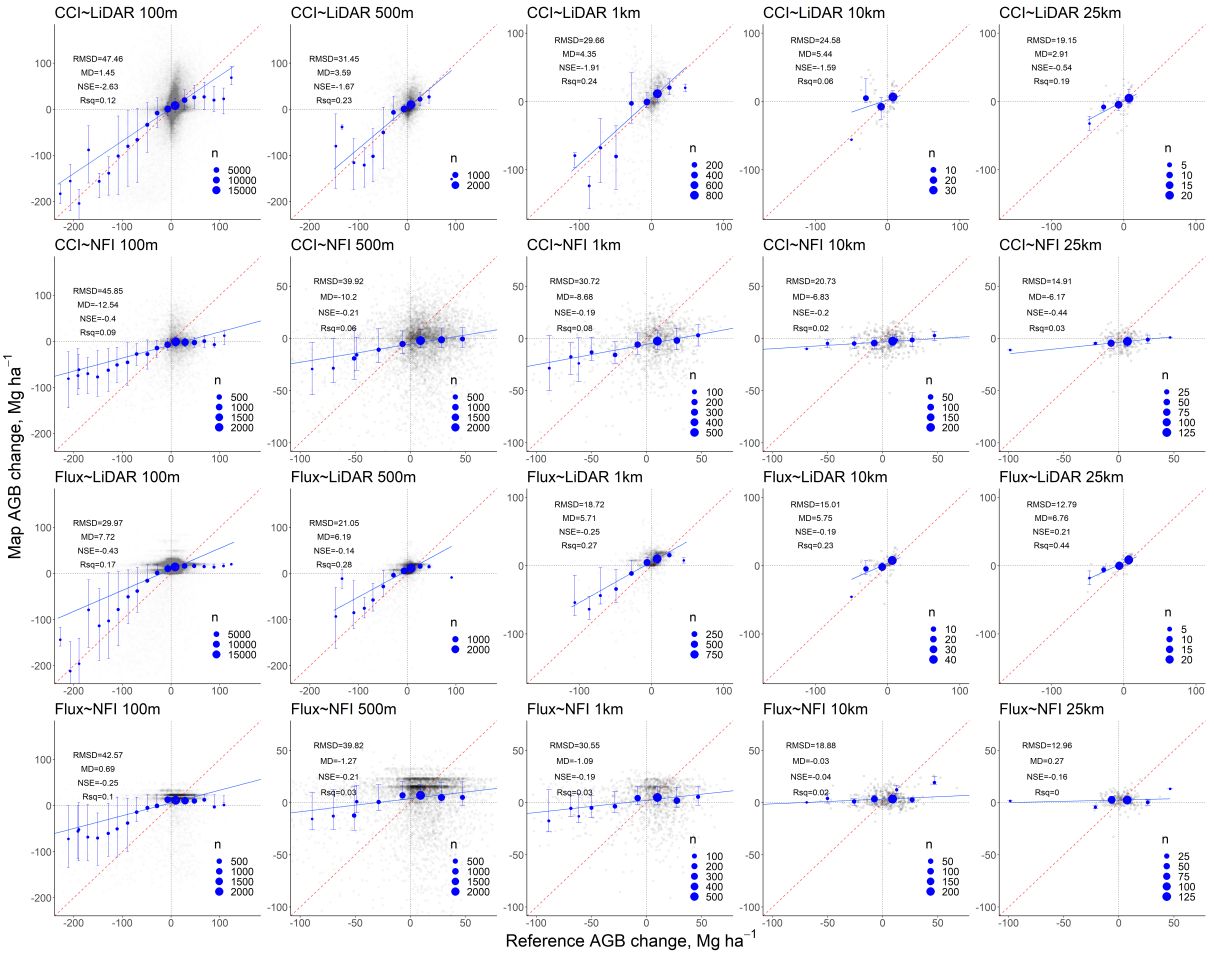

Figure 3.4: ΔAGB comparisons between the originally 100 m map products (CCI and Flux), and the LiDAR and NFI reference data. The binning symbol size (circles) depends on the number of data, with whiskers indicating the 25th and 75th quartile of the ΔAGB map. The bins for the 25 km results are lesser than in Figure 3.6. Be aware also of the different axes for NFI and LiDAR assessment i.e., narrower axis > 1km onwards to increase the visibility of comparisons. Coefficients R^2 and NSE are also shown.

maps of these hotspot regions are shown in Figure S4. Map disagreements are further emphasized in Figure S5 where correlation coefficients (r) among maps range from 0.11 to 0.29. The majority of the pixels are classified as "no change" as shown in Figure 3.7(b). They constitute 66% of total while the other classes constitute: disagree = 21%, gain = 8% and loss = 5%.

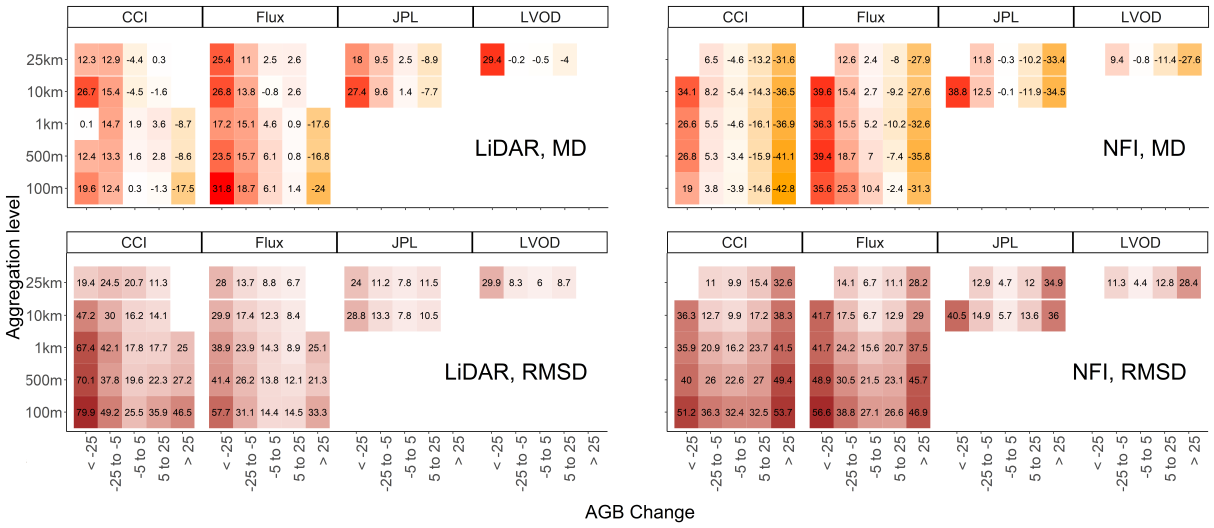

Figure 3.5: Matrices of MD and RMSD derived from the comparisons at different aggregation levels and ΔAGB bins using NFI and LiDAR data as reference. The colour gradient from light to dark depicts low to high values. For the MD matrix, red gradient refers to AGB loss underestimation while yellow gradient depicts AGB gain underestimation.

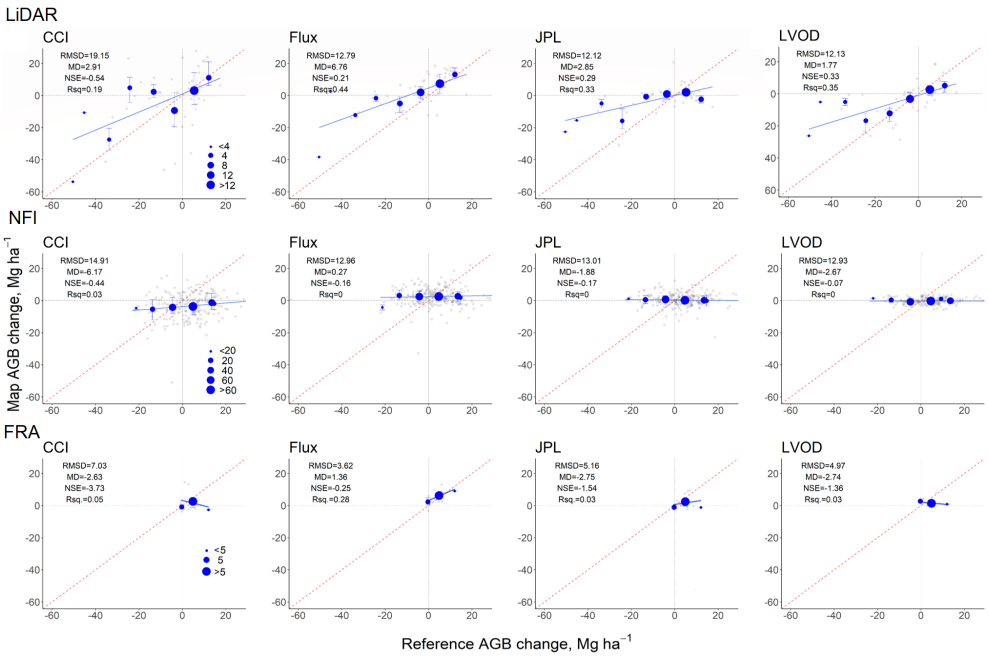

Figure 3.6: Comparisons of 25 km ΔAGB estimates between the map products and the three types of reference data. The binning symbol size (circles) depends on the number of data, with whiskers indicating the 25th and 75th quartile of the map-based ΔAGB. Also shown are the regression line (blue) and the 1:1 line (red). Coefficients R^2 and NSE are also shown.

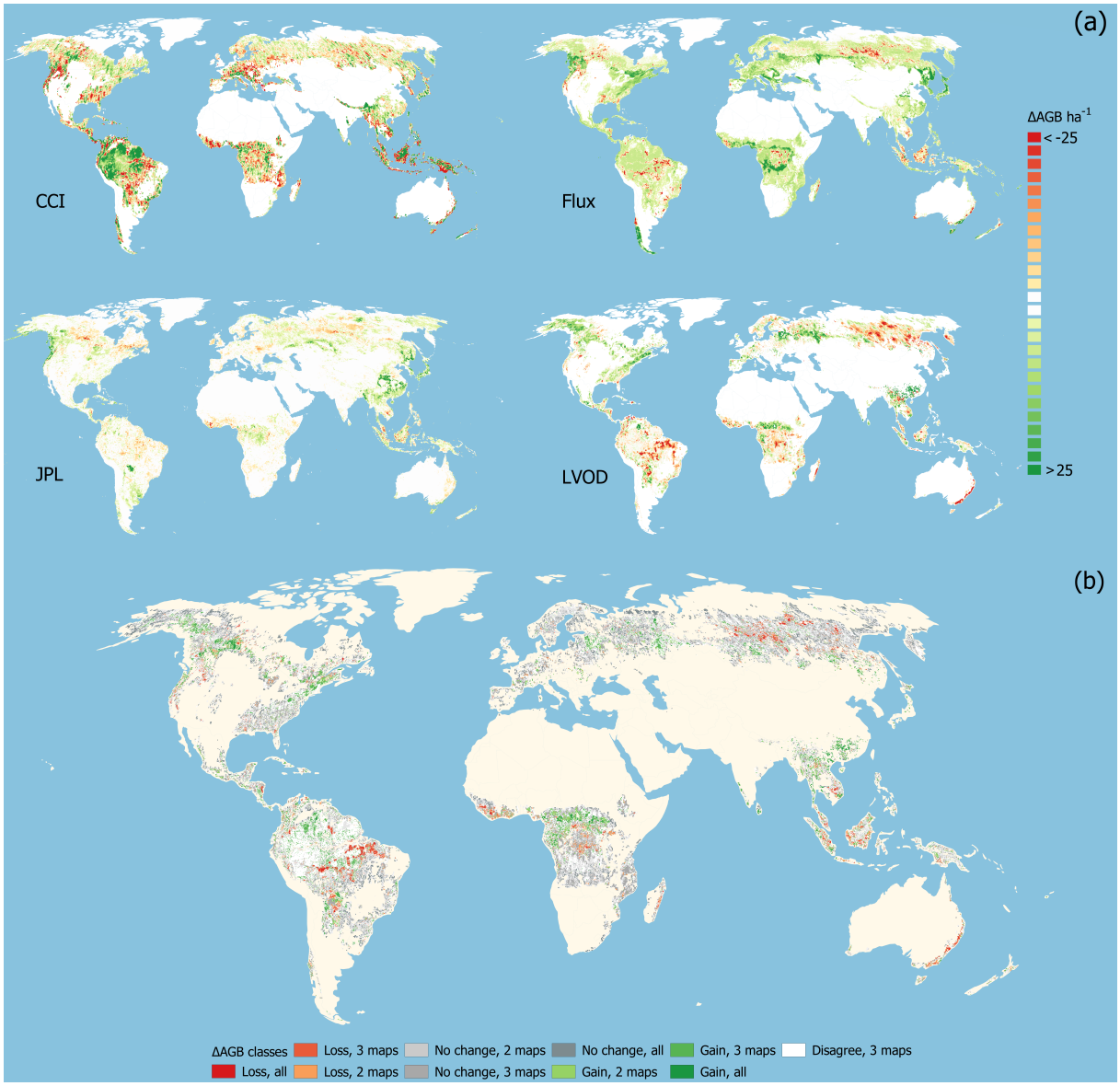

Figure 3.7: (a) Map-based ΔAGB at 25 km resolution; and (b) Overlap of ΔAGB among map products particularly the gain, loss and no change pixels i.e., the stronger the colour, the more agreement there is. The white pixels depict disagreement among 3 products. The rest are areas outside the forest boundary and the masked-out LVOD pixels.

3.4 Discussion

3.4.1 Reference data quality assessment

Current NFI and LiDAR reference data sources under-represent most ecological zones especially in the tropics. We used three European NFIs and one NFI in the tropics, as NFIs are commonly government data and requesting access is often a long process. Aside from crowd-sourcing platforms, online tools such as the *Plot2Map* tool by Araza et al. (2022b) can facilitate access to NFI data. Through the Multi-Mission Algorithm Platform (Albinet et al., 2019), the use of *Plot2Map* has been demonstrated in three countries already. Like for NFIs, the LiDAR reference data were currently limited to specific regions, but there has been an increasing interest and coverage of permanent forest plots with LiDAR campaigns worldwide (Chave et al., 2019a). We used NFIs mostly located in European forest plantations while LiDAR data mostly overlapped both disturbed and stable forests. The forest type where the reference data are situated also drives the distribution of ΔAGB observed in Figure 3.3. Future reference data should also represent different forest land uses.

As the availability of reference datasets increases, the criteria for selecting them for global map assessments can become stricter. While the size of plots may need to be large enough (i.e., >1 ha) to fully cover the pixels of map products (Réjou-Méchain et al., 2019), this will limit the reference data to permanent research plots which are always preferentially sampled. Here the effects of plot size are considered when we weighted our reference data according to plot size-driven uncertainty, and when we excluded grid cells with plots fewer than the minimum number of plots criterion. Stricter grid cell selection can be implied at coarse aggregation levels. The minimum number of plots per grid cell can be increased (Moreno et al., 2016) or grid cells with locally representative plots can only be selected (Araza et al., 2022a). Moreover, additional analysis on global data representativeness and sampling intensity could be initiated. Findings from these can support decisions on whether potential data are still necessary for certain regions (Figure 3.2) and identify regions that need more attention for data requests and measurement campaigns. In cases where NFIs and ΔAGB maps need integration for national ΔAGB estimates and rigorous map accuracy assessments, the NFI sampling design should be considered (Nesha et al., 2022). Further caution is needed because NFIs are not primarily designed for map comparisons and plots do not properly sample mapped ΔAGB especially at coarse aggregation levels. Moreover, NFIs can have different sub-plot configurations that cannot be tessellated over the entire mapped area. If only LiDAR is available for country ΔAGB estimation, one should also consider the effect of LiDAR data being preferentially sampled in particular forest types. Lastly, only reference data with estimated uncertainties are preferred for map assessments for uncertainty-weighted AGB averaging. Table S4 summarises the above discussions geared toward current and future reference data suitability.

ΔAGB comparisons at different aggregation levels

Comparisons of ΔAGB between the reference data and maps from 100 m to 25 km levels of aggregation revealed a decrease of scattering in the ΔAGB comparisons (i.e., smaller RMSD), and the persistent underestimation of AGB losses, owing mostly to map systematic differences (MD), see Figure 3.5. Hence, the MD problem exists regardless of the map product and spatial resolution. It is expected for AGB maps to overestimate smaller AGB and underestimate greater AGB (Réjou-Méchain et al., 2019; Araza et al., 2022a) and this MD is carried over into ΔAGB, especially for deforestation and plantation clear-cutting events, e.g., a map-based ΔAGB from 350 to 5 Mg ha^{-1} where reference data ΔAGB shows 450 to 0 Mg ha^{-1}. Similarly, gains spanning 9 years were also expected to be underestimated because of this systematic error.

The comparisons from fine to coarse levels were influenced by the reference data (Figure 3.4). The comparisons using NFI and LiDAR at aggregation levels up to 1 km showed moderate agreement with maps and were able to assess large changes i.e., deforestation, clear-cuts and regrowth (Figure 3.3). These kinds of ΔAGB at fine resolutions are more important when map users require ΔAGB maps such as for carbon MRV reporting and ecosystem accounting. Beyond 1 km comparisons where the ΔAGB between NFIs and maps disagreed, the NFI plots we used likely missed to represent local heterogeneous areas with different forest types and forest management activities in Europe (Figure S2). This result is consistent with Herold et al. (2022) where the ΔAGB of NFIs and CCI map were similar when using at least 25 European NFI plots in comparisons aggregated to 12 km. Also using all European NFIs, Moreno et al. (2016) reported that increasing the aggregation level from 1 to 5-25 km is optimal because of increased plot representation over grid cells. The country-level ΔAGB comparisons using FRA as reference depicted varying results among maps (Figure 3.6). This variation can be attributed to the different forest definitions and AGB estimation methods of countries. Metadata of the FRA dataset is needed as basis to harmonize the map-based estimates and make them more comparable with the FRA. Nevertheless, country-level variations also reflect that there is disagreement of ΔAGB among maps.

Spatial analysis and map-map differences

The purpose of inter-comparing the ΔAGB maps was to assess where maps indicate the same changes. Agreement among maps was gauged by the sign and magnitude of reported ΔAGB, and the ΔAGB cross-correlation results ranged between 0.11 and 0.29 r (Figure S5). The map products were produced by different remote sensing data types and AGB retrieval methodologies (Section 3.2.2). The CCI ΔAGB is obtained by subtracting the 2018 and 2010 maps i.e., stock change approach. AGB maps are indirect estimates from remote sensing signals and changes in signals are not always equivalent to ΔAGB. Past and current spaceborne radar datasets used for CCI lack sufficient sensitivity to

measure gradual changes associated with regrowth and degradation especially in dense forests (Santoro & Cartus, 2019). For the Flux model, a gain-loss approach, the IPCC 2019 growth rates were one of the bases for years beyond >2012. Such rates can be very uncertain in Europe (Harris et al., 2021). Interestingly, the CCI and Flux yielded contrasting ΔAGB in certain regions (Figure 3.7) despite using the same CCI 2010 map as a baseline. This regional variation illustrates the different results obtained by stock change and gain-loss approaches. The latter can be strongly influenced by the localized activity data i.e., land uses (McRoberts et al., 2020). Compared to the CCI and Flux, the JPL and LVOD time series products reported smaller ΔAGB magnitude especially for AGB gains. Lastly, the ΔAGB differences among the maps may also be affected by the different remote sensing data and mapping methods employed by map producers and the slight variations in the map epochs (Table S2).

The overlap of ΔAGB maps in Figure 3.7 showed that current maps mostly capture AGB losses in known deforestation hotspot regions (Feng et al., 2022). It is known that the satellite signal before and after deforestation is less prone to noise than signals concerning gradual changes like regrowth or degradation (Ryan et al., 2011). Moreover, both JPL and Flux used the same tree cover loss product (Hansen et al., 2013b), while the LVOD used the CCI precursor, the GlobBiomass (Santoro et al., 2021), for AGB calibration. All maps reported sinks of carbon in parts of Europe, China, Canada and African savannah, which coincides with several global and regional studies that used remote sensing and in-situ data (Bastin et al., 2017; Tubiello et al., 2021). In contrast, map disagreement was evident in the central Amazon basin - being the largest and most complex carbon pool region. Previous work of Phillips et al. (2017) reported contrasting views on whether the basin is a source or sink. Most ΔAGB pixels were within the interval between -7 and 7 Mg ha^{-1}, which were classified as "no change". These pixels occur mostly in intact and non-forest areas that sequester little to no carbon (Lesiv et al., 2022).

Application of the work and outlook

This work provides a confluence of evidence from ΔAGB map-reference data and map-map comparisons, which is a source of information for both map producers and users. Map producers can revisit their AGB retrieval process in areas where most maps disagree. We anticipate improvements of the current ΔAGB maps. Future releases of the CCI maps will make use of repeated observations instead of a single observation in the form of an image mosaic. In addition, the AGB retrieval will be supported by a much denser dataset of spaceborne LiDAR observations. The Flux model will implement improved activity data and removal factors. In terms of map users, global carbon and climate modellers mainly use global ΔAGB maps (Herold et al., 2019; Quegan et al., 2019). An unpublished survey among these users revealed that most modellers prefer >1 km maps from multiple periods (Peylin et al., 2019). At such levels, the ΔAGB is more pronounced compared to 100 m level. Moreover, the >1 km map-reference data comparisons showed that LiDAR data can

be a reliable source of reference data. More airborne LiDAR campaigns are expected in the coming years, spearheaded by initiatives such as Supersites and GEO-Trees. LiDAR data from two periods were found useful to validate even annual AGB dynamics in stable forests (Nguyen et al., 2020). For national applications, we showed that both NFIs and LiDAR have a certain level of agreement with maps and capture large changes until 1 km, which is useful if users aim to assess specific ΔAGB drivers, e.g., deforestation or reforestation-driven changes.

The variability in the 25 km map-reference data comparisons and the map-map comparisons reflect potential limitations of the current global ΔAGB assessment. One approach to deal with map disagreements is to produce a new map from an ensemble of existing global AGB maps using model-based approaches (Zhang & Liang, 2020). However, doing so requires a suitable global reference dataset and does not guarantee producing accurate ΔAGB estimates. Worth exploring though is the direct mapping of ΔAGB using the global ΔAGB products and other remote sensing auxiliary data in countries with reference data. The resulting country ΔAGB map would benefit national applications that require ΔAGB map inputs e.g., for carbon MRV (Csillik et al., 2022), and ecosystem accounting (Hein et al., 2020b). Such mapping exercise should account for the uncertainty of sampling variability. This caution also applies for sub-national to national carbon accounting using rigorous estimation methods such as an NFI-based model-assisted ΔAGB estimation.

3.5 Conclusions

We compared ΔAGB derived from four recent multi-date global AGB maps with three reference datasets. The comparison was undertaken at spatial scales between 100 m and 25 km. We conclude the following:

1. The map-based estimates of ΔAGB agreed most with the LiDAR-based values regardless of the spatial scale. When compared to ΔAGB values derived from NFI data, the agreement was instead moderate below 1 km and poor for coarser spatial scales. The comparison with country averages reported in the FRA revealed different levels of agreement depending on the map. The assessments revealed systematic differences in mapped ΔAGB compared to the reference data, i.e., mapped AGB loss was smaller owing to the underestimation of AGB in baseline maps (2010).

2. Our investigation should be considered exploratory because of the current representation of our reference dataset for most eco-zones and continents. Nonetheless, it is foreseen that this limitation will be alleviated in the nearest future thanks to upcoming multiple airborne LiDAR data acquisitions in several regions of the world. Also, the use of NFI data can be enhanced if more countries decide to support online map assessment tools like *Plot2Map* and data crowd-sourcing platforms. Reference

data with uncertainty estimates and within areas where we lack representation in both geographic and feature space (e.g., eco-zones) are preferred for future global ΔAGB map assessments.

3. The maps all identified AGB losses in known deforestation hotspots, while also identifying regions that act as sinks. The remaining disagreement among maps (e.g., in the Amazon basin) reflects the different methodology applied such as stock differencing for CCI and gain-loss for Flux; while the two time series products had smaller ΔAGB magnitudes. To assure comparable ΔAGB among maps and with reference data, preliminary steps were necessary including a new carbon flux model (Flux) and applying a standard forest mask.

The map disagreements and biases need to be understood and addressed to increase the reliability of the maps for applications that require biomass change estimation and information.

Chapter 4

Spatial predictions and uncertainties of forest carbon fluxes for environmental-economic accounting

This chapter is based on:

Araza, A., De Bruin, S., Hein, L., & Herold, M. Spatial predictions and uncertainties of forest carbon fluxes for environmental-economic accounting. (Under review as of May 20, 2023).

Abstract

Countries have pledged to different national and international environmental agreements, most prominently the climate change mitigation targets of the Paris Agreement. Accounting for carbon stocks and flows (fluxes) is essential for countries that have recently adopted the United Nations System of Environmental-Economic Accounting – ecosystem accounting framework (UNSEEA) as a global statistical standard. In this paper, we analyze how spatial carbon fluxes can be used in support of the UNSEEA carbon accounts in five case countries with available in-situ data. Using global multi-date biomass map products and other remotely sensed data, we mapped the 2010-2018 carbon fluxes in Brazil, the Netherlands, the Philippines, Sweden and the USA using National Forest Inventory (NFI) and local biomass maps from airborne LiDAR as reference data. We identified areas that are unsupported by the reference data within environmental feature space (6-47% of vegetated country area); cross-validated an ensemble machine learning (RMSE=9-39 C Mg ha^{-1} and R^2=0.16-0.71) used to map carbon fluxes with prediction intervals; and assessed spatially correlated residuals (<5 km) before aggregating carbon fluxes from 1-ha pixels to UNSEEA forest classes. The resulting carbon accounting tables revealed that natural forests (broadleaved, coniferous, mixed forest and mangroves) mostly depict net carbon sequestrations while plantations and other woody vegetation show otherwise. The carbon fluxes were inter-compared with UN-Forest Resource Assessment and similar recent studies to find that our estimates were consistent with them except for Brazil. The Brazil case used a highly clustered sample prone to incorrect predictions via extrapolation even though the results of cross-validation are promising. We finally provide recommendations to mitigate the effect of under-sampling and to better account for the uncertainties once carbon stocks and flows need to be aggregated in relatively smaller countries. These actions are timely given the global initiatives that aim to upscale UNSEEA carbon accounting.

Introduction

Under the increasing threat of climate change, countries have reaffirmed the Paris Agreement commitments at the 2021 COP26 and the 2022 COP27 toward reducing CO_2 emissions and increasing CO_2 removals through forest protection and tree planting (Nabuurs et al., 2022). The "biocarbon" or the combined above-ground, below-ground and soil carbon of forests have contributed 23-30% of the total anthropogenic Greenhouse Gas (GHG) emissions worldwide (Goetz et al., 2009; Nabuurs et al., 2022). To track country commitments, regular accounting of biocarbon (herein called carbon) serves as a primary source of information. Countries report their GHG inventories according to the United Nations Framework Convention on Climate Change (UNFCCC). Countries are also encouraged to develop carbon accounts under the UN System of Environmental-Economic Accounting - ecosystem accounting framework (UNSEEA), which is now an international statistical standard (UN, 2021). The UNFCCC and UNSEEA carbon accounting follow complementary measurement methods of forest carbon stocks and flows. Their quantification of flows involves both carbon emissions (stock reduction) and sequestration (stock addition). The two systems differ in the way UNSEEA accounts for all stocks and flows of carbon(UN, 2021), whereas UNFCCC focuses on reporting human-influenced emissions. Furthermore, UNSEEA is a spatially explicit system that analyze ecosystems, where national or subnational maps of ecosystem type, condition and ecosystem services are compiled. The UNSEEA carbon stocks and flows are commonly aggregated and reported by ecosystem type under the UN Land Cover Classification System (UN, 2021).

Forest carbon accounting benefits from remotely sensed data (Buendia et al., 2019; UN, 2021). Remote sensing data are integrated with country in-situ data such as national forest inventories (NFI) for mapping carbon stocks (Rodríguez-Veiga et al., 2016; Araza et al., 2021a). The flows of carbon can also be estimated depending on whether countries repeatedly acquire in-situ data in repeated NFIs and even from airborne LiDAR surveys. For such countries, flows can be obtained either by direct mapping of carbon fluxes or by indirect mapping where separate maps of opening and closing stocks are subtracted. Most past studies favoured direct mapping to avoid propagation of mapping errors from two models (Esteban et al., 2020). Direct mapping often uses machine learning predictive models that relate in-situ biomass change to auxiliary remote sensing variables. In the absence of repeated in-situ data, countries can rely on forest change maps and associated land use and land cover (LULC) changes, and this case is more common especially in developing countries (McRoberts et al., 2020; Nesha et al., 2022). There are around 24 countries that have relied on remote sensing data to generate their carbon stocks and flows in compliance with the UNSEEA framework (Hein et al., 2020a). All of them used alternative methods of flow estimation such as using periodic LULC maps (Hein et al., 2020b) and proxy indicators of flows like maps of Net Primary Productivity (Vargas et al., 2018).

The availability of global remote sensing datasets useful for carbon accounting are increasing. For instance, the World Resource Institute (WRI) mapped 2000-2019 carbon fluxes globally at 30 m based on Landsat (Harris et al., 2021). Other sources of global carbon fluxes include the 100 m multi-date biomass maps (2010, 2017 and 2018) from European Space Agency Climate Change Initiative (CCI) mainly based on ALOS-PALSAR (Santoro & Cartus, 2019) and the 10 km 2000-2020 JPL time series biomass maps based on MODIS (Xu et al., 2021). There exist a 100 m multi-date carbon maps that combined ALOS-PALSAR, Landsat and MODIS data but these maps are limited to the United States (Yu et al., 2022).

Carbon accounting based on remote sensing products is affected by large uncertainty in the input data used (Houghton et al., 2012; Yanai et al., 2020). The main input of carbon accounts is the carbon flux map, which tends to underestimate carbon losses owing to remote sensing signal saturation in dense forests (Araza et al., 2023). Additionally, remote sensing signals from gradual carbon changes such as forest degradation and regrowth are most vulnerable to signal noise (Ryan et al., 2011). Moreover, carbon flux maps that are derived using in-situ data can be inaccurate depending on how biomass is estimated and how plots are sampled. For instance, a clustered sample may result in preferential sampling of the spatial variability both in geographic and feature space - the latter refers to a set of environmental regions defined by the remote sensing data in relation to carbon flux. A clustered sample leads to overly optimistic accuracy estimates assessed by cross-validation (de Bruin et al., 2022). Several studies analyzed the representativeness of samples in environmental feature space (Labrière et al., 2022). Such analysis can support decisions on whether to integrate additional samples to minimize the sampling uncertainty (Shettles et al., 2015) or constrain the mapping in areas where predictions are supported by the sample resulting in an incomplete map (Meyer & Pebesma, 2021).

The UNSEEA carbon accounting requires map inputs with a high spatial resolution to account for all kinds of fluxes (flows) even those from small land cover changes (Hein et al., 2020a; Keith et al., 2019). Furthermore, high-resolution maps are required for evaluating policies and implementations that concern carbon retention in ecosystems. The need for high-resolution maps favours the use of global carbon flux datasets from WRI (30 m) and ESA (100 m). While it is practical to use either one or create an ensemble of their carbon fluxes, they showed low to moderate agreement against in-situ data in terms of biomass change (Araza et al., 2023). Map-based carbon fluxes are derived using either of two different methods. Subtracting the 2018 and 2010 CCI maps results in a stock difference, while the WRI follows a gain-loss method that incorporates spatial carbon emissions and removals based on activity data. Aside from the global biomass maps, other remote sensing data like height, tree cover and vegetation indices may also be related to biomass change i.e., as covariates.

The main objective of this paper is to analyze how spatial carbon fluxes can be used

in support of the UNSEEA carbon accounting of the above-ground carbon pool in five case countries with available in-situ data. Particularly, we use global biomass and other environmental data as covariates together with in-situ data from NFI and local AGB maps from airborne LiDAR as reference for an ensemble machine learning framework. First, we directly map 2010 to 2018 net biomass change and hence derive the carbon flux. The carbon flux map units (pixels) need to be aggregated for every forest type recommended by UNSEEA. Here we also report the uncertainties associated with the spatial aggregation step (e.g., of stocks and flow residuals) as this component is outside the framework of machine learning models (Heuvelink & Webster, 2022). Lastly, we include non-forest woody vegetation in the carbon accounting. Our specific objectives are:

1. Assess to what extent spatial predictions of carbon fluxes are supported by the country data.
2. Conduct ensemble machine learning to map carbon fluxes at national scale using global biomass and other remotely sensed data as covariates.
3. Use the resulting carbon flux map to develop UNSEEA carbon accounts with reported uncertainties, identified limitations and a list of recommendations toward upscaling to other countries.

Methods

Overview

The methodology overview is shown in Figure 4.1, where the main steps include: (1) mapping the carbon flux using a cross-validated ensemble machine learning with remote sensing data as covariates and in-situ data (NFI or LiDAR) as reference and (2) compilation of the carbon accounts including the aggregation of the carbon flux map to each UNSEEA class. The carbon accounts represent an opening stock in 2010 derived from the CCI map 2010 and a closing stock in 2018 as the difference between the opening stock and the carbon fluxes. The overall methodology also includes intermediate steps such as estimating reference data uncertainties, investigating multi-collinearity among covariates, hyperparameter tuning of spatial models and variogram analysis. An independent step is the feature space analysis to identify areas that are not supported by the country data relative to the set of covariates used for carbon flux mapping.

Study area and reference data

The national ecosystem carbon accounting is demonstrated using five country cases: Brazil (BRA), the Netherlands (NLD), the Philippines (PHL), Sweden (SWE) and the United States of America (USA). The selection of countries was mainly based on reference data availability and representation of major climatic zones. See Figure 2 for maps of the study and the reference data sampling locations. The Netherlands and Sweden data are

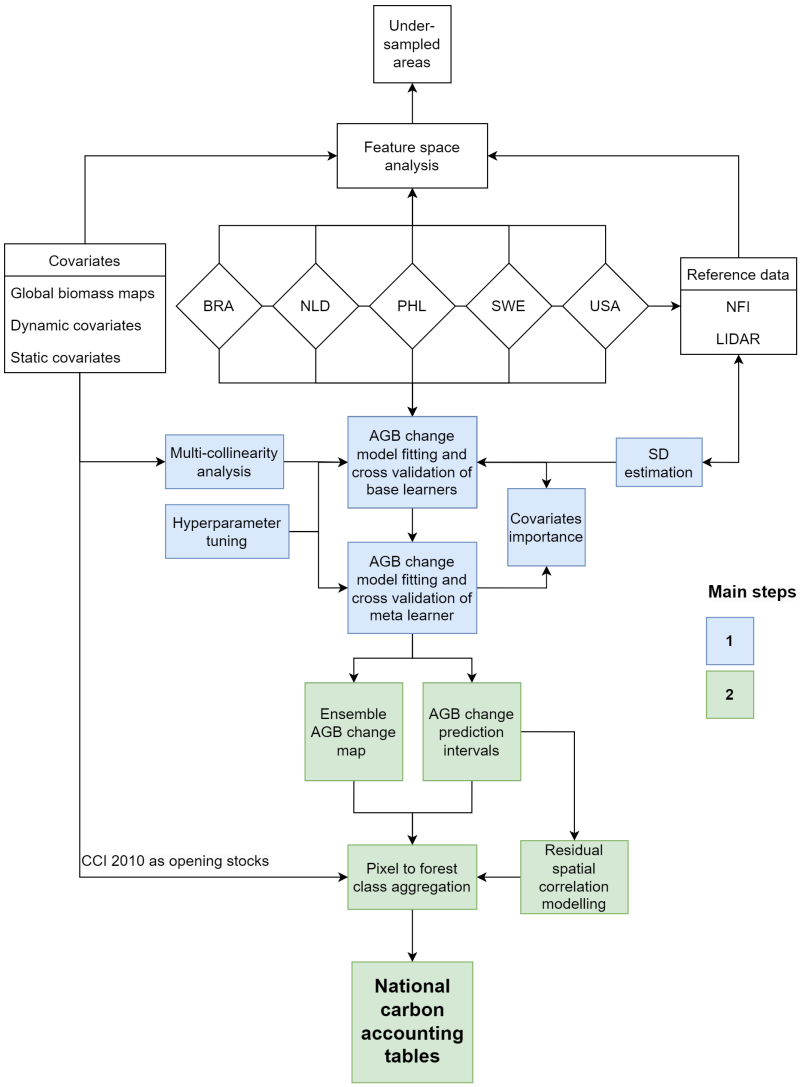

Figure 4.1: Flowchart of the steps undertaken to derive the carbon accounting tables as the final output.

NFIs, accessed from the European NFI database (Schelhaas et al., 2018). The Philippines data is also from an NFI and was accessed directly from the Philippine environmental office. The others are high-quality local biomass maps from airborne LiDAR campaigns in Brazil (Longo et al., 2016) and the USA (Johnson et al., 2010). The NFI data were acquired by probability sampling: Sweden and Philippines NFIs use systematic samples while the Netherlands NFI applies stratified random sampling. The USA LiDAR data also follows a systematic sample but not all sites have repeated LiDAR surveys (Johnson et al., 2010) while the Brazil LiDAR datasets are mostly sampled in secondary forests. These datasets underwent quality filtering as elaborated in our recent study (Araza et al., 2023). The number of observations are as follows: BRA=28,607, NLD=1,562, PHL=587, SWE=12,887 and USA=110,939. The LiDAR reference data have associated uncertainty layers while the NFI plot measurement uncertainties were estimated using error propa-

gation method as described in our previous work (Araza et al., 2022a). We particularly estimated the largest plot uncertainty contributor originating from tree measurement errors and the use of allometric models in estimating biomass. Finally, we converted the biomass change of all reference data to carbon flux (C Mg ha $^{-1}$) using a 0.49 multiplier. See Table S1 for the technical details of the reference datasets.

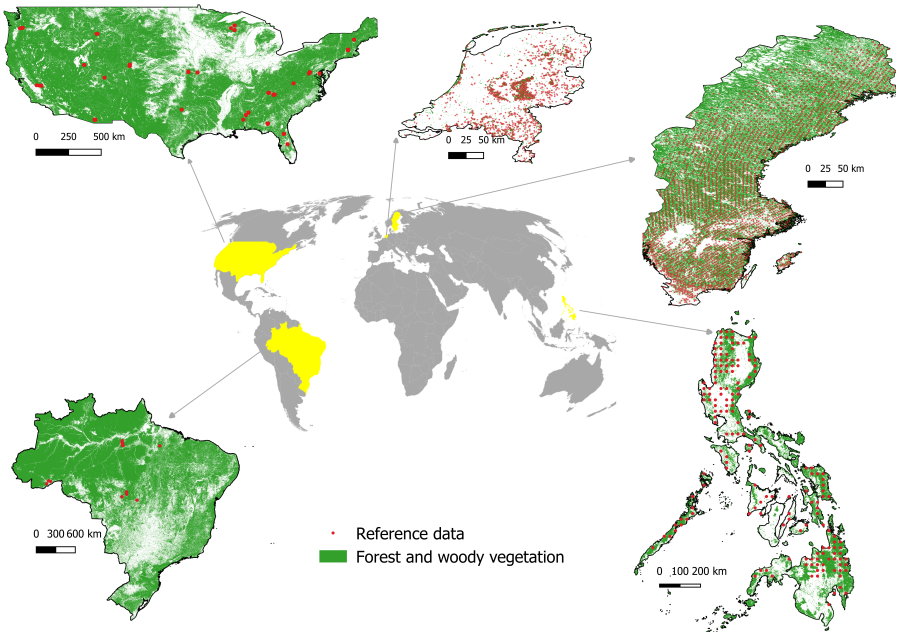

Figure 4.2: Country cases and the sampling of reference data within the forest and other woody vegetation described in Table 4.2 and Figure S1. Note that the size of each country map is relative. Note also that the USA and Brazil are LiDAR footprints where observations are BRA=28,607 and USA=110,939.

Spatial covariates

The list of spatially exhaustive covariates used and their description are shown in Table 4.1. The first set of covariates includes global biomass maps derived from the ESA and WRI sources herein called CCI maps and WRI Flux, respectively. The local variability of biomass changes from these high-resolution inputs was also considered. We computed their textural variables using Gray-Level Co-Occurrence Matrix (GLCM (Gebejes & Huertas, 2013)), particularly the mean, variance, homogeneity and contrast of biomass changes in a 300 x 300 m window. We also used a coarse time series biomass (JPL) (Xu et al., 2021) and a periodic biomass dataset (CONUS, USA only) (Yu et al., 2022). All biomass maps are produced without the use of our reference data. The next set of covariates were forest height and forest cover dynamics using height data from spaceborne LiDAR (Potapov et al., 2021) and tree cover data from optical satellites (Defourny et al., 2012; Sexton et al., 2013), respectively. Datasets that represent forest management (Grantham et al., 2021; Lesiv et al., 2022) and land cover changes (Defourny et al., 2012) were also

included. For European countries, we included gap-filled quarterly composites of Normalized Vegetation Difference Index (NDVI) (Witjes et al., 2022), being readily available and cloud-free i.e., never been reproduced for large and tropical countries. The remaining covariates were static variables such as forest type, elevation, slope and biomes. In total, we started with 28 covariates for European countries, 25 for the USA and 24 for Brazil and the Philippines - all from open-access data. We finally constrained all covariates within the recommended classes by UNSEEA as described in Table 4.2 and Figure S1.

All covariates were cross-correlated to assess multicollinearity among them as a precaution to avoid model overfitting and misinterpretation of the covariates model importance (see Figure S2). We randomly sampled 5000 pixels for each country for the cross-correlation. We found only a few covariate pairs that exhibit a strong correlation, particularly pairs that include global biomass maps and an associated textural property (*texMean* and *texVar*). We excluded the latter since they also highly correlate with other map textural properties.

Table 4.1: Spatial data used as covariates and their technical details. Note that the "Epochs used" column also denotes whether a covariate is dynamic or static.

Spatial data	Category	Covariates name and definition	Units	Country used	Pixel size	Epochs used	RS and in situ data	Reference
CCI	CCI	agb10_cci = CCI AGB 2010	Mg ha $^{-1}$	All	100 m	2010-2018	ALOS2-PALSAR2, Sentinel 1	Santoro & Cartus (2019)
		agb18_cci = CCI AGB 2018	Mg ha $^{-1}$					
		diff_cci = CCI biomass change	Mg ha $^{-1}$					
		texContrast_cci = Textural contrast of diff_cci	relative					
		texHomo_cci = Textural homogeneity of diff_cci	relative					
		texMean_cci = Textural mean of diff_cci	relative					
		texVar_cci = Textural variance of diff_cci	relative					
WRI	Flux	diff_flux = WRI Flux biomass change	Mg ha $^{-1}$	All	100 m	2010-2019	CCI 2010, Global Forest Change (GFC) and IPCC activity data	Harris et al. (2021)
		texContrast_flux = Textural contrast of diff_flux	relative					
		texHomo_flux = Textural homogeneity of diff_flux	relative					
		texMean_flux = Textural mean of diff_flux	relative					
		texVar_flux = Textural variance of diff_flux	relative					
JPL	AGB	diff_jpl = JPL biomass change	Mg ha $^{-1}$	All	10 km	2010-2019	MODIS, ICESat, ALOS-PALSAR	Xu et al. (2021)
CONUS	CONUS	diff_conus = CONUS biomass change	Mg ha $^{-1}$	All	100 m	2010-2017	ALOS2-PALSAR2, MODIS	Yu et al. (2022)
Forest height loss	Environmental (envi)	height_envi = forest height loss	meters	All	30 m	2010-2020	ICESat, GEDI	Potapov et al. (2021)
Forest dynamics	Environmental	forType_envi = forest dynamics	categorical	All	30 m	2010-2020	ICESat, GEDI	
VCF dynamics	Environmental	tc_envi = tree cover change						
NDVI quarterly composites	Environmental	ndviQ1_envi = 1st quarter NDVI change composites	-1 to 1	SWE, NLD	30 m	2010-2019	Landsat archive	Witjes et al. (2022)
		ndviQ2_envi = 2nd quarter NDVI change composites	-1 to 1					
		ndviQ3_envi = 3rd quarter NDVI change composites	-1 to 1					
		ndviQ4_envi = 4th quarter NDVI change composites	-1 to 1					
Land cover change	Land Cover (LC)	lcov10 = CCI Land Cover 2010	categorical	All	300 m	2010-2019	MERIS	Defourny et al. (2012)
		lcov18 = CCI Land Cover 2018	categorical					
		lcovDiff = Land cover change	categorical					
Forest Management	Forest management (mgmt)	mgmt_mgmt = 2015 forest management	categorical	All	100 m	2015	PROBA-V	Lesiv et al. (2022)
Forest Landscape Integrity Index	Forest management	flii_mgmt = Relative forest integrity index	0-100	All	300 m	2019	GFC data; Curtis et al., data	Grantham et al. (2021)
Elevation	Topography (topo)	elev_topo = Elevation	meters	All	30 m	2000	SRTM	Jarvis et al. (2008)
Slope	Topo	slope_topo = Slope	degrees	All	30 m	2000	SRTM	
Biome	Climate	bio_climate = major climatic zones	categorical	All	10 km	2017	Protected area network	Dinerstein et al. (2017)

Feature space representation of reference data

This step is needed to assess how the reference data represent the spatial variability of feature space, which is becoming a prerequisite for spatial prediction models. This analysis identifies potentially under-sampled areas or those areas that exhibit high dissimilarity based on distances from the reference data in the multidimensional feature space (Meyer & Pebesma, 2021). The latter is spanned by the covariates listed in Table 4.1 that are used in a spatially cross-validated model to calculate dissimilarity. The non-covered areas are prone to extrapolation of the machine learning models where less credible spatial predictions are expected. Awareness of the extent of these non-covered areas is crucial not only for our carbon accounting demonstration but also as decision-support towards improving the current accounts i.e., the need for additional samples and forest masking. Here we identified under-sampled areas countrywide and for each UNSEEA carbon accounting class in Table 4.2 and Figure S1.

Prediction models of carbon fluxes

An ensemble model of three machine learning models was developed under a model generalization framework (Wolpert, 1992). The main idea of the framework is that a generic model (meta learner) fitted from predictions of individual models (base learners) has superior predictive performance than individual predictions. Models of random forest (RFM), extreme gradient boosting and support vector machine served as base learners where each model resulted in their own predictions of carbon flux. These predictions were then used as covariates to a meta learner (RFM). Any RFM implementation starts by bootstrapping the reference data and these resamples are used to create regression trees. Through bagging the data and sub-sampling the candidate covariates at each split, the trees are aimed to be mutually uncorrelated. The random forest algorithm averages predictions over all trees to produce a final prediction. To estimate the uncertainty of the carbon flux predicted by the RFM meta learner, we used quantile regression forest where decision trees are trained on different quantile levels of the carbon flux and derive an entire distribution of carbon flux predictions(Meinshausen & Ridgeway, 2006). We particularly used the 5^{th} and 95^{th} quantiles as prediction intervals. We employed case weights using inverse variance weighting to give preference to less uncertain reference data in the random forest bootstrapping procedure. The descriptions of other individual ML models are provided in the supplementary materials.

All base learners underwent model tuning whereas models that use unique combinations of hyperparameters were iterated (grid search). The optimal hyperparameters combination was determined if an objective function i.e., Root Mean Square Error (RMSE) is attained. See Table S2 for the chosen hyperparameters for each country case.

Model evaluation

A five-fold random cross-validation was applied using all reference data to evaluate model performance. Independent folds were used by the base learners and the meta learner to avoid overfitting the latter. Three metrics were used to evaluate the models: RMSE, which is the squared difference between population means of reference data $z(s_i)$ and predictions $\hat{z}(s_i)$; Mean Error (ME) or the mean difference between $z(s_i)$ and $\hat{z}(s_i)$; and coefficient of determination (R^2) as the goodness of fit measure.

$$RMSE = \sqrt{\frac{1}{n}\sum_{i=1}^{n}\left(z\left(s_i\right) - \hat{z}\left(s_i\right)\right)^2} \tag{4.1}$$

$$ME = \frac{1}{n}\sum_{i=1}^{n} z\left(s_i\right) - \hat{z}\left(s_i\right) \tag{4.2}$$

$$R^2 = 1 - \frac{\sum_{i=1}^{n}\left(z\left(s_i\right) - \hat{z}\left(s_i\right)\right)^2}{\sum_{i=1}^{n}\left(z\left(s_i\right) - \bar{z}\right)^2} \tag{4.3}$$

Influence of covariates on models

The importance values based on covariate data permutation were quantified for each base learner. The RMSE before and after the permutation is computed and the increase in RMSE indicates the covariate importance. This comparison was done for each fold of the cross-validation and then averaged among the folds. The final importance values we used were weighted averages based on the importance score of base learners to the meta learner. The resulting importance scores were first presented individually for each covariate per country. Second, the importance values were ranked and averaged with respect to their data categories (Table 4.1). The second set of results is helpful to highlight the influence of global biomass data in mapping carbon fluxes. All covariates importance values range from 0-100% .

Carbon accounting tables and their uncertainties

We first derived the carbon flux standard deviation SD_{flux} from the prediction interval, particularly the 95^{th} quantile (Q) and 5^{th} Q limits for a 90% prediction interval:

$$\text{SD}_{\text{flux}} = \frac{95^{th}Q - 5^{th}Q}{2} * 1.64 \tag{4.4}$$

Then, the 100 m carbon flux maps needed aggregation for every UNSEEA class in Table 4.2. Aside from the carbon flux, the associated uncertainties also need to be aggregated while taking into account the covariance of map errors. Moreover, the variance of map

errors may vary over space i.e., owing to heteroscedasticity. Hence, we modelled the spatial correlation of the carbon flux map standardized residuals at reference data locations using variograms. We also did the same procedure for the opening stocks interchanging SD_{flux} with the SD layer of CCI 2010 SD_{open}. The full details of this step including the standardization of carbon flux residuals are shown in the supplementary materials.

Denoting SD_{open} and SD_{flux} as σ, we derived the covariances of the map error component $\sigma_{i,j}$ of pixel pairs i and j $(1 \ldots \text{n})$, equation 4.5. The covariances were aggregated for each UNSEEA class to derive the variance and hence the SD of each class SD_{fc} (equation 4.5). The resulting aggregated variance of the opening stock and fluxes were added to obtain the closing stock variance assuming error independence among the two random variables. We finally took the square root of the aggregated variances of the opening stocks, fluxes and closing stocks, and reported them in the carbon accounts.

$$\text{SD}_{\text{fc}} = \sqrt{\sum_{i=1}^{n}\sum_{j=1}^{n}\sigma_{i,j}} \tag{4.5}$$

The minimum requirement to define the UNSEEA carbon accounting classes are land cover inputs that distinguish broadleaved, coniferous, mixed and mangrove forests (Level 1 classes). Areas with dominant and partial woody grassland, shrublands and scrubs were included and aggregated into one UNSEEA class "Other woody vegetation", see Table S3 for the reclassification details. Multiple continental to global land cover data exist and we preferred the dataset with higher resolution and accuracy. A forest plantation dataset (Lesiv et al., 2022) was integrated into the land cover maps to distinguish between natural forests and plantations since the latter is required by UNSEEA. The land cover inputs were resampled to 100 m using nearest neighbor interpolation. Then, the land cover and carbon stocks and flows inputs were projected into an equal area projection to avoid geographic area distortion especially in places far from the equator. Table 4.2 shows further details about the carbon accounting data inputs.

We then derived the total country net carbon fluxes and inter-compared them with similar estimates from other sources. We also reported the emissions and removals separately and further disaggregated the emissions as supplementary results. The latter involved using the associated 2018 land cover dataset to separate emissions driven by land-use changes (forest conversions).

Table 4.2: Details of the datasets used for the UNSEEA recommended carbon accounting classes. The forest plantation class was derived by integrating a plantation forest dataset (Lesiv et al., 2022)

Country	LC dataset	UNSEEA classes	Pixel size (m)
Brazil	CCI-LC	Broadleaved forest, Coniferous forest, Mixed forest, Mangroves, Other woody vegetation, Forest plantations	300
Netherlands	CORINE	Broadleaved forest, Coniferous forest, Mixed forest, Other woody vegetation, Forest plantations	100
Philippines	CCI-LC	Broadleaved forest, Coniferous forest, Mixed forest, Mangroves, Other woody vegetation, Forest plantations	300
Sweden	CORINE	Broadleaved forest, Coniferous forest, Mixed forest, Other woody vegetation, Forest plantations	100
USA	CCI-LC	Broadleaved forest, Coniferous forest, Mixed forest, Other woody vegetation, Forest plantations	300

Results

Under-sampled areas

Maps of under-sampled areas according to feature space coverage are shown in Figure 4.3. Notice the large extent of these areas are for Brazil and the USA. The majority of southeastern Brazil and western USA is not supported by the current sample. Per country, the relative spatial extent of non-covered areas is: NLD=6%, PHL=7%, SWE=14% BRA=32%, and USA=47% of the total vegetated areas of these countries. The breakdown of the non-covered areas for each UNSEEA carbon accounting class is shown in Figure S3. The classes with the highest proportion of under-sampled areas (>50% of total class area) are mostly found in Brazil and USA, particularly coniferous, mixed, other woody vegetation and mangroves (Brazil only) forests, see Figure S3. Among all countries, the class with the largest proportion of areas unsupported by the sample is other woody vegetation. This reflects the fact that the NFI and LiDAR reference data are mainly forest samples.

Cross-validation of spatial models

The model evaluation results using five-fold cross-validation for each country are shown in Table 4.3. Overall, the cross-validation range are: RMSE=9-39 C Mg ha^{-1}, ME=-0.3-0.2 C Mg ha^{-1} and R^2=0.16-0.71. The cross-validation results differ between countries. The Netherlands and the Philippines have different results than the other countries notable in the standard deviations of the three accuracy metrics. Brazil and USA show almost similar results for every validation fold and even show the best fit with reference data. These countries used spatially explicit LiDAR, but recall also that such samples are clustered (LiDAR footprints) and may produce conservative cross-validation results.

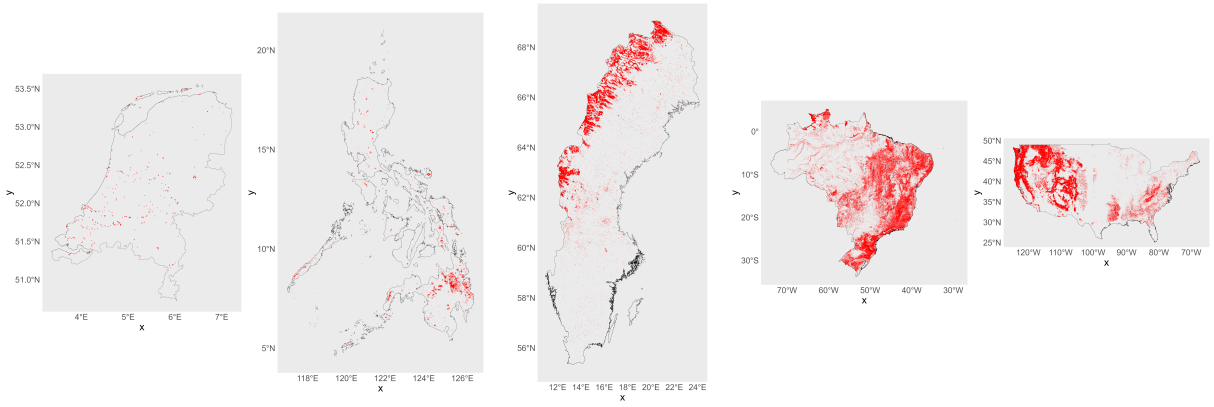

Figure 4.3: Maps showing how the current reference data represents environmental feature space.

Table 4.3: Accuracy metrics of the cross-validated spatial models of carbon fluxes and the standard deviation over the five-fold cross-validation

Country	RMSE C Mg ha^{-1}	ME C Mg ha^{-1}	R^2
Brazil	9.3 ±0.4	0.1 ±0.1	0.71 ±0.02
Netherlands	23.9 ±4.6	0.1 ±2.1	0.21 ±0.10
Philippines	39.4 ±7.7	-0.3 ±5.5	0.16 ±0.21
Sweden	18.6 ±0.5	0.2 ±0.4	0.34 ±0.01
USA	11.8 ±0.5	-0.1 ±0.5	0.63 ±0.02

Covariates importance

The weighted importance values of the ensemble learner are shown in Figure 4.4. The colored matrix shows the importance of individual covariates where models of most countries are highly influenced by the WRI Flux, CCI maps and canopy height changes. Textural variables show moderate influence on the models and quarterly NDVI to the models of European countries. The static covariates and even dynamic LC data show the least influence on most models. An exception to this is the high influence of elevation on the models of tropical countries Brazil and the Philippines. Using the mean importance of each covariate, the categorical importance values further highlight the influence of global AGB maps (bar graphs of Figure 4.5). This influence accounts for 51-70% of the importance scores of covariates.

Map predictions

The predicted carbon flux maps and their prediction intervals are shown in Figure 4.6. Spatial patterns of the past-decade carbon dynamics can be observed. Areas with evident carbon losses exist in all countries except the Netherlands. Evident also are losses that appear as regional hotspots particularly southern Philippines, central Brazil and southwest USA. The hotspots are less pronounced for Netherlands and Sweden. Forest carbon

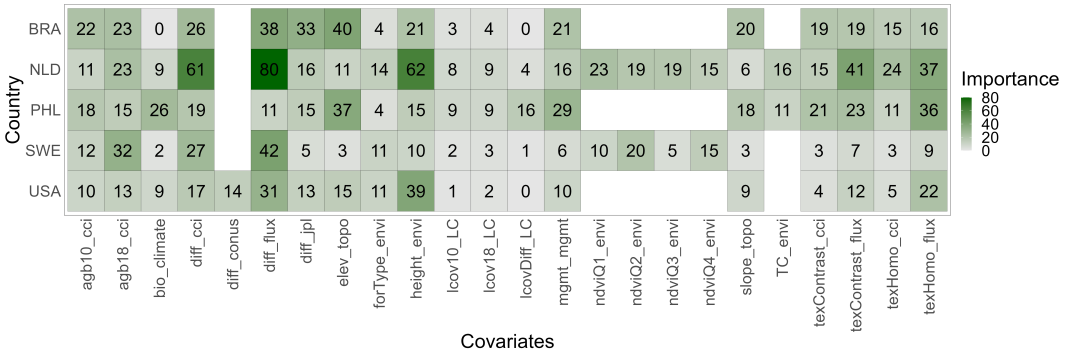

Figure 4.4: Permutation-based importance values (0-100%) of each covariate to country spatial models. Refer to Table 4.1 for the covariate names.

.

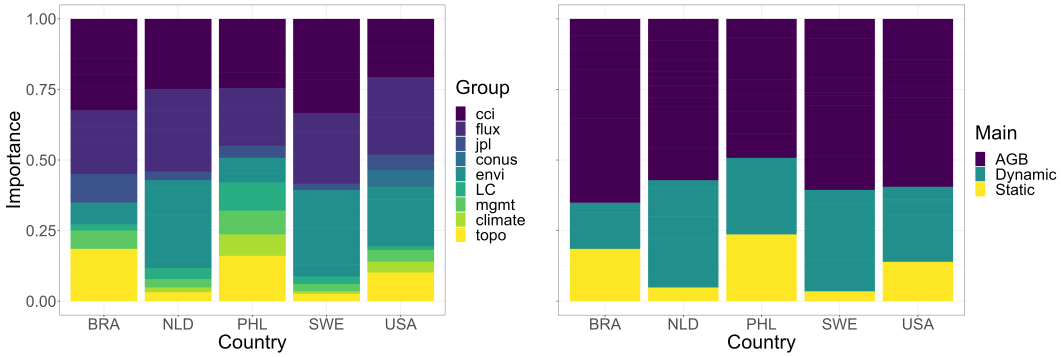

Figure 4.5: Proportion of the importance values (0-1) for each covariate group shown in Table 4.1. The left graph shows the category of covariates that distinguish each biomass global product along with other dynamic environmental inputs (height, tree cover and NDVI), land cover, management, climate and topography. The right graph further generalizes the covariates into categories that distinguish global AGB maps from other dynamic covariates, along with the static covariates.

sequestrations are also observed in all countries. Most are small carbon sequestrations of around 5-25 C Mg ha^{-1}, most evident in the Amazon basin in Brazil. Such small carbon sequestration in eight years is normal for an old-growth intact forest (Amazon) while the other cases can be attributed to natural disturbances that hinder tree growth like droughts. The loss and sequestration spatial patterns are also pronounced in the prediction intervals. The highest uncertainties of the predictions are observed in the USA map.

Spatial aggregation and carbon accounts

The spatial correlation of carbon flux residuals depicted by the variograms is shown in Figure S5. Spatially correlated residuals are evident in relatively short distances of 100-5500 m. The variability depicted by variogram sills ranges from 0.32-0.63. For the 2010

carbon stocks, a similar short-distance correlation of residuals is observed but in a slightly wider range and higher sill than the carbon flux. These results are basis to ignore spatially correlated residuals when aggregating map errors for each UNSEEA class.

The resulting carbon accounting table is shown in Table 4.3, while the table where emissions are further disaggregated is shown in Table S4. Net fluxes of carbon emissions are mostly evident and highest in number in Brazil and USA, particularly plantations and other woody vegetation of at least 95.23±11.07 Tg. All other countries mostly depict net carbon sequestrations notably USA broadleaved = 188.01±6.3 Tg, Sweden coniferous = 5.59±0.84 Tg and Philippines broadleaved = 3.87±2.57 Tg. The natural forests that consist of broadleaved, coniferous, mixed and mangroves are showing net carbon sequestrations than plantations except in Brazil where all classes are found as carbon emitters. The observation in Brazil is also consistent with the reports from UNFRA (see Table S5). Most emissions are driven by land-use changes in all countries, while the emissions within forest areas are logically occurring mostly in plantations. The uncertainty estimates of carbon fluxes are generally higher than the stocks, while the closing stocks are more uncertain than the opening stocks.

Discussion

Implications of reference data sample to carbon accounting

The reference data for the carbon flux spatial predictions did not cover the entire environmental space, wherein 6-47% of the combined forests and other woody vegetation areas appeared to be under-sampled. In such case, one recommendation is to consider limiting the predictions without the under-sampled areas (Meyer & Pebesma, 2021). However, incomplete carbon accounting in the context of UNSEEA is inadvisable (UN, 2021). Hence, the results in the accounting table of countries with LiDAR samples particularly mixed forest and other woody vegetation (Figure S3) should be treated with caution. Moving forward, we elaborate on a series of recommendations in cases where the country data sample would hamper the application of the mapped carbon flux for UNSEEA carbon accounting:

1. **Additional samples**. If additional field samples are not feasible, synthetic samples can be integrated into the current sample (Taghizadeh-Mehrjardi et al., 2020). As proof of concept to this recommendation, we show the implications of adding synthetic samples within the under-sampled areas in Figure S6. The current under-sampled areas are significantly reduced after adding pseudo loss samples based on forest loss data (Hansen et al., 2013b). Gradual changes in forests such as from degradation and regrowth need to be sampled as well. Samples provided by forest dynamics monitoring tools can be explored (Decuyper et al., 2022). Adding synthetic samples also means that a highly gapped clustered sample (Brazil) can

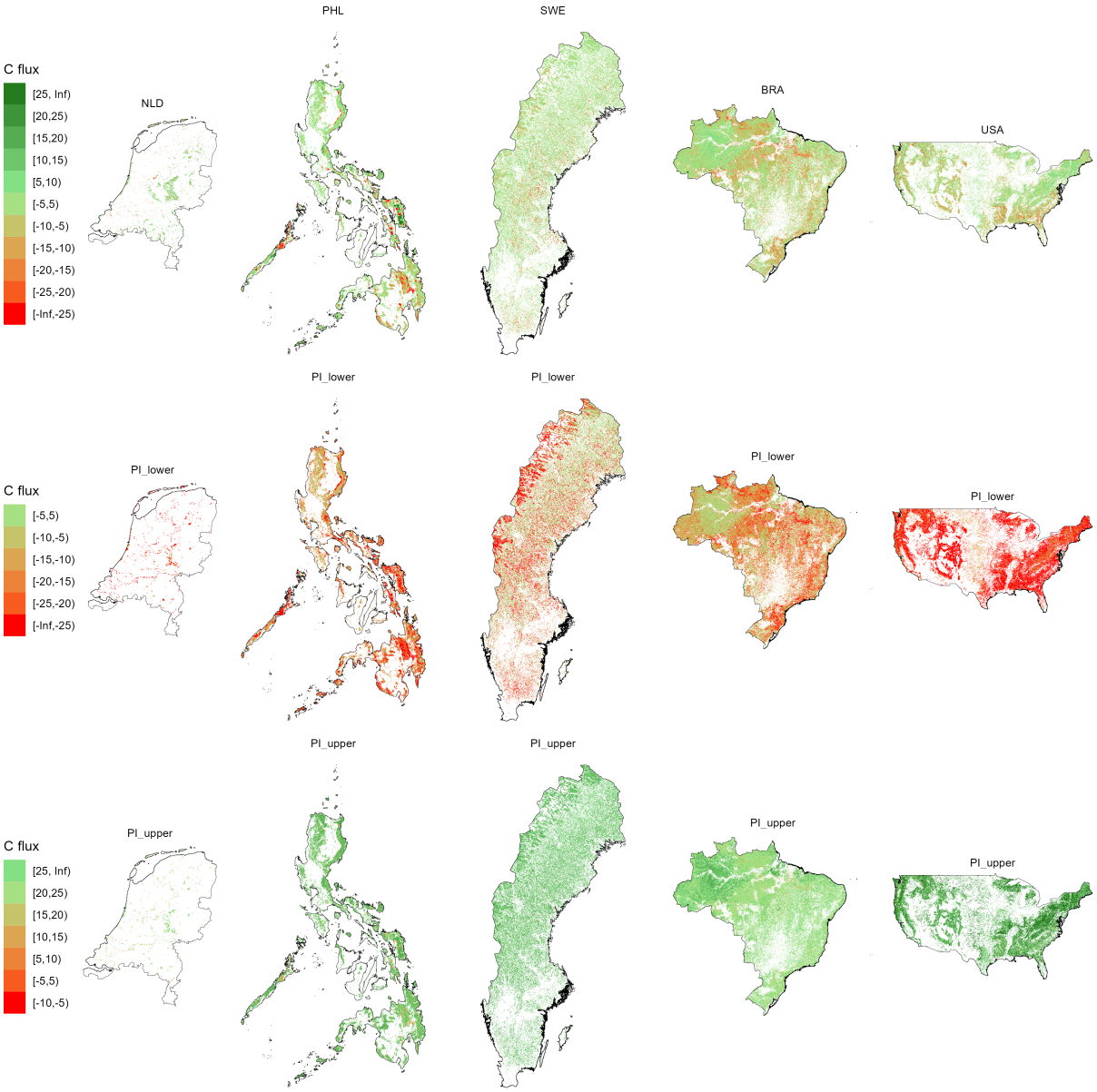

Figure 4.6: Predicted carbon flux maps for all countries and their prediction intervals. Map units are C Mg ha $^{-1}$. Note that colors can be different between the prediction and prediction intervals.

turn into a moderately gapped clustered data. In any case, a more suitable cross-validation should be used instead of the conventional *k-fold* cross-validation. For instance, cross-validation weighted by sampling intensity is suitable when using moderately clustered samples (de Bruin et al., 2022).

2. **Substitute the mapped carbon flux with the carbon flux from global products**. For UNSEEA classes that are not supported by country data such as mixed forests and non-forest woody areas in this study, the mapped carbon flux can

Table 4.4: Carbon accounting tables for 2010-2018 of the five case countries. Negative values denote net emissions, net sequestration otherwise. Also shown are the 2010 areas of each UNSEEA class.

UNSEEA class	Area ('000 km^2)	Opening 2010 (Tg)	Net fluxes (Tg)	Closing 2018 (Tg)
BRA				
Broadleaved	3485634	49541.1 ±30.175	-43.18 ±4.961	49497.92 ±29.765
Coniferous	153277	1059.03 ±3.905	-22.76 ±1.083	1036.27 ±3.752
Mixed	735145	1988.52 ±5.121	-156.02 ±2.390	1832.50 ±4.529
Mangroves	166677	794.79 ±3.496	-0.48 ±1.010	794.31 ±3.347
Other woody vegetation	1140095	4015.19 ±8.232	-403.50 ±3.069	3611.69 ±7.638
Plantations	1320002	3380.46 ±6.601	-421.18 ±3.112	2959.28 ±5.822
NLD				
Broadleaved	3008	0.33 ±0.064	0.00 ±0.030	0.33 ±0.057
Coniferous	4962	0.25 ±0.082	0.00 ±0.015	0.25 ±0.081
Mixed	5487	2.2 ±0.164	0.02 ±0.033	2.22 ±0.161
Other woody vegetation	54494	1.93 ±0.253	0.02 ±0.214	1.95 ±0.135
Plantations	15199	5.41 ±0.254	0.02 ±0.063	5.43 ±0.247
PHL				
Broadleaved	57334	427.45 ±4.060	3.87 ±2.476	431.32 ±3.218
Coniferous	3008	14.42 ±0.669	0.14 ±0.457	14.56 ±0.488
Mixed	4962	12.19 ±0.659	-0.28 ±0.511	11.91 ±0.416
Mangroves	5487	7.71 ±0.640	-1.10 ±0.583	6.61 ±0.263
Other woody vegetation	54494	297.88 ±3.191	1.83 ±1.770	299.71 ±2.654
Plantations	15199	45.6 ±1.280	-0.86 ±0.858	44.74 ±0.949
SWE				
Broadleaved	4588	13.26 ±0.254	0.32 ±0.114	13.58 ±0.227
Coniferous	109355	501.12 ±2.169	5.59 ±0.844	506.71 ±1.999
Mixed	8396	34.52 ±0.574	1.41 ±0.241	35.93 ±0.521
Other woody vegetation	88573	254.33 ±2.021	-1.27 ±1.541	253.06 ±1.306
Plantations	61354	293.69 ±1.987	-0.68 ±0.651	293.01 ±1.877
USA				
Broadleaved	529916	2849.44 ±9.183	188.01 ±6.277	3037.45 ±6.703
Coniferous	959568	6069.88 ±15.075	-23.96 ±7.608	6045.92 ±13.015
Mixed	665106	1482.73 ±7.573	-34.70 ±5.873	1448.03 ±4.781
Other woody vegetation	2351583	1023.21 ±11.507	-95.23 ±11.074	927.98 ±3.125
Plantations	1084568	2919.96 ±9.789	-239.26 ±7.460	2680.70 ±6.338

be substituted by global products (e.g., CCI and WRI). Either one or an average of the global products can be the alternative input data. This holds the rationale of a remote sensing-based carbon accounting. As a pre-requisite, an assessment of the global product can be initiated even at country scales using UN Forest Resource Assessment (UNFRA) as reference (Xu et al., 2021; Araza et al., 2023). A good agreement of the country carbon fluxes between the global product and the UNFRA would justify the use of the former for carbon accounting.

3. **Limit the accounting classes**. If the global carbon flux disagrees with the UNFRA data especially for top-tier countries according to UNFRA standards (Nesha et al., 2022), the last resort would be the exclusion of certain UNSEEA classes such

as mixed forests and other woody vegetation in our case. These classes have minimal carbon stocks among the carbon accounting classes. The latter can also be affected by highly variable non-forest woody definitions. An option also is to mask out areas that sequester little to no carbon ("no change" forests) equivalent to those intact old-growth forests.

4. **Estimation of the uncertainty from sampling variability**. Quantification of the uncertainty from sampling variability alongside mapping the under-sampled areas is our last recommendation. This sampling uncertainty can be estimated by bootstrapping methods that derive pairwise covariances of predicted carbon fluxes (McRoberts et al., 2022). This step, however, is computationally demanding and was demonstrated only at local scales from one study (Esteban et al., 2020). Aside from easing computational demands for country scales, worth testing is the quantification of sampling uncertainty with and without the pseudo samples.

Accuracy and uncertainty of the spatial models

The predictive performance of our spatial models yielded: RMSE=9-39 C Mg ha^{-1}, ME=-0.3-0.2 C Mg ha^{-1} and R^2=0.16-0.71. These results are relatively higher when compared to our previous assessment of the biomass changes from global data (R^2=0.09-0.21)(Araza et al., 2023). Nevertheless, mapping the changes in biomass and carbon using remote sensing is challenging. Pixel-level changes except for abrupt losses from deforestation can be very uncertain. For instance, the map producers of CCI maps cautioned about the use of their 100 m biomass change product due to uncertainties attributed to gradual changes in forests (Santoro & Cartus, 2019). Similarly, Santoro et al. (2022a) found at least 40% relative uncertainty of biomass change in Sweden at 20 m pixel size. This map evaluation similarly used NFI as reference but their mapping used the indirect method of deriving biomass change by differencing two maps. Indirect methods are known to add up model errors from two epochs. Moreover, environmental dynamic inputs useful for direct carbon flux mapping were unavailable until 2021. Recent efforts already estimated carbon fluxes with high precision using direct methods. Esteban et al. (2020) for instance produced wall-to-wall growing stock volume (convertible to biomass) from combined NFI and airborne LiDAR as auxiliary data. McRoberts et al. (2022) used a similar approach to estimate uncertainties from both residual and sampling variability intended for large-scale biomass mapping. More studies like this are anticipated considering the increasing number of permanent LiDAR sites as support for upcoming satellite missions (Chave et al., 2019a). This will strengthen our carbon accounting demonstration, where inputs are leaning towards time series data (e.g., LiDAR (Zhao et al., 2018)) also enabling current machine learning models from spatial to spatio-temporal. Lastly, additional base learners may also help improve the current ensemble model.

Uncertainty sources of the carbon accounts

The carbon accounting required aggregation from pixel to UNSEEA class of carbon stocks (from CCI AGB 2010) and fluxes. From the variograms in Figure S5, we found short-range correlation (<5 km) at country scales, which is consistent with previous studies particularly in Brazil (Mauro et al., 2019) and USA (Popescu et al., 2004). This basis allowed us to ignore spatial correlation during the aggregation step. This decision is case-to-case basis and needs reconsideration especially when the target country is relatively small i.e., where spatially correlated errors of around 5-50 km are already non-negligible. The variogram analysis also revealed the magnitude of autocorrelated scaled residuals (0-1) were all below 1. This suggests that we overestimate the map prediction error. This caution was also evident in 3 out of 4 global biomass maps in a previous study (Araza et al., 2022a). Here we focused on quantifying the uncertainty from residual variability, but missed to quantify the uncertainty from sampling variability (see 4th recommendation above). Another uncertainty source is the land cover input. Here we used the Level 1 UNSEEA classes but once countries require Levels 2 UNSEEA classes where, for instance, broadleaved is sub-classified into broadleaved closed canopy and broadleaved open canopy (Table S3), the uncertainty from land cover inputs needs consideration. Mapping more forest classes lead to a higher misclassification tendency among sub-classes. To account for this, land cover probabilities and geostatistical approaches are needed for potential area corrections among land cover units (de Bruin, 2000). This correction also concerns the carbon accounting table where emissions and removals are reported separately and emission sources are disaggregated (Table S4). Should countries require such a table, the spatial dependency between emissions and removals needs to be accounted for as well. We finally emphasize that any reference data have a degree of uncertainty. We account for this uncertainty when we applied a weighted bootstrapping in the ensemble model that preferred samples with low measurement error uncertainty. An exactly similar approach was implemented by Araza et al. (2022a) and Takoutsing & Heuvelink (2022). The latter example found no striking difference between a random forest model with and without the weighted bootstrapping.

Influence of the covariates

The most influential covariates in the carbon flux predictions were global biomass products, which accounted for 51-70% of the overall importance scores of covariates. The carbon fluxes from CCI and WRI contributed the most to this score. This result seems to be expected and self-explanatory. What is more surprising is that we learned that other dynamic environmental datasets were also important covariates. Particularly, height dynamics was important for the spatial models of the Netherlands (62%) and USA (39%) as well as the 1st and 2nd NDVI quarterly composites for the European countries with at most 23% importance score. Height and vegetation indices are commonly used variables for biomass mapping because of their correlation to biomass (Rodríguez-Veiga et al.,

2016). To our knowledge, this is the first attempt to use their dynamic variables to model biomass change (dynamic height dataset is relatively new). Moreover, elevation also had high importance score for Brazil (40%) and the Philippines (37%). This suggests that biomass change is topography-driven in the tropics. Recent studies even revealed that biomass change in the tropics is seasonal (Csillik et al., 2022). Aside from including seasonal covariates, we aim to explore other descriptive analysis of covariates to biomass change such as the use of partial dependence plots and Shapley values.

Country carbon fluxes

Overall, the carbon accounting tables depicted net carbon sequestration in natural forests except for Brazil, while net carbon loss was observed in other woody vegetation and plantations (except for the Netherlands). As a good practice, we summarized the carbon fluxes and forest areas at country scales and compared them to similar results in the literature, see Table S5. In comparison with the UNFRA and other similar studies (Santoro & Cartus, 2019; Harris et al., 2021; Santoro et al., 2022a; Yu et al., 2022), our estimates were mostly consistent for the Netherlands, the Philippines and Sweden. In these countries, our estimates were often in between the estimates of UNFRA and similar studies suggesting we conservatively estimated carbon fluxes. While there is a large discrepancy in forest areas (since we included other woody non-forests) and a few years difference in the monitoring period, the comparisons in the results of Brazil and USA showed we overestimated carbon loss compared to other sources. Our next carbon flux maps of the two countries will benefit from the anticipated USA Forest Inventory Analysis plots and additional re-measured LiDAR data for both USA and Brazil. Nevertheless, our estimates included reported uncertainties at the country level among the other sources.

Outlooks in carbon accounting based on remote sensing

The next generation UNSEEA carbon accounts are aiming toward carbon flux maps as inputs. This transpired in the last Advancing Earth Observation for Ecosystem Accounting conference in December 2022 `https://eo4ea-2022.esa.int/`. Remote sensing is also central to international initiatives that aim to upscale UNSEEA carbon accounting such as the following:

1. Mapping and Assessment for Integrated Ecosystem Accounting (MAIA, `https://maiaportal.eu/`)
2. Artificial Intelligence for Environment and Sustainability (ARIES, `https://seea.un.org/content/aries-for-seea`)
3. Open Earth Monitor project `https://earthmonitor.org/`

Our current carbon accounting spans eight years due to data availability for 2010 and 2018, but the suggested period of UNSEEA should either be annual or every five years. This periodic carbon accounting is complimented by the further increase of remote sensing

data for forest monitoring due to upcoming satellite missions.

Carbon stocks and fluxes maps are always subject to map assessments and integration with reference data especially now that country NFIs are increasing even in developing countries in the tropics (Nesha et al., 2022). Given these country data in addition to the upcoming LiDAR sites (Chave et al., 2019a), sufficient global data would allow map errors of the global carbon fluxes to be modelled and minimized using our bias modelling approach (Araza et al., 2022a). A bias-adjusted global carbon flux welcomes the possibility of carbon accounting for all countries. This would not only benefit UNSEEA carbon accounting, but also the UNFCCC GHG reporting and even the UNFCCC Global Stocktake.

Conclusions

To provide the needed carbon flux input for UNSEEA carbon accounting, we spatially predict the 2010-2018 net carbon flux using ensemble machine learning in five countries. Our learning from the study are as follows:

1. The reference data may not support the environmental and geographic space of UNSEEA classes especially when using clustered samples. To minimize the undersampling, we have provided recommendations including the need for additional samples, cases where global products can substitute as carbon accounting input and when to exclude certain UNSEEA classes. Most of these actions are also applicable to similar mapping efforts based on machine learning spatial models.
2. Mapping the changes in biomass and carbon at high resolution is challenging, judging by the variability in map accuracy results. While our predictions were mostly influenced by data from global biomass products and even dynamic height and NDVI data, these remote sensing data are all uncertain to gradual forest changes. Moreover, the reference data can be uncertain also if they have a spatial and temporal mismatch with remote sensing data. Time series reference data is anticipated and that would lead to prediction models that account for both spatial and temporal properties of carbon fluxes.
3. The carbon accounting tables mostly depicted net carbon sequestration in natural forests, while net carbon loss was observed in other woody vegetation and plantations. These findings are mostly consistent with results from Forest Resource Assessment and several recent studies; except our results for Brazil and partly for USA.
4. We found short-range correlation of carbon flux map errors that can be considered negligible when we aggregate the carbon flux from pixel to UNSEEA. For relatively smaller countries, even short-range correlations (e.g., 5-50 km) need to be accounted. This caution is also true when carbon accounting requires Level 2 UNSEEA classes (e.g., broadleaved into closed forest broadleaved and open forest broadleaved). This step will require area corrections i.e., using land cover probabilities and geostatistical

approaches.

Our study is the first demonstration of a UNSEEA and remote sensing-based carbon accounting with reported uncertainties. The approach is reproducible for countries with reference data through this repository `https://github.com/arnanaraza/SEEA_RS` and interactively once we set up a dedicated online platform. These access options would help assure transparent UNSEEA annual carbon accounting.

Chapter 5

Rapid remote monitoring reveals spatial and temporal hotspots of carbon loss in Africa's rainforests

This chapter is based on: Csillik, O., Reiche, J., De Sy, V., Araza, A., & Herold, M. (2022). Rapid remote monitoring reveals spatial and temporal hotspots of carbon loss in Africa's rainforests. *Communications Earth & Environment, 3*(1), 48.

Abstract

Spatially explicit monitoring of tropical forest aboveground carbon is an important prerequisite for better targeting and assessing forest conservation efforts and more transparent reporting of carbon losses. Here, we combine near-real-time forest disturbance alerts based on all-weather radar data with aboveground carbon stocks to provide carbon loss estimates at high spatial and temporal resolution for the rainforests of Africa. We identified spatial and temporal hotspots of carbon loss for 2019 and 2020 for the 23 countries analyzed, led by different drivers of forest disturbance. We found that 75.7% of total annual carbon loss in the Central African Republic happened within the first three months of 2020, while 89% of the annual carbon loss in Madagascar occurred within the last five months of 2020. Our detailed spatiotemporal mapping of carbon loss creates opportunities for much more transparent, timely, and efficient assessments of forest carbon changes both at the level of specific activities, for national-level GHG reporting, and large area comparative analysis.

5.1 Introduction

Conserving and reducing the loss of rainforests is among the most effective solutions for mitigating climate change and for preserving key ecosystem services (Bastin et al., 2019). International and national initiatives related to the Paris Climate Agreement stimulate and implement targeted activities for avoiding tropical forest loss (Bos et al., 2019). Their success, however, depends on suitable information on where and why forests are changing to define suitable policies and actions, to support implementation and enforcement on the ground, and to provide robust reporting on the progress and performance of such activities (Gibbs et al., 2007; Nesha et al., 2021). Forest carbon monitoring efforts have evolved, but limited spatial detail and timeliness hinder their usefulness for tracking collective progress towards forest-specific climate mitigation goals. This is a particular issue for Africa's humid forest changes that remain poorly understood and quantified (Dupuis et al., 2020; Shapiro et al., 2021). The fact that the most recent national forest inventories (NFIs) of countries in this region are 4.5±3.2 years old (Supplementary Table 1) highlights that available data are not serving the action-oriented nature of ongoing forest-related mitigation schemes.

Rapid detection of forest disturbances in Africa has already proven to decrease the probability of deforestation by 18%, with an estimated social cost of carbon for avoided deforestation between US$149 million and US$696 million (Moffette et al., 2021). Two main causes of forest disturbance in the Congo basin between 2000 and 2014 were small-scale clearing for agriculture (84%) and selective logging (10%), with regional differences (Tyukavina et al., 2018). For example, more than 60% of forest disturbances in Gabon are due to selective logging and more than 90% of disturbances in the Democratic Republic of the Congo (DRC) and the Central African Republic are due to small-scale agriculture (Tyukavina et al., 2018). West and East African tropical forests, including Madagascar, have lost almost all the forest extent in the last decades (Aleman et al., 2017), while the last two largest tropical forest fragments in Africa, both located in the DRC are at immediate threat due to continuing expansion of rural populations into remote forests (Hansen et al., 2020). A long-term future prediction indicates a decline in the African tropical forest carbon sink (Hubau et al., 2020).

Monitoring forest carbon changes using remote sensing technologies has become increasingly feasible (Csillik et al., 2019; Harris et al., 2021; Xu et al., 2021) driven by the abundance of multi-source satellite time-series data for tracking forest changes (Woodcock et al., 2020; Hansen et al., 2013b) and forest biomass and carbon stocks (Xu et al., 2021; Santoro et al., 2021). Driven by the open access availability of Sentinel-1 data, radar-based approaches are now operationally available to overcome cloud-cover issues in large area tropical forest monitoring and assess small-scale disturbances in a matter of days at 10m spatial scale (Reiche et al., 2021). Such information can be used to track changes at spatiotemporal scales at which human activities affecting forests and land

use are operating. This creates opportunities for much more transparent, timely, and efficient assessments of forest carbon changes both at the level of specific activities, for national-level GHG reporting, and large area comparative analysis.

Here, we present a high-resolution spatially explicit rapid monitoring of local carbon loss in Africa's humid tropical forest by combining data of radar-based forest change alerts and spatial carbon stock estimates. We define local carbon loss as the complete or partial potential loss of carbon that can later be emitted into the atmosphere. We analyzed the spatiotemporal dynamics of carbon loss in 2019 and 2020 by combining aboveground carbon estimates, derived from a combination of best available remote sensing and field data, with near-real-time radar-based forest disturbance alerts, at a spatial scale of 10 m with monthly intervals. We separate between high and low confidence alerts and provide uncertainty estimates at the pixel and country-level by combining the uncertainties of the carbon map with commission and omission errors of the alerts. We analyzed 23 countries with a wide variety of spatiotemporal patterns of carbon loss and found correlations between the two years analyzed reaching up to 0.94.

5.2 Material and methods

5.2.1 Study area

The study area is represented by the primary tropical humid forest of Africa and covers 23 countries. The primary tropical forest is defined as mature natural tropical forest cover that has not been completely cleared and regrown in recent history (Turubanova et al., 2018). We created a reference primary tropical humid forest mask for 2018 using the extent of these forests in 2001 (Turubanova et al., 2018), from which we excluded the forest loss between 2001 – 2018 (Hansen et al., 2013b) and mangroves (Bunting et al., 2018).

5.2.2 Forest disturbance alerts

We used the RADD alerts (Radar for Detecting Deforestation) based on Sentinel-1 data for the years 2019 and 2020 (Reiche et al., 2021). Forest disturbance is defined as the complete or partial removal of tree cover within a 10 x 10 m pixel (0.01 ha) Complete removal of tree cover is associated with a stand-replacement disturbance at the pixel scale, while partial removal mainly represents disturbances associated with boundary pixels and selective logging. The alerts are based on Sentinel-1 radar satellite time-series data and a forest disturbance alert is triggered and confirmed with high confidence after multiple consecutive observations using Bayesian updating. There are two types of alerts: (1) low confidence alerts are provided for a forest disturbance probability >0.85 and (2) high confidence alerts for forest disturbance probabilities >0.975, within a maximum period of 90 days from first detection. Due to this timeframe of confirming alerts, analyzing

2019 and 2020 alerts will result in the last three months of 2020 having both high and low confidence alerts. We used an MMU of 0.2 ha since at this MMU the alerts were validated. The user's and producer's accuracies of high confidence alerts of forest disturbance larger than or equal to 0.2 ha were 97.6% and 95.0%, respectively, using stratified random sampling and a buffer zone around alerts to ensure a good estimate of the omission error (Olofsson et al., 2020). For each alert pixel, we computed the number of neighboring alert pixels in an eight connected direction and separated between core alerts (pixels fully surrounded by 8 alert pixels) and boundary alerts (pixels with less than 8 neighboring alert pixels) (Reiche et al., 2021).

5.2.3 Aboveground biomass estimation

We used the single-date spatially explicit ESA Climate Change Initiative (CCI) Version 2 aboveground biomass map for 2018 with per-pixel associated accuracy (standard deviation) at a spatial resolution of 100 m (Santoro & Cartus, 2021). The map was obtained based on Sentinel-1 C-band and ALOS-2 PALSAR-2 L-band data using an algorithm that inverts a semi-empirical model relating the forest backscatter to canopy density and height and then transformed to AGB using allometric equations. The per-pixel standard deviation is calculated by propagating individual uncertainties of the SAR measurement and the modeling framework. The AGB estimates for the wet tropics depend solely on the L-band backscatter data that is prone to local biases related to wet conditions and limited sensitivity to biomass in moderate to high biomass forests. This resulted in a non-uniform bias or the overestimation of low biomass and underestimation of high biomass (>250MgC/ha), the latter being driven by signal saturation of remote sensing images (Réjou-Méchain et al., 2019). This map bias can be modeled since different forest types, climatic gradients, topography, and aboveground biomass itself have been found to affect bias in biomass predictions (Chave et al., 2004; Rodríguez-Veiga et al., 2019). Map bias can be modeled only after accounting for the sources of uncertainties from the map and the plot data used for validation (Araza et al., 2022a).

A collection of research and forestry plots was compared with the CCI Biomass map for 2018 to derive the map bias (Araza et al., 2022a). Then, bias was modeled as a function of the AGB map and its textural properties as well as other spatially exhaustive covariates such as biome (Dinerstein et al., 2017), topographic variables (aspect and slope), forest fractional cover (Buchhorn et al., 2020), and the standard deviation layer of the AGB map using a random forest model (Breiman, 2001). The bias model followed a 10-fold cross-validation and was assessed through Root Mean Square Error (RMSE) (42.24Mg/ha) and Mean Absolute Error (MAE) (29.25Mg/ha). The predictive power of the covariates was also evaluated using variable importance measures while the sensitivity of the modeled trends to its inputs was assessed using partial dependence plots (Greenwell, 2017). Statistical significance of predicted bias was assessed using the prediction standard errors obtained with the infinitesimal jack-knife approach (Wager et al., 2014).

Only those statistically significant bias pixels were used to correct AGB map pixels. We ultimately converted the bias-adjusted AGB and associated standard deviation to carbon values using a conversion factor of 0.47 (Buendia et al., 2019).

5.2.4 Aboveground carbon loss and uncertainties

We combined the forest disturbance alerts and aboveground carbon stocks to estimate local carbon loss at two different spatial scales, 10m (0.01ha) and 100m (1ha). The two spatial scales matched those of the two main datasets used, the alerts and biomass estimates, and thus easier integration with either of them can be achieved. Carbon loss at 10m was calculated as the percentage of the 0.01ha of the alert pixel within the 1ha area of an aboveground carbon pixel (1%). Losses at 1ha were computed as the percentage of disturbance alerts within a 1ha pixel from the total aboveground carbon stored by that 1ha pixel. For both approaches, a distinction between high and low confidence and core and boundary disturbance alerts was made. We considered complete removal of tree cover and, therefore, complete carbon loss (100%) for core alerts and partial carbon loss (50%) for boundary alerts.

We estimated the uncertainty of carbon loss estimates per pixel and at the country level based on the propagation of the AGB standard deviation and the commission and omission errors of the alerts.

We defined a model of carbon loss (CL) (Eq. 5.1):

$$CL = AGC \times i \tag{5.1}$$

where AGC represents the aboveground carbon in forest biomass in a certain pixel and i is an indicator that is 1 if a pixel is labeled as disturbed and 0 otherwise. For the case a pixel is labeled as being disturbed, we combined the variance of AGC and the commission error of the alerts (2.4%). The probability of a pixel labeled as disturbed ($i = 1$) to actually be disturbed is 0.976 and the variance of this binomial trial is 0.0234. We further used the formula for the variance of a product of two uncorrelated random variables, resulting in the variance of carbon loss estimate (var(CL)) to be computed as (Eq. 5.2).

$$\mathrm{var}(CL) = AGC^2 \times 0.0234 + 0.976^2 \times \mathrm{stdev}_{AGC}{}^2 + 0.0234 \times \mathrm{stdev}_{AGC}{}^2 \tag{5.2}$$

For the case a pixel was not labeled as being disturbed, thus considered intact forest ($i = 0$), it has an expected disturbance probability of 0.05 due to the omission error of the alerts. Its variance would then be 0.0475 and applying the corresponding formula from above would result in the variance of the carbon loss for an undisturbed pixel to be (Eq. 5.3).

$$\mathrm{var}(CL) = AGC^2 \times 0.0475 + 0.05^2 \times \mathrm{stdev}_{AGC}{}^2 + 0.0475 \times \mathrm{stdev}_{AGC}{}^2 \tag{5.3}$$

We assumed complete dependence of the uncertainties when we scaled up to the country level, which resulted in a conservative approach since data dependence always results in larger uncertainty values (Roman-Cuesta et al., 2016). As a first step, we calculated the standard deviation at the aggregated country scale as the sum of standard deviations at the pixel level (Roman-Cuesta et al., 2016). In computing carbon loss uncertainties, we did not consider land cover successions or the main drivers of carbon loss. We then expanded the formula above to calculate the variance of a product of multiple uncorrelated random variables (AGC, commission, omission errors, and their variances) and computed the country-scale variance of carbon loss ($\mathrm{var(CL)_{country}}$) as (Eq. 5.4):

$$\begin{aligned}\mathrm{var}(CL)_{\mathrm{country}} &= \left(\mathrm{stdev}(AGC)^2 + AGC^2\right) \times \left(0.0234 + 0.976^2\right) \\ &\quad \times \left(0.0475 + 0.05^2\right) - AGC^2 \times 0.976^2 \times 0.05^2\end{aligned} \tag{5.4}$$

Ultimately, we calculated the square root of the resulted variances and expressed the per-pixel and country-scale carbon loss statistics and uncertainties as mean±standard deviation.

5.3 Results and discussion

5.3.1 Continental, regional, and local spatiotemporal patterns of carbon loss

For Africa's primary tropical humid forest, carbon losses due to forest disturbances reached 42.2±5.1MtCyr1 (mean±standard deviation, where MtCyr1 is one million metric tons of carbon loss per year) in 2019 and 53.4±6.5MtCyr1 in 2020. Just 9 countries out of the 23 analyzed accounted for 95.0% of total gross losses in 2019 and 94.3% in 2020. These countries contain about 95.7% of all primary tropical humid forests of Africa, with the DRC accounting for 52.8%, Gabon 11.8%, the Republic of the Congo 11.0%, and Cameroon 9.8%. Of these, DRC and Cameroon were responsible for 49.3% and 19.1% of losses in 2019 and 44.7% and 20.6% in 2020. DRC and Cameroon had an annual increase of 15.0% and 36.5% respectively, between 2019 and 2020. From countries with at least 1 MtC emitted in the two years analyzed, Madagascar had the highest annual increase in carbon loss (+153.9%), while Equatorial Guinea is the only country with a decrease in carbon loss (20.1%). Extending the carbon loss analysis for both past and future will help to better understand these variations and whether the COVID-19 global pandemic had any influence on the general increase between 2019 and 2020 (Brancalion et al., 2020). While the absolute numbers for carbon loss estimates should be treated carefully and a

sample-based approach should be preferred for an unbiased estimate of absolute numbers (Wernick et al., 2021), we focused our analysis on the trends of carbon loss at the continental, country, and local scale (Figure 5.1 and Supplementary Figure 1).

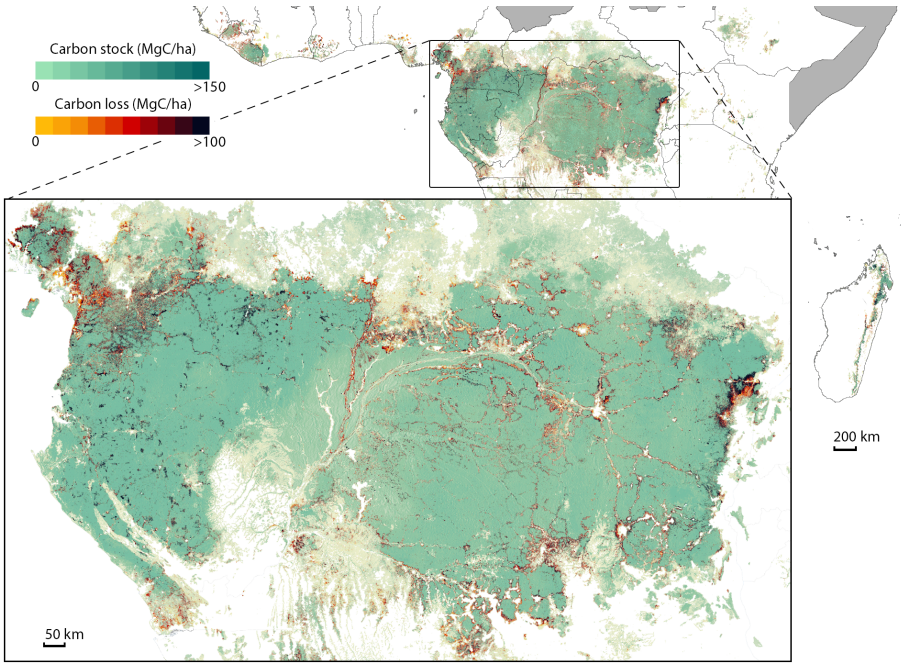

Figure 5.1: Carbon loss across Africa's rainforests. We analyzed 23 countries containing primary moist forest. The aboveground carbon stock (green palette) underlies the carbon loss estimations (red palette). Several hotspots can be seen across these regions. The uncertainties of the carbon loss estimations are expressed as standard deviations and shown in Supplementary Figure 1.

The high temporal detail of the analysis revealed various monthly patterns of carbon losses for countries, highly related to local rainfall patterns (Reiche et al., 2021) (Figure 5.2). Countries like Cameroon, Liberia, Nigeria, Central African Republic (CAR), and Madagascar showed a clear dry-wet seasonal variation in carbon loss per year, while the Republic of the Congo and the DRC, due to their latitudinal extent, exhibited two dry-wet season variations per year with varying intensities (Figure 5.2). The seasonal variation can be explained by higher accessibility to forests during the dry months when activities related to smallholder agriculture and logging are more feasible than in the wet season when many roads become inaccessible.

One of the highest differences between the months with the most and the least carbon losses was found for Madagascar (72 times more carbon loss in March compared to November 2019). In CAR, the three consecutive months with the highest cumulative carbon loss (January to March 2020) contributed to 75.7% of the total annual loss (between February and April 2020), in Nigeria 73.9% (January to March 2020), Liberia 73.1% (February to April 2020), Madagascar 70.7% (September to November 2020), and Cameroon 62.2%

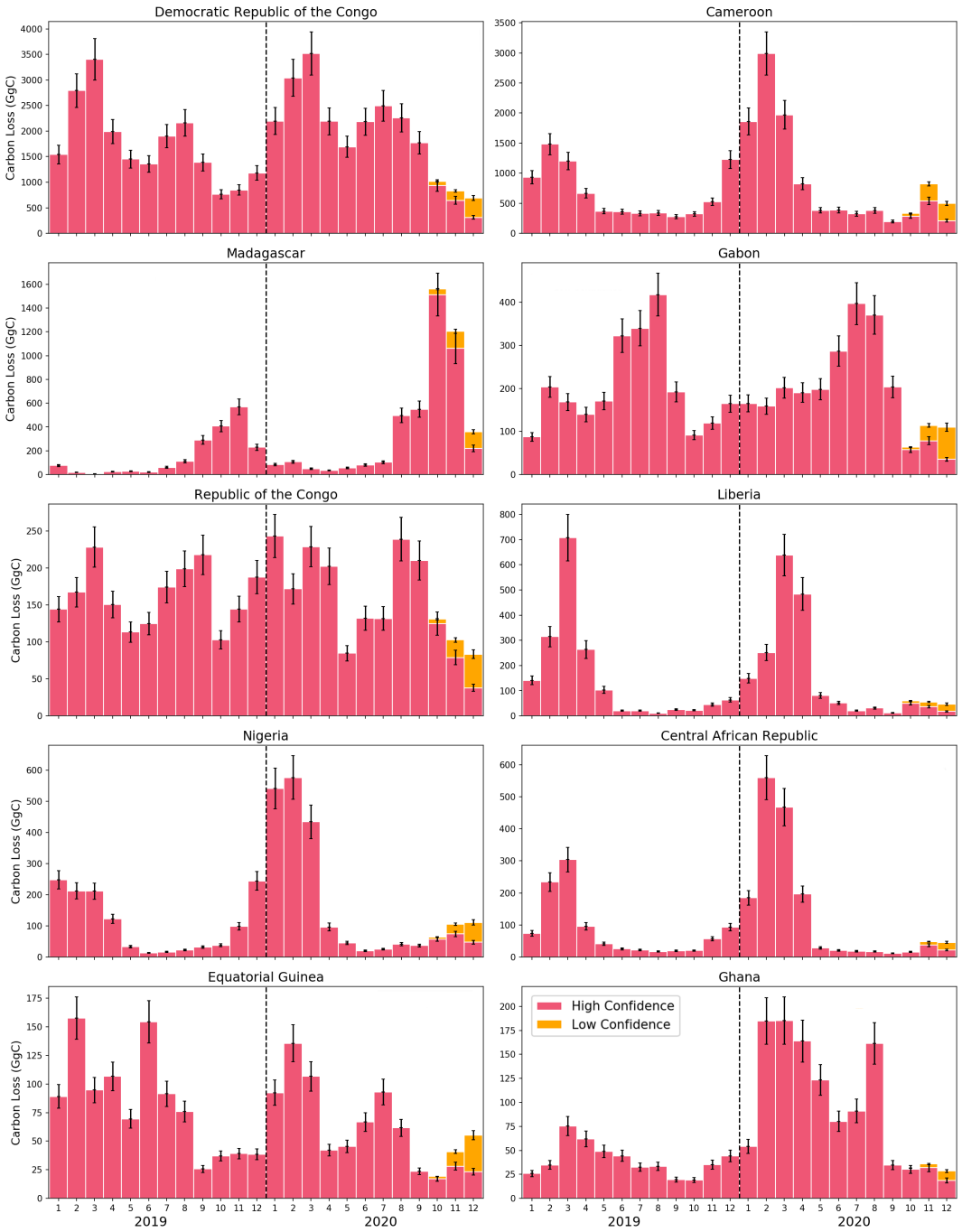

Figure 5.2: Temporal patterns of carbon loss for the top 10 countries. We show monthly statistics for 2019 and 2020 and the associated uncertainty (black lines). We separate between high (red bars) and low (yellow bars) confidence alerts, the latter showing up for the last 3 months of 2020.

(January to March 2020). Lower percentages were found for countries with mixed seasonality and patterns, like DRC 36.7% (January to March 2020), and the Republic of the Congo 32.8% (January to March 2020) (Figure 5.2). For the latter two countries, we

expect better-defined peaks of carbon loss at local scales, where climatic conditions are not mixed. The annual cumulative carbon loss (%) per country (Figure 5.3) showed that Liberia, Nigeria, CAR, and Cameroon reached between 70-90% of their annual carbon loss in April, while Madagascar reached 60% in October. The DRC, Gabon, Republic of the Congo, Equatorial Guinea, and Ghana have a more gradual monthly increase of cumulative carbon loss with less contrasting seasonality effects. Monthly patterns of carbon losses between the two years analyzed resulted in a correlation coefficient of 0.94 for the CAR, 0.92 for the DRC, 0.91 for Madagascar, 0.90 for Gabon, and 0.83 for Cameroon (Supplementary Figure 2). For the Republic of the Congo, the two years correlated 0.51. Knowing the peak months of carbon loss for each country and that these patterns are repeatable from one year to another can contribute to better target and prioritize enforcement activities, as well as predicting future patterns and early reporting of annual forest carbon losses.

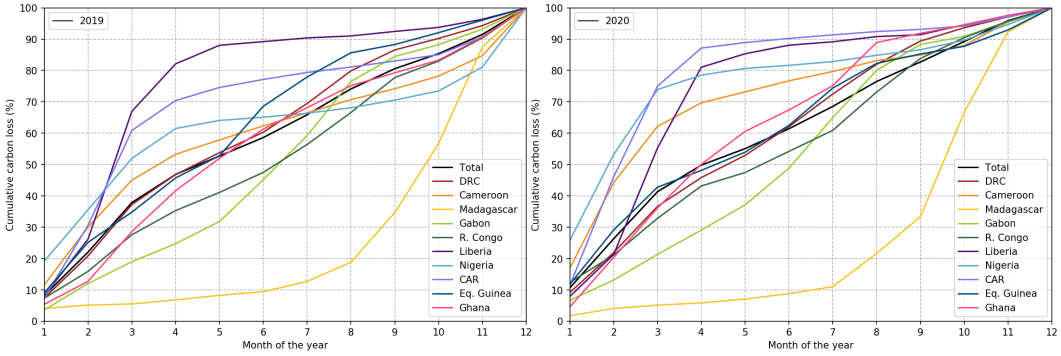

Figure 5.3: Annual cumulative carbon loss (%) for both years analyzed, 2019 and 2020. Africa's total cumulative carbon loss is shown with a black line. The 10 topmost emitting countries out of 23 countries analyzed are shown and represented by distinct colored lines.

Several hotspots of carbon losses can be seen in Figure 5.1. The high spatial and temporal details of our analysis are shown in Figure 5.3, where several local examples with different drivers of forest disturbances are shown, like logging roads, selective logging, mining, oil palm plantations, urban expansion, and small-holder agriculture. This kind of information, coupled with auxiliary datasets (e.g., legal concessions, protected areas) can identify the legality of forest disturbance (Araza et al., 2021c).

5.3.2 Implications of rapid monitoring of local carbon loss

Near-real time alerts combined with biomass maps result in spatially explicit forest carbon loss, unlike global tabular statistics of national data (Achard et al., 2014; UN-FAO, 2020). We provide new insights into the spatiotemporal dynamics of carbon loss with consistent assessment of accuracy that could enable transparency and completeness for countries reporting on their REDD+progress to the UNFCCC (Sandker et al., 2021). We provide monthly carbon loss estimates that could play a key role in local, national, and

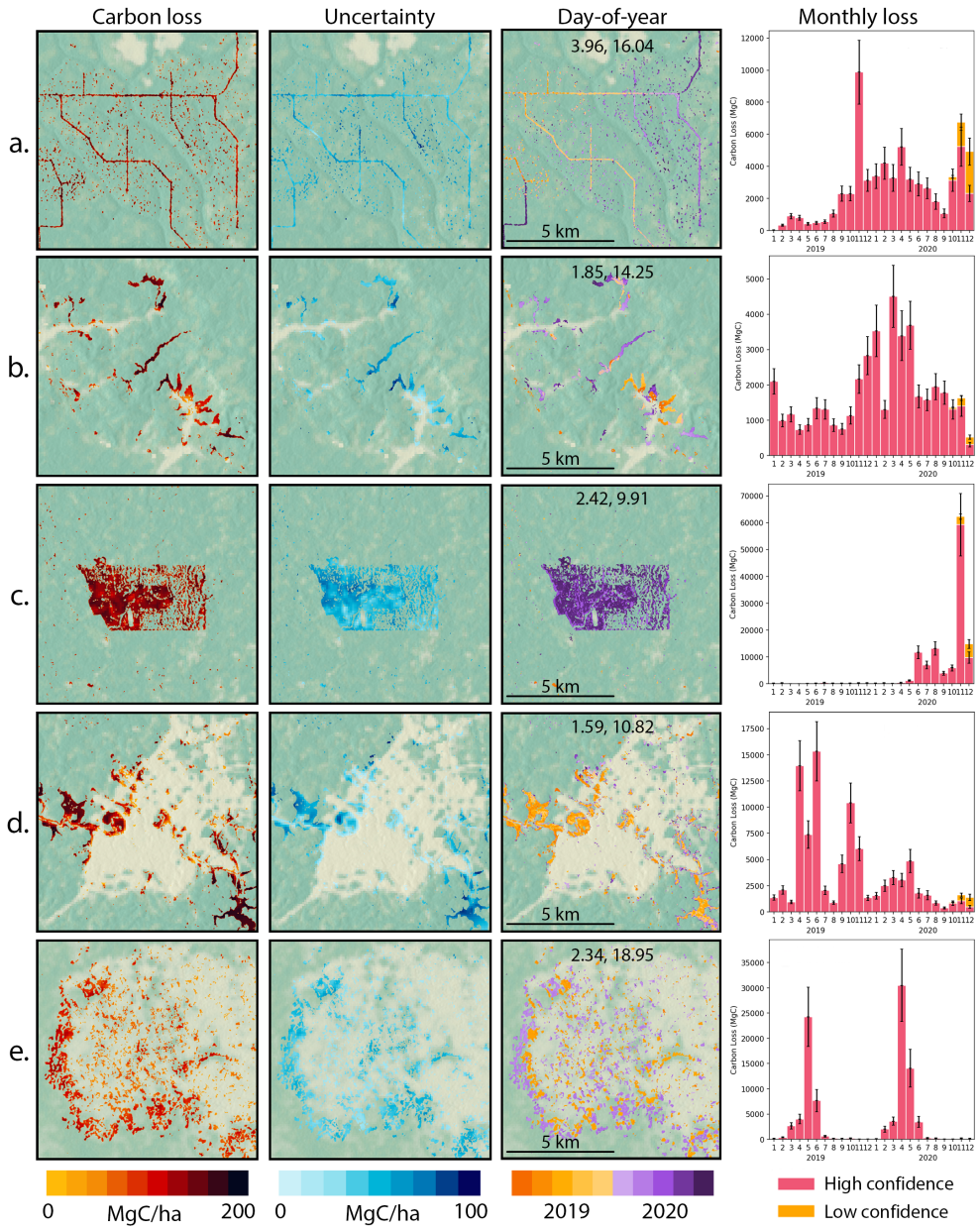

Figure 5.4: Local examples of approximately 10×10km in extent showing different spatiotemporal patterns and drivers of carbon loss. The first column shows the carbon loss, the second column the associated uncertainty, the third column the day-of-the-year when the loss occurred, and the last column shows the monthly distribution of carbon loss and associated uncertainty for each local example. The center coordinates of each location are shown in the third column as latitude and longitude. Exact locations are shown in Supplementary Figure 5.3. (a) Logging roads and selective logging in the Central African Republic, (b) mining of gold and titanium in the Republic of the Congo, (c) development of an oil palm plantation in Cameroon, (d) forest disturbance related to building a new capital city in Equatorial Guinea, and (e) small-scale agriculture expansion at the edge of the forest in the DRC.

international forest initiatives for global carbon policy goals (Finer et al., 2018). Such a system can be implemented with minimal costs and is based on open-source datasets and Google Earth Engine cloud computing platform Gorelick et al. (2017), thus enabling cost-effective national monitoring of forest carbon loss (Moffette et al., 2021). Providing rapid reporting on the location, time, and amount of carbon lost across Africa's primary humid forest will help undertake immediate action to protect and conserve carbon-rich threatened forests. Furthermore, countries will be able to predict and estimate their annual carbon loss before a reporting period ends, thus having the opportunity to adjust their practices to meet their country-specific commitments for climate change mitigation initiatives.

5.3.3 Limitations and future improvements

We used the RADD alerts (Radar for Detecting Deforestation) (Reiche et al., 2021) with a minimum mapping unit (MMU) of 0.2ha as accuracy estimates were available for this MMU. Events smaller than 0.2ha would add to the total carbon loss but are by nature associated with higher uncertainties (Reiche et al., 2021). The implications of the RADD alerts using a global humid tropical forest product as a forest baseline for 2018 (Hansen et al., 2013b; Turubanova et al., 2018; Bunting et al., 2018) are twofold. First, the global nature of this product might result in inconsistencies at the local level (Reiche et al., 2021). Second, because the forest cover loss information used to generate the forest baseline is based on optical Landsat data, persistent cloud cover in the second half of 2018 in some areas led to missed reporting of forest disturbances, thus being detected at the beginning of 2019 by the RADD alerts. This possible overestimation of carbon loss at the start of 2019 is not an issue for a near-real-time alerting system since later months are not affected. Furthermore, the alerts do not distinguish between human-induced disturbances and natural forest disturbances (Reiche et al., 2021). When a new forest disturbance alert is detected, it will be confirmed or rejected within 90 days by subsequent Sentinel-1 images (Reiche et al., 2021). That is why our carbon loss reporting separates between high and low confidence alerts for the last three months of 2020, which is common for most forest disturbance alerting products (Reiche et al., 2021; Hansen et al., 2016). We separated all the alerts into core and boundary pixels. Core alerts represent complete tree cover removal and we assumed complete carbon loss within a pixel. For boundary alerts, we assumed a 50% carbon loss since these mainly represent forest disturbances with partial tree cover removal. Detecting and quantifying the level of degradation remains challenging and future developments will minimize this uncertainty by providing variable percentages of degraded forest (Hoekman et al., 2020). The timeliness and spatial details of future forest disturbance alerting products will improve with the availability of open access long-wavelength radar data from near-future satellite missions (e.g., NISAR L-band SAR in 2023 (Rosen et al., 2017)), by using a combination of optical and radar forest disturbance alert products, and integration with high-resolution satellite products.

We relied on an aboveground biomass baseline map from 2018 (Santoro et al., 2021), prior to RADD alerts starting from 2019. Biomass estimation for the tropical moist forests is based on ALOS-2 PALSAR-2 L-band satellite and its usage needs to account for the local biases, especially underestimating AGB values higher than 250 Mg/ha((Santoro et al., 2021)). Although we reduced this underestimation by adjusting the AGB map based on ground field data, more research is needed on providing up-to-date high-resolution aboveground carbon estimates (Csillik & Asner, 2020) that could further increase the accuracy of local carbon loss estimation. Radar-based estimation of forest carbon stocks is challenging over mountainous terrain and is less accurate in complex canopies (Gibbs et al., 2007) and future integration of radar and optical satellite data will provide more robust estimates (Csillik & Asner, 2020). Nevertheless, new spaceborne missions (e.g., GEDI (Dubayah et al., 2020), BIOMASS (Quegan et al., 2019)) will provide an unprecedented amount of forest structure samples that will improve the algorithms and thus the final accuracy of aboveground biomass estimates.

We focused on exploring and analyzing local carbon losses and showing high temporal and spatial patterns of carbon losses. We showed the country statistics to emphasize the temporal dynamics of carbon losses and compare the temporal profiles across our study region. Our approach was not to provide stratified area estimations (Olofsson et al., 2020) associated with forest disturbances but we used this concept in the sense that we had a stratified sample of higher quality reference data (Reiche et al., 2021) to estimate the omission and commission errors and consider those in our uncertainty estimation on the pixel level. The analysis showed that omission and commission errors are small and rather balanced, and thus do not result in a major area bias for the forest disturbances. The uncertainties of the aboveground biomass product (Santoro et al., 2021) were adjusted for known regional biases using regional forest biomass plot data sources. With this approach, the original aboveground biomass map bias was partly corrected using a model-based approach deemed to be an alternative to a sample-based approach whenever country data are unavailable (Næsset et al., 2020). Our uncertainty analysis and error reduction showed that we expect only minor bias in the forest disturbance and the biomass data and the remaining uncertainties are propagated in our pixel-based uncertainty layer.

5.4 Conclusions

We introduce an analysis framework to estimate tropical forest aboveground carbon loss with high-spatial and temporal resolution that provides suitable information to enhance implementation and enforcement on the ground. This type of spatially explicit analysis will benefit all actors involved in climate change mitigation policies and actions, with improved transparency, transferability, and speed of reporting carbon losses promptly. Our framework provides a continentally comprehensive dataset on carbon losses that can be easily adapted to ingest new datasets, thus providing a benchmarking approach that

will enhance the capacity of countries to track the progress towards the goals of the Paris Agreement at multiple scales.

Chapter 6

Synthesis

6.1 Main findings

This section highlights the main findings of the thesis related to each research question posed in Chapter 1. Included also are discussions and recommendations related to each main finding.

6.1.1 How can the accuracy and uncertainty of global AGB maps be assessed using different reference data sources?

The increasing global AGB maps and the need to validate them are the main motivations of this thesis. Challenged by the lack of an ideal global reference sample, the map assessment framework developed in this thesis has enabled the comparison of the biomass from a collection of reference data and several global AGB maps after considering and accounting for both of their uncertainties. Such uncertainty assessment has never been done in past large-scale studies concerning AGB map validation. Aside from the plot uncertainty estimation itself (section 6.1.2), preliminary steps were needed. Reference data were collected using the existing plot database from the GlobBiomass project and data requests from online platforms e.g., from Forest Observation System (FOS). Plot data were also provided by several sources but under data-use agreements. The collated reference data underwent strict filtering based on several quality criteria. This step excluded around half of the original data. The strict filtering standardized the biomass of the reference data as those estimated only from plots with >10 cm trees. Some datasets had to be excluded because of imprecise coordinates despite their plots being located in less represented regions. The estimated AGB of most plots was provided by the data sources themselves using estimation methods deemed appropriate with respect to forest types and countries. The plots without information about AGB estimation were automatically discarded. Using the strictly filtered plots, plot uncertainties were estimated (section 6.1.2) and were used to calculate the minimum-variance linear unbiased estimates of the mean forest AGB when averaged to 0.1°, which were then compared with the map averages at 0.1° resolution. The comparisons evaluated the maps over bins of reference AGB using the metrics root mean square difference (RMSD), mean difference (MD) and an error conformity metric that indicates whether maps are optimistic or pessimistic about their precision.

The comparisons paved the way for the uncertainty modelling component of the framework, which both included bias and precision. The bias modelling predicted map bias as a function of AGB and other environmental data using a random forest regression model trained using data from less uncertain plots (mostly large plots). Using random forest involves resampling the original data through bootstrapping with replacement, meaning data can be duplicated. The uncertainties from this kind of resampling were accounted using Infinitesimal Jack-knifing, a method that estimates variances of bagged learners like random forest (Wager et al., 2014). The method was used for computing the standard

error of the predicted bias which was used to derive confidence intervals. The predicted bias at 0.1° resolution was most sensitive to biomass and tree cover (Chapter 2), while the most important bias predictors at 100 m resolution were biomass and its textural properties over 900 x 900 m^2 (Chapter 5). These dependencies were quantified and visualized using partial dependence plots, which are tools that help interpret machine learning models. Similar bias modelling approaches have recently been demonstrated such as Zhang et al. (2022) where a bias-adjusted map was produced after harmonizing global AGB maps based on global reference data. After the bias modelling step, the aim was to derive the pantropical total biomass. This step accounted for spatially correlated AGB residuals using variograms. The variograms in Chapter 2 also accounted for plot measurement error and then revealed spatial correlation up to 104 km. Such autocorrelation is caused by patches of forest types and landscape features that are sampled by NFIs at country scales (Saatchi et al., 2011a). Using variograms and map error covariances, the uncertainty of the pantropical AGB was derived.

The steps concerning the map assessment framework are implemented in the *Plot2Map* online tool (Araza et al., 2022b). The applications of the tool are further described in section 6.3.

6.1.2 Which sources of uncertainty affect the assessment and applications of global AGB maps?

The map assessment framework acknowledges that reference data are not error-free and their uncertainties from error sources need to be estimated and accounted for. While there already exists a list of plot uncertainty sources in Chapter 4 of the CEOS validation protocol (Duncanson et al., 2022), the majority of them concern the uncertainties from tree measurements and the use of allometric models. It was shown how these uncertainties can be predicted using a two-step approach that first uses an error propagation tool designed to estimate measurement error uncertainties from trees to plots (Rejou-Mechain et al., 2017; Gonzalez-Akre et al., 2021), and a meta-model that predicts such uncertainty for all plots. Chapter 2 showed that the main contributor at pixel levels is the combined uncertainties from tree measurements and allometric models as a consequence of using many small plots <0.3 ha. In Chapters 2-3, plot data providers were encouraged to either provide tree-level data or estimated plot-level uncertainties.

Another major plot uncertainty source concerns how the plots are sampled locally and globally. At the pixel level, the second highest uncertainty contributor appeared to be the spatial mismatch between plots and pixels (within-pixel variability, Chapter 2). This uncertainty increases whenever small plots (<0.3 ha) are compared with coarser resolution maps especially when the forest structure tends to be non-uniform over short distances. Imprecise geo-locations add to this uncertainty. At 0.1° grid cells, the representativity of the plots can be questionable especially when research plots are used. Permanent

research plots are mostly located in specific forest types and hence prone to preferential sampling. Hence, a representativity analysis in Chapter 2 was implemented and it was found that the effect of preferential sampling was less for NFIs than for research plots, which can be explained by the design of NFIs that aims to capture the local variability of biomass. A substitute for using research plots are local AGB maps from airborne LiDAR (Duncanson et al., 2021). The footprints of these local LiDAR maps usually cover 0.1° grid cells. Regarding global representativeness, a representativity analysis is helpful to determine regions that are under-sampled and hence require additional data collection. For instance, the Chapter 2 reference data would benefit from additional data for most parts of the boreal zones, southwest USA and south Africa as indicated by yellow and red areas (Figure 6.1). In Chapter 4, the area of applicability approach was used to determine priority areas for additional data at country scales (Meyer & Pebesma, 2021). Such analysis served as the basis to recommend additional samples and the caveats when interpreting carbon accounts of UNSEEA classes prone to under-sampling such as mixed forests and other woody vegetation.

Chapter 2 applied an adjustment of plot-level AGB if the plots have a temporal mismatch with map epochs of about ±10 years. The uncertainties introduced from these adjustments were estimated using information from the growth data used from the revised IPCC guidelines (Buendia et al., 2019). However, the IPCC growth data may introduce large uncertainties in certain regions and forest types e.g., in European forests (Harris et al., 2021). In such cases, it would be better to narrow the criterion to implement the temporal adjustment e.g. <5 years.

The map assessment framework estimates uncertainties of residuals which are needed when map pixels need to be aggregated for country summary statistics like AGB totals. This uncertainty source, however, is deemed to be of little importance when the aggregation involves large countries. The larger uncertainty contributor in such cases comes from sampling variability. This component is not fully accounted for in this thesis. The information needed to estimate sampling uncertainty should be provided by map producers. While most map producers provide associated SD layers, these data concern the residual prediction error rather than sampling uncertainty. The uncertainty from sampling variability is currently being dealt with in an extension of Chapter 2 using a more representative global plot than the plots used in Chapter 2.

6.1.3 What is the effect of spatial aggregation on ΔAGB assessments?

In Chapter 3, the past decade ΔAGB was estimated using four maps at different aggregation levels. The reference data were also aggregated and compared with map estimates. The reference data used were NFIs, LiDAR-based AGB maps and Forest Resource Assessment data. The comparisons of ΔAGB between the reference data and maps from 100 m to 25 km levels of aggregation revealed a decrease of scattering (smaller RMSD

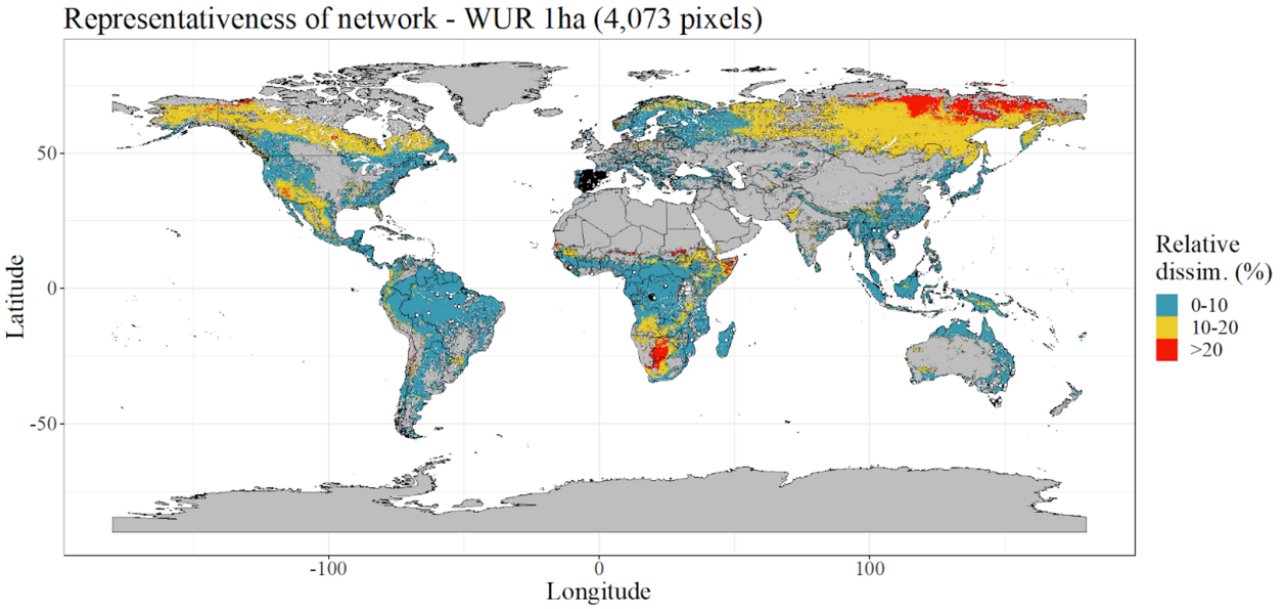

Figure 6.1: Representativeness of large reference data over environmental feature space. The image was taken from an intermediate analysis as part of the CCI Biomass project and produced by Nicolas Labriere.

and higher R^2) in the ΔAGB comparisons. This refers to random errors that tend to average out in the aggregation. However, regardless of the aggregation level, the map-based estimates showed smaller AGB loss and gain than the reference data owing mostly to map systematic differences (MD). The bias from 2010 maps is carried over into ΔAGB especially for deforestation and plantation clear-cutting events. Bias cannot be removed by averaging. The bias modelling in Chapter 2 can be used to reduce this bias once there is a more suitable ΔAGB reference data at global scale (Chapter 3). Biases of either the ΔAGB itself or the individual 2010 and 2018 maps can be predicted using the Chapter 2 framework, the resulting 2010 and 2018 maps can be differenced after.

The comparisons from fine to coarse aggregation levels affected the range of assessed ΔAGB. A wider range of comparisons was observed at 100 m from -220 to 120 Mg ha^{-1}, while the 25 km comparisons were confined to -100 to 20 Mg ha^{-1}. Assessment of ΔAGB attributed to deforestation (>100 Mg ha^{-1}) is important to countries that implement REDD+ MRV and ecosystem accounting. The range of observations was further diminished to -10 to 20 Mg ha^{-1} when using country averages (FRA). Country scales have more pronounced "net effect" ΔAGB compared to pixel-level ΔAGB (100 m). Changes in AGB totals can be compared instead of ΔAGB when using FRA reports.

The ΔAGB from LiDAR data agreed the most with map-based ΔAGB regardless of the aggregation level. The main reason for this is that LiDAR and map-based estimates both come from maps. The agreement when using NFI was sustained until the 1 km level. First, the NFIs are not entirely designed to measure changes in forest variables. The

NFIs used in Chapter 3 were <0.1 ha in size and mostly from European countries with active forest management such as pruning, thinning and salvage cutting. Moreover, the NFI plots may not properly represent grid cells e.g., only 12 plots over 25 km grid cells on average. Hence, grid cells may need a different selection criterion i.e., based on plot representativeness. Lastly, the comparisons of the ΔAGB between maps and FRA data showed different results despite using data from top-tier countries (Chapter 3). This is mainly affected by the different forest definitions set by countries. It is also possible that maps can be inconsistent for estimates of net carbon fluxes at country scales.

6.1.4 How global AGB maps and their assessment support both global and national map users?

Chapters 2 and 5 demonstrated that the framework is beneficial to both global and national users. Global AGB maps are inputs to Earth System models of climate scientists and to carbon cycle models of carbon scientists. National users particularly the REDD+ countries also benefit from global AGB maps for their reporting. Both user groups have the following map preferences in common according to the user consultation report of Quegan & Ciais (2018): (1) has global spatial coverage of biomass; (2) annual map availability; (3) underwent independent validation and uncertainty assessment; (4) preferably unbiased; and (5) accessible and open access. Regarding map spatial resolution, >1 km maps are preferred by global users while countries prefer higher resolution (<100 m).

The map assessment framework can assess any global AGB map with associated uncertainty from epochs 2000 and beyond. Biases from these maps can be modelled and adjusted as demonstrated in Chapter 2. Using a bias-adjusted map reduces the underestimation of AGB losses when used as the baseline AGB map (Araza et al., 2023). Maximizing the use of these map products requires constant communication with the global modellers. In 2020, a dataset of bias-adjusted 2000, 2010 and 2018 global 0.1° AGB maps was provided to them after conducting a user needs survey (Peylin et al., 2019). The same multi-date maps can also be helpful for global carbon budget reporting. These maps were also downloaded online by online users as of February 2023.

Chapter 5 showed how national users especially REDD+ countries can benefit from an MRV system that uses a bias-adjusted AGB map as baseline AGB while estimating monthly emissions from disturbed forest areas of at least 0.01 ha. Both the AGB and disturbance data uncertainties were accounted for when estimating the uncertainty of country emissions. An assessment concerning all 60 REDD+ countries revealed that most countries are still using the forest reference level approach where emission rates are estimated from forest area changes instead of actual AGB (Yanai et al., 2020).

Chapter 4 is one of the first carbon accounting demonstrations that used spatially explicit carbon stocks and flows. Chapter 4 used four global ΔAGB maps as covariates to predict the needed carbon fluxes to compile carbon accounts in five countries following the UN-

SEEA 2021 guidelines. The CCI 2010 map was also used to derive opening stocks being the only high-resolution map with an associated SD layer. Keith et al. (2021) reviewed current carbon accounting systems and they defined comprehensive carbon accounting as one that accounts not only for flows but also stocks. They added that common frameworks such as the UNFCCC carbon accounting and the previous UNSEEA framework in 2014 lack such comprehensiveness. Chapter 4 also showed around that 71% of the variation in the predictions of spatial carbon flux models can be explained by the global ΔAGB covariates. Using global ΔAGB maps as covariates to the carbon flux maps in Chapter 4 also resolves the issue of map selection for users.

6.2 Outlooks in global AGB map assessments

6.2.1 Upcoming global AGB maps

Global AGB maps are expected to further increase at a fast rate considering around half of all existing maps were produced in the past 3-4 years and given the upcoming EO missions for forest monitoring. The BIOMASS mission boarded by the first P-band sensor in space will produce an AGB map due in 1-2 years. What makes the mission unique is that P-band backscatter is in general more sensitive to AGB than higher frequencies. Moreover, the mission will include tomographic data used to generate 3D forest structures that enable accurate retrieval of canopy height and hence biomass (Quegan et al., 2019). The mission plans to produce global maps for each observation cycle and hence allows ΔAGB to be derived. The BIOMASS is complimented by the upcoming L-band NISAR mission and the ongoing GEDI mission in terms of attaining global coverage, see Figure 10 of Quegan et al. (2019). Similarly, the map integration of the GEDI pantropical map and the ICESat boreal map will produce the first global AGB map solely based on spaceborne LiDAR. Fusion methods of spaceborne LiDAR data already showed promising results at regional scales (Silva et al., 2021). Any upcoming global map of mangrove biomass produced using allometries specific to mangroves should also be used and integrated.

Updated and improved versions of current maps can also be expected. The next GEDI AGB map will have lesser spatial gaps than the current map once the recent footprints are integrated. For the CCI maps, the next versions would use the original ALOS-PALSAR datasets instead of annual mosaics. The CCI map producers also plan to release maps for the 2020 and 2021 epochs. Global maps produced using the gain-loss method like the carbon flux model will benefit from the recent Global Land Cover and Land Use Change dataset 2000-2020 (including forest gains) that come at 30 m spatial resolution (Potapov et al., 2022). These datasets can be used as activity data. The coarse maps based on SMOS-LVOD data may produce a version with better biomass retrieval in the boreal forests. Even the AGB retrieval method from scatterometer data tested in Santoro et al. (2022b) is about to produce maps that cover the 1990-2020 epochs.

6.2.2 Upcoming reference data

Datasets useful as reference data for AGB and ΔAGB map assessments are anticipated. The GEO-Trees initiative defined as the Forest Biomass Reference System from Tree-by-Tree Inventory Data has started. The goal of GEO-Trees involves collating a biomass reference dataset with tree-level data and LiDAR measurements and making them open-source. The initiative collaborates with the FOS which offers freely available plot data and the SuperSites system where permanent LiDAR-based globally sampled reference data is planned. GEO-Trees include not only airborne LiDAR but also terrestrial LiDAR. The latter is particularly important as it captures the whole tree structure including below the canopy. A recent study that used terrestrial LiDAR found a large underestimation of biomass in temperate forests when biomass is estimated using allometric models based on the diameter and height of trees (Calders et al., 2022). Research plots with terrestrial LiDAR surveys can be used to correct for the bias induced by allometric models. Reference data from NFIs is also promising. Countries with NFI data were found to be increasing even in developing countries, Figure 6.2 (Nesha et al., 2022). There are many countries with complete coverage NFIs (full), see Figure 6.2e. Most of them are highly forested countries like Brazil and African countries. Europe remains to have the most re-measurements but some tropical countries are catching up (Figure 6.2b). Another potential source of reference data is crowd-sourced plot data obtainable through interactive platforms like the FOS system. The Global Forest Biodiversity Initiative (GFBI) also has a similar system of reference data collection and provision through formal data requests.

6.2.3 Spaceborne and ground-based AGB integration

The integration of space-based and ground-based data for biomass estimates over unit areas is deemed necessary (Nesha et al., 2022). This thesis demonstrated an integration in the context of map assessment that includes a model-based approach to reduce map bias using global reference data. The integration can be more complicated especially when using country data as a reference. While this thesis focused mostly on the effect of plot size on the integration, there can be other causal factors such as the sampling configurations and completeness of the country data (NFIs) and even country forest definitions. Here are the considerations worth to be re-iterated and mentioning. Most are insights from our recent literature reviews and ongoing studies:

NFI sampling and configurations

Several issues may hamper the integration process (plot-map comparisons) when using NFI data. Incomplete NFI surveys are possible due to inaccessible forest areas, conflict areas and funding issues. Moreover, the way NFIs are configured has implications in the map integration process (Málaga et al., 2022). Countries have the flexibility in adopting

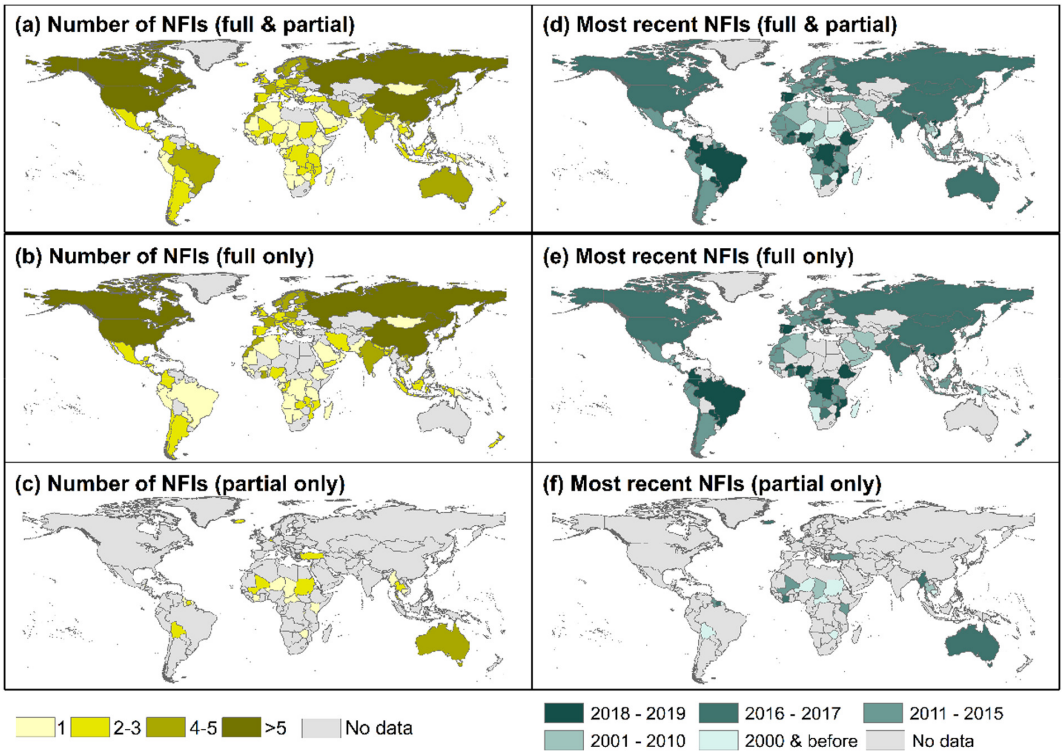

Figure 6.2: The total number of NFIs and the extent and temporality of the latest NFIs in 236 countries and territories from 2000 to 2020 according to FRA (both ongoing and completed NFI). Per country, the number of full and partial NFIs (2a); the number of full NFIs only (2b); the number of partial NFIs only (2c); most recent NFIs - both full and partial (2d); most recent NFIs - full only (2e); and most recent NFIs – partial only (2f). No data means that countries didn't implement any NFI up to the FRA 2020 report. Image and image caption from (Nesha et al., 2022)

sampling designs since the guidelines set by UN-FAO are implicit and may need updating. For instance, the guidelines do not consider the spatial autocorrelation of biomass when setting the distance between plots and subplots in fixed designs. Autocorrelation also matters when designing the dimension and shapes of transects. For countries with >1 NFIs, it is possible that the next NFI cycle is not actual re-measurements. Common reasons for this include changes in the sampling design, incomplete surveys (same as the reasons above) and missing plot markers from the first surveys. A full NFI survey often takes years to finish since surveys are implemented one region at a time especially for large countries. The uncertainties of these temporal mismatches also apply when the integration is aimed at deriving country ΔAGB statistics. The uncertainties from temporal mismatches may worsen when the order of regions between the first and second surveys is different.

Forest definition consistency

The integration also needs to consider the consistency of forest definitions between the ground data and maps. Global map producers may or may not use a forest mask to estimate pixel-level forest biomass. The pixel-level biomass of maps with and without forest mask can be very different if pixels have non-forest areas. Map users may also want biomass information from non-forest woody vegetation such as savannas, shrublands and grasslands. The commonly used forest mask datasets include tree cover data from Global Forest Change data and land cover data like the CCI Land Cover map. Similarly, countries define their own forest areas despite the standard definition set by UN-FAO that is $> 10\%$ tree cover. The variation in the forest definition of countries needs a harmonization process if the biomass information will be used and compared with map estimates (Avitabile & Camia, 2018). An example is the forest fraction correction applied in Chapter 2. Any modification of forest areas from the guidelines like setting different tree cover thresholds needs to be explicitly reported when they submit their Forest Resource Assessment to UN (Tomppo et al., 2010). Such is important information when comparing country and map-based estimates as mentioned in Chapter 3.

6.2.4 Remaining issues for the reference data

A globally sampled reference data is extremely important. Recently, Labrière et al. (2022) conducted a global biomass plot representativity analysis of around 200 sites that best represent different environmental conditions, geographical space and factors specific to forest structure. The authors pinpointed regions and countries that are under-sampled in the context of map assessment similar to Figure 6.1. These areas definitely need priority for data collection, requests for government data or the use of online map assessment tools. Alternatively, synthetic samples can be integrated to minimize under-sampling.

An unbalanced sample can be a consequence of using a collection of global samples (opportunistic) especially those with many nested plots i.e., subplots are used as reference data. One way to deal with unbalanced sampling is to account for the sampling intensity especially when used as training data for bias modelling.

Any selected reference data for map assessments need to be independent of the maps i.e., not used for map calibration. Several LiDAR-based reference data were used during the calibration phase of AGB models specific to GEDI and even BIOMASS data.

Lastly, small trees (4-9 cm in diameter) may need to be included in the plot-level biomass estimation to better account for forest understorey especially in natural forests (Le et al., 2018). This was demonstrated in producing the first Philippine AGB map in a parallel study (Araza et al., 2021b).

6.2.5 Remaining issues for the global AGB and ΔAGB maps

Uncertainty owing to sampling variability

The variability owing to the use of sample-based data (for calibration data) needs to be accounted for. Map producers are encouraged to provide the necessary metadata and McRoberts et al. (2022) describe a bootstrapping method to facilitate this.

Sensitivity to gradual biomass changes

Gradual changes in biomass from forest degradation and natural growth can be unreliable owing to our uncertainty about their magnitudes. One foreseen scenario is that map producers find better retrieval solutions for gradual changes. Otherwise, map post-processing using time series algorithms is an option. Several of these algorithms have been developed and mainly tested using Landsat archive such as *LandTrendr* (Kennedy et al., 2010), *BFAST* (Verbesselt et al., 2010) and *AVOCADO* (Decuyper et al., 2022). There exist several global AGB time series maps and additional epochs for the CCI maps are also targeted to extend its monitoring period (2010-2021). It is timely to use these AGB datasets as time series inputs to the algorithms. The time series algorithms require training and validation data of biomass time series, which can be complemented by the increasing reference data sources (see section 6.2.2).

6.3 Increasing country uptake of global AGB maps

Countries that use global AGB maps to produce carbon accounts for different reporting frameworks (UNFCCC and UNSEEA) and compliance with REDD+ requirements are expected to increase. Their uptake of global inputs depends on how well they understand the added value of the global maps on top of their national data. The following subsections describe aspects related to the increased use of global AGB maps for country-level assessments.

6.3.1 Online tools and data platforms

Online platforms and tools have helped in higher user uptake of the framework. The *Plot2Map* tool implements the framework and is publicly available through `https://github.com/arnanaraza/PlotToMap`. The tool is suited for both global and national users, especially in cases where the latter cannot share the reference data (private data) (Araza et al., 2022b). The tool includes options to incorporate country data into the reference data geodatabase and then immediately update priority areas where the current reference data are lacking. The *Plot2Map* tool has been tested in five countries namely Wales, Japan, the Philippines, Mexico and India through the Multi-Mission Algorithm

Platform (MAAP) (Albinet et al., 2019). Using *Plot2Map* in the MAAP allows transparent map assessment and inter-comparison of current global AGB maps for map selection purposes. The tool will soon include an estimation of the uncertainty from sampling variability when deriving AGB totals and assessment of ΔAGB maps.

Platforms with a collection of global AGB maps are useful. Consider this platform as a one-stop-shop of maps and other remotely sensed data with full description and metadata. Known data portals such as Google Earth Engine and Global Forest Watch only have 1-2 available global AGB maps. Platforms dedicated to ecosystem accounting like the ARtificial Intelligence for Environment and Sustainability (ARIES) are still not using recent global biomass datasets. Recently, the Open Earth Monitor Project (OEMP) was launched with the overarching goal of building a platform for global environmental applications including UNSEEA carbon accounting. The OEMP system would ingest most global AGB maps and would include functionalities to derive carbon accounting tables building up from Chapters 4 and 5 of this thesis. This system will be implemented in all European countries and several tropical countries.

6.3.2 Compliance to different carbon accounting frameworks

Countries may regularly need to compile carbon accounts for different requirements including both the UNFCCC and the UNSEEA. Aside from the UNFCCC GHG reporting, countries need to contextualize their reports for the Global Stocktake, an event where country climate change plans undergo a comprehensive evaluation. This evaluation includes carbon accounts of both national and sub-national units. The first Global Stocktake took place at the United Nations Climate Change Conference (COP) in 2021 and will be repeated in 2028 and 2033. Countries under the REDD+ programme have the option to report emissions from deforestation or degradation depending on their capacity. The main requirement for them to receive carbon credits is to properly account for emission uncertainties (Yanai et al., 2020). Helpful to meet this requirement are methodological frameworks and demonstrations in hotspot countries that show timeliness and transparency in carbon MRV (Csillik et al., 2022). Under the UNSEEA, carbon accounts of other carbon pools aside from the above-ground component are needed i.e., the below-ground and soil components. Useful in compiling these accounts are global datasets of below-ground biomass (Spawn et al., 2020; Huang et al., 2021) and soil carbon with uncertainty (Poggio et al., 2021). The below-ground biomass (BGB) datasets are both confined to single epochs and may need to be harmonized with the multi-date AGB maps to derive ΔBGB.

The actual carbon stocks and flows of the UNFCCC and UNSEEA frameworks at the country level can be compared. The UNSEEA separately accounts for managed forests (mostly plantations) that are comparable with the UNFCCC flows from human-induced changes. Existing comparisons of the two frameworks in the literature are limited to

theoretical complementation and differences (Keith et al., 2019).

6.3.3 Policy implications of the carbon accounts

The UNSEEA framework is a spatial explicit system that accounts for the loss of ecosystem services due to conversions from forest to other land uses. The UNSEEA accounts are the basis for creating, reforming and implementing policies from local to national scales (bottom-up approach). The UNSEEA also involves monetary valuation based on the physical accounts (e.g., carbon accounts) used as basis for public incentive schemes that promote sustainable forest management e.g., payment for ecosystem services (PES). Like in the REDD+ context, payment schemes under the UNSEEA context need to consider the uncertainties of physical units and monetized units when evaluating incentives. Oppositely, a disincentive system is implemented by the Organisation for Economic Cooperation and Development (OECD) that uses information on carbon emission to set appropriate carbon prices and taxes in the international market trade of goods and services. Carbon accounts will also play a role in the recent European Green Deal. Lastly, the accounts can be used for land use planning based on nature-based solutions.

The carbon emission spatial and temporal hotspots in Chapter 5 have strong policy implications. Aside from the identification of hotspot countries, local hotspot areas for each country can be monitored. Important to know such a monitoring system is the actual driver of hotspot areas. Drivers of forest disturbances have distinct spatial and temporal characteristics (Araza et al., 2021c). For instance, slash-and-burn agriculture is usually encroaching on the forests and such practice is repeated in the same forest land every 5-10 years. Deforested patches of forest lands due to landslides occur during typhoon season in steep slopes. These characteristics enabled the classification of different hotspots using emerging hotspot analysis in a parallel study to this thesis (Araza et al., 2021c). Such analysis enables the prioritization of forest protection activities especially needed by developing countries. Using such an approach will further characterize the hotspots in Chapter 5.

Summary

The global terrestrial forest and woody vegetation are vital assets of our planet because of the enormous ecosystem services they provide to mankind. Forests store and sequester atmospheric carbon, which is the most valuable ecosystem service in the context of climate change. This climate regulating service has made forest above-ground biomass (AGB) an Essential Climate Variable by the United Nations. For three decades, the development of AGB mapping is evident from the rapid increase of maps and associated scientific papers. Maps of AGB at global scales are becoming common, thanks to the availability of Earth Observation (EO) data and increasing satellite missions.

Just like any EO product, global AGB maps have a degree of uncertainty mainly because satellite data are indirect measures of biomass. Converting satellite signals into biomass requires the actual biomass information of trees, which is obtainable from in-situ forest measurements or deterministic models that also originated using these measurements. Global AGB maps should undergo independent map validation to evaluate accuracy and uncertainties. This protocol is the main stipulation of the recently published CEOS AGB Validation Protocol (Duncanson et al., 2021) and the main content of Chapter 2 (Araza et al., 2022a). To validate global AGB, reference data are needed but the common sources of these data such as National Forest Inventories (NFI), research plots and local maps from airborne LiDAR are also not error-free. Hence, map assessments (and not validation) should consider the uncertainties of both maps and reference data before their AGB comparisons. Chapter 2 showed how reference data were selected and how uncertainties from plot measurement and allometric model error, sampling error and temporal mismatch were estimated. These uncertainty estimates were used to derive weighted biomass averages. Four global AGB maps were assessed at 0.1° aggregated level (around 10 km), the preferred spatial resolution of global climate and carbon modellers that use AGB maps as model inputs. The aggregation also allowed random errors to be reduced and the systematic differences between AGB estimates of maps and reference data (map bias) to be modelled. Chapter 2 demonstrated a model-based prediction of map bias as a function of biomass, tree cover, and other environmental variables. This step allowed bias adjustment in areas where bias is predicted with confidence and further allowed the estimation of AGB totals and their uncertainty while considering the spatial correlation of map errors.

Recently, multi-date AGB maps at global scales were produced. The biomass change (ΔAGB) derived from these maps can have a higher user interest and a wider range of applications than maps of single epochs. Map-based ΔAGB are derived either from differencing two maps or using a baseline map, forest changes data, and associated carbon emission and removal (gain-loss method). The ΔAGB maps also need to be assessed. In Chapter 3, four ΔAGB maps representing the past decade were assessed and intercompared using reference data from NFI and LiDAR at different aggregation levels preferred by map users (Araza et al., 2023). The uncertainty of reference data was again estimated and accounted for in the aggregation step using the Chapter 2 methodology. There was an agreement between the map-based ΔAGB and LiDAR data from 100 m until 25 km since their estimates both come from maps. Such agreement was observed until 1 km when using NFI as a reference mainly because of sparse NFI plots at coarser aggregates. Map-map comparisons revealed that maps all captured AGB losses from deforestation hotspot regions, but maps showed ΔAGB disagreement in highly forested regions such as the Amazon basin. This key finding has an implication on whether current ΔAGB maps are reliable for national applications. Chapter 3 included recommendations towards a more suitable global reference data for ΔAGB assessment.

Using global ΔAGB maps and other dynamic environmental EO data, the 2010-2018 carbon fluxes were predicted and used for carbon accounting under the United Nations System of Environmental-Economic Accounting (UNSEEA) (Chapter 4, Araza et al., under review). This EO-based carbon accounting was demonstrated in five case countries using the Chapter 3 reference data. An ensemble of machine learning was used to predict carbon fluxes with prediction intervals. Aside from the global AGB maps, changes in height and tree cover were found as important covariates for all countries, while topography was found important for tropical countries. The predicted ΔAGB was aggregated to forest classes recommended by the UNSEEA framework while considering the spatial correlation of map errors. In parallel, the representativity of the reference data was assessed in environmental feature space. Results from this analysis served as the basis for recommendations on how to mitigate the effects of under-sampling when implementing EO-based carbon accounting. Recommendations include the option to add synthetic samples and the exclusion of certain UNSEEA classes unsupported by the reference data sample. The carbon accounting is targeted to be updated annually and for more case countries.

For Chapter 5, carbon emission hotspots were identified and reported for all African countries (Csillik et al., 2022). The main inputs of this system were a bias-adjusted AGB map (Chapter 2) as baseline biomass and forest disturbance alerts that allowed the estimation of succeeding emissions (Reiche et al., 2021). The associated carbon emission uncertainty considered the standard deviation layer of the baseline AGB and the omission-commission errors of the forest disturbance data. The main finding of the study was the seasonal pattern of emissions where 76% of all emissions in Africa happened in the early

months of 2020. Highlighted also was the spatial pattern of carbon loss which can be the focus of forest protection. The estimated emissions and the workflow can be used for transparent and efficient monitoring of ΔAGB for national reporting and accounting purposes.

This thesis emphasized the need to assess the increasing global AGB products under a framework that accounts for uncertainties of the reference dataset used. This thesis also showed that associated uncertainties need to be accounted when using global AGB maps for national applications. The map assessment framework and the *Plot2Map* tool provide the means for global AGB maps to be more reliable (plot-map integration) for global and national applications. While the need for additional reference data is highly emphasized in the thesis especially for ΔAGB assessment, the analysis and information about priority areas for additional data is equally important. Also important is the quantification of sampling uncertainties from using global samples. These and other outlooks mentioned in Chapter 6 are all helpful to further understand the current plot-map and map-map differences revealed in this thesis.

Supplementary materials

Supplementary materials of Chapter 2

Table S1. Metadata of the plot dataset.

ID	Scale	Type	Count	Avg. inventory year	Avg. size (ha)	Avg. AGB (Mg ha -1)	Dominant biome	Reference
AFR2	Regional	Research plot	593	2007	0.69	118.51	Tropical rainforest	Lindsell & Klop (2013)
AFR4	Local	Research plot	110	2005	0.25	13.72	Tropical mountain system	De Vries et al. (2012)
AFR5	Local	Research plot	71	2008	0.16	118.6	Tropical rainforest	Laurin et al. (2016)
AFR6	Local	Research plot	24	2008	0.54	358.85	Tropical rainforest	Willcock et al. (2014)
AFR7	Local	Research plot**	19	2008	0.64	32.58	Tropical rainforest	Lewis et al. (2013)
AFR8	National	NFI	105	2010	0.25	187.67	Tropical moist forest	Carreiras et al. (2012)
AFR9	Local	Research plot	41	2006	0.12	164.16	Tropical dry forest	Carreiras et al. (2013)
AFR10	Local	Research plot	18	2012	0.13	216.29	Tropical rainforest	Mitchard et al. (2011)
AFR11	National	NBS*	726	2012	0.08	266.36	Tropical rainforest	Drichi (2003); Avitabile et al. (2012)
AFR12	National	NFI	108	2009	0.67	371.28	Tropical rainforest	Avitabile et al. (2012)
AFR13	Local	Research plot	25	2012	1	243.52	Tropical rainforest	Mitchard et al. (2009)
AFR14	Local	Research plot	88	2008	0.13	70.37	Tropical dry forest	Mitchard et al. (2009)
AFR15	National	NFI	680	2011	0.13	25.35	Tropical mountain system	Vieilledent et al. (2016)
AFR FOS	Regional	Research plot**	527	2013	0.44	287.77	Tropical rainforest	?
ASI CH	National	NFI	1267	2008	0.1	129.39	Subtropical mountain system	Zhang et al. (2019)
ASI FOS	Local	Research plot	15	2006	0.4	308.6	Tropical rainforest	?
ASI IND	Local	Research plot	96	1996	1	272.43	Tropical rainforest	Ramesh et al. (2010)
ASI PH	National	NFI	1210	2004	0.43	58.04	Tropical rainforest	Araza et al. (2021a)
ASI1	Regional	NFI	2903	2008	0.05	108.19	Tropical mountain system and rainforest	Avitabile et al. (2016)
ASI2	Local	Research plot	119	2011	0.11	181.03	Tropical dry forest	WWF and OBf, 2013
ASI3	Local	Research plot	92	2007	1	163.45	Tropical rainforest	Morel et al. (2011)
ASI4	Local	Research plot	70	2010	0.02	208.48	Tropical dry forest	Wijaya et al. (2015)
ASI5	Local	Research plot	28	2015	3.07	35.93	Tropical rainforest	Slik et al. (2013)
ASI8	Local	Research plot	31	2008	0.02	304.81	Tropical dry forest	Murdiyarso et al. (2009)
ASI9	Regional	Research plot	74	2012	0.13	309.16	Tropical rainforest	Avitabile et al. (2016)
AUS FOS	Local	Research plot	3	2004	0.68	168.37	Tropical dry forest	?
AUS INJ	National	NFI	5001	2000	0.25	76.66	Subtropical steppe	Tickle et al. 2016
AUS1	National	NFI	9113	2008	0.13	268.57	Tropical dry forest	Auscover (2016)
CAM FOS	Local	Research plot	19	2012	0.97	248.66	Tropical rainforest	?
CAM1	National	NFI	4045	2006	0.16	82.3	Tropical dry/moist/rain forest	de Jong (2013)
EU FOS	Regional	Research plot	170	2014	0.27	194.02	Boreal coniferous forest	?
EU1	National	NFI	16819	2011	0.01	76.37	Temperate broadleaf and Boreal forests	NA
EU2	National	NFI	58185	2003	0.2	60.45	Mediterranean forests	NA
EU3	National	NFI	3021	2013	0.06	190.98	Temperate oceanic forest	Schelhaas et al. (2014)
EU4	National	NFI	5967	2007	0.06	176.07	Temperate broadleaf and Mediterranean forests	NA
NAM1	National	NFI	588	2010	0.04	96.01	Boreal coniferous forest	Liang et al. (2015)
NAM2	Local	Research plot	75	2004	0.04	293.55	Temperate mountain system	Luyssaert et al. (2008)
NAM3	Regional	NFI	586	2010	0.03	130.93	Temperate continental forest	NA
NAM4	Regional	NFI	2798	2010	0.04	79.42	Temperate continental forest	NA
SAM FOS	Regional	Research plot**	161	2010	0.47	333.25	Tropical rainforest	?Mitchard et al. (2014)
SAM2	National	Research plot**	281	2013	0.34	208.65	Tropical rainforest	dos Santos et al. (2019)
SAM3	National	NFMS***	111	2011	0.13	395.3	Tropical rainforest	Brown et al. (2014)
SAM4	Local	Research plot	7	2014	0.15	352.51	Tropical rainforest	Goodman et al. (2013)
SAM5	Local	Research plot	23	2014	0.6	144.11	Tropical rainforest	NA
SAM TAP	Local	Research plot	46	2009	0.25	217.71	Tropical rainforest	Bispo et al. (2014)
SAM BAJO	Local	Research plot	122	2017	0.26	74.52	Tropical rainforest	a Pacheco-Pascagaza et al. (2018)

*National Biomass System and ***National Forest Monitoring System, both comparable to NFIs; **Include key long-term sites supported by the Amazon Forest Inventory Network (RAINFOR) and African Tropical Rainforest Observatory Network (AfriTRO

Table S2. Summary statistics of plot data per major climatic zone and continent used for 2000, 2008/10, and 2017 map comparisons, respectively.

Major climatic zone and continent	Plot (n)	Avg. year	Avg. size $\pm SD(ha)$	Avg. AGB (min. - max) (Mg ha^{-1})
Boreal	**5783**	**2008.5**	**0.02 ±0.06**	**56.4 (0 - 360.4)**
Europe	5443	2008.5	0.02 ±0.06	54.1 (0 - 360.4)
N.America	340	2009.0	0.04 ±0	93.3 (0.1 - 247.2)
Subtropical	**56880**	**2003.4**	**0.19 ±0.04**	**55.8 (0 - 1212.5)**
Asia	1149	2008.0	0.1 ±0	114.6 (0.3 - 691.5)
Australia	3938	2001.8	0.2 ±0.1	113 (0 - 1212.5)
C.America	50	2006.0	0.16 ±0	50.8 (0.4 - 223)
Europe	51743	2003.6	0.19 ±0.02	45.2 (0 - 629.3)
Temperate	**17892**	**2005.8**	**0.11 ±0.08**	**133.8 (0 - 5676.1)**
Australia	1223	2007.4	0.08 ±0.04	298.4 (0.5 - 5676.1)
Europe	14480	2005.1	0.12 ±0.08	129.3 (0 - 973)
N.America	2189	2008.9	0.04 ±0.02	71.1 (0 - 937.1)
Tropical	**12307**	**2006.8**	**0.22 ± 0.42**	**109.7 (0 - 869.8)**
Africa	3534	2007.5	0.3 ±0.19	150.3 (0 - 863.1)
Asia	3900	2006.9	0.17 ±0.23	84.5 (0 - 830.9)
Australia	238	2005.3	0.32 ±1.62	31 (0 - 238.5)
C.America	3990	2006.0	0.16 ±0	67.3 (0 - 859.2)
S.America	645	2008.8	0.46 ±1.33	330.6 (18 - 869.8)

Major climatic zone and continent	Plot (n)	Avg. year	Avg. size $\pm SD(ha)$	Avg. AGB (min. - max) (Mg ha^{-1})
Boreal	**11865**	**2010.6**	**0.02 ±0.05**	**67.7 (0 - 429.4)**
Europe	11289	2010.6	0.02 ±0.05	66.2 (0 - 429.4)
N.America	576	2010	0.04 ±0.01	97.1 (0.2 - 273.4)
Subtropical	**63297**	**2003.7**	**0.19 ±0.05**	**79.6 (0 - 2096.4)**
Asia	1268	2008	0.1 ±0.01	131.5 (7.9 - 691.5)
Australia	9746	2003.2	0.19 ±0.11	138.4 (0 - 2096.4)
C.America	51	2006	0.16 ±0.01	70.3 (11.3 - 223)
Europe	52232	2003.6	0.19 ±0.02	67.4 (7.2 - 647.3)
Temperate	**26674**	**2008**	**0.09 ±0.12**	**179.9 (0.1 - 6822.4)**
Australia	2978	2010.7	0.08 ±0.1	475.9 (0.3 - 6822.4)
Europe	20290	2007.3	0.1 ±0.14	147.8 (0.2 - 1071.2)
N.America	3406	2009.8	0.04 ±0.02	93.2 (0.1 - 937.1)
Tropical	**14345**	**2007.4**	**0.25 ± 0.51**	**150.2 (0 - 1268.8)**
Africa	4285	2008.4	0.31 ±0.43	191.7 (0 - 980.6)
Asia	4449	2006.7	0.21 ±0.39	118.1 (2.1 - 1268.8)
Australia	316	2006.9	0.29 ±1.41	53.4 (0 - 276.2)
C.America	4006	2006	0.16 ±0.06	98.8 (16.2 - 865.2)
S.America	1289	2010.7	0.41 ±1.07	306.9 (1.5 - 876.8)

Major climatic zone and continent	Plot (n)	Avg. year	Avg. size $\pm SD(ha)$	Avg. AGB (min. - max) (Mg ha^{-1})
Boreal	**11661**	**2010.6**	**0.02 ±0.03**	**74.8 (3.7 - 437.1)**
Europe	11088	2010.6	0.02 ±0.03	73.3 (3.7 - 437.1)
N.America	573	2010.0	0.04 ±0	104.8 (7 - 281.9)
Subtropical	**21004**	**2006.8**	**0.18 ±0.06**	**101.9 (8.6 - 2103.4)**
Asia	1149	2008.0	0.1 ±0	136.4 (25.4 - 691.5)
Australia	2472	2009.7	0.14 ±0.15	186 (8.6 - 2103.4)
C.America	50	2006.0	0.16 ±0	83.9 (28.8 - 223)
Europe	17333	2006.3	0.19 ±0.04	87.7 (25.4 - 651.9)
Temperate	**20889**	**2009.6**	**0.06 ±0.13**	**204.7 (7.3 - 6823.9)**
Australia	2716	2011.3	0.08 ±0.1	519.8 (12.8 - 6823.9)
Europe	14970	2009.1	0.07 ±0.14	168.7 (7.3 - 1080.4)
N.America	3203	2010.0	0.04 ±0.01	105.8 (16 - 465.8)
Tropical	**11545**	**2008.1**	**0.22 ± 0.5**	**181.3 (7 - 991.5)**
Africa	3395	2009.2	0.32 ±0.22	234.1 (7 - 991.5)
Asia	3113	2008.2	0.09 ±0.4	139.3 (25.9 - 703.3)
Australia	217	2008.7	0.3 ±1.7	70.4 (20.4 - 283)
C.America	3609	2006.0	0.16 ±0.06	125.8 (43.5 - 862.8)
S.America	1211	2010.6	0.4 ±1.08	326.5 (27.1 - 883.8)

Table S3. List of global and pantropical biomass maps epoch 2000 onwards.

AGB map	Spatial scale	Forest mask data	Pixel size	Epoch	RS and in situ data	Open access (OA)	OA uncertainty layer	Reference
Avitabile	pantropical	-	1km	2000-2008	Fusion of Saatchi and Baccini Pantropical	Yes	Yes	Avitabile et al. (2016)
Baccini Global	global	GLAS data and tree canopy cover thresholds	30m	2000	GLAS, MODIS, SRTM	Yes	Yes[1]	GlobalForestWatch (2002)
Baccini Pantropical	pantropical	-	1km	2007-2008	GLAS, MODIS, SRTM	Yes	Yes	Baccini et al. (2012)
Chen	global	GLC2000 forest and VCF threshold	1km	2007-2008	MODIS-NBAR	No	No	Chen et al. (2018)
CCI Biomass	global	-	100m	2017	ALOS2 PALSAR2, Sentinel 1	Yes	Yes	Santoro & Cartus (2019)
Hu	global	MODIS Land Cover	1km	2004	GLAS, MODIS, SRTM	No	No	Hu et al. (2016)
Kindermann	global	FRA forest area	55km	2005	FAO statistics, modelled NPP	No	No	Kindermann et al. (2008)
Liu	global	MODIS Land Cover forest	27.5km	1993-2012	L-VOD	No	No	Liu et al. (2015)
GEOCARBON	global	GLC2000 forests	1km	2007-2010	Fusion of Avitabile and Santoro	Yes	Yes	Avitabile et al. (2014); Santoro et al. (2015)
GlobBiomass	global	-	100m	2010	ALOS-PALSAR, ENVISAT, ASAR	Yes	Yes	Santoro et al. (2020)
Ruesch-Gibbs	global	GLC2000 forests	1km	2000	GLC2000, IPCC data	No	No	Ruesch & Gibbs (2008)
Saatchi	pantropical	-	1km	2000	GLAS, MODIS, QSCAT, SRTM, forest plots	No	No	Saatchi et al. (2011b)
Yang	global	Per continent based on secondary data	1km	2005	VCF, GLASS LAI, forest plots, regional maps	No	No	Yang et al. (2020)
Zhang	global	GFC tree cover threshold	1km	2000	Fusion of local and global maps	No	No	Zhang & Liang (2020)

[1]Currently accessible at Google Earth Engine (`https://code.earthengine.google.com/11b2fe70fd7019cd70fafa375bb3a525`),but will be re-uploaded to its original repository at global forest watch platform.

Fig. S1. Comparison of the assessments when using the grid cells from the current approach and after strict filtering to mitigate preferential sampling. The latter involved the following steps: (1) Use of the plot dataset used to assess the 2010 GlobBiomass map, and the 30-m Hansen 2010 tree cover (TC) as a proxy for AGB variability (Avitabile & Camia, 2018). (2) Compute the mean TC of the grid cell and at plot locations, and their difference (mean plot TC – mean grid cell TC). The standard error of the mean TC at plot locations is also computed. Assuming the difference is normally distributed, a grid cell is accepted if the mean of the exhaustively sampled TC is within the 90% confidence interval of the true mean TC. (3) Assess the effect of preferential sampling through GlobBiomass assessments using grid cells from strict filter and the current approach. The slight differences between the two comparisons, even for the >300 Mg ha^{-1} bins, indicate that preferential sampling is unlikely to have much impact on our analysis. This can be attributed to our use of more NFIs than research plots and the fact that many of the research plots used are within forests which visually exhibit homogeneous canopy cover.

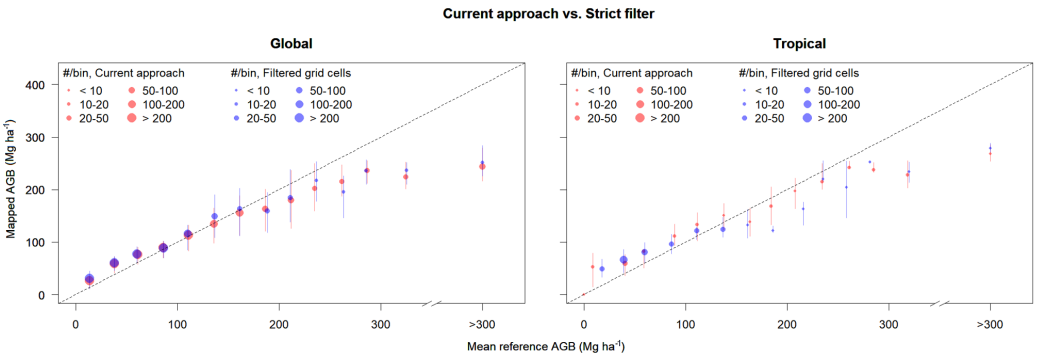

Fig. S2. Locations of all possible pantropical grid cells and those selected under both the current approach and strict filtering in high AGB tropical areas wherein 77% of the grid cells chosen under the current approach are also chosen after strict filtering. The average number of plots inside selected 0.1° grid cells is 10.89 for the current approach and 11.59 for the strict filter.

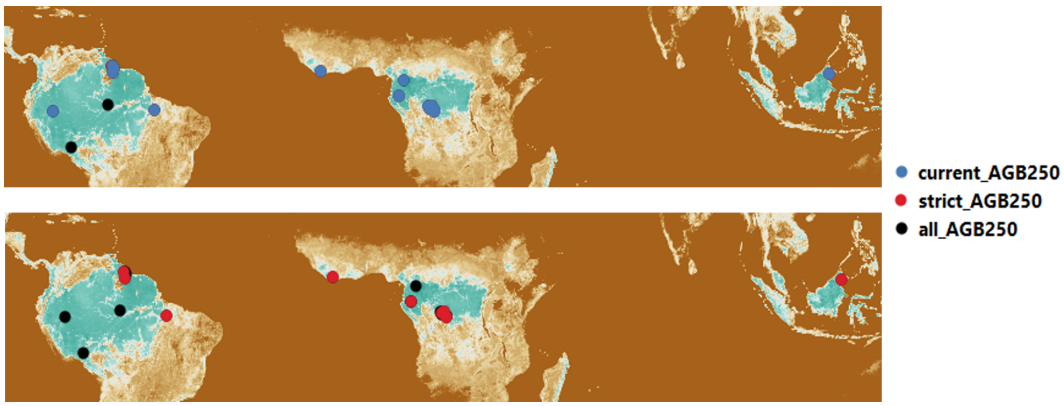

Table S4. Summary results for the weighted RF models used for bias modelling with the explained trend (%) and the rank and percentage of the Variable Importance Measure (VIM) values per covariate. The covariates in the Baccini model exclude the SD layer (currently only available for the pantropics) to enable global bias prediction.

RF model	Explained trend (%)	VIM rank	VIM proportion (%)
Baccini	36	Above-ground Biomass map (AGB), Tree Cover (TC), Slope (SL), Aspect (ASP)	49,32,12,7
GEOCARBON	24	AGB, TC, Standard Deviation layer (SD), SL, ASP	30,27,17,15,11
GlobBiomass	27	TC, AGB, SD, SLP, ASP	27,26,19,17,11
CCI Biomass	33	AGB, TC, SD, SL, ASP	26,22,19,17,17

Fig. S3. Partial Dependence Plots of predicted bias as a function of a covariate pair in the CCI Biomass map: (a) AGB map and tree cover at 0.1° ; and (b) slope and aspect at original map pixel size of 100 m.

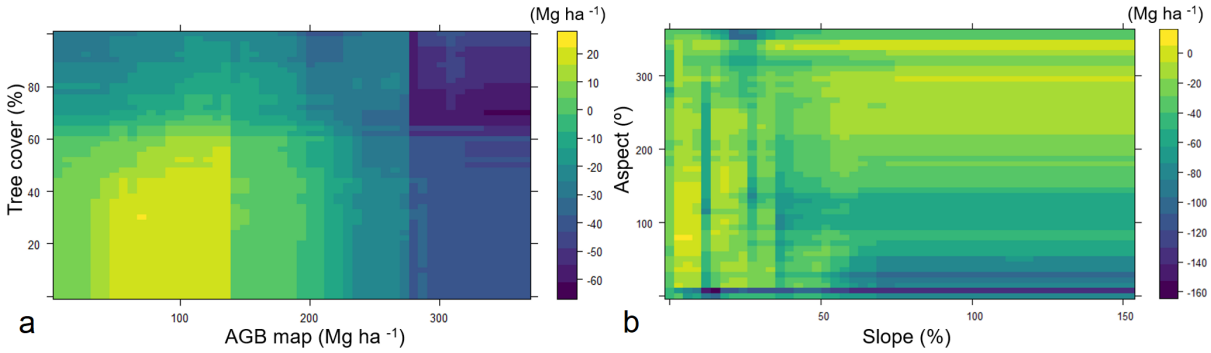

Fig. S4. Plot-to-map comparison for the bias-corrected AGB maps indicating an increase in map accuracy (relative to Fig. 4). The comparisons used a third of the total grid cells, independent to the ones used for the bias modelling: Baccini=2187, GEOCARBON=2174, GlobBiomass=2067 and CCI Biomass=871. Each circle represents an AGB bin and its size indicates the number of plot data while the whiskers correspond to the 25^{th} and 75^{th} quartile range of the map AGB.

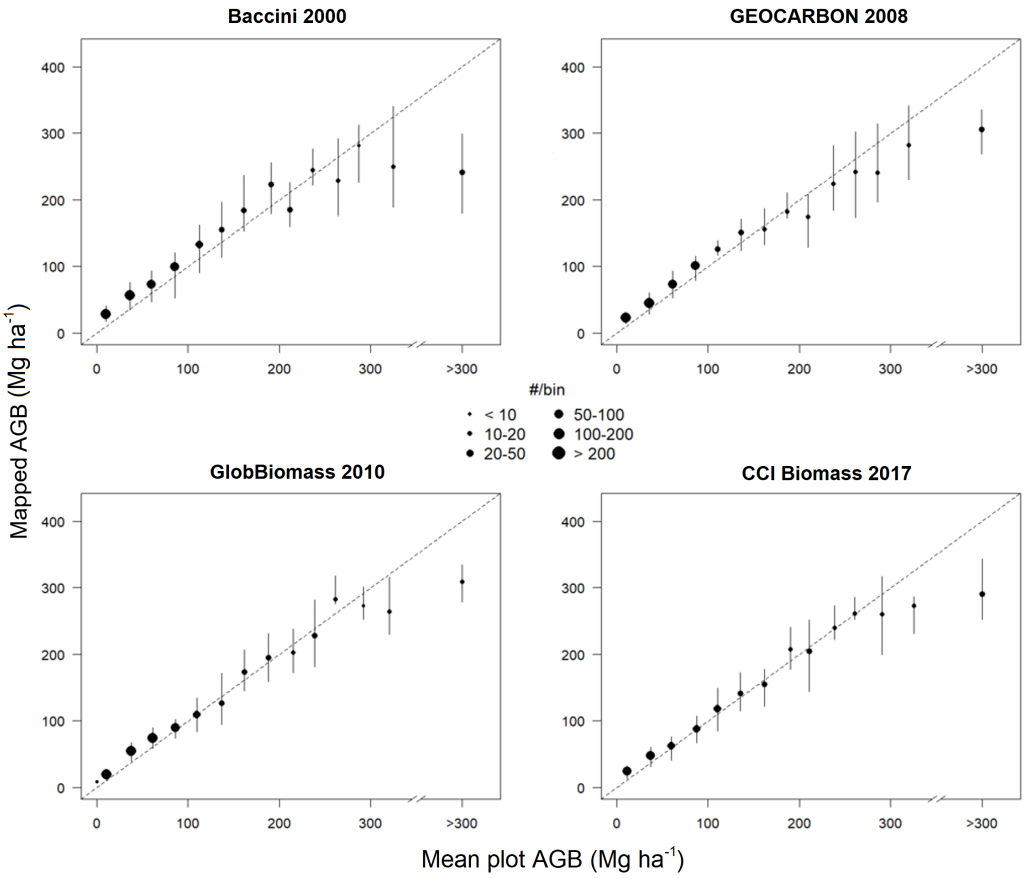

Fig. S5. Variogram models (VMs) fitted to data from the four AGB maps: (1) default VMs, (2) VMs adjusted by plot measurement error, and (3) convoluted VMs.

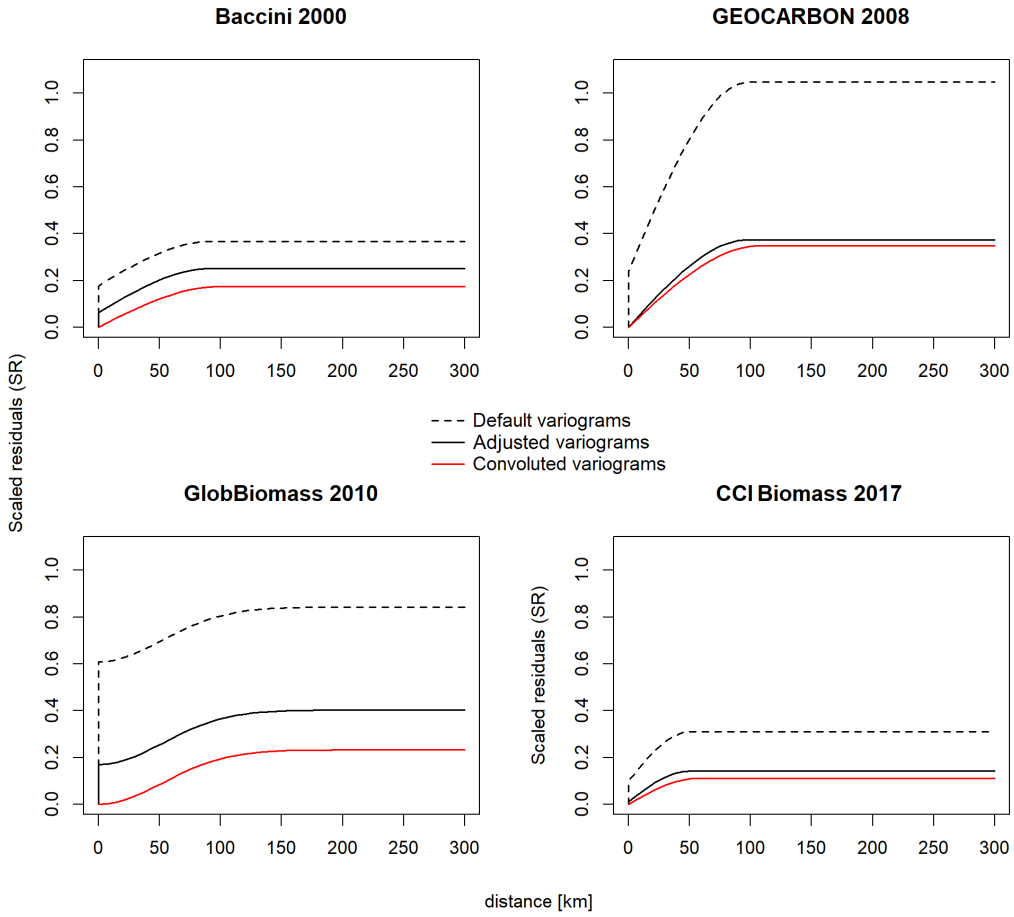

Fig. S6. The SD layers at original map pixel size (default SD) and the modified SD layers at 0.1° used for uncertainty aggregation in the pantropics. The modified maps account for spatial autocorrelation when averaging from original map resolution to 0.1°.

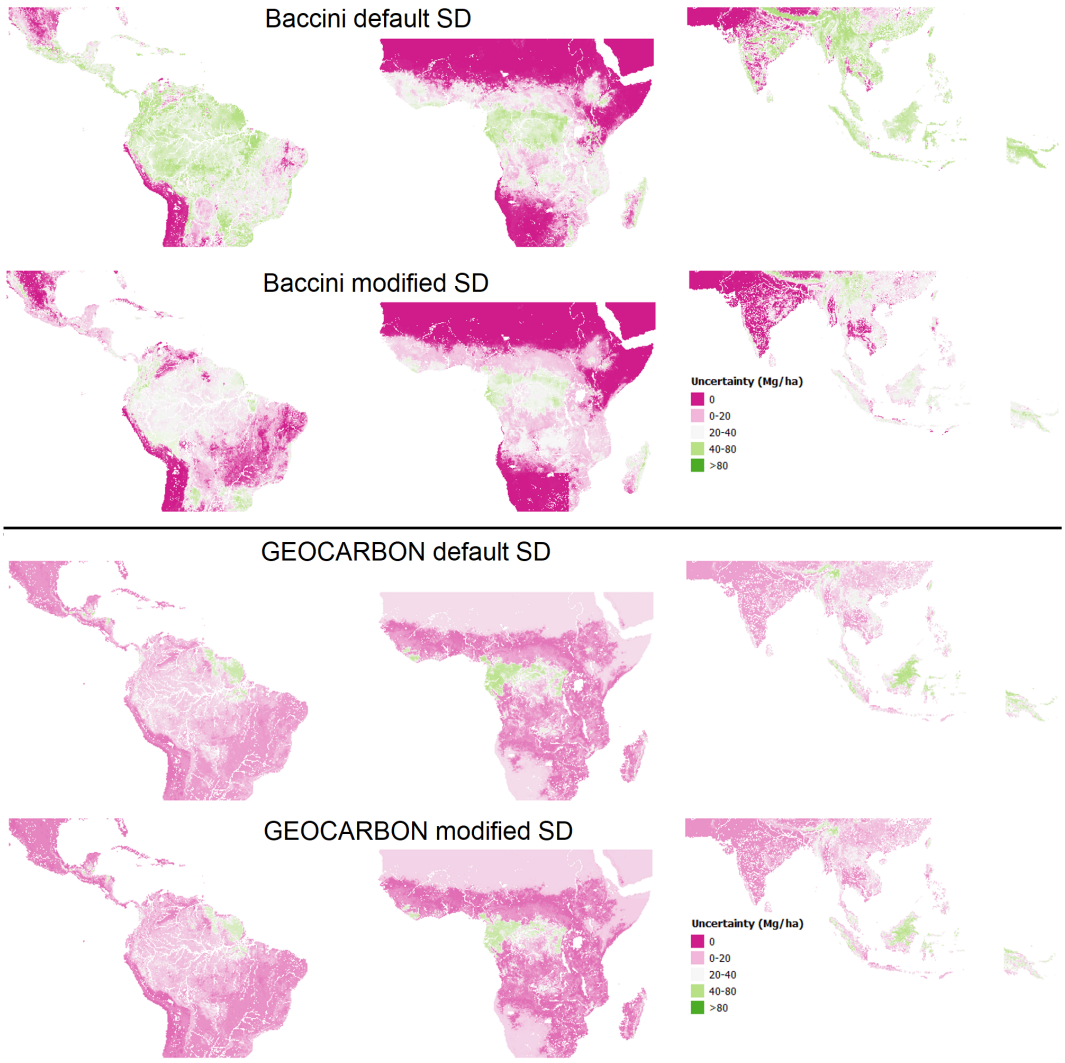

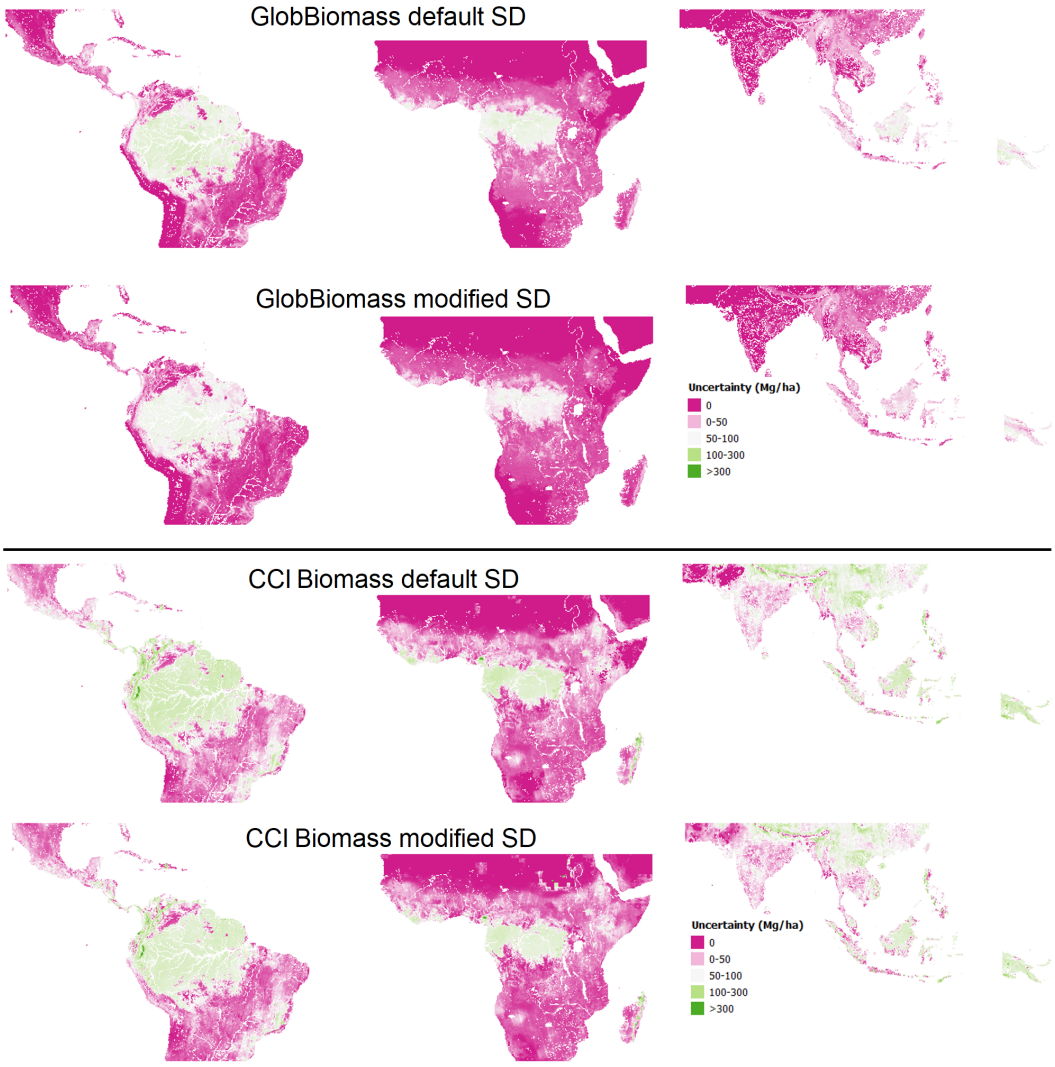
GlobBiomass default SD
GlobBiomass modified SD
CCI Biomass default SD
CCI Biomass modified SD
Uncertainty (Mg/ha)
0
0-50
50-100
100-300
>300

Supplementary materials of Chapter 3

Table S1. List of ΔAGB reference data and their key details. Data sources with uncertainty estimate all followed error propagation methods using Monte Carlo approach. These included propagation of tree measurement parameters (diameter, height and wood density) and the allometric model parameters for the plot data; and the parameters of the height-AGB regression model for LiDAR datasets.

Country	Data type	Dominang forest type	Measurement n (n)		Inventory year	Original size (ha)	Mean ΔAGB (Mg ha^{-1})	SD estimate	Eco-region	Reference
Belgium	NFI	Plantation	3	668	2003-2019	0.1	-2.8	no	Temperate broadleaf and mixed forests	Schelhaas et al. (2018)
Netherlands	NFI	Plantation	3	1562	2007-2019	0.04	11.8	no	Temperate broadleaf and mixed forests	Schelhaas et al. (2018)
Philippines	NFI	Natural	2	587	2003-2014	0.5	2.8	yes	Tropical rainforest	Araza et al. (2021a)
Sweden	NFI	Plantation	3	12887	2008-2017	0.03	4.9	yes	Boreal forest	Johnson et al. (2010)
Alaska	LiDAR	Natural	2	48552	2013-2019	0.5	1.76	yes	Tropical rainforest	Longo et al. (2016)
Brazil	LiDAR	Natural	2	28607	2011-2018	0.5	-17.8	yes	Tropical rainforest	Longo et al. (2016)
Bulgaria	LiDAR	Plantation	2	1946	2006-2016	1	0.12	yes	Temperate conifer forests	Dmitrov et al., under preparation
Czech Republic	LiDAR	Plantation	2	75	2014-2020	0.05	2	yes	Temperate conifer forests	Brovkina et al. (2017)
Costa Rica	LiDAR	Natural	2	9342	2010-2018	1	-0.6	no	Tropical rainforest	Cushman et al. (2021)
Poland	LiDAR	Plantation	2	770	2005- 2019	1	6.5	no	Temperate broadleaf and mixed forests and Boreal forests	Laurin et al. (2020)
Spain	LiDAR	Plantation	2	54058	2010-2016	0.5	0.86	no	Mediterranean forests	Mariano et al., under preparation
USA	LiDAR	Natural	2	110939	2013-2019	0.5	1.76	yes	Temperate broadleaf and Boreal forests	Johnson et al. (2010)

Table S2. List of ΔAGB map data sources and their key details. It can be noticed that the maps are different mainly in terms of remote sensing data, pixel size, forest mask and validation.

Maps	Forest mask	Pixel size	Selected epochs	RS and in situ data	Open access (OA)	Uncertainty layer	Validation	Reference
CCI	-	100 m	2010, 2018	ALOS2-PALSAR2, Sentinel 1	Yes	Yes	Each epoch using independent plots	Santoro & Cartus (2019)
Flux	>30% tree cover	100 m	2010, 2019	CCI 100 m 2010 AGB, GFC data and IPCC activity data	Yes	No	None	Harris et al. (2021)
JPL	>30% tree cover	10 km	2009-2011, 2017-2019	MODIS, ICESat, ALOS-PALSAR	Yes	No	Selected epochs using FRA country statistics	Xu et al. (2021)
LVOD	-	25 km	2011, 2019	L-band VOD from SMOS, GlobBiomass 2010	No	No	None	Yang et al. (2022)

Fig. S1. Histograms of AGB for each reference data highlighting changes through time. The numerous LiDAR data (hundred thousand pixels) is randomly sampled to emphasize the changes.

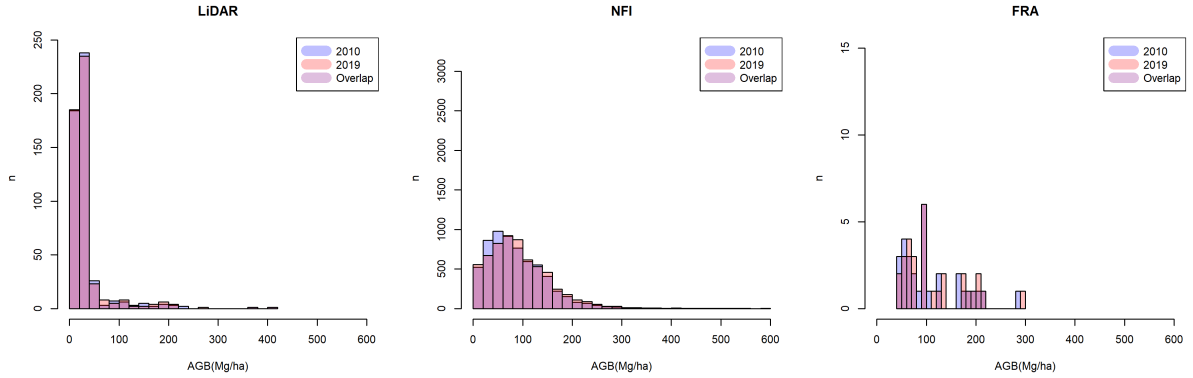

Fig. S2. (a) Key country reference data and (b) sample grid cell with plot locations for NFI (left) and LiDAR (right).

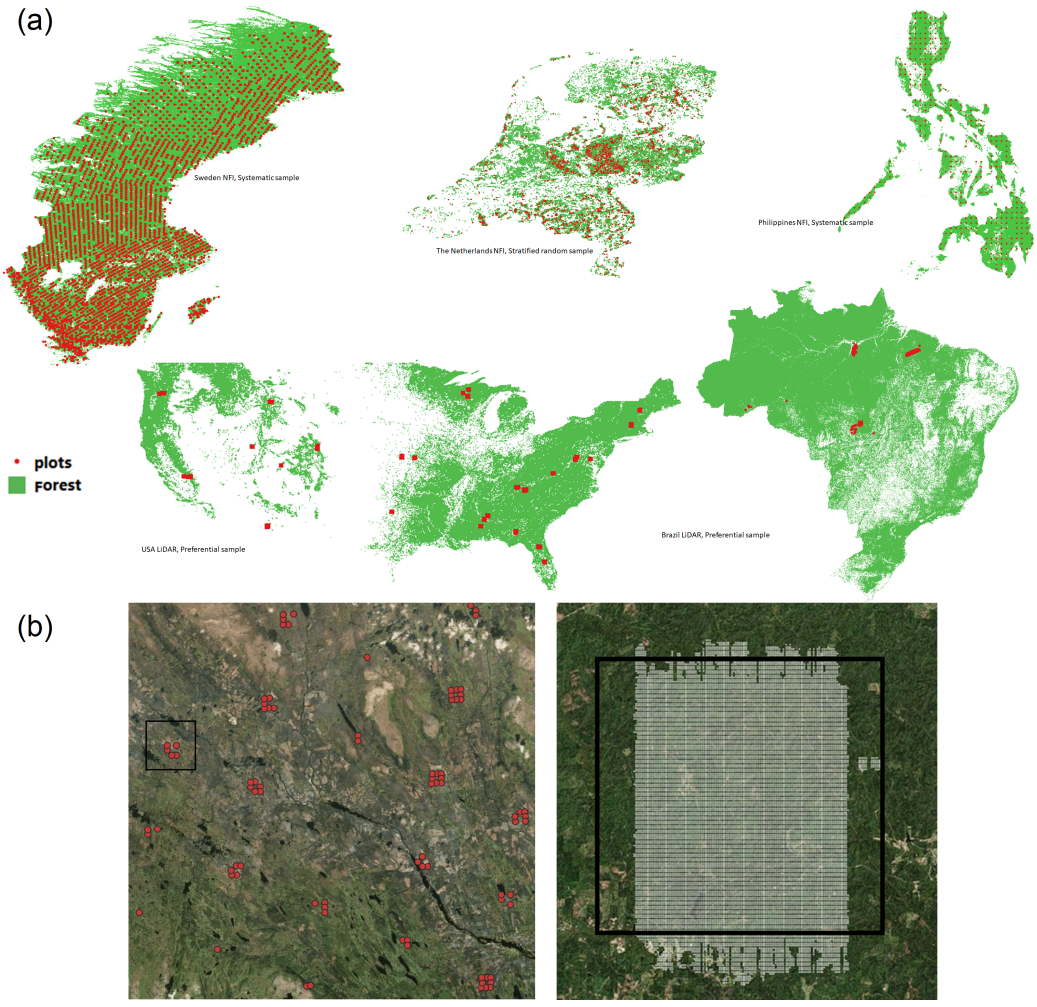

Table S3. FRA data of the selected countries based on quality filter.

Country	Code	Region	NFI 2010 capacity	NFI 2020 capacity	RS 2020 capacity	Δ forest (thousand ha)
Austria	AUT	Europe	Good	Good	Low	35.95
Canada	CAN	North and Central America	Very good	Very good	Very good	-394.11
Switzerland	CHE	Europe	Very good	Very good	Low	34.39
Germany	DEU	Europe	Very good	Very good	Low	10
Finland	FIN	Europe	Very good	Very good	Low	167
France	FRA	Europe	Very good	Very good	Low	834
India	IND	Asia	Very good	Very good	Very good	2664
Mexico	MEX	North and Central America	Very good	Very good	Very good	-1251.23
Netherlands	NLD	Europe	Very good	Very good	Good	-3.98
Norway	NOR	Europe	Very good	Very good	Low	78
New Zealand	NZL	Oceania	Very good	Very good	Very good	44.47
Portugal	PRT	Europe	Very good	Very good	Low	60
Russian Federation	RUS	Europe	Very good	Very good	Very good	176
Sweden	SWE	Europe	Very good	Very good	Low	-93
United States of America	USA	North and Central America	Very good	Very good	Low	1075
Canada	CAN	North and Central America	Very good	Very good	Very good	-394.11
Chile	CHL	South America	Good	Good	Very good	1485.44
Ghana	GHA	Africa	Intermediate	Intermediate	Very good	42.78
Haiti	HTI	North and Central America	Low	Low	Very good	-4
Sri Lanka	LKA	Asia	Good	Good	Very good	9.4
Myanmar	MMR	Asia	Good	Good	Very good	-2897.11
Senegal	SEN	Africa	Good	Good	Very good	-400
Venezuela	VEN	South America	Low	Low	Good	-1274.1
Ghana	GHA	Africa	Intermediate	Intermediate	Very good	42.78
Indonesia	IDN	Asia	Good	Very good	Very good	-7526

Fig. S4. Latitudinal profiles of ΔAGB using 25 km maps.

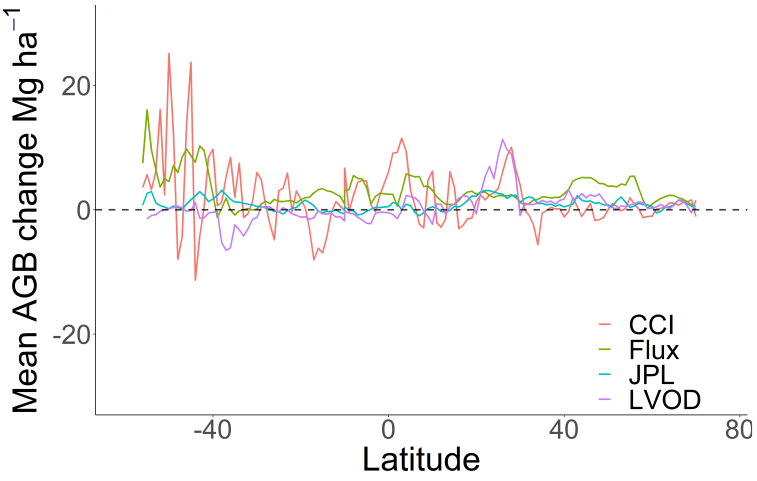

Fig. S5. Regions where most maps depict net AGB loss (1-3) and net AGB gains (3-5). The third inset concerns regions that show consistent net AGB gains among maps in China and consistent net AGB loss in Indonesia and nearby countries. Here we used 10 km maps (LVOD was resampled) for better visualization purposes.

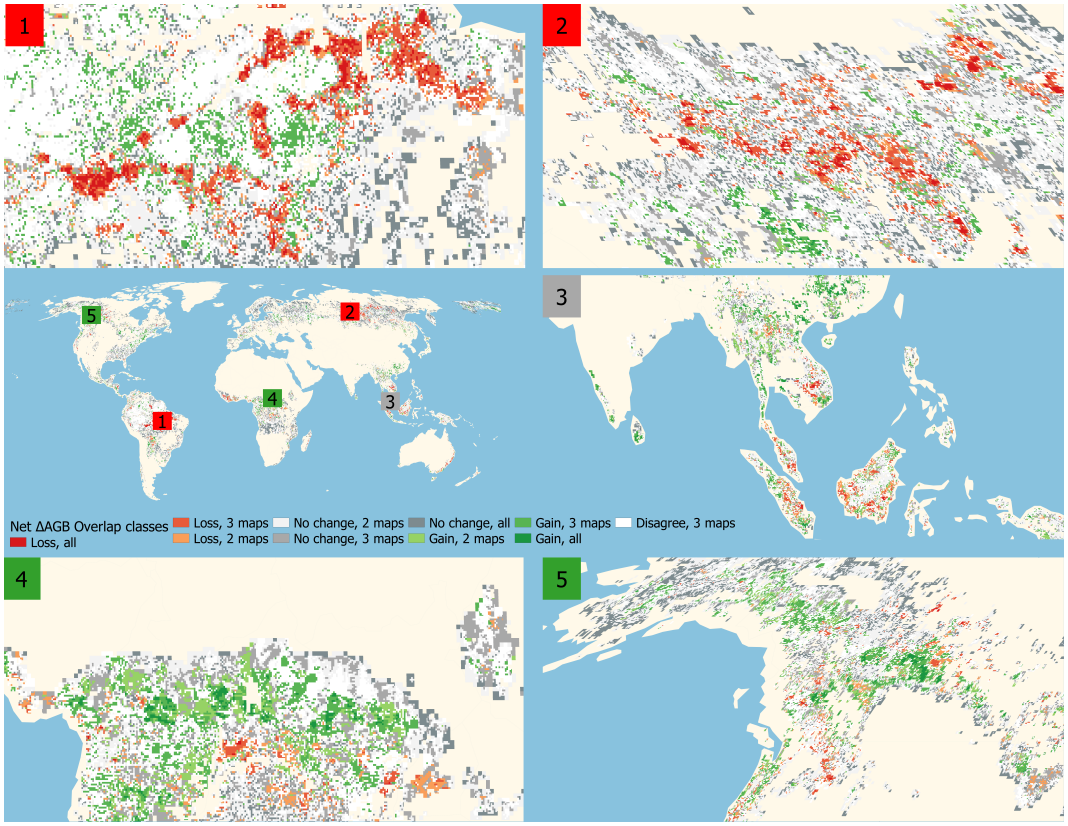

Fig. S6. Cross-correlation results (r) among the four maps at 25 km aggregation level.

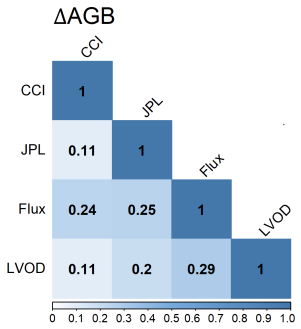

Table S4. Summary of the findings on the use of current reference data relative to key aspects of map assessment.

Map assessment aspect	Reference data	Advantages	Disadvantages	Issues/opportunities
Regional to Global representativeness	NFI	Nationwide coverage; Reasonable coverage in temperate and boreal forest regions	Missing multi-date NFI datasets in many tropical regions, NFI data access limitations	*Plot2map* tool can be used for map assessment if original plot data cannot be shared
	LiDAR	Different regions covered mostly from dedicated research programs (US, Europe, Australia, Brazil)	Limited regional coverage (almost no multi-date LIDAR in Africa)	Supersite measurement efforts such GEO-Trees using LiDAR data
	FRA	Potentially wider coverage	Rely on country-reported estimates - varying type and quality data sources used	Forest definition applies
Local representativeness (grid cells)	NFI	NFI sampling designs and remeasurements cover local variability (e.g., <10 km)	Many data are excluded for coarser-scale assessments, small plots and representativeness varies by NFI design	Local mapping at the grid cell level
		Re-measured research plots often of high quality	Available only to limited areas	Forest fraction correction needed
		-	-	Time periods
	LiDAR	LiDAR change footprints cover full "landscapes" including non-forests	Some >10 km grid cells partially covered (footprint edges)	Forest fraction correction needed
	FRA	-	Not locally representative	-
Issues of AGB change estimates	NFI	AGB change estimation can be provided by source	Missing uncertainty estimates from source data, data quality varies	Tree-level data for localized error propagation
		-	Limited quality control for remeasurements	Weighted average if nested plots
	LiDAR	Most suitable source for assessing biomass change integrating with space-based data	Missing SD layers	SD as a quality requirement
	FRA	Focus on "high capacity" countries	Only "proxies" for uncertainty, and many countries not covered	Recommendation to include country SD estimate

Supplementary materials of Chapter 4

Table S1. Reference data technical description

Country	Data type	Dominant forest type	Measurement (n)	Count (n)	Inventory year	Size (ha)	Mean ΔAGB (Mg ha^{-1})	SD estimate	Eco-region
Brazil	LiDAR	Natural	2	28607	2011-2018	1	-17.8	yes	Tropical rainforest
Netherlands	NFI	Plantation	3	1562	2007-2016	0.04	11.8	no	Temperate broadleaf and mixed forests
Philippines	NFI	Natural	2	587	2003-2014	0.5	2.8	yes	Tropical rainforest
Sweden	NFI	Plantation	3	12887	2008-2013	0.03	4.9	no	Temperate broadleaf and Boreal forests
USA	LiDAR	Natural	2	110939	2013-2019	1	1.76	yes	Temperate broadleaf and Boreal forests

Figure S1. Sample locations to highlight plot configurations of reference data.

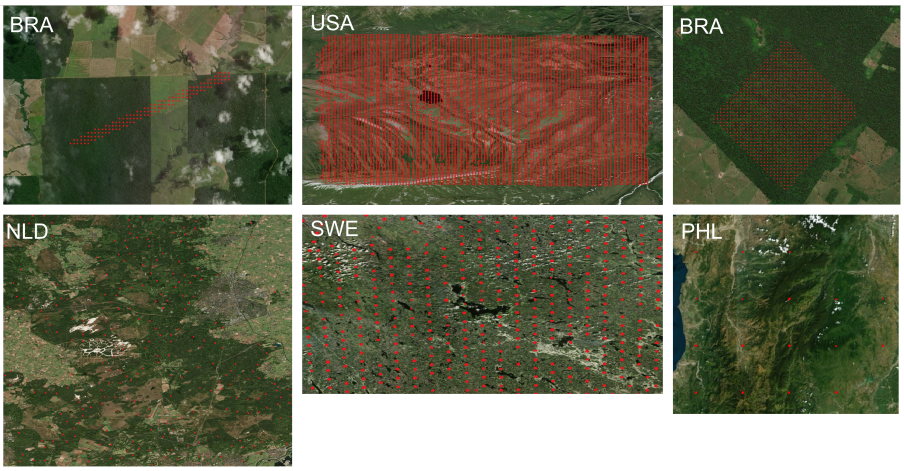

Other base learners

We used extreme gradient boosting modelsChen & Guestrin (2016) (XGM) as base learner. Like other boosting models, XGM is capable of extrapolating beyond the range of the training data i.e., the under-sampled areas in our case (see Figure S4). This boosting model also grows decision trees sequentially and create an ensemble after final predictions. Unlike other boosting models, XGM can optimize how trees are grown by applying weighted decision trees as tree pruning basis. Moreover, XGM extends the optimization of an objective function from first-order to second-order Taylor expansion. The objective function (i.e., loss gradient) is the optimization metric that should be as minimized as possible after model fitting. The model can also perform

Table S2. Hyperparameter tuning results

Country	Model	Final parameters
BRA	SVM	C=0.2546
	XGM	nrounds=2000, max_depth=5, eta=0.03, gamma=0.01, colsample_bytree=0.75, min_child_weight=5, subsample=0.5
	RFM	min.node.size=5, mtry=18
NLD	SVM	C=0.0523
	XGM	nrounds = 500, max_depth = 5, eta = 0.01, gamma = 0.5, colsample_bytree = 0.75, min_child_weight = 10, subsample = 0.5
	RFM	min.node.size=5, mtry=2
PHL	SVM	C=0.0314
	XGM	nrounds=500, max_depth=5, eta=0.01, gamma=0.5, colsample_bytree=0.75, min_child_weight=1, subsample=0.5
	RFM	min.node.size=5, mtry=2
SWE	SVM	C=15.032
	XGM	nrounds = 500, max_depth = 5, eta = 0.01, gamma = 0.1, colsample_bytree = 0.75, min_child_weight = 10, subsample = 0.5
	RFM	min.node.size=5, mtry=12
USA	SVM	C=2.864
	XGM	nrounds=2000, max_depth=5, eta=0.1, gamma=0.01, colsample_bytree=0.75, min_child_weight=1, subsample=0.5
	RFM	min.node.size=5, mtry=10

parallel computing, data imputation and, like RFM, minimizes model overfitting but using a regularization term instead of decorrelating trees. Another base learner is support vector machineHearst et al. (1998) (SVM), an algorithm that tries to find the line or boundary (hyperplane) that best fits the data. Instead of separating two classes like in classification, the SVM is trying to fit the data optimally. The SVM tries to find the hyperplane that minimizes the distance between the data points and the hyperplane, while also maximizing the distance between the hyperplane and the nearest data points. The model is controlled by a regularization term (C) or a trade-off between the complexity of the model and the amount of training error that is tolerated.

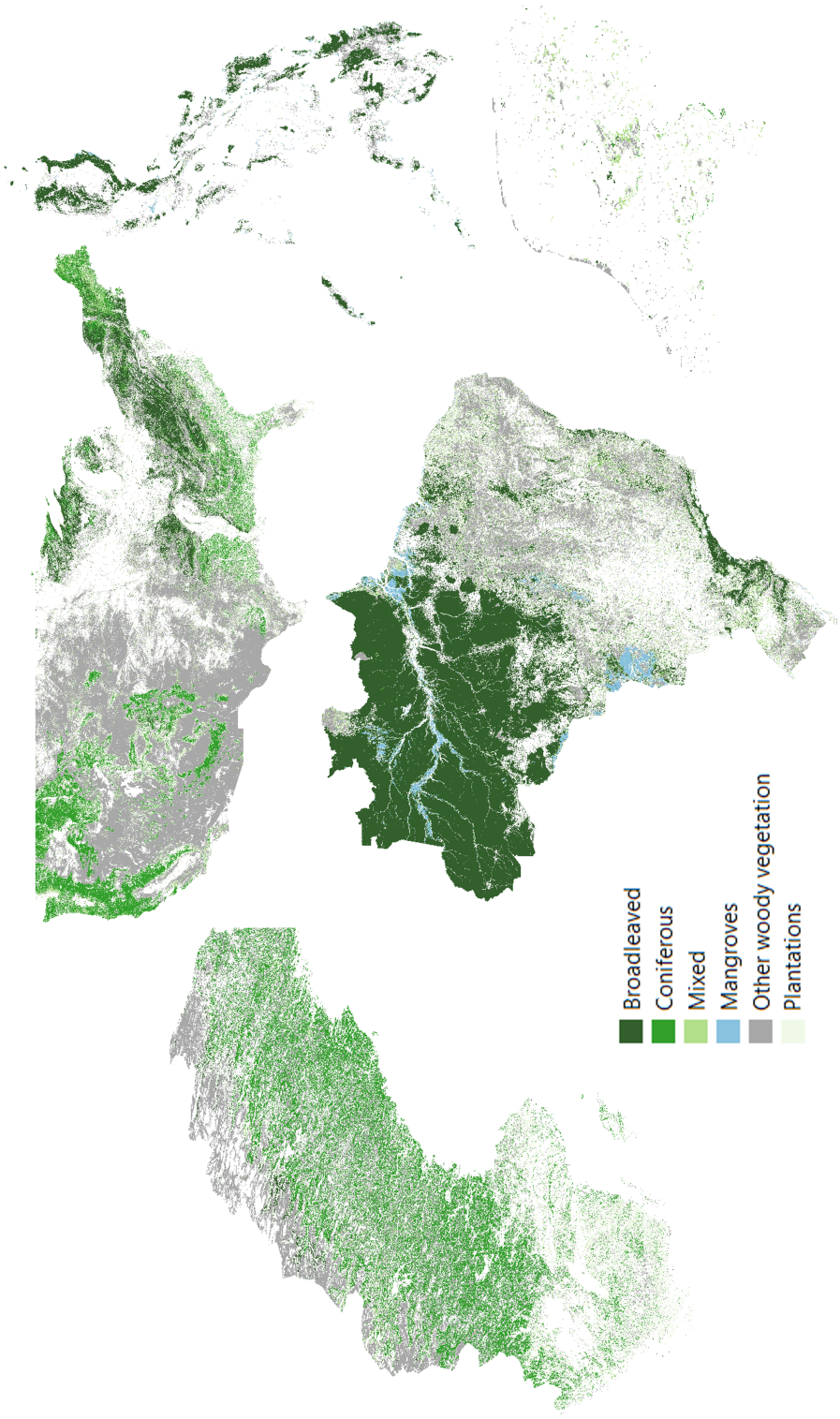

Figure S2. Forest classes of each country. We used QGIS 3.4.3 to layout this map.

Table S3. Reclassification of land cover datasets into Level 1 UN-SEEA classes. Note that the 2nd column denotes the actual class number of the land cover dataset.

CCI Land Cover Defourny et al. (2012)	50 = Tree cover, broadleaved, evergreen, closed to open (>15%) 70-72 = Tree cover, needleleaved, evergreen, closed to open (>15%) 90 = Tree cover, mixed leaf type (broadleaved and needleleaved) 100 = Mosaic tree and shrub (>50%) / herbaceous cover (<50%) 160 = Tree cover, flooded, fresh or brackish water 170 = Tree cover, flooded, saline water 180 = Shrub or herbaceous cover, flooded, fresh/saline/brakish water	1 = Broadleaved forest 2 = Coniferous forest 3 = Mixed forest 4 = Mangroves
CORINE Büttner (2014)	23 = Broadleaved forest 24 = Coniferous forest 25 = Mixed forest 26 = Natural grassland	1 = Broadleaved forest 2 = Coniferous forest 3 = Mixed forest 5 = Other woody vegetation
IIASA data Lesiv et al. (2022)	31 = Planted forests (rotation >15 years) 32 = Plantation forest (rotation <15 years) 40 = Oil palm plantations years 53 = Agroforestry	6 = Forest plantation

Figure S3. Correlation matrix of covariates for the five case countries.

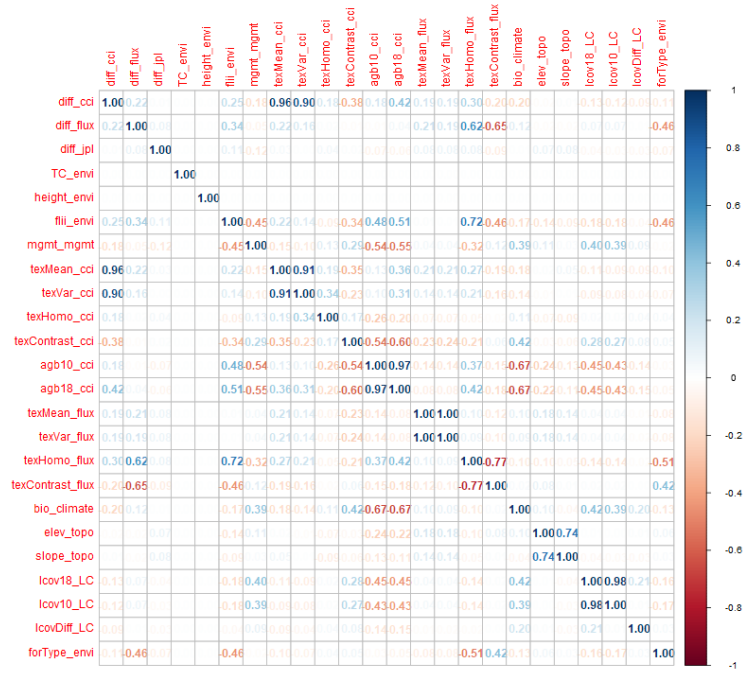

Brazil

Residual spatial correlation modelling

The resulting carbon flux map from the spatial predictions were multiplied by 0.49 to derive carbon fluxes. The carbon flux map residuals $MR(i)$, defined as map-reference data carbon flux difference at plot location i, was scaled by the map SD (SD_{m}); this assumes the SD of the residuals is proportional to the SD_{m} at that point (equation 6.1). This scaling was assumed to transform the residuals to homoscedasticity $SR(x)$. For carbon stocks, we used the existing SD layer of CCI 2010 multiplied by 0.49.

$$SR(x) = \frac{MR(x)}{SD_m(x)} \tag{6.1}$$

Models of semivariances, $\gamma(h)$ in equation 6.2, allow estimation of the spatial correlation of SR at spatial lag h, where x is a plot location, and the errors are assumed to be statistically stationary:

$$\gamma(h) = \frac{1}{2}\,\mathrm{Var}[SR(x) - SR(x+h)] \tag{6.2}$$

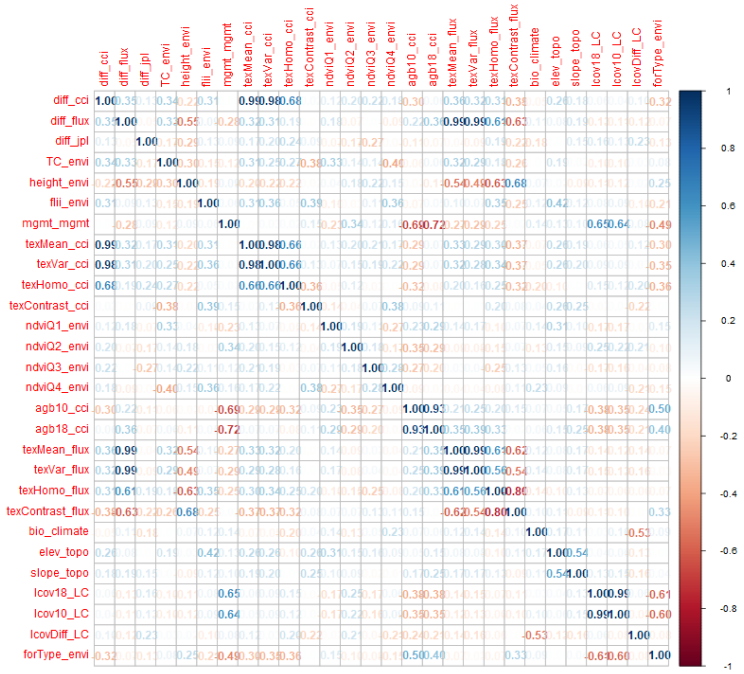

Netherlands

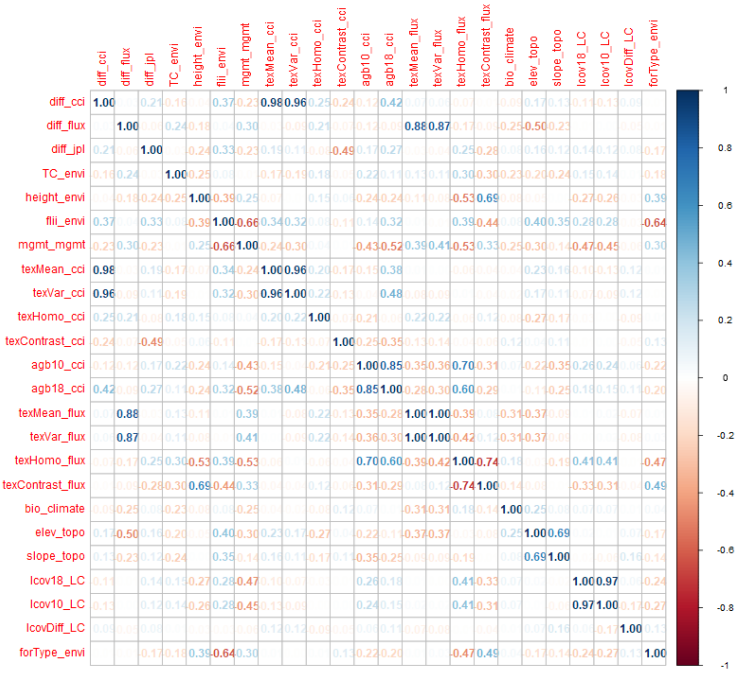

Philippines

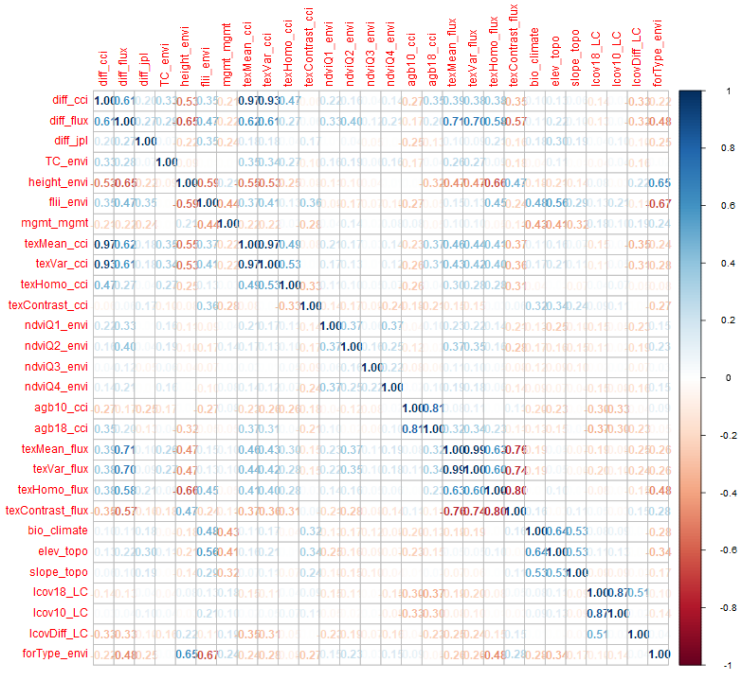
diff_cci
diff_flux
diff_jpl
TC_envi
height_envi
flii_envi
mgmt_mgmt
texMean_cci
texVar_cci
texHomo_cci
texContrast_cci
ndviQ1_envi
ndviQ2_envi
ndviQ3_envi
ndviQ4_envi
agb10_cci
agb18_cci
texMean_flux
texVar_flux
texHomo_flux
texContrast_flux
bio_climate
elev_topo
slope_topo
lcov18_LC
lcov10_LC
lcovDiff_LC
forType_envi
1
0.8
0.6
0.4
0.2
0
-0.2
-0.4
-0.6
-0.8
-1

Sweden

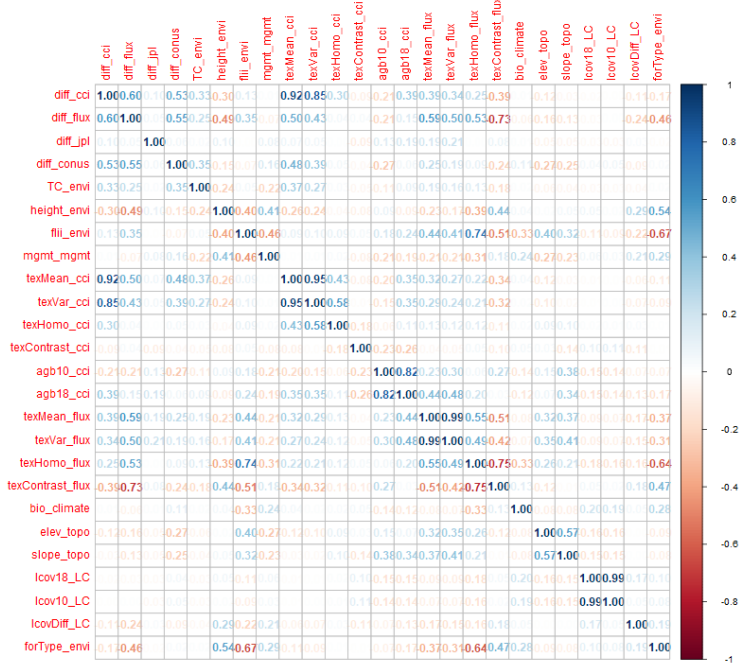
diff_cci
diff_flux
diff_jpl
diff_conus
TC_envi
height_envi
flii_envi
mgmt_mgmt
texMean_cci
texVar_cci
texHomo_cci
texContrast_cci
agb10_cci
agb18_cci
texMean_flux
texVar_flux
texHomo_flux
texContrast_flux
bio_climate
elev_topo
slope_topo
lcov18_LC
lcov10_LC
lcovDiff_LC
forType_envi
1
0.8
0.6
0.4
0.2
0
-0.2
-0.4
-0.6
-0.8
-1

USA

Figure S4. Proportion of under-sampled areas per UN-SEEA carbon accounting classes for each country

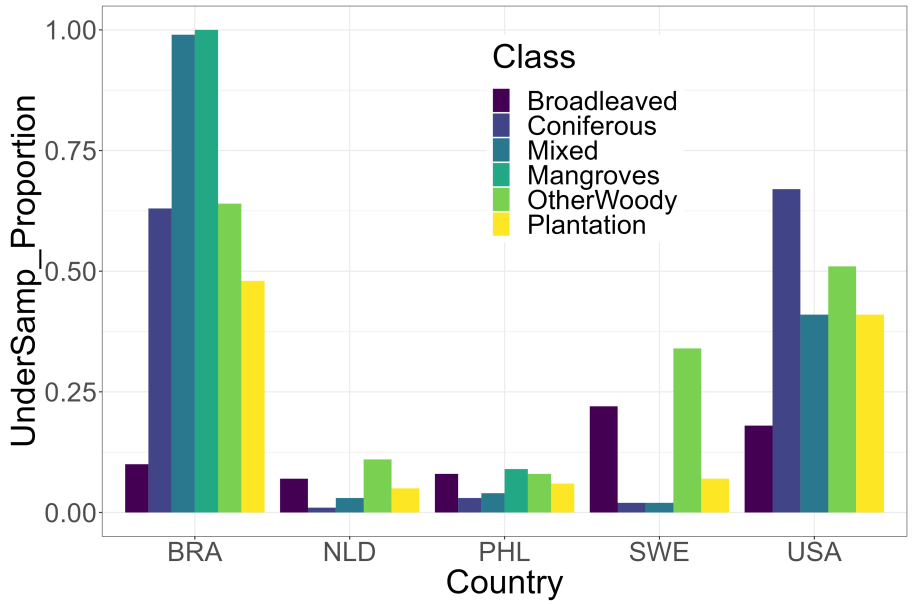

Figure S5. Prediction comparison of random forest and extreme gradient boosting when using systematic and preferential samples.

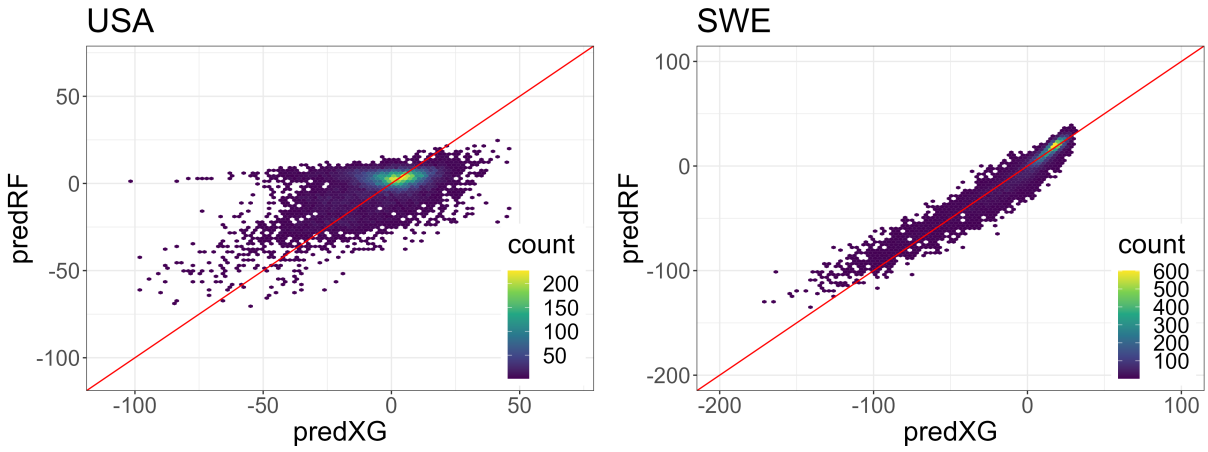

Figure S6. Variograms of stocks and flow residuals.

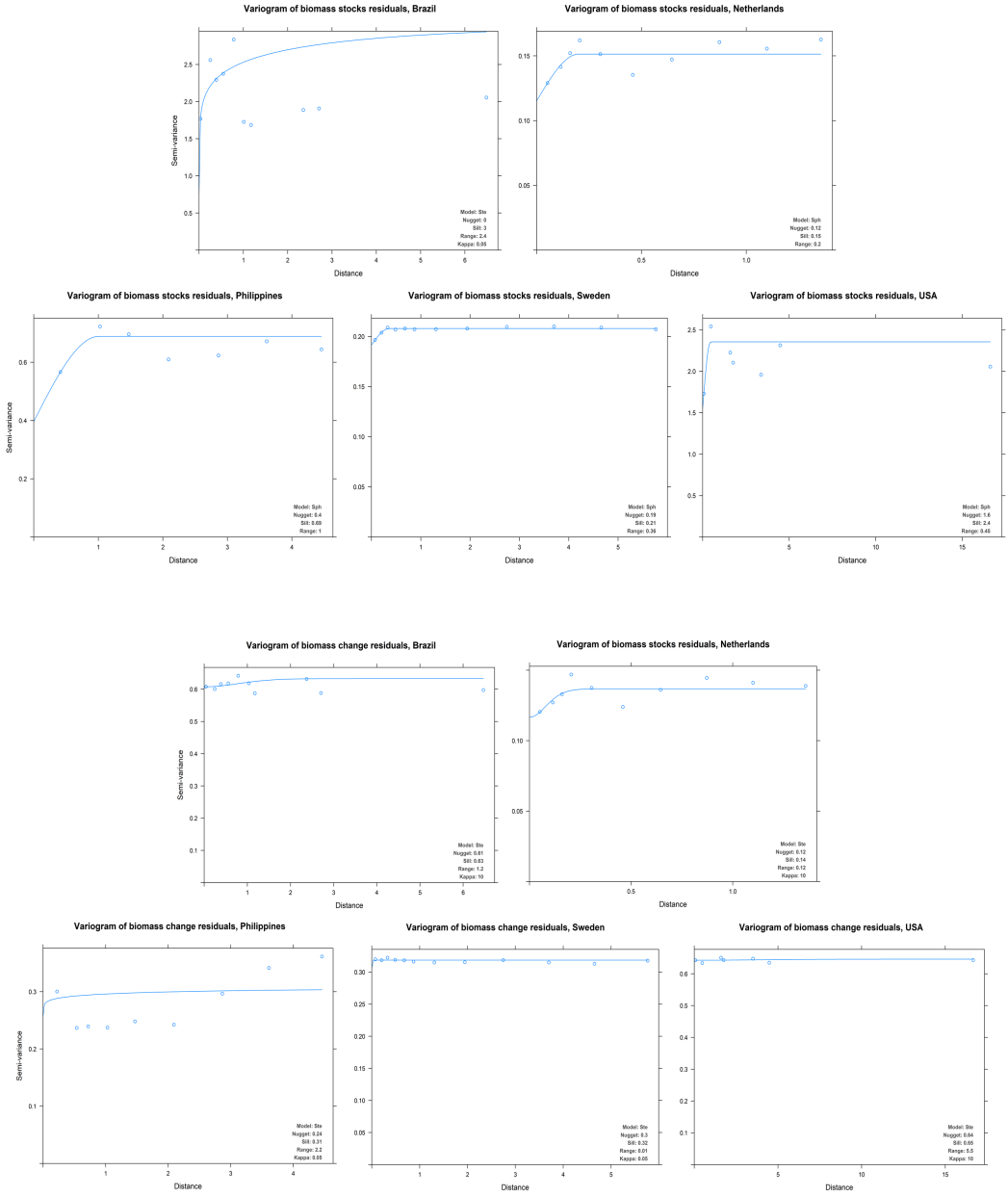

Figure S7. Impact of pseudo loss data to the under-sampled areas(a) with and (b) without pseudo loss samples. The randomly selected pseudo samples are limited to 10% of the total country reference data and sampled within the under-sampled areas in (b). We used *ggplot2* in R to layout this map.

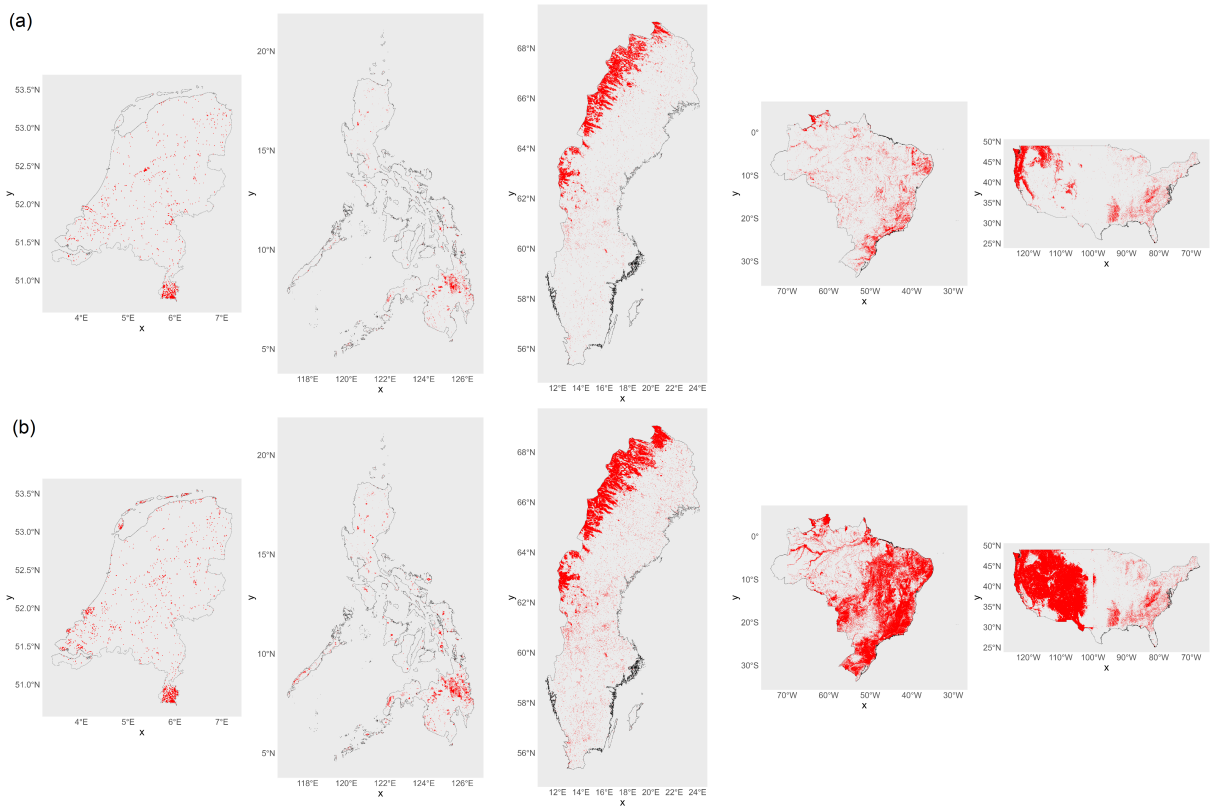

Table S4. Carbon accounting table with emissions and removals. The emissions are further disaggregated whether as a result of land use change (forest conversion) of emissions within forest (likely forest degradation). Aside from the 2010 land cover dataset, we used the associated 2018 land cover for this disaggregations.

Countries	UN-SEEA classes	Forest area 2010 ('000 ha)	Net emissions (C Mg ha $^{-1}$)	Emissions from land-use change (C Mg ha $^{-1}$)	% contribution	Emissions within forest (C Mg ha $^{-1}$)	% contribution	Net sequestration (C Mg ha $^{-1}$)	Net fluxes (C Mg ha $^{-1}$)
Brazil	Broadleaved	3485634	-127.43	-127.26	99.87%	-0.17	0.13%	84.25	-43.18
	Coniferous	153277	-3543.74	-3543.74	100.00%	0.00	0.00%	3520.98	-22.76
	Mixed	735145	-479.66	-479.66	100.00%	0.00	0.00%	323.64	-156.02
	Mangroves	166677	-1.81	-1.79	98.90%	-0.02	1.10%	1.33	-0.48
	Other woody vegetation	1140095	-673.62	-664.73	98.68%	-8.88	1.32%	270.12	-403.50
	Plantation	1320002	-738.59	-728.48	98.63%	-10.10	1.37%	317.41	-421.18
Netherlands	Broadleaved	89	-0.002	0.00	98.78%	0.00	1.22%	0.01	0.002
	Coniferous	103	-0.001	0.00	98.97%	0.00	1.03%	0.001	0.001
	Mixed	530	-0.002	0.00	99.09%	0.00	0.91%	0.02	0.02
	Other woody vegetation	1109	-0.21	-0.20	98.98%	0.00	0.00%	0.23	0.02
	Plantation	1206	-0.02	-0.01	98.96%	0.00	1.04%	0.04	0.02
Philippines	Broadleaved	57334	-4.95	-4.90	99.09%	0.00	0.00%	8.81	3.87
	Coniferous	3008	-0.21	-0.21	98.93%	0.00	0.00%	0.35	0.14
	Mixed	4962	-0.80	-0.77	95.23%	0.00	0.00%	0.52	-0.28
	Mangroves	5487	-2.58	-2.50	96.88%	0.00	0.00%	1.48	-1.10
	Other woody vegetation	54494	-5.48	-5.48	100.00%	0.00	0.00%	7.31	1.83
	Plantation	15199	-4.91	-4.46	90.90%	-0.45	9.10%	4.05	-0.86
Sweden	Broadleaved	4588	-0.04	-0.04	98.46%	0.00	1.54%	0.36	0.32
	Coniferous	109355	-7.19	-7.11	98.85%	-0.08	1.15%	12.78	5.59
	Mixed	8396	-0.40	-0.40	100.00%	0.00	0.00%	1.81	1.41
	Other woody vegetation	88573	-17.80	-17.76	99.80%	-0.04	0.20%	16.53	-1.27
	Plantation	61354	-5.04	-4.95	98.11%	-0.10	1.89%	4.36	-0.68
USA	Broadleaved	529916	-61.89	-59.60	96.29%	-2.30	3.71%	249.90	188.01
	Coniferous	959568	-418.90	-398.79	95.20%	-20.12	4.80%	394.94	-23.96
	Mixed	665106	-161.11	-161.11	100.00%	0.00	0.00%	126.41	-34.70
	Other woody vegetation	2351583	-292.89	-276.10	94.27%	0.00	0.00%	197.65	-95.23
	Plantation	1084568	-420.88	-408.62	97.09%	-12.26	2.91%	181.62	-239.26

Table S5. Summary of country net carbon fluxes 2010-2018 and inter-comparison with other sources. Reported also are the 2010 forest area and the % change of the 2010 stocks relative to the 2010-2018 fluxes.

Country	Area ('000 km^2)	C Flux (Tg)	% change
BRA			
This study	7000830	-1,047.12	-0.015%
CCI	7000830	2,173.22	0.031%
WRI	7000830	599.80	0.009%
FRA	5115810	-435.6	-0.085%
NLD			
This study	3037	0.06	0.002%
CCI	3037	-0.11	-0.004%
WRI	3037	0.41	0.014%
FRA	3735	0.911	0.024%
PHL			
This study	125285	4.46	0.004%
CCI	125285	51.23	0.041%
WRI	125285	50.98	0.041%
FRA	68397	-4.03	-0.006%
SWE			
This study	272266	5.37	0.002%
CCI	272266	-30.71	-0.011%
WRI	272266	618.25	0.227%
FRA	280730	37.65	0.013%
Santoro 2010-2015	254646	12	0.005%
USA			
This study	5590741	-205.14	-0.004%
CCI	5590741	-30.71	-0.001%
WRI	5590741	618.25	0.011%
FRA	3087200	644.67	0.021%
CONUS 2010-2017	4313653	224.5	0.005%

Supplementary materials of Chapter 5

Supplementary Figure 1. Uncertainty of carbon loss across Africa's primary humid tropical forest expressed as standard deviation

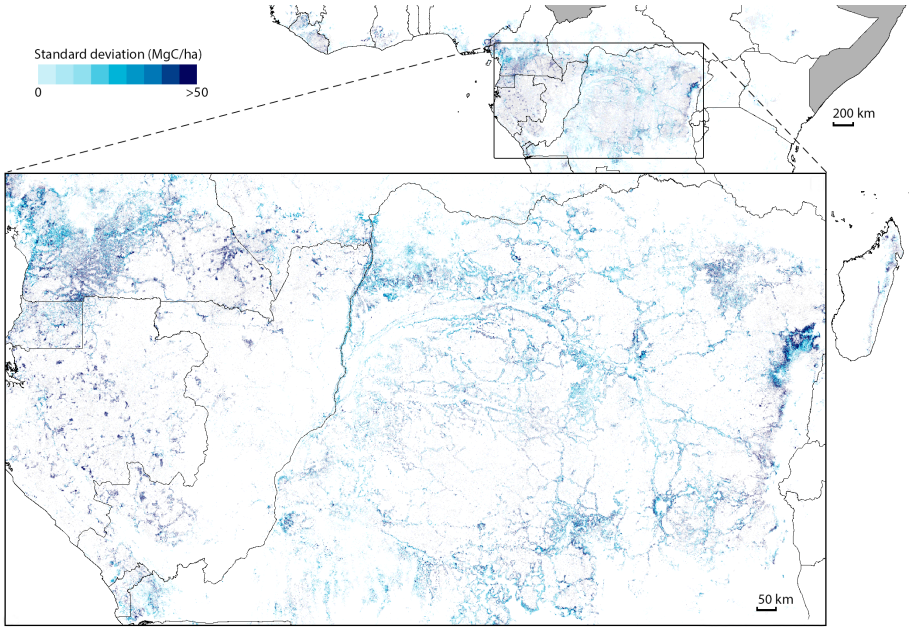

Supplementary Figure 2. Radar charts comparing the monthly carbon loss for each year for the topmost emitting countries. Pearson's correlation of coefficient (r) is shown in italics at the bottom of each chart. Note that the vertical axis depicting the total amount of carbon loss is expressed in Tg C and varies for each country.

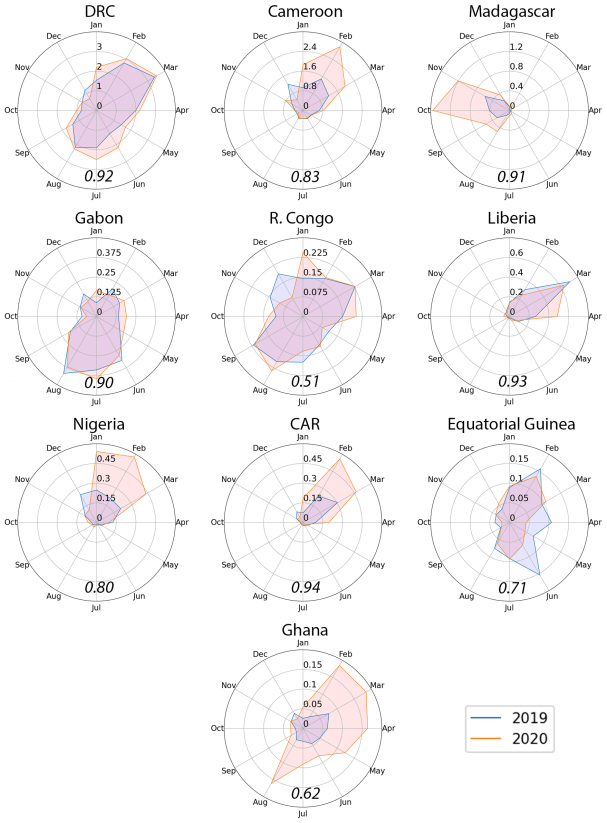

Supplementary Figure 3. Locations of the local examples from Figure 4. The locations are shown with a black square inside the blue circles. Background data represents the carbon stock, carbon loss, and countries' borders.

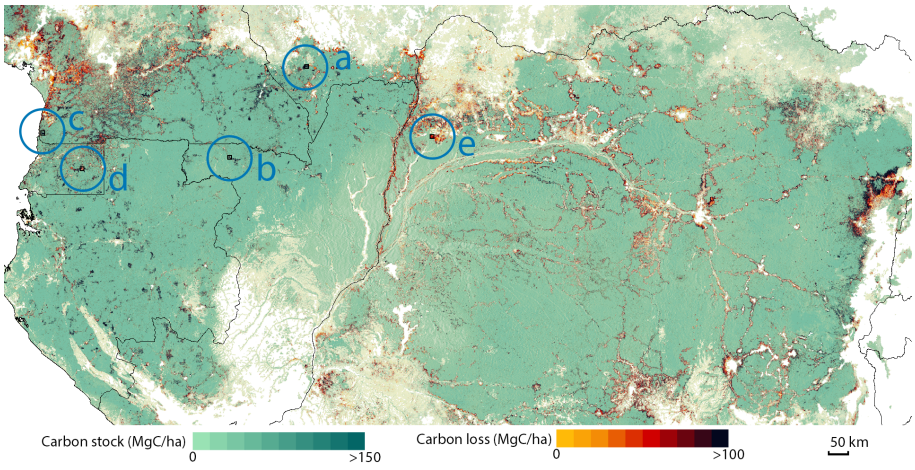

Table 6.1: Supplementary Table 1. Emissions reporting by country and year

Country	FRA - RS	FRA - NFI	NDC	BUR	NC	NIR	GHG
Angola	2015	2015	2020s, 2021u	NA	2012	NA	NA
Benin	2007	2008	2017	2019	2019	2019	NA
Burundi	1979	1976	2018	NA	2019	NA	NA
Cameroon	2004	2004	2016	NA	2012	NA	NA
CAR	2008	1994	2016	NA	2015	NA	NA
Congo	2004	2017	2017	NA	2009	NA	NA
Cote d'Ivoire	2016	2017	2016	2018	2017	NA	NA
DRC	2010	2019	2017	NA	2015	NA	NA
Equatorial Guinea	2014	1991	2018	NA	2019	NA	NA
Ethiopia	2016	2018	2017 s, 2020 u	NA	2016	NA	NA
Gabon	2015	2000	2016	NA	2011	NA	NA
Ghana	2017	2017	2016	2019	2020	2020	2001
Guinea	NA	2017	2016	NA	2018	NA	NA
Kenya	2018	2014	2016 s, 2020 u	NA	2015	NA	NA
Liberia	2014	NA	2018	2021	2021	NA	NA
Madagascar	2010	1996	2016	NA	2017	NA	NA
Nigeria	2018	2018	2017 s, 2021 u	2018	2020	NA	NA
Rwanda	2008	2007	2016 s, 2020 u	NA	2018	NA	NA
Sierra Leone	1986	NA	2016	NA	2018	NA	NA
South Sudan	2013	NA	2021	NA	2019	NA	NA
Togo	2014	2016	2017	2017	2015	2017	NA
Uganda	2017	2018	2016	2019	2014	NA	NA
Zambia	2014	2014	2016 s, 2020 u	2020	2020	NA	NA

References

Achard, F. et al. (2014). Determination of tropical deforestation rates and related carbon losses from 1990 to 2010. *Global Change Biology*, *20*, 2540–2554. doi:10.1111/gcb.12605.

Alaniz, A. J., Carvajal, M. A., Marquet, P. A., Vergara, P. M., Meneses, L., & Moreira-Arce, D. (2022). Analyzing the spatiotemporal patterns of forests carbon sink and sources between 2000 and 2019. *Earth's Future*, *10*. doi:10.1029/2021ef002560.

Albinet, C. et al. (2019). A joint ESA-NASA multi-mission algorithm and analysis platform (MAAP) for biomass, NISAR, and GEDI. *Surveys in Geophysics*, *40*, 1017–1027. doi:10.1007/s10712-019-09541-z.

Aleman, J. C., Jarzyna, M. A., & Staver, A. C. (2017). Forest extent and deforestation in tropical africa since 1900. *Nature Ecology &amp Evolution*, *2*, 26–33. doi:10.1038/s41559-017-0406-1.

Anacioco, K. P., Gorio, J. A. L., Padsico, M. R. S., Lumbres, R. I. C., Doyog, N. D., & Lee, Y. J. (2018). Fitting and evaluation of height-diameter models for alnus japonica in la trinidad, benguet, philippines. *Journal of Mountain Science*, *15*, 2422–2432. doi:https://doi.org/10.1007/s11629-018-4866-9.

Araza, A. et al. (2022a). A comprehensive framework for assessing the accuracy and uncertainty of global above-ground biomass maps. *Remote Sensing of Environment*, *272*, 112917. doi:10.1016/j.rse.2022.112917.

Araza, A. et al. (2023). Past decade above-ground biomass change comparisons from four multi-temporal global maps. *International Journal of Applied Earth Observation and Geoinformation, 2nd revision*, *000*, 000000.

Araza, A., Bruin, S. D., & Herold, M. (2022b). Plot-to-map: an open-source r workflow for above-ground biomass independent validation. In *IGARSS 2022 - 2022 IEEE International Geoscience and Remote Sensing Symposium*. IEEE. doi:10.1109/igarss46834.2022.9884831.

Araza, A., Herold, M., Hein, L., & Quinones, M. (2021a). The first above-ground biomass map of the philippines produced using remote sensing and machine learning. In *2021 IEEE International Geoscience and Remote Sensing Symposium IGARSS*. IEEE.

doi:10.1109/igarss47720.2021.9553225.

Araza, A., Herold, M., Hein, L., & Quiñones, M. (2021b). The first above-ground biomass map of the philippines produced using remote sensing and machine learning. In *2021 IEEE International Geoscience and Remote Sensing Symposium IGARSS* (pp. 6897–6900). IEEE. doi:https://doi.org/10.13140/RG.2.2.19978.62400.

Araza, A. B., Castillo, G. B., Buduan, E. D., Hein, L., Herold, M., Reiche, J., Gou, Y., Villaluz, M. G. Q., & Razal, R. A. (2021c). Intra-annual identification of local deforestation hotspots in the philippines using earth observation products. *Forests*, *12*, 1008. doi:10.3390/f12081008.

Auscover, T. (2016). Biomass plot library-national collation of tree and shrub inventory data, allometric model predictions of above and below-ground biomass, australia. *Made available by the AusCover facility of the Terrestrial Ecosystem Research Network (TERN)*, .

Avitabile, V., Baccini, A., Friedl, M. A., & Schmullius, C. (2012). Capabilities and limitations of landsat and land cover data for aboveground woody biomass estimation of uganda. *Remote Sensing of Environment*, *117*, 366–380. doi:https://doi.org/10.1016/j.rse.2011.10.012.

Avitabile, V., & Camia, A. (2018). An assessment of forest biomass maps in europe using harmonized national statistics and inventory plots. *Forest Ecology and Management*, *409*, 489–498. doi:https://doi.org/10.1016/j.foreco.2017.11.047.

Avitabile, V., Herold, M., Henry, M., & Schmullius, C. (2011). Mapping biomass with remote sensing: a comparison of methods for the case study of uganda. *Carbon Balance and Management*, *6*. doi:https://doi.org/10.1186/1750-0680-6-7.

Avitabile, V. et al. (2016). An integrated pan-tropical biomass map using multiple reference datasets. *Global Change Biology*, *22*, 1406–1420. doi:https://doi.org/10.1111/gcb.13139.

Avitabile, V. et al. (2014). Comparative analysis and fusion for improved global biomass mapping. In *Book of abstracts of the International Conference Global Vegetation Monitoring and Modeling (GV2M)* (pp. 251–252).

Baccini, A., Friedl, M., Woodcock, C., & Zhu, Z. (2007). Scaling field data to calibrate and validate moderate spatial resolution remote sensing models. *Photogrammetric Engineering & Remote Sensing*, *73*, 945–954. doi:https://doi.org/10.14358/pers.73.8.945.

Baccini, A., Goetz, S. J., Walker, W. S., Laporte, N. T., Sun, M., Sulla-Menashe, D., Hackler, J., Beck, P. S. A., Dubayah, R., Friedl, M. A., Samanta, S., & Houghton, R. A. (2012). Estimated carbon dioxide emissions from tropical deforestation improved by carbon-density maps. *Nature Climate Change*, *2*, 182–185. doi:https://doi.org/10.1038/nclimate1354.

Baccini, A., Walker, W., Carvalho, L., Farina, M., Sulla-Menashe, D., & Houghton, R. A. (2017). Tropical forests are a net carbon source based on aboveground measurements of gain and loss. *Science*, *358*, 230–234. doi:10.1126/science.aam5962.

Balk, D., & Yetman, G. (2004). The global distribution of population: evaluating the gains in resolution refinement. *New York: Center for International Earth Science Information Network (CIESIN), Columbia University*, .

Bastin, J.-F. et al. (2017). The extent of forest in dryland biomes. *Science*, *356*, 635–638. doi:10.1126/science.aam6527.

Bastin, J.-F., Finegold, Y., Garcia, C., Mollicone, D., Rezende, M., Routh, D., Zohner, C. M., & Crowther, T. W. (2019). The global tree restoration potential. *Science*, *365*, 76–79. doi:10.1126/science.aax0848.

Besnard, S. et al. (2021). Mapping global forest age from forest inventories, biomass and climate data. *Earth System Science Data*, *13*, 4881–4896. doi:10.5194/essd-13-4881-2021.

Bispo, P. C., Santos, J. R., Valeriano, M. M., Touzi, R., & Seifert, F. M. (2014). Integration of polarimetric PALSAR attributes and local geomorphometric variables derived from SRTM for forest biomass modeling in central amazonia. *Canadian Journal of Remote Sensing*, *40*, 26–42. doi:https://doi.org/10.1080/07038992.2014.913477.

Bojinski, S., Verstraete, M., Peterson, T. C., Richter, C., Simmons, A., & Zemp, M. (2014). The concept of essential climate variables in support of climate research, applications, and policy. *Bulletin of the American Meteorological Society*, *95*, 1431–1443. doi:10.1175/bams-d-13-00047.1.

Bos, A. B., Sy, V. D., Duchelle, A. E., Herold, M., Martius, C., & Tsendbazar, N.-E. (2019). Global data and tools for local forest cover loss and REDD performance assessment: Accuracy, uncertainty, complementarity and impact. *International Journal of Applied Earth Observation and Geoinformation*, *80*, 295–311. doi:https://doi.org/10.1016/j.jag.2019.04.004.

Bradford, J. B., Weishampel, P., Smith, M.-L., Kolka, R., Birdsey, R. A., Ollinger, S. V., & Ryan, M. G. (2010). Carbon pools and fluxes in small temperate forest landscapes: Variability and implications for sampling design. *Forest Ecology and Management*, *259*, 1245–1254. doi:https://doi.org/10.1016/j.foreco.2009.04.009.

Brancalion, P. H. et al. (2020). Emerging threats linking tropical deforestation and the COVID-19 pandemic. *Perspectives in Ecology and Conservation*, *18*, 243–246. doi:10.1016/j.pecon.2020.09.006.

Breiman, L. (2001). Random forests. *Machine learning*, *45*, 5–32.

Brovkina, O., Novotny, J., Cienciala, E., Zemek, F., & Russ, R. (2017). Mapping forest aboveground biomass using airborne hyperspectral and lidar data in the mountainous

conditions of central europe. *Ecological Engineering*, *100*, 219–230.

Brown, S., Goslee, K., Casarim, F., Harris, N., & Petrova, S. (2014). Sampling design and implementation plan for guyana's redd+ forest carbon monitoring system (fcms): version 2. *Submitted by Winrock International to the Guyana Forestry Commission*, .

de Bruin, S. (2000). Predicting the areal extent of land-cover types using classified imagery and geostatistics. *Remote Sensing of Environment*, *74*, 387–396. doi:10.1016/s0034-4257(00)00132-2.

de Bruin, S., Brus, D. J., Heuvelink, G. B., van Ebbenhorst Tengbergen, T., & Wadoux, A. M.-C. (2022). Dealing with clustered samples for assessing map accuracy by cross-validation. *Ecological Informatics*, *69*, 101665. doi:10.1016/j.ecoinf.2022.101665.

de Bruin, S., Herold, M., & Araza, A. (2019). *Product Validation Plan*. Technical Report, European Space Agency.

de Bruin, S., Herold, M., Araza, A., & Lucas, R. (2020). Cci biomass product validation plan year 2 version 2.0: D2. 5. ESA.

Buchhorn, M., Lesiv, M., Tsendbazar, N.-E., Herold, M., Bertels, L., & Smets, B. (2020). Copernicus global land cover layers—collection 2. *Remote Sensing*, *12*, 1044. doi:10.3390/rs12061044.

Buendia, E., Tanabe, K., Kranjc, A., Baasansuren, J., Fukuda, M., Ngarize, S., Osako, A., Pyrozhenko, Y., Shermanau, P., & Federici, S. (2019). Refinement to the 2006 ipcc guidelines for national greenhouse gas inventories. *IPCC: Geneva, Switzerland*, .

Bunting, P., Rosenqvist, A., Lucas, R., Rebelo, L.-M., Hilarides, L., Thomas, N., Hardy, A., Itoh, T., Shimada, M., & Finlayson, C. (2018). The global mangrove watch—a new 2010 global baseline of mangrove extent. *Remote Sensing*, *10*, 1669. doi:10.3390/rs10101669.

Burt, A., Calders, K., Cuni-Sanchez, A., Gómez-Dans, J., Lewis, P., Lewis, S. L., Malhi, Y., Phillips, O. L., & Disney, M. (2020). Assessment of bias in pan-tropical biomass predictions. *Frontiers in Forests and Global Change*, *3*. doi:https://doi.org/10.3389/ffgc.2020.00012.

Büttner, G. (2014). CORINE land cover and land cover change products. In *Land Use and Land Cover Mapping in Europe* (pp. 55–74). Springer Netherlands. doi:10.1007/978-94-007-7969-3_5.

Calders, K., Verbeeck, H., Burt, A., Origo, N., Nightingale, J., Malhi, Y., Wilkes, P., Raumonen, P., Bunce, R. G. H., & Disney, M. (2022). Laser scanning reveals potential underestimation of biomass carbon in temperate forest. *Ecological Solutions and Evidence*, *3*. doi:10.1002/2688-8319.12197.

Carreiras, J., Melo, J., & Vasconcelos, M. (2013). Estimating the above-ground biomass in miombo savanna woodlands (mozambique, east africa) using l-band synthetic aper-

ture radar data. *Remote Sensing*, *5*, 1524–1548. doi:https://doi.org/10.3390/rs5041524.

Carreiras, J. M., Vasconcelos, M. J., & Lucas, R. M. (2012). Understanding the relationship between aboveground biomass and ALOS PALSAR data in the forests of guinea-bissau (west africa). *Remote Sensing of Environment*, *121*, 426–442. doi:https://doi.org/10.1016/j.rse.2012.02.012.

de Castilho, C. V., Magnusson, W. E., de Araújo, R. N. O., Luizão, R. C., Luizão, F. J., Lima, A. P., & Higuchi, N. (2006). Variation in aboveground tree live biomass in a central amazonian forest: Effects of soil and topography. *Forest Ecology and Management*, *234*, 85–96. doi:https://doi.org/10.1016/j.foreco.2006.06.024.

Chave, J., Condit, R., Aguilar, S., Hernandez, A., Lao, S., & Perez, R. (2004). Error propagation and scaling for tropical forest biomass estimates. *Philosophical Transactions of the Royal Society of London. Series B: Biological Sciences*, *359*, 409–420.

Chave, J., Coomes, D., Jansen, S., Lewis, S. L., Swenson, N. G., & Zanne, A. E. (2009). Towards a worldwide wood economics spectrum. *Ecology Letters*, *12*, 351–366. doi:https://doi.org/10.1111/j.1461-0248.2009.01285.x.

Chave, J. et al. (2019a). Ground data are essential for biomass remote sensing missions. *Surveys in Geophysics*, *40*, 863–880. doi:10.1007/s10712-019-09528-w.

Chave, J., Davies, S. J., Phillips, O. L., Lewis, S. L., Sist, P., Schepaschenko, D., Armston, J., Baker, T. R., Coomes, D., Disney, M. et al. (2019b). Ground data are essential for biomass remote sensing missions. *Surveys in Geophysics*, (pp. 1–18).

Chave, J., Réjou-Méchain, M., Búrquez, A., Chidumayo, E., Colgan, M. S., Delitti, W. B., Duque, A., Eid, T., Fearnside, P. M., Goodman, R. C. et al. (2014). Improved allometric models to estimate the aboveground biomass of tropical trees. *Global change biology*, *20*, 3177–3190.

Chen, A., Peng, S., & Fei, S. (2018). Mapping global forest biomass and its changes over the first decade of the 21st century. *Science China Earth Sciences*, *62*, 585–594. doi:https://doi.org/10.1007/s11430-018-9277-6.

Chen, Q., Laurin, G. V., & Valentini, R. (2015). Uncertainty of remotely sensed aboveground biomass over an african tropical forest: Propagating errors from trees to plots to pixels. *Remote Sensing of Environment*, *160*, 134–143.

Chen, T., & Guestrin, C. (2016). XGBoost. In *Proceedings of the 22nd ACM SIGKDD International Conference on Knowledge Discovery and Data Mining*. ACM. doi:10.1145/2939672.2939785.

Christensen, W. F. (2011). Filtered kriging for spatial data with heterogeneous measurement error variances. *Biometrics*, *67*, 947–957. doi:https://doi.org/10.1111/j.1541-0420.2011.01563.x.

Csillik, O., & Asner, G. P. (2020). Near-real time aboveground carbon emissions in peru. *PLOS ONE*, *15*, e0241418. doi:10.1371/journal.pone.0241418.

Csillik, O., Kumar, P., Mascaro, J., O'Shea, T., & Asner, G. P. (2019). Monitoring tropical forest carbon stocks and emissions using planet satellite data. *Scientific Reports*, *9*. doi:https://doi.org/10.1038/s41598-019-54386-6.

Csillik, O., Reiche, J., Sy, V. D., Araza, A., & Herold, M. (2022). Rapid remote monitoring reveals spatial and temporal hotspots of carbon loss in africa's rainforests. *Communications Earth &amp Environment*, *3*. doi:10.1038/s43247-022-00383-z.

Cushman, K. C., Burley, J. T., Imbach, B., Saatchi, S. S., Silva, C. E., Vargas, O., Zgraggen, C., & Kellner, J. R. (2021). Impact of a tropical forest blowdown on aboveground carbon balance. *Scientific Reports*, *11*. doi:10.1038/s41598-021-90576-x.

De Vries, B., Avitabile, V., Kooistra, L., & Herold, M. (2012). Monitoring the impact of redd+ implementation in the unesco kafa biosphere reserve ethiopia. *Sensing a Changing World*, .

Decuyper, M., Chávez, R. O., Lohbeck, M., Lastra, J. A., Tsendbazar, N., Hackländer, J., Herold, M., & Vågen, T.-G. (2022). Continuous monitoring of forest change dynamics with satellite time series. *Remote Sensing of Environment*, *269*, 112829. doi:10.1016/j.rse.2021.112829.

Defourny, P., Kirches, G., Brockmann, C., Boettcher, M., Peters, M., Bontemps, S., Lamarche, C., Schlerf, M., & Santoro, M. (2012). Land cover cci. *Product User Guide Version*, *2*, 325.

Dieck, R. H. (2007). *Measurement uncertainty: methods and applications*. ISA.

Dinerstein, E. et al. (2017). An ecoregion-based approach to protecting half the terrestrial realm. *BioScience*, *67*, 534–545. doi:10.1093/biosci/bix014.

Drichi, P. (2003). *National Biomas Study of Uganda*. Technical Report, .

Dubayah, R. et al. (2020). The global ecosystem dynamics investigation: High-resolution laser ranging of the earth's forests and topography. *Science of Remote Sensing*, *1*, 100002. doi:10.1016/j.srs.2020.100002.

Dubayah, R. O., & Drake, J. B. (2000). Lidar remote sensing for forestry. *Journal of forestry*, *98*, 44–46.

Duncanson, L., Armston, J., Disney, M., Avitabile, V., Barbier, N., Calders, K., Carter, S., Chave, J., Herold, M., MacBean, N. et al. (2021). Aboveground woody biomass product validation good practices protocol, . doi:https://doi.org/doi:10.5067.

Duncanson, L. et al. (2022). Aboveground biomass density models for NASA's global ecosystem dynamics investigation (GEDI) lidar mission. *Remote Sensing of Environment*, *270*, 112845. doi:10.1016/j.rse.2021.112845.

Dupuis, C., Lejeune, P., Michez, A., & Fayolle, A. (2020). How can remote sensing help monitor tropical moist forest degradation?—a systematic review. *Remote Sensing*, *12*, 1087. doi:10.3390/rs12071087.

Eggleston, H., Buendia, L., Miwa, K., Ngara, T., & Tanabe, K. (2006). 2006 ipcc guidelines for national greenhouse gas inventories, . *5*.

Esteban, J., McRoberts, R. E., Fernández-Landa, A., Tomé, J. L., & Marchamalo, M. (2020). A model-based volume estimator that accounts for both land cover misclassification and model prediction uncertainty. *Remote Sensing*, *12*, 3360. doi:10.3390/rs12203360.

Fazakas, Z., Nilsson, M., & Olsson, H. (1999). Regional forest biomass and wood volume estimation using satellite data and ancillary data. *Agricultural and Forest Meteorology*, *98-99*, 417–425. doi:https://doi.org/10.1016/s0168-1923(99)00112-4.

Feldpausch, T. R. et al. (2012). Tree height integrated into pantropical forest biomass estimates. *Biogeosciences*, *9*, 3381–3403. doi:https://doi.org/10.5194/bg-9-3381-2012.

Feng, Y., Zeng, Z., Searchinger, T. D., Ziegler, A. D., Wu, J., Wang, D., He, X., Elsen, P. R., Ciais, P., Xu, R. et al. (2022). Doubling of annual forest carbon loss over the tropics during the early twenty-first century. *Nature Sustainability*, (pp. 1–8).

Finer, M., Novoa, S., Weisse, M. J., Petersen, R., Mascaro, J., Souto, T., Stearns, F., & Martinez, R. G. (2018). Combating deforestation: From satellite to intervention. *Science*, *360*, 1303–1305. doi:10.1126/science.aat1203.

Friedlingstein, P. et al. (2022). Global carbon budget 2021. *Earth System Science Data*, *14*, 1917–2005. doi:10.5194/essd-14-1917-2022.

GCOS (2016). The global observing system for climate: Implementation needs, gcos-200.

Gebejes, A., & Huertas, R. (2013). Texture characterization based on grey-level cooccurrence matrix. *Databases*, *9*, 375–378.

Gibbs, H. K., Brown, S., Niles, J. O., & Foley, J. A. (2007). Monitoring and estimating tropical forest carbon stocks: making REDD a reality. *Environmental Research Letters*, *2*, 045023. doi:10.1088/1748-9326/2/4/045023.

GlobalForestWatch (2002). Global forest watch. *World Resources Institute, Washington, DC. Available from http://www. globalforestwatch.org (accessed March 2020)*, .

Goetz, S. J., Baccini, A., Laporte, N. T., Johns, T., Walker, W., Kellndorfer, J., Houghton, R. A., & Sun, M. (2009). Mapping and monitoring carbon stocks with satellite observations: a comparison of methods. *Carbon Balance and Management*, *4*. doi:10.1186/1750-0680-4-2.

Gonzalez-Akre, E. et al. (2021). iallodb/i : An r package for biomass estimation at globally distributed extratropical forest plots. *Methods in Ecology and Evolution*, *13*, 330–338.

doi:10.1111/2041-210x.13756.

Goodman, R. C., Phillips, O. L., del Castillo Torres, D., Freitas, L., Cortese, S. T., Monteagudo, A., & Baker, T. R. (2013). Amazon palm biomass and allometry. *Forest Ecology and Management*, *310*, 994–1004. doi:https://doi.org/10.1016/j.foreco.2013.09.045.

Gorelick, N., Hancher, M., Dixon, M., Ilyushchenko, S., Thau, D., & Moore, R. (2017). Google earth engine: Planetary-scale geospatial analysis for everyone. *Remote Sensing of Environment*, *202*, 18–27. doi:10.1016/j.rse.2017.06.031.

Grantham, H. S. et al. (2021). Anthropogenic modification of forests means only 40% of remaining forests have high ecosystem integrity. *Nature Communications*, *12*. doi:10.1038/s41467-021-20999-7.

Greenwell, B. M. (2017). pdp: an r package for constructing partial dependence plots. *The R Journal*, *9*, 421–436.

GTOPO30-global, U. (2002). 30-arc second elevation data. *US geological survey. National Mapping Division, EROS Data Center. Available from: http://edcdaac.usgs.gov/gtopo30/gtopo30.html*, .

Guitet, S., Hérault, B., Molto, Q., Brunaux, O., & Couteron, P. (2015). Spatial structure of above-ground biomass limits accuracy of carbon mapping in rainforest but large scale forest inventories can help to overcome. *PLoS One*, *10*, e0138456.

Hansen, M. C., Krylov, A., Tyukavina, A., Potapov, P. V., Turubanova, S., Zutta, B., Ifo, S., Margono, B., Stolle, F., & Moore, R. (2016). Humid tropical forest disturbance alerts using landsat data. *Environmental Research Letters*, *11*, 034008. doi:10.1088/1748-9326/11/3/034008.

Hansen, M. C., Potapov, P. V., Moore, R., Hancher, M., Turubanova, S., Tyukavina, A., Thau, D., Stehman, S., Goetz, S., Loveland, T. R. et al. (2013a). High-resolution global maps of 21st-century forest cover change. *Science*, *342*, 850–853.

Hansen, M. C. et al. (2013b). High-resolution global maps of 21st-century forest cover change. *Science*, *342*, 850–853. doi:10.1126/science.1244693.

Hansen, M. C., Wang, L., Song, X.-P., Tyukavina, A., Turubanova, S., Potapov, P. V., & Stehman, S. V. (2020). The fate of tropical forest fragments. *Science Advances*, *6*, eaax8574. doi:https://doi.org/10.1126/sciadv.aax8574.

Harmon, M. E., Fasth, B., Halpern, C. B., & Lutz, J. A. (2015). Uncertainty analysis: an evaluation metric for synthesis science. *Ecosphere*, *6*, 1–12. doi:https://doi.org/10.1890/es14-00235.1.

Harris, N. L. et al. (2021). Global maps of twenty-first century forest carbon fluxes. *Nature Climate Change*, . doi:10.1038/s41558-020-00976-6.

Hearst, M. A., Dumais, S. T., Osuna, E., Platt, J., & Scholkopf, B. (1998). Support

vector machines. *IEEE Intelligent Systems and their applications*, *13*, 18–28.

Hein, L. et al. (2020a). Progress in natural capital accounting for ecosystems. *Science*, *367*, 514–515. doi:10.1126/science.aaz8901.

Hein, L., Remme, R. P., Schenau, S., Bogaart, P. W., Lof, M. E., & Horlings, E. (2020b). Ecosystem accounting in the netherlands. *Ecosystem Services*, *44*, 101118. doi:10.1016/j.ecoser.2020.101118.

Hernández-Stefanoni, J. L., Castillo-Santiago, M. Á., Mas, J. F., Wheeler, C. E., Andres-Mauricio, J., Tun-Dzul, F., George-Chacón, S. P., Reyes-Palomeque, G., Castellanos-Basto, B., Vaca, R., & Dupuy, J. M. (2020). Improving aboveground biomass maps of tropical dry forests by integrating LiDAR, ALOS PALSAR, climate and field data. *Carbon Balance and Management*, *15*. doi:https://doi.org/10.1186/s13021-020-00151-6.

Herold, M., Araza, A., Schelhaas, M.-J., Nabuurs, G.-J., Lerink, B., & Winkler, K. (2022). *National forest inventory and high-resolution forest cover for Eastern Europe*. Technical Report, European Union.

Herold, M., Carter, S., Avitabile, V., Espejo, A. B., Jonckheere, I., Lucas, R., McRoberts, R. E., Næsset, E., Nightingale, J., Petersen, R. et al. (2019). The role and need for space-based forest biomass-related measurements in environmental management and policy. *Surveys in Geophysics*, *40*, 1–22. doi:10.1007/s10712-019-09510-6.

Heuvelink, G. B., & Webster, R. (2022). Spatial statistics and soil mapping: A blossoming partnership under pressure. *Spatial Statistics*, *50*, 100639. doi:10.1016/j.spasta.2022.100639.

Hoekman, D., Kooij, B., Quiñones, M., Vellekoop, S., Carolita, I., Budhiman, S., Arief, R., & Roswintiarti, O. (2020). Wide-area near-real-time monitoring of tropical forest degradation and deforestation using sentinel-1. *Remote Sensing*, *12*, 3263. doi:10.3390/rs12193263.

Houghton, R. A., House, J. I., Pongratz, J., van der Werf, G. R., DeFries, R. S., Hansen, M. C., Quéré, C. L., & Ramankutty, N. (2012). Carbon emissions from land use and land-cover change. *Biogeosciences*, *9*, 5125–5142. doi:10.5194/bg-9-5125-2012.

Hu, T., Su, Y., Xue, B., Liu, J., Zhao, X., Fang, J., & Guo, Q. (2016). Mapping global forest aboveground biomass with spaceborne LiDAR, optical imagery, and forest inventory data, . *8*, 565. doi:10.3390/rs8070565.

Huang, Y., Ciais, P., Santoro, M., Makowski, D., Chave, J., Schepaschenko, D., Abramoff, R. Z., Goll, D. S., Yang, H., Chen, Y., Wei, W., & Piao, S. (2021). A global map of root biomass across the world's forests. *Earth System Science Data*, *13*, 4263–4274. doi:10.5194/essd-13-4263-2021.

Hubau, W. et al. (2020). Asynchronous carbon sink saturation in african and

amazonian tropical forests. *Nature*, *579*, 80–87. doi:https://doi.org/10.1038/s41586-020-2035-0.

Iremonger, S., & Gerrand, A. (2011). Global ecological zones for fao forest reporting, 2010. *Unpublished report. Rome, FAO*, .

Jarvis, A., Reuter, H. I., Nelson, A., Guevara, E. et al. (2008). Hole-filled srtm for the globe version 4. *available from the CGIAR-CSI SRTM 90m Database (http://srtm. csi. cgiar. org)*, *15*, 25–54.

Johnson, B. R., Kuester, M. A., Kampe, T. U., & Keller, M. (2010). National ecological observatory network (NEON) airborne remote measurements of vegetation canopy biochemistry and structure. In *2010 IEEE International Geoscience and Remote Sensing Symposium*. IEEE. doi:10.1109/igarss.2010.5654121.

de Jong, B. H. (2013). Spatial distribution of biomass and links to reported disturbances in tropical lowland forests of southern mexico. *Carbon Management*, *4*, 601–615. doi:https://doi.org/10.4155/cmt.13.60.

Keith, H., Vardon, M., Obst, C., Young, V., Houghton, R. A., & Mackey, B. (2021). Evaluating nature-based solutions for climate mitigation and conservation requires comprehensive carbon accounting. *Science of The Total Environment*, *769*, 144341. doi:10.1016/j.scitotenv.2020.144341.

Keith, H., Vardon, M., Stein, J., & Lindenmayer, D. (2019). Contribution of native forests to climate change mitigation – a common approach to carbon accounting that aligns results from environmental-economic accounting with rules for emissions reduction. *Environmental Science & Policy*, *93*, 189–199. doi:10.1016/j.envsci.2018.11.001.

Kellogg, K. et al. (2020). NASA-ISRO synthetic aperture radar (NISAR) mission. In *2020 IEEE Aerospace Conference*. IEEE. doi:https://doi.org/10.1109/aero47225.2020.9172638.

Kennedy, R. E., Yang, Z., & Cohen, W. B. (2010). Detecting trends in forest disturbance and recovery using yearly landsat time series: 1. LandTrendr — temporal segmentation algorithms. *Remote Sensing of Environment*, *114*, 2897–2910. doi:10.1016/j.rse.2010.07.008.

Kindermann, G., McCallum, I., Fritz, S., & Obersteiner, M. (2008). A global forest growing stock, biomass and carbon map based on FAO statistics. *Silva Fennica*, *42*. doi:https://doi.org/10.14214/sf.244.

Kyriakidis, P. C. (2004). A geostatistical framework for area-to-point spatial interpolation. *Geographical Analysis*, *36*, 259–289. doi:https://doi.org/10.1111/j.1538-4632.2004.tb01135.x.

Labrière, N. et al. (2022). Toward a forest biomass reference measurement system for remote sensing applications. *Global Change Biology*, . doi:10.1111/gcb.16497.

Labriere, N. et al. (2018). italicin situ/italic reference datasets from the TropiSAR and AfriSAR campaigns in support of upcoming spaceborne biomass missions. *IEEE Journal of Selected Topics in Applied Earth Observations and Remote Sensing*, *11*, 3617–3627. doi:https://doi.org/10.1109/jstars.2018.2851606.

Langner, A., Achard, F., & Grassi, G. (2014). Can recent pan-tropical biomass maps be used to derive alternative tier 1 values for reporting redd+ activities under unfccc? *Environmental Research Letters*, *9*, 124008. doi:10.1088/1748-9326/9/12/124008.

Laurin, G. V., Hawthorne, W., Chiti, T., Paola, A. D., Gatti, R. C., Marconi, S., Noce, S., Grieco, E., Pirotti, F., & Valentini, R. (2016). Does degradation from selective logging and illegal activities differently impact forest resources? a case study in ghana. *iForest - Biogeosciences and Forestry*, *9*, 354–362. doi:https://doi.org/10.3832/ifor1779-008.

Laurin, G. V., Puletti, N., Grotti, M., Stereńczak, K., Modzelewska, A., Lisiewicz, M., Sadkowski, R., Kuberski, Ł., Chirici, G., & Papale, D. (2020). Species dominance and above ground biomass in the białowieża forest, poland, described by airborne hyperspectral and lidar data. *International Journal of Applied Earth Observation and Geoinformation*, *92*, 102178. doi:10.1016/j.jag.2020.102178.

Le, A., Paull, D., & Griffin, A. (2018). Exploring the inclusion of small regenerating trees to improve above-ground forest biomass estimation using geospatial data. *Remote Sensing*, *10*, 1446. doi:10.3390/rs10091446.

Lesiv, M. et al. (2022). Global forest management data for 2015 at a 100 m resolution. *Scientific Data*, *9*. doi:10.1038/s41597-022-01332-3.

Lewis, S. L. et al. (2013). Above-ground biomass and structure of 260 african tropical forests. *Philosophical Transactions of the Royal Society B: Biological Sciences*, *368*, 20120295. doi:https://doi.org/10.1098/rstb.2012.0295.

Liang, J. et al. (2016). Positive biodiversity-productivity relationship predominant in global forests. *Science*, *354*. doi:10.1126/science.aaf8957.

Liang, J., Zhou, M., Tobin, P. C., McGuire, A. D., & Reich, P. B. (2015). Biodiversity influences plant productivity through niche–efficiency. *Proceedings of the National Academy of Sciences*, *112*, 5738–5743. doi:https://doi.org/10.1073/pnas.1409853112.

Lindsell, J. A., & Klop, E. (2013). Spatial and temporal variation of carbon stocks in a lowland tropical forest in west africa. *Forest Ecology and Management*, *289*, 10–17. doi:10.1016/j.foreco.2012.09.045.

Liu, Y. Y., van Dijk, A. I. J. M., de Jeu, R. A. M., Canadell, J. G., McCabe, M. F., Evans, J. P., & Wang, G. (2015). Recent reversal in loss of global terrestrial biomass, . *5*, 470–474. doi:10.1038/nclimate2581.

Liu, Y. Y., van Dijk, A. I. J. M., McCabe, M. F., Evans, J. P., & de Jeu, R. A. M. (2012). Global vegetation biomass change (1988-2008) and attribution to environmental and human drivers. *Global Ecology and Biogeography*, *22*, 692–705. doi:10.1111/geb.12024.

Longo, M., Keller, M., dos Santos, M. N., Leitold, V., Pinagé, E. R., Baccini, A., Saatchi, S., Nogueira, E. M., Batistella, M., & Morton, D. C. (2016). Aboveground biomass variability across intact and degraded forests in the brazilian amazon. *Global Biogeochemical Cycles*, *30*, 1639–1660. doi:10.1002/2016gb005465.

Lucas, R., Milne, A., Cronin, N., Witte, C., & Denham, R. (2000). The potential of synthetic aperture radar (SAR) for quantifying the biomass of australia's woodlands. *The Rangeland Journal*, *22*, 124. doi:10.1071/rj0000124.

Luyssaert, S., Schulze, E. D., Börner, A., Knohl, A., Hessenmöller, D., Law, B. E., Ciais, P., & Grace, J. (2008). Old-growth forests as global carbon sinks. *Nature*, *455*, 213–215. doi:https://doi.org/10.1038/nature07276.

Mahanta, D. J., & Borah, M. (2014). Parameter estimation of weibull growth models in forestry. *parameters*, *1*, 5.

Málaga, N., de Bruin, S., McRoberts, R. E., Olivos, A. A., de la Cruz Paiva, R., Montesinos, P. D., Suarez, D. R., & Herold, M. (2022). Precision of subnational forest AGB estimates within the peruvian amazonia using a global biomass map. *International Journal of Applied Earth Observation and Geoinformation*, *115*, 103102. doi:10.1016/j.jag.2022.103102.

Mascaro, J., Asner, G. P., Knapp, D. E., Kennedy-Bowdoin, T., Martin, R. E., Anderson, C., Higgins, M., & Chadwick, K. D. (2014). A tale of two "forests": Random forest machine learning aids tropical forest carbon mapping. *PLoS ONE*, *9*, e85993. doi:https://doi.org/10.1371/journal.pone.0085993.

Mauro, F., Ritchie, M., Wing, B., Frank, B., Monleon, V., Temesgen, H., & Hudak, A. (2019). Estimation of changes of forest structural attributes at three different spatial aggregation levels in northern california using multitemporal LiDAR. *Remote Sensing*, *11*, 923.

McRoberts, R., Næsset, E., Sannier, C., Stehman, S., & Tomppo, E. (2020). Remote sensing support for the gain-loss approach for greenhouse gas inventories. *Remote Sensing*, *12*, 1891. doi:10.3390/rs12111891.

McRoberts, R. E., Chen, Q., Domke, G. M., Ståhl, G., Saarela, S., & Westfall, J. A. (2016). Hybrid estimators for mean aboveground carbon per unit area. *Forest Ecology and Management*, *378*, 44–56. doi:https://doi.org/10.1016/j.foreco.2016.07.007.

McRoberts, R. E., Holden, G. R., Nelson, M. D., Liknes, G. C., & Gormanson, D. D. (2005). Using satellite imagery as ancillary data for increasing the precision of estimates

for the forest inventory and analysis program of the USDA forest service. *Canadian Journal of Forest Research*, *35*, 2968–2980. doi:10.1139/x05-222.

McRoberts, R. E., Næsset, E., & Gobakken, T. (2015). The effects of temporal differences between map and ground data on map-assisted estimates of forest area and biomass. *Annals of Forest Science*, *73*, 839–847. doi:https://doi.org/10.1007/s13595-015-0485-6.

McRoberts, R. E., Næsset, E., Liknes, G. C., Chen, Q., Walters, B. F., Saatchi, S., & Herold, M. (2019a). Using a finer resolution biomass map to assess the accuracy of a regional, map-based estimate of forest biomass. *Surveys in Geophysics*, *40*, 1001–1015. doi:https://doi.org/10.1007/s10712-019-09507-1.

McRoberts, R. E., Næsset, E., Saatchi, S., Liknes, G. C., Walters, B. F., & Chen, Q. (2019b). Local validation of global biomass maps. *International Journal of Applied Earth Observation and Geoinformation*, *83*, 101931. doi:https://doi.org/10.1016/j.jag.2019.101931.

McRoberts, R. E., Næsset, E., Saatchi, S., & Quegan, S. (2022). Statistically rigorous, model-based inferences from maps. *Remote Sensing of Environment*, *279*, 113028. doi:10.1016/j.rse.2022.113028.

McRoberts, R. E., & Tomppo, E. O. (2007). Remote sensing support for national forest inventories. *Remote sensing of environment*, *110*, 412–419. doi:10.1016/j.rse.2006.09.034.

Meinshausen, N., & Ridgeway, G. (2006). Quantile regression forests. *Journal of machine learning research*, *7*.

Menlove, J., & Healey, S. P. (2020). A comprehensive forest biomass dataset for the USA allows customized validation of remotely sensed biomass estimates. *Remote Sensing*, *12*, 4141. doi:10.3390/rs12244141.

Meyer, H., & Pebesma, E. (2021). Predicting into unknown space? estimating the area of applicability of spatial prediction models. *Methods in Ecology and Evolution*, *12*, 1620–1633. doi:10.1111/2041-210x.13650.

Meyer, H., Reudenbach, C., Wöllauer, S., & Nauss, T. (2019). Importance of spatial predictor variable selection in machine learning applications – moving from data reproduction to spatial prediction. *Ecological Modelling*, *411*, 108815. doi:https://doi.org/10.1016/j.ecolmodel.2019.108815.

Mitchard, E., Saatchi, S., Lewis, S., Feldpausch, T., Woodhouse, I., Sonké, B., Rowland, C., & Meir, P. (2011). Measuring biomass changes due to woody encroachment and deforestation/degradation in a forest–savanna boundary region of central africa using multi-temporal l-band radar backscatter. *Remote Sensing of Environment*, *115*, 2861–2873. doi:https://doi.org/10.1016/j.rse.2010.02.022.

Mitchard, E. T., Saatchi, S. S., Baccini, A., Asner, G. P., Goetz, S. J., Harris, N. L., & Brown, S. (2013). Uncertainty in the spatial distribution of tropical forest biomass: a comparison of pan-tropical maps. *Carbon Balance and Management*, *8*. doi:https://doi.org/10.1186/1750-0680-8-10.

Mitchard, E. T. A. et al. (2014). Markedly divergent estimates of amazon forest carbon density from ground plots and satellites. *Global Ecology and Biogeography*, *23*, 935–946. doi:https://doi.org/10.1111/geb.12168.

Mitchard, E. T. A., Saatchi, S. S., Woodhouse, I. H., Nangendo, G., Ribeiro, N. S., Williams, M., Ryan, C. M., Lewis, S. L., Feldpausch, T. R., & Meir, P. (2009). Using satellite radar backscatter to predict above-ground woody biomass: A consistent relationship across four different african landscapes. *Geophysical Research Letters*, *36*. doi:https://doi.org/10.1029/2009gl040692.

Moffette, F., Alix-Garcia, J., Shea, K., & Pickens, A. H. (2021). The impact of near-real-time deforestation alerts across the tropics. *Nature Climate Change*, *11*, 172–178. doi:10.1038/s41558-020-00956-w.

Morel, A. C., Saatchi, S. S., Malhi, Y., Berry, N. J., Banin, L., Burslem, D., Nilus, R., & Ong, R. C. (2011). Estimating aboveground biomass in forest and oil palm plantation in sabah, malaysian borneo using ALOS PALSAR data. *Forest Ecology and Management*, *262*, 1786–1798. doi:https://doi.org/10.1016/j.foreco.2011.07.008.

Moreno, A., Neumann, M., & Hasenauer, H. (2016). Optimal resolution for linking remotely sensed and forest inventory data in europe. *Remote Sensing of Environment*, *183*, 109–119. doi:10.1016/j.rse.2016.05.021.

Murdiyarso, D., Donato, D., Kauffman, J. B., Kurnianto, S., Stidham, M., & Kanninen, M. (2009). Carbon storage in mangrove and peatland ecosystems: A preliminary account from plots in indonesia. *Working paper 48. Bogor Banat, Indonesia: Center for International Forestry Research. 35 p.*, (pp. 1–35).

Nabuurs, G.-J., Harris, N., Sheil, D., Palahi, M., Chirici, G., Boissière, M., Fay, C., Reiche, J., & Valbuena, R. (2022). Glasgow forest declaration needs new modes of data ownership. *Nature Climate Change*, . doi:10.1038/s41558-022-01343-3.

Næsset, E., Bollandsås, O. M., Gobakken, T., Solberg, S., & McRoberts, R. E. (2015). The effects of field plot size on model-assisted estimation of aboveground biomass change using multitemporal interferometric SAR and airborne laser scanning data. *Remote Sensing of Environment*, *168*, 252–264. doi:https://doi.org/10.1016/j.rse.2015.07.002.

Næsset, E., McRoberts, R. E., Pekkarinen, A., Saatchi, S., Santoro, M., Trier, Ø. D., Zahabu, E., & Gobakken, T. (2020). Use of local and global maps of forest canopy height and aboveground biomass to enhance local estimates of biomass in miombo woodlands in tanzania. *International Journal of Applied Earth Observation and Geoinformation*,

89, 102138. doi:https://doi.org/10.1016/j.jag.2020.102138.

Nascimento, H. E., & Laurance, W. F. (2002). Total aboveground biomass in central amazonian rainforests: a landscape-scale study. *Forest Ecology and Management*, *168*, 311–321. doi:https://doi.org/10.1016/s0378-1127(01)00749-6.

Nesha, K., Herold, M., Sy, V. D., de Bruin, S., Araza, A., Málaga, N., Gamarra, J. G., Hergoualc'h, K., Pekkarinen, A., Ramirez, C., Morales-Hidalgo, D., & Tavani, R. (2022). Exploring characteristics of national forest inventories for integration with global space-based forest biomass data. *Science of The Total Environment*, *850*, 157788. doi:10.1016/j.scitotenv.2022.157788.

Nesha, M. K., Herold, M., Sy, V. D., Duchelle, A. E., Martius, C., Branthomme, A., Garzuglia, M., Jonsson, O., & Pekkarinen, A. (2021). An assessment of data sources, data quality and changes in national forest monitoring capacities in the global forest resources assessment 2005-2020. *Environmental Research Letters*, . doi:https://doi.org/10.1088/1748-9326/abd81b.

Nguyen, T. H., Jones, S., Soto-Berelov, M., Haywood, A., & Hislop, S. (2019). Landsat time-series for estimating forest aboveground biomass and its dynamics across space and time: A review. *Remote Sensing*, *12*, 98. doi:10.3390/rs12010098.

Nguyen, T. H., Jones, S. D., Soto-Berelov, M., Haywood, A., & Hislop, S. (2020). Monitoring aboveground forest biomass dynamics over three decades using landsat time-series and single-date inventory data. *International Journal of Applied Earth Observation and Geoinformation*, *84*, 101952. doi:https://doi.org/10.1016/j.jag.2019.101952.

Nightingale, J., Schaepman-Strub, G., Nickeson, J., Baret, F., & Herold, M. (2010). Assessing satellite-derived land product quality for earth system science applications: results from the ceos lpv sub-group, .

Olofsson, P., Arévalo, P., Espejo, A. B., Green, C., Lindquist, E., McRoberts, R. E., & Sanz, M. J. (2020). Mitigating the effects of omission errors on area and area change estimates. *Remote Sensing of Environment*, *236*, 111492. doi:10.1016/j.rse.2019.111492.

a Pacheco-Pascagaza, A. M., Garcia, M., Guez-Veiga, P. R., & Balzter, H. (2018). The use of multifrequency sar data for assessing levels of forest disturbance in bajo calima colombia. In *IGARSS 2018-2018 IEEE International Geoscience and Remote Sensing Symposium* (pp. 7015–7018). IEEE.

Peylin, P., Broquet, G., Chevallier, F., Palmer, P., Thompson, R., Bousquet, P., Maenhout, G., Lequere, C., Kutsch, W., DeCola, P. et al. (2019). Verify: a new european project to derive an observation-based system for monitoring and verification of greenhouse gases. In *Geophysical Research Abstracts*. volume 21.

Phillips, O. L., , & Brienen, R. J. W. (2017). Carbon uptake by mature amazon forests has mitigated amazon nations' carbon emissions. *Carbon Balance and Management*,

12. doi:10.1186/s13021-016-0069-2.

Ploton, P. et al. (2020a). A map of african humid tropical forest aboveground biomass derived from management inventories. *Scientific Data*, *7*. doi:https://doi.org/10.1038/s41597-020-0561-0.

Ploton, P. et al. (2020b). Spatial validation reveals poor predictive performance of large-scale ecological mapping models. *Nature Communications*, *11*. doi:https://doi.org/10.1038/s41467-020-18321-y.

Poggio, L., de Sousa, L. M., Batjes, N. H., Heuvelink, G. B. M., Kempen, B., Ribeiro, E., & Rossiter, D. (2021). SoilGrids 2.0: producing soil information for the globe with quantified spatial uncertainty. *SOIL*, *7*, 217–240. doi:10.5194/soil-7-217-2021.

Popescu, S. C., Wynne, R. H., & Scrivani, J. A. (2004). Fusion of small-footprint lidar and multispectral data to estimate plot-level volume and biomass in deciduous and pine forests in virginia, usa. *Forest Science*, *50*, 551–565.

Potapov, P. et al. (2022). The global 2000-2020 land cover and land use change dataset derived from the landsat archive: First results. *Frontiers in Remote Sensing*, *3*. doi:10.3389/frsen.2022.856903.

Potapov, P. et al. (2021). Mapping global forest canopy height through integration of GEDI and landsat data. *Remote Sensing of Environment*, *253*, 112165. doi:10.1016/j.rse.2020.112165.

Quegan, S., & Ciais, P. (2018). *User Requirement Document*. Technical Report, European Space Agency.

Quegan, S. et al. (2019). The european space agency BIOMASS mission: Measuring forest above-ground biomass from space. *Remote Sensing of Environment*, *227*, 44–60. doi:10.1016/j.rse.2019.03.032.

Ramesh, B., Venugopal, P. D., Pélissier, R., Patil, S. V., Swaminath, M., & Couteron, P. (2010). Mesoscale patterns in the floristic composition of forests in the central western ghats of karnataka, india. *Biotropica*, *42*, 435–443.

Reiche, J. et al. (2021). Forest disturbance alerts for the congo basin using sentinel-1. *Environmental Research Letters*, *16*, 024005. doi:10.1088/1748-9326/abd0a8.

Réjou-Méchain, M. et al. (2019). Upscaling forest biomass from field to satellite measurements: Sources of errors and ways to reduce them. *Surveys in Geophysics*, *40*, 881–911. doi:https://doi.org/10.1007/s10712-019-09532-0.

Rejou-Mechain, M., Muller-Landau, H. C., Detto, M., Thomas, S., Toan, T. L., Saatchi, S., Barreto-Silvia, J., Bourg, N., Bunyavejchewin, S., Butt, N. et al. (2014). Local spatial structure of forest biomass and its consequences for remote sensing of carbon stocks. *Biogeosciences Discussions*, *11*, 5711.

Rejou-Mechain, M., Tanguy, A., Piponiot, C., Chave, J., & Herault, B. (2017). biomass:

an r package for estimating above-ground biomass and its uncertainty in tropical forests. *Methods in Ecology and Evolution*, *8*, 1163–1167.

Rodríguez-Veiga, P. et al. (2019). Forest biomass retrieval approaches from earth observation in different biomes. *International Journal of Applied Earth Observation and Geoinformation*, *77*, 53–68. doi:https://doi.org/10.1016/j.jag.2018.12.008.

Rodríguez-Veiga, P., Saatchi, S., Tansey, K., & Balzter, H. (2016). Magnitude, spatial distribution and uncertainty of forest biomass stocks in mexico. *Remote Sensing of Environment*, *183*, 265–281. doi:https://doi.org/10.1016/j.rse.2016.06.004.

Rodríguez-Veiga, P., Wheeler, J., Louis, V., Tansey, K., & Balzter, H. (2017). Quantifying forest biomass carbon stocks from space. *Current Forestry Reports*, *3*, 1–18. doi:https://doi.org/10.1007/s40725-017-0052-5.

Roman-Cuesta, R. M. et al. (2016). Hotspots of gross emissions from the land use sector: patterns, uncertainties, and leading emission sources for the period 2000–2005 in the tropics. *Biogeosciences*, *13*, 4253–4269. doi:10.5194/bg-13-4253-2016.

Rosen, P. A., Kim, Y., Kumar, R., Misra, T., Bhan, R., & Sagi, V. R. (2017). Global persistent SAR sampling with the NASA-ISRO SAR (NISAR) mission. In *2017 IEEE Radar Conference (RadarConf)*. IEEE. doi:10.1109/radar.2017.7944237.

Ruesch, A., & Gibbs, H. (2008). New global biomass carbon map for the year 2000 based on ipcc tier-1 methodology. *Oak Ridge National Laboratory's Carbon Dioxide Information Analysis Center: Oak Ridge, USA. Available online from the Carbon Dioxide Information Analysis Center, URL: http://cdiac. ornl. gov*, .

Ryan, C. M., Hill, T., Woollen, E., Ghee, C., Mitchard, E., Cassells, G., Grace, J., Woodhouse, I. H., & Williams, M. (2011). Quantifying small-scale deforestation and forest degradation in african woodlands using radar imagery. *Global Change Biology*, *18*, 243–257. doi:10.1111/j.1365-2486.2011.02551.x.

Saatchi, S., Marlier, M., Chazdon, R. L., Clark, D. B., & Russell, A. E. (2011a). Impact of spatial variability of tropical forest structure on radar estimation of aboveground biomass. *Remote Sensing of Environment*, *115*, 2836–2849. doi:https://doi.org/10.1016/j.rse.2010.07.015.

Saatchi, S. S., Harris, N. L., Brown, S., Lefsky, M., Mitchard, E. T., Salas, W., Zutta, B. R., Buermann, W., Lewis, S. L., Hagen, S. et al. (2011b). Benchmark map of forest carbon stocks in tropical regions across three continents. *Proceedings of the national academy of sciences*, *108*, 9899–9904. doi:https://doi.org/10.1073/pnas.1019576108.

Saatchi, S. S., Houghton, R. A., Alvala, R. C. D. S., Soares, J. V., & Yu, Y. (2007). Distribution of aboveground live biomass in the amazon basin. *Global Change Biology*, *13*, 816–837. doi:10.1111/j.1365-2486.2007.01323.x.

Sandker, M., Carrillo, O., Leng, C., Lee, D., d'Annunzio, R., & Fox, J. (2021). The importance of high–quality data for REDD monitoring and reporting. *Forests*, *12*, 99. doi:10.3390/f12010099.

Santoro, M. (2020). *CCI Biomass Product User Guide v2*. Technical Report, European Space Agency.

Santoro, M., Beaudoin, A., Beer, C., Cartus, O., Fransson, J. E., Hall, R. J., Pathe, C., Schmullius, C., Schepaschenko, D., Shvidenko, A., Thurner, M., & Wegmüller, U. (2015). Forest growing stock volume of the northern hemisphere: Spatially explicit estimates for 2010 derived from envisat ASAR. *Remote Sensing of Environment*, *168*, 316–334. doi:https://doi.org/10.1016/j.rse.2015.07.005.

Santoro, M., Beer, C., Cartus, O., Schmullius, C., Shvidenko, A., McCallum, I., Wegmüller, U., & Wiesmann, A. (2011). Retrieval of growing stock volume in boreal forest using hyper-temporal series of envisat ASAR ScanSAR backscatter measurements. *Remote Sensing of Environment*, *115*, 490–507. doi:https://doi.org/10.1016/j.rse.2010.09.018.

Santoro, M., & Cartus, O. (2019). Esa biomass climate change initiative (biomass_cci): Global datasets of forest above-ground biomass for the year 2017, v1. doi:https://doi.org/10.5285/BEDC59F37C9545C981A839EB552E4084.

Santoro, M., & Cartus, O. (2021). Esa biomass climate change initiative (biomass_cci): Global datasets of forest above-ground biomass for the year 2017, v2. doi:10.5285/BEDC59F37C9545C981A839EB552E4084.

Santoro, M. et al. (2020). The global forest above-ground biomass pool for 2010 estimated from high-resolution satellite observations, . doi:https://doi.org/10.5194/essd-2020-148.

Santoro, M. et al. (2021). The global forest above-ground biomass pool for 2010 estimated from high-resolution satellite observations. *Earth System Science Data*, *13*, 3927–3950. doi:10.5194/essd-13-3927-2021.

Santoro, M., Cartus, O., & Fransson, J. E. (2022a). Dynamics of the swedish forest carbon pool between 2010 and 2015 estimated from satellite l-band SAR observations. *Remote Sensing of Environment*, *270*, 112846. doi:10.1016/j.rse.2021.112846.

Santoro, M., Cartus, O., Wegmüller, U., Besnard, S., Carvalhais, N., Araza, A., Herold, M., Liang, J., Cavlovic, J., & Engdahl, M. E. (2022b). Global estimation of above-ground biomass from spaceborne c-band scatterometer observations aided by LiDAR metrics of vegetation structure. *Remote Sensing of Environment*, *279*, 113114. doi:10.1016/j.rse.2022.113114.

dos Santos, M., Keller, M., & Morton, D. (2019). Lidar surveys over selected forest research sites, brazilian amazon, 2008-2018. doi:https://doi.org/10.3334/ORNLDAAC/1644.

Schelhaas, M., Clerkx, A., Daamen, W., Oldenburger, J., Velema, G., Schnitger, P., Schoonderwoerd, H., & Kramer, H. (2014). *Zesde Nederlandse bosinventarisatie: methoden en basisresultaten*. Technical Report, Alterra, Wageningen-UR.

Schelhaas, M.-J. et al. (2018). Actual european forest management by region, tree species and owner based on 714, 000 re-measured trees in national forest inventories. *PLOS ONE*, *13*, e0207151. doi:https://doi.org/10.1371/journal.pone.0207151.

Schepaschenko, D., Chave, J., Phillips, O. L., Lewis, S. L., Davies, S. J., Réjou-Méchain, M., Sist, P., Scipal, K., Perger, C., Hérault, B. et al. (2019). The forest observation system, building a global reference dataset for remote sensing of forest biomass. *Scientific data*, *6*, 1–11. doi:10.1038/s41597-019-0196-1.

Schimel, D., Pavlick, R., Fisher, J. B., Asner, G. P., Saatchi, S., Townsend, P., Miller, C., Frankenberg, C., Hibbard, K., & Cox, P. (2015). Observing terrestrial ecosystems and the carbon cycle from space. *Global Change Biology*, *21*, 1762–1776. doi:https://doi.org/10.1111/gcb.12822.

Sexton, J. O., Song, X.-P., Feng, M., Noojipady, P., Anand, A., Huang, C., Kim, D.-H., Collins, K. M., Channan, S., DiMiceli, C., & Townshend, J. R. (2013). Global, 30-m resolution continuous fields of tree cover: Landsat-based rescaling of MODIS vegetation continuous fields with lidar-based estimates of error. *International Journal of Digital Earth*, *6*, 427–448. doi:10.1080/17538947.2013.786146.

Shapiro, A. C., Grantham, H. S., Aguilar-Amuchastegui, N., Murray, N. J., Gond, V., Bonfils, D., & Rickenbach, O. (2021). Forest condition in the congo basin for the assessment of ecosystem conservation status. *Ecological Indicators*, *122*, 107268. doi:10.1016/j.ecolind.2020.107268.

Shettles, M., Temesgen, H., Gray, A. N., & Hilker, T. (2015). Comparison of uncertainty in per unit area estimates of aboveground biomass for two selected model sets. *Forest Ecology and Management*, *354*, 18–25. doi:10.1016/j.foreco.2015.07.002.

Silva, C. A., Duncanson, L., Hancock, S., Neuenschwander, A., Thomas, N., Hofton, M., Fatoyinbo, L., Simard, M., Marshak, C. Z., Armston, J., Lutchke, S., & Dubayah, R. (2021). Fusing simulated GEDI, ICESat-2 and NISAR data for regional aboveground biomass mapping. *Remote Sensing of Environment*, *253*, 112234. doi:10.1016/j.rse.2020.112234.

Sinha, S., Jeganathan, C., Sharma, L. K., & Nathawat, M. S. (2015). A review of radar remote sensing for biomass estimation. *International Journal of Environmental Science and Technology*, *12*, 1779–1792. doi:10.1007/s13762-015-0750-0.

Slik, J. W. F. et al. (2013). Large trees drive forest aboveground biomass variation in moist lowland forests across the tropics. *Global Ecology and Biogeography*, *22*, 1261–1271. doi:https://doi.org/10.1111/geb.12092.

Spawn, S. A., Sullivan, C. C., Lark, T. J., & Gibbs, H. K. (2020). Harmonized global

maps of above and belowground biomass carbon density in the year 2010. *Scientific Data*, *7*. doi:10.1038/s41597-020-0444-4.

Suarez, D. R. et al. (2019). Estimating aboveground net biomass change for tropical and subtropical forests: Refinement of IPCC default rates using forest plot data. *Global Change Biology*, *25*, 3609–3624. doi:https://doi.org/10.1111/gcb.14767.

Taghizadeh-Mehrjardi, R., Schmidt, K., Eftekhari, K., Behrens, T., Jamshidi, M., Davatgar, N., Toomanian, N., & Scholten, T. (2020). Synthetic resampling strategies and machine learning for digital soil mapping in iran. *European Journal of Soil Science*, *71*, 352–368. doi:10.1111/ejss.12893.

Takoutsing, B., & Heuvelink, G. B. (2022). Comparing the prediction performance, uncertainty quantification and extrapolation potential of regression kriging and random forest while accounting for soil measurement errors. *Geoderma*, *428*, 116192. doi:10.1016/j.geoderma.2022.116192.

Toan, T. L., Quegan, S., Davidson, M., Balzter, H., Paillou, P., Papathanassiou, K., Plummer, S., Rocca, F., Saatchi, S., Shugart, H., & Ulander, L. (2011). The BIOMASS mission: Mapping global forest biomass to better understand the terrestrial carbon cycle. *Remote Sensing of Environment*, *115*, 2850–2860. doi:https://doi.org/10.1016/j.rse.2011.03.020.

Tomppo, E., Gschwantner, T., Lawrence, M., & McRoberts, R. E. (Eds.) (2010). *National Forest Inventories*. Springer Netherlands. doi:10.1007/978-90-481-3233-1.

Tsutsumida, N., Rodríguez-Veiga, P., Harris, P., Balzter, H., & Comber, A. (2019). Investigating spatial error structures in continuous raster data. *International Journal of Applied Earth Observation and Geoinformation*, *74*, 259–268. doi:https://doi.org/10.1016/j.jag.2018.09.020.

Tubiello, F. N., Conchedda, G., Wanner, N., Federici, S., Rossi, S., & Grassi, G. (2021). Carbon emissions and removals from forests: new estimates, 1990–2020. *Earth System Science Data*, *13*, 1681–1691. doi:10.5194/essd-13-1681-2021.

Tucker, C., Vanpraet, C., Sharman, M., & Ittersum, G. V. (1985). Satellite remote sensing of total herbaceous biomass production in the senegalese sahel: 1980–1984. *Remote Sensing of Environment*, *17*, 233–249. doi:10.1016/0034-4257(85)90097-5.

Turubanova, S., Potapov, P. V., Tyukavina, A., & Hansen, M. C. (2018). Ongoing primary forest loss in brazil, democratic republic of the congo, and indonesia. *Environmental Research Letters*, *13*, 074028. doi:10.1088/1748-9326/aacd1c.

Tyukavina, A., Baccini, A., Hansen, M. C., Potapov, P. V., Stehman, S. V., Houghton, R. A., Turubanova, S., & Goetz, S. J. (2018). Aboveground carbon loss in natural and managed tropical forests from 2000 to 2012 (2015 environ. res. lett. 10 074002). *Environmental Research Letters*, *13*, 109501. doi:10.1088/1748-9326/aae31e.

UN (2021). *System of Environmental-Economic Accounting— Ecosystem Accounting (SEEA EA)*.

UN-FAO (2010). *Global Forest Resources Assessment 2010: Main report*. Technical Report, .

UN-FAO (2020). *Global Forest Resources Assessment 2020*. Technical Report, .

Vargas, L., Willemen, L., & Hein, L. (2018). Assessing the capacity of ecosystems to supply ecosystem services using remote sensing and an ecosystem accounting approach. *Environmental Management*, *63*, 1–15. doi:10.1007/s00267-018-1110-x.

Verbesselt, J., Hyndman, R., Zeileis, A., & Culvenor, D. (2010). Phenological change detection while accounting for abrupt and gradual trends in satellite image time series. *Remote Sensing of Environment*, *114*, 2970–2980. doi:10.1016/j.rse.2010.08.003.

Vieilledent, G., Gardi, O., Grinand, C., Burren, C., Andriamanjato, M., Camara, C., Gardner, C. J., Glass, L., Rasolohery, A., Ratsimba, H. R., Gond, V., & Rakotoarijaona, J.-R. (2016). Bioclimatic envelope models predict a decrease in tropical forest carbon stocks with climate change in madagascar. *Journal of Ecology*, *104*, 703–715. doi:https://doi.org/10.1111/1365-2745.12548.

Wager, S., Hastie, T., & Efron, B. (2014). Confidence intervals for random forests: The jackknife and the infinitesimal jackknife. *The Journal of Machine Learning Research*, *15*, 1625–1651.

Wernick, I. K., Ciais, P., Fridman, J., Högberg, P., Korhonen, K. T., Nordin, A., & Kauppi, P. E. (2021). Quantifying forest change in the european union. *Nature*, *592*, E13–E14. doi:10.1038/s41586-021-03293-w.

Whittaker, R. (1975). Whittaker biome diagram.

Wigneron, J.-P., Li, X., Frappart, F., Fan, L., Al-Yaari, A., Lannoy, G. D., Liu, X., Wang, M., Masson, E. L., & Moisy, C. (2021). SMOS-IC data record of soil moisture and l-VOD: Historical development, applications and perspectives. *Remote Sensing of Environment*, *254*, 112238. doi:10.1016/j.rse.2020.112238.

Wijaya, A., Liesenberg, V., Susanti, A., Karyanto, O., & Verchot, L. V. (2015). Estimation of biomass carbon stocks over peat swamp forests using multi-temporal and multi-polratizations SAR data. *ISPRS - International Archives of the Photogrammetry, Remote Sensing and Spatial Information Sciences*, *XL-7/W3*, 551–556. doi:https://doi.org/10.5194/isprsarchives-xl-7-w3-551-2015.

Willcock, S. et al. (2014). Quantifying and understanding carbon storage and sequestration within the eastern arc mountains of tanzania, a tropical biodiversity hotspot. *Carbon Balance and Management*, *9*. doi:https://doi.org/10.1186/1750-0680-9-2.

Witjes, M. et al. (2022). A spatiotemporal ensemble machine learning framework for generating land use/land cover time-series maps for europe (2000–2019) based on LUCAS,

CORINE and GLAD landsat. *PeerJ*, *10*, e13573. doi:10.7717/peerj.13573.

Wolpert, D. H. (1992). Stacked generalization. *Neural Networks*, *5*, 241–259. doi:10.1016/s0893-6080(05)80023-1.

Woodcock, C. E., Loveland, T. R., Herold, M., & Bauer, M. E. (2020). Transitioning from change detection to monitoring with remote sensing: A paradigm shift. *Remote Sensing of Environment*, *238*, 111558. doi:10.1016/j.rse.2019.111558.

Wright, M. N., & Ziegler, A. (2017). ranger: A fast implementation of random forests for high dimensional data in c and r. *Journal of Statistical Software*, *77*. doi:https://doi.org/10.18637/jss.v077.i01.

Xu, L. et al. (2021). Changes in global terrestrial live biomass over the 21st century. *Science Advances*, *7*, eabe9829. doi:10.1126/sciadv.abe9829.

Xu, L., Saatchi, S. S., Yang, Y., Yu, Y., & White, L. (2016). Performance of non-parametric algorithms for spatial mapping of tropical forest structure. *Carbon Balance and Management*, *11*. doi:https://doi.org/10.1186/s13021-016-0062-9.

Yanai, R., Wayson, C., Lee, D., Espejo, A., Campbell, J. L., Green, M. B., Zukswert, J. M., Yoffe, S., Aukema, J., Lister, A., Kirchner, J. W., & Gamarra, J. G. P. (2020). Improving uncertainty in forest carbon accounting for REDD mitigation efforts. *Environmental Research Letters*, . doi:10.1088/1748-9326/abb96f.

Yang, H. et al. (2022). Climatic and biotic factors influencing regional declines and recovery of tropical forest biomass from the 2015/16 el niño. *Proceedings of the National Academy of Sciences*, *119*. doi:10.1073/pnas.2101388119.

Yang, L., Liang, S., & Zhang, Y. (2020). A new method for generating a global forest aboveground biomass map from multiple high-level satellite products and ancillary information. *IEEE Journal of Selected Topics in Applied Earth Observations and Remote Sensing*, *13*, 2587–2597. doi:https://doi.org/10.1109/jstars.2020.2987951.

Yu, Y., Saatchi, S., Domke, G. M., Walters, B., Woodall, C., Ganguly, S., Li, S., Kalia, S., Park, T., Nemani, R., Hagen, S. C., & Melendy, L. (2022). Making the US national forest inventory spatially contiguous and temporally consistent. *Environmental Research Letters*, *17*, 065002. doi:10.1088/1748-9326/ac6b47.

Zhang, Q., Liang, Y., & He, H. (2018). Tree-lists estimation for chinese boreal forests by integrating weibull diameter distributions with MODIS-based forest attributes from kNN imputation. *Forests*, *9*, 758. doi:https://doi.org/10.3390/f9120758.

Zhang, X., Duan, A., Zhang, J., & Xiang, C. (2014). Estimating tree height-diameter models with the bayesian method. *The Scientific World Journal*, *2014*, 1–9. doi:https://doi.org/10.1155/2014/683691.

Zhang, Y., & Liang, S. (2020). Fusion of multiple gridded biomass datasets for generating a global forest aboveground biomass map. *Remote Sensing*, *12*, 2559. doi:https://

doi.org/10.3390/rs12162559.

Zhang, Y., Liang, S., & Yang, L. (2019). A review of regional and global gridded forest biomass datasets. *Remote Sensing*, *11*, 2744. doi:https://doi.org/10.3390/rs11232744.

Zhang, Y., Ma, J., Liang, S., Li, X., & Liu, J. (2022). A stacking ensemble algorithm for improving the biases of forest aboveground biomass estimations from multiple remotely sensed datasets. *GIScience &amp Remote Sensing*, *59*, 234–249. doi:10.1080/15481603.2021.2023842.

Zhao, K., Suarez, J. C., Garcia, M., Hu, T., Wang, C., & Londo, A. (2018). Utility of multitemporal lidar for forest and carbon monitoring: Tree growth, biomass dynamics, and carbon flux. *Remote Sensing of Environment*, *204*, 883–897. doi:10.1016/j.rse.2017.09.007.

Zhao, P., Lu, D., Wang, G., Wu, C., Huang, Y., & Yu, S. (2016). Examining spectral reflectance saturation in landsat imagery and corresponding solutions to improve forest aboveground biomass estimation. *Remote Sensing*, *8*, 469. doi:https://doi.org/10.3390/rs8060469.

Acknowledgements

Until now, the possibility of being a "doctor" is still not sinking into my mind. This four-year roller-coaster working-mostly-from-home journey is finally ending - and it's really ending because I'm now writing the Acknowledgement page (May 2023)!

Doing and finishing this unexpected PhD is impossible without the constant help of my supervisors. Martin's bright ideas and analytical mind helped a lot in shaping my PhD papers. His trust also gave me exposure to the international research scene. I appreciate his quotable phrases whenever I needed motivation and reminders. I'll always be thankful for Sytze's technical inputs, on-point and constructive reviews and commitment all throughout the PhD. He is indeed the daily supervisor you can count on. I thank Lars not only for the ecosystem accounting flavor of my PhD but more importantly for his constant concern for me and my family's welfare being expats in the Netherlands.

To the GRS and ESA colleagues, though I'm not always around during coffee breaks and lunch outs, I appreciate our limited but meaningful small talk and hi-hello. I always get inspired to see how you guys talk about your individual research and I feel proud whenever you publish something cool. I also learned a lot from the random talks about food and culture. I will miss the busy Monday feels at GRS, the room 332 meetings and perhaps even Truus' reminders to fill up the time sheets :-). Special thanks to the GRS board for funding my IGARSS 2022 conference in Malaysia.

Many thanks to the PE&RC for the relaxing and informative PhD weekends. Thanks to Claudius and Lennart for the guidance needed by PhDs.

Salamat sa WUR pinoys 2016-2023; mga pinoy families dito; at sa mga sobrang bait na ate dito at sa inyong mga mister na Dutch na naging tropang dikit ko. Ang ating mga inuman, kwentuhan, baraha, gala, basketbol, tambay sa rhine river at mga mukbang na parang walang bukas ay talagang nakawala nang istres.

My lifetime gratitude to my first love, April Ann, first for giving me my *Chingbuching* Amity and second for sacrificing a lot to build a family with me here in the Netherlands. The other half of my achievements should be yours. But now that the PhD is ending, it's time to make our 2nd baby! To my family and friends in the Philippines that I always miss, I would say you fueled my tank whenever I needed it the most.

To The Almighty, your plan to make me a “scientist” has also challenged my faith several times. Challenges only make things stronger. To God be the glory!

About the author

The author was born and raised in the province of Laguna, Philippines. He comes from a family of teachers and had the unique opportunity to be a student of both his grandmother (kindergarten) and mother (high school). The author studied Certificate in Forestry and BS Forestry from 2003 to 2009 at the University of the Philippines and became a professional Forester afterward. That journey has connected him with nature. In 2006, the author joined the Upsilon Sigma Phi fraternity where striving for excellence is inculcated. He also did public service as an elected local government official (*Sangguniang Barangay*) from 2008 to 2014. He was also an active choir member at the *San Agustin* Parish Church back then.

For his first work experience, he traveled throughout the Philippines climbing mountains to measure and identify trees, and meeting not just local people but also snakes and killer bees in the mountains. Then he learned and practiced Geographic Information System (GIS) used for different land use plans of local governments. Then he did consultancy work, the most memorable are the Phil-WAVES and ProFor ecosystem accounting pilot projects in 2016 by the World Bank where he provided the needed spatial models and other GIS-related work. The author also met Lars Hein there who encouraged him to do graduate studies at Wageningen University. That plan obviously materialized after a year but it was a bittersweet moment as the author needed to go abroad while leaving his 3-month-old daughter in the Philippines.

The author took Masters's in Geo-information Science (2016-2018) where the author efficiently learned a lot about remote sensing and programming, experienced daily discussions with groupmates and appreciated how impactful research could be. The author's MSc thesis and internship topics were still about forests, but with a touch of data-driven approaches and in the context of climate change. After the MGI, the author was offered a temporary research job by his MSc supervisor Martin Herold - which eventually turned into a PhD and the rest is history. The author will contribute to Open Earth Monitor and SELINA projects as a post-doctoral researcher. He will also continue doing advocacy research work in the Philippines.

In terms of hobbies, the author tries to stay fit by smashing shuttlecocks and shooting basketballs. The author is also a self-declared chef while staying abroad, thanks to Youtube.

He also likes to drink coffee and beer (hours apart) while thinking of business ideas and research topics for his home country. He and his family enjoy renting *OV fiets* to cycle around different cities and places in the Netherlands.

Peer-reviewed publications

Araza, A., De Bruin, S., Herold, M., Quegan, S., Labriere, N., Rodriguez-Veiga, P., ... & Lucas, R. (2022). A comprehensive framework for assessing the accuracy and uncertainty of global above-ground biomass maps. *Remote Sensing of Environment, 272,* 112917.

Araza, A., Herold, M., De Bruin, S., Ciais, P., Gibbs, D. A., Harris, N., ... & Hein, L. (2023). Past decade above-ground biomass change comparisons from four multi-temporal global maps. *International Journal of Applied Earth Observation and Geoinformation, 118,* 103274.

Araza, A., De Bruin, S., Hein, L., & Herold, M. Spatial predictions and uncertainties of forest carbon fluxes for environmental-economic accounting. *Nature Scientific Reports* (Minor revision as of May 20, 2023).

Csillik, O., Reiche, J., De Sy, V., Araza, A., & Herold, M. (2022). Rapid remote monitoring reveals spatial and temporal hotspots of carbon loss in Africa's rainforests. *Communications Earth & Environment, 3*(1), 48.

Araza, A. B., Castillo, G. B., Buduan, E. D., Hein, L., Herold, M., Reiche, J., ... & Razal, R. A. (2021). Intra-annual identification of local deforestation hotspots in the Philippines using earth observation products. *Forests, 12*(8), 1008.

Santoro, M., Cartus, O., Carvalhais, N., Rozendaal, D., Avitabile, V., Araza, A., ... & Willcock, S. (2021). The global forest above-ground biomass pool for 2010 estimated from high-resolution satellite observations. *Earth System Science Data, 13*(8), 3927-3950.

Santoro, M., Cartus, O., Wegmüller, U., Besnard, S., Carvalhais, N., Araza, A., ... & Engdahl, M. E. (2022). Global estimation of above-ground biomass from spaceborne C-band scatterometer observations aided by LiDAR metrics of vegetation structure. *Remote Sensing of Environment, 279*, 113114.

Nesha, K., Herold, M., De Sy, V., De Bruin, S., Araza, A., Málaga, N., ... & Tavani, R. (2022). *Exploring characteristics of national forest inventories for integration with global space-based forest biomass data. Science of the Total Environment, 850*, 157788.

Conferences publications

Araza, A., Herold, M., Hein, L., Quiñones, M. (2021, July). The first Above-ground Biomass map of the Philippines produced using Remote sensing and Machine learning. *In 2021 IEEE International Geoscience and Remote Sensing Symposium IGARSS* (pp. 6897-6900). IEEE.

Araza, A., De Bruin, S., Herold, M. (2022, July). Plot-To-Map: an Open-Source R Workflow For Above-Ground Biomass Independent Validation. *In IGARSS 2022-2022 IEEE International Geoscience and Remote Sensing Symposium* (pp. 5575-5577). IEEE.

Peer-reviewed book chapter

Villanueva, L. A., Gatumbato, E. A., Araza, A. Fragmentation drivers and community education for coastal biodiversity reconstruction. *In Routledge Handbook of Seascapes* (pp. 399-410). Routledge.

Other scientific publications

Araza, A., Perez, M., Cruz, R.V., Aggabao, L.F. and Soyosa, E., (2020). Probable streamflow changes and its associated risk to the water resources of Abuan watershed, Philippines caused by climate change and land use changes. *Stochastic environmental research and risk assessment, 35*, pp.389-404.

Dida, J. J. V., Araza, A. B., Eduarte, G. T., Umali, A. G. A., Malabrigo Jr, P. L., & Razal, R. A. (2021). Towards nationwide mapping of bamboo resources in the Philippines: testing the pixel-based and fractional cover approaches. *International Journal of Remote Sensing, 42*(9), 3380-3404.

PE&RC Training and Education Statement

With the training and education activities listed below the PhD candidate has complied with the requirements set by the C.T. de Wit Graduate School for Production Ecology and Resource Conservation (PE&RC) which comprises of a minimum total of 32 ECTS (= 22 weeks of activities)

Writing of project proposal (4.5 ECTS)

- Assessment, Uncertainties and Applications of global Above-ground biomass maps from Earth Observation

Post-graduate courses (2.1 ECTS)

- OpenGeoHub Summer School (2020)
- R and Big Data; PE&RC (2020)

Invited review of (unpublished) journal manuscript (5 ECTS)

- Central Mindanao University Journal of Science: Sensitivity analysis in modeling streamflow of the Taganibong watershed (2021)
- International Journal of Remote Sensing: Analysis of maximum fractional vegetation cover from 2001 to 2016 (2021)
- International Conference on Computer Science and Application Engineering: Remote Sensing Monitoring of Afforestation Its Interaction with Climate in Saihanba Mechanical Forest Farm in Recent 45 (2022)
- Earth's Future: Analyzing the Spatiotemporal Patterns of Forests Carbon Sink and Sources Between 2000 and 2019 (2022)
- Geo-Carto International: Bamboo forest mapping using sub-region combined with optical and SAR satellite data in Google Earth Engine (2022)

Competence strengthening / skills courses (2.4 ECTS)

- Scientific publishing; PE&RC (2020)
- Reviewing a paper; PE&RC (2020)
- Scientific writing; PE&RC (2020)

PE&RC Annual meetings, seminars and the PE&RC weekend (1.5 ECTS)

- PE&RC PhD Weekend (2020)
- PE&RC last year of PhD (2022)

Discussion groups / local seminars / other scientific meetings (5.3 ECTS)

- GRS Time Series Group; WUR (2020)
- National Research Council of the Philippines annual meeting; NRCP (2021)
- Climate Change Initiative and Biomass Harmonization; ESA-NASA (2020-2023)
- Earth Observation for Ecosystem Accounting; EO4EA (2022)

International symposia, workshops and conferences (12.8 ECTS)

- EO3S Symposium; poster presentation; The Hague, Netherlands (2020)
- ESA POLINSAR; oral presentation; Online (2021)
- IGARSS 2021; oral presentation; Online (2021)
- 9th Annual International Conference on Environmental Science; poster presentation; Online (2021)
- PhilGEOS 2021; poster presentation; Online (2021)
- 3rd International Conference on Integrated Natural Resources and Environment Management; oral presentation; Online (2021)
- NCG Symposium; oral presentation; Wageningen, Netherlands (2022)
- Living Planet Symposium 2022; oral presentation; Bonn, Germany (2022)
- IGARSS 2022; oral presentation; Kuala Lumpur, Malaysia (2022)
- ForestSAT 2022; oral presentation; Berlin, Germany (2022)

Lecturing / supervision of practical's / tutorials (1.2 ECTS)

- Good practices on the use of open data for research; online; Philippines (2021)
- GIS for Local Climate Change Action Plan; online; Philippines (2021)
- Spatial Data Science for mapping obesity; Philippines (2022)
- MOOC for Land Biophysical parameters; EO College; (2022)

Supervision of MSc students

- Analyzing the link between deforestation and flashfloods in Malawi using data-driven methods (2021)

This research received funding from European Space Agency and European Union.

The printing of the PhD booklets is funded by Wageningen University.

Cover design by Arnan Araza